Alma Mater Studiorum – Università di Bologna

DOTTORATO DI RICERCA IN

GEOFISICA

Ciclo XXVI

Settore Concorsuale di afferenza: 04 / A4

Settore Scientifico disciplinare: GEO / 10 GEOFISICA DELLA TERRA SOLIDA

ADVANCED MODELLING OF TIME DOMAIN ELECTROMAGNETIC DATA WITH UPDATED HYDROGEOLOGICAL INTERPRETATIONS

Presentata da: Vincenzo Sapia

Coordinatore Dottorato

Prof. Michele Dragoni

Relatore

Dott. Marco Marchetti

Esame finale anno 2014

Index

Chapter 3.

Investigate the role of a priori information into the inversion of AEM data: the case study of Spiritwood Valley Aquifer.

A*cknowledgements*

There are a huge number of people I would like to thank. Above all, my heartfelt thanks go to ***Andrea Viezzoli*** *and* ***Greg Oldenborger***. *Andrea initiated me into the complex field of Airborne Electromagnetics. He patiently followed my progress, skillfully clarifying my numerous misunderstandings of EM theory, data modeling, etc. His enthusiasm for airborne geophysics combined with his friendship have been of primary importance in completing this work.*

Greg generously gave me his unwavering support and always guided me in the right direction. Despite the distance, he has been a fundamental presence throughout the study period, supporting me almost daily! It was a wonderful experience spending time in Canada and working with him at the Geological Survey.

I wish to thank my supervisor ***Marco Marchetti*** *for participating with great enthusiasm and for all kind of support he gave me whenever needed.*

I'm grateful to ***Antonio Menghini*** *for his willingness and unconditional help. He initiated me in the ground TEM field work, providing me with his huge experience acquired over the year.*

Many thanks to ***Flemming Jorgensen*** *for his training in EM data interpretation, 3D modeling, and many other forms of support when I was in Denmark. It has been a important opportunity for me to work with him.*

I am also very grateful to ***Esben Auken, Bjarke Roth, Cyril Schamper, Giulio Vignoli*** *and* ***Gianluca Fiandaca*** *for their critical suggestions in data processing and inversion.*

Thanks to ***Andrè Pugin, Heather Crow, Charles Logan, David Sharpe,*** *and* ***Hazen Russel****, for our stimulating discussions when I was in Canada. I also thank the University of Bologna, which gave me the opportunity of studying a PhD in Geophysics and awarded me a scholarship.*

Last, but not least, my gratitude to my parents, my brother, my wife, and all of my friends who make my life so enjoyable.

It might be possible I did forget to acknowledge some people..Beyond doubt, I really wish to thank everyone who shared his time with me in the last three years!!

Introduction, scope and results of the thesis

The research on which this thesis is founded was developed with the purpose of improving the resolution of Airborne Electromagnetic (AEM) results used to target and map subsurface conductivity structures. Most of the theory surrounding EM is well established, but for high-resolution mapping and calibration of acquired data, there is still room for improvement, and this provided the inspiration for the present dissertation.

Several countries have acquired, over the past decades, large amounts of area covering Airborne Electromagnetic data. The original applications were most often for promoting mineral exploration but in the last three decades, airborne electromagnetic (AEM) systems have been used for many groundwater exploration purposes. This contribution of airborne geophysics for both groundwater resource mapping and water quality evaluations and management has increased dramatically over the last 10 years proving how those systems are appropriate for large-scale and efficient groundwater surveying. One of the major reasons for its popularity are the time and cost efficiency in producing spatially extensive datasets that can be applied to multiple purposes.

As an example, in Canada many electromagnetic surveys are proprietary, and few of these data are public domain, duly compiled in accessible databases. Some are well described, documented and stored, others miss crucial parts of ancillary information. The type and quality of the data also varies significantly from older datasets from the 90's or earlier to more modern ones (either magnetic and both in frequency and time domain). Many AEM surveys were flown with different purposes over the past 40. The significant developments in data processing and modelling of the last few years, accompanied by novel approaches to integration of multiple datasets of different types, are driving research in revisiting these existing datasets. One approach to reconciling multiple data sets, data from different systems, or different generations of data is through calibration and/or joint inversion of extensive less-robust data with less extensive high quality data.

We start with processing and inversion of two AEM dataset from two different systems:

1) the AeroTEM III dataset, commissioned by the Geological Survey of Canada in 2010 as part of an buried valleys aquifer mapping campaign for the Spiritwood Valley in Manitoba, Canada and 2) the "Full Waveform VTEM" dataset, collected and tested over the Spiritwood Valley area, during the fall 2011. In fact, this system was developed in order to improve the shallow imaging capability of the VTEM helicopter EM system, obtaining more accurate early-time data.

It's well know in literature that buried valleys are important hydrogeological structures in Canada and other glaciated terrains, that provide sources of groundwater for drinking, agriculture, and industrial applications. Hydrgeological exploration methods such as pumping tests, borehole coring, or ground-based geophysical methods alone (seismic and electrical resistivity tomography) provide limited spatial information and are inadequate to efficiently predict the sustainability of these aquifers on a regional scale. On the contrary, airborne geophysics can be used to significantly improve geological and hydrogeological knowledge on a regional scale.

As one of the main achievements of this study, we demonstrate that in the presence of multiple datasets, either AEM and ground data, due processing, inversion, post-processing, data integration and data correction (calibration) is the proper approach capable of providing reliable and consistent resistivity models. The output model can then be interpreted for geological and or hydrogeological purposes and, in turn, it can be of interest to many end users, ranging from Geological Surveys, Universities to Private Companies dealing with hydrogeological mapping. In general, the deliverables from contractors often include raw data and Conductivity Depth Images. These are imaging products based on approximations, and not a full inversion based on accurate forward modelling. As such, they can be inadequate for providing accurate rendering of the subsurface resistivity variations required for rigorous hydrogeological mapping. Also, processing of the data used as input for the CDIs can introduce artifacts example if it fails to address correctly, for example, system bias, noise levels, or coupling with infrastructure. We therefore set to a complete reprocessing and inversion of the raw data. In this thesis, the reader is conducted through the entire AEM data handling workflow, which involves data processing and inversion.

As is known, very raw data are always influenced by electromagnetic coupling to man-made structures. Such noisy data need to be carefully culled from the dataset to avoid uncoupled data being distorted by coupled data which would directly affect inversion results. Appropriate modeling of the waveform, time gates, transmitter area, number of turns, etc. (all part of the system transfer function) are of primary importance when attempting AEM data inversion. If the system transfer function is not modeled accurately, the errors introduced may migrate to the model's earth or geometry related parameters. These data were then used as input to a Spatially Constrained Inversion.

Despite careful processing, examination of preliminary inversion results from both AEM datasets reveal several inadequacies in the recovered models. AEM data often suffer from significant inaccuracies in the early-time or near-surface data – a problem that can lead to errors in the inverse model or limited near-surface resolution in the event that early time gates are removed.

In this study we investigate the general assumption that data integration, or combination of several complimentary types of geophysical data collected over the same survey area, can improve inversions, reduce ambiguity and deliver high resolution results for the very near-surface. However, data integration is a loose term in the geophysical literature. For instance, existing examples in literature where knowledge from high resolution reflection seismic data is used to improve airborne time-domain electromagnetic data inversion are few and far between.

To this end, reflection surfaces picked from high-resolution seismic reflection data are used as a-priori information to define layer depths in the inversion of both AEM dataset. This leverages the high-resolution architectural nature of the seismic data against the material property sensitivity of the AEM data and results in consistency between the data sets, but does not necessarily yield an inversion result that is in agreement with geological knowledge. Adding a priori from seismic data results in improved near-surface resistivity and a more continuous bedrock layer with a sharper contact. Moreover, bedrock seismic constraints reduce uncertainty in the resistivity values of the overlying layers, although no a-priori resistivity information is added directly to those layers.

For the VTEM results, preliminary inversion showed margin for improvement in the rendering of the shallowest layers. It was found that the description of the waveform used was not accurate. The modelling was therefore revisited redefining the waveform description of the VTEM data using the ERT as a reference model. Quantitative application of ERT results as constraint information is not as straightforward as for the seismic data since layer boundaries are not well defined from ERT. The VTEM model was calibrated to the supporting data via a small time-shift in the VTEM data gates relative to ramp-off. The source of the time shift was attributed to timing or turn-off errors, but the calibration procedure is independent of the source of noise. The calibrated VTEM model exhibits detailed delineation of the very near surface and other resistive anomalies associated with the valley fill. Many of the issues described in this paper could be relevant to other AEM datasets collected over the world. The suggested approach can be applied to any airborne EM dataset for which some reference model can be established.

This is a pragmatic approach in that we do not attempt to identify the source of timing error, but rather, consider recovery of a consistent and acceptable model as justification of the procedure. It is important to note that the reference model should be of high quality and that any errors or uncertainty in the reference model will be propagated to the calibration and the recovered models.

In this approach, we use both model-space constraints and iterative model-and data-space calibration based on ancillary information from other survey types. We further combine the time-shift calibration with the seismic bedrock constraint and we obtain more structure in the valley-fill sediments and increased consistency of the bedrock contact.

The result is a model that benefits from the near-surface resolution of the ERT and a methodology that can be a applied to the entire HTEM survey area.

Calibration procedure is adapted from that applied in Denmark to AEM data using reference models derived from ground TEM data. By applying calibration to an entire data set, the advantages of the regional extent and high spatial density of AEM can be fully utilized. Consistency across data sets

results in increased confidence in the near surface model that is critical for groundwater mapping on which management decisions are based.

With respect to the calibration time shift, there are several issues in Airborne TEM data collection that can potentially affect the correct location of data gates with respect to the transmitter waveform, especially at early time. These include transmitter-receiver synchronization, imperfect bucking of large primary fields or parasitic capacitance. There can also be a degree of subjectivity in choosing to use ramp-off as a time reference for the receiver data gates. As a result, there can be a significant amount of current still flowing in the transmitter loop during the early off-time gates. It is unlikely that a single optimal time-shift exists for a large data set with multiple flights, although our utilization of a time shift obtained over one line of collocated data produces acceptable results survey-wide. The entire processing and calibration procedure in itself is model independent and should work in all geological domains of the survey area.

All things mentioned above do not constitute the only goals of this study. We attempted to move further from the data processing and inversion itself. therefore, we decided to use the final, most reliable resistivity models as a solid basis for a knowledge-driven 3D geological modeling. In addition, the impact of an AEM dataset towards hydrogeological mapping and 3D hydrogeological modelling, comparing it to having only a ground based TEM dataset (even if large and dense), and\or to having only boreholes is also described in detail. From the latter, we describe the shortcomings in hydrogeological interpretation and management that could have arisen if the AEM survey had been substituted by a ground TEM survey in the same area. Output resistivity models and the derived 3D geological model, clearly reveal how the mapping of hydrogeological features, like main buried valleys as well as minor valley networks, could be inaccurate and poorly detailed in terms of structures morphology. On the contrary, AEM provides, rapidly and cost effectively, robust results in terms of aquifer geometry and vulnerability mapping, much detailed 3D hydro\geological model, all things that concur to being solid basis for i.e. subsequent flow modeling. A 3D Voxel-based model of the AeroTEM survey data was realized and presented in this

dissertation. For the VTEM dataset, we also present a 3D voxel model obtained with the original VTEM waveform in order to illustrate how the voxel models would have differed in terms of derived hydro\geological interpretation. Fidelity of electrical resistivity derived from the AEM inversion is of great significance when attempting to assess the hydrogeological importance of geological units.

A voxel approach allows a quantitative understanding of the hydrogeological setting of the area, and it can be further used to estimate the aquifers volumes (potential amount of groundwater resources) as well as hydrogeological flow model. The 3-D modelling was carried out in two steps: first, 3D surfaces were previously interpreted and interpolated based on AEM (AeroTEM) resistivity grids and, subsequently, those surfaces were used to constrain the 3-D lithological model. Since different resistivity values are due to variations in filling materials (higher resistivity for coarse-grained materials and lower resistivity for finer-clayey ones), each lithology were interpreted based on picked resistivity values directly from the AeroTEM resistivity grids.

Differences in the output 3D geological models are highlighted in detail. In general we learned that the 3D geological model derived from a AEM dataset matches all available ancillary information (ERT, seismic, boreholes, prior geological knowledge). Conversely, un-calibrated AEM dataset give rise to inaccurate and unreliable 3D geological model for many reasons, including a) artificial ubiquitous shallow conductive (clay) cap cover that would prevent surficial recharge, shows, b) erroneous depth estimate of buried valleys, c) overestimation of aquifers porosity. Extraction or management of the GW resources based on this model would most likely bring unwelcomed consequences. Ongoing development within the AEM world is increasing the value, relevance and applicability of this methodology. Improvements or revisiting of hardware, modelling, procedures deployed for the task and interpretation, they are all contributing towards this result.

Chapter 1

A review of EM theory, airborne EM systems, and data inversion.

Introduction

A brief summary is provided below of basic EM theory, the wide range of applications for Airborne EM systems, together with some information regarding AEM data inversion. The purpose is to establish a adequate conceptual foundation to understand developments in airborne time domain electromagnetic prospecting. Perhaps, it is important to comprehend EM fields, depth of penetration, and transition waveforms in order to optimize the choice of AEM system for different surveying contexts. Maxwell's equations form the basis for electromagnetism and it would be pointless to repeat here what other well known authors have already explained (Grant and West, 1965; West and Macnae, 1991, Nabighian, 1998a; Nabighian, 1998b; Wait, 1982). Reviews of EM geophysical methods, with extensive bibliographical references, were also published recently by Christiansen et al. (2009), and Nabighian and Macnae (2005). Having premised the above, this chapter will outline only the basic elements required for an explanation of EM, and in particular Airborne TEM systems, and Airborne TEM data inversion. This will serve as a foundation for the discussion of further parameters in greater detail in the following chapters. Geophysical inversion is a methodology for estimating the consistency of Earth model(s) parameters with a geophysical observation set, also taking data noise into consideration. This can be approached from two main perspectives which can be termed deterministic or probabilistic. Both approaches tend to generate comparable results (cf. Brodie 2013). However, in this work a deterministic methodology for data inversion is applied, and summarized below. An outline is provided for a laterally constrained (Auken et al., 2004), and spatially constrained (Viezzoli et al., 2008) inversions. Many different types of data have effectively been processed using one dimensional spatial and lateral inversion techniques. Examples include vertical electrical soundings (Auken and Christiansen 2004; Auken et al. 2005a), seismic surface waves (Wisén and Christiansen 2005), transient electromagnetics

(Auken et al. 2008; Viezzoli et al. 2008), frequency-domain electromagnetics (Monteiro Santos 2004; Brodie and Sambridge 2006; Triantafilis and Monteiro Santos 2009), magnetic resonance soundings (Behroozmand et al. 2012a), and time domain induced polarization (Fiandaca et al. 2012b, Fiandaca et al. 2012a). Since the aim of the present chapter is to provide an overview, without presenting any innovations in EM theory or inversion, there is an intentionally large number of references to all the most important works by the many scientists and researchers in this field.

How the time domain electromagnetic method works

A transient magnetic field is generated by varying the flow of current around a transmitter loop. The high air-surface impedance causes the primary EM field to diffuse downwards in the form of a plane wave. By abruptly interrupting the current in the transmitter loop, it generates very marked variations in the magnetic field which in turn induces an electromotive force (emf) in the medium according to Faraday's Law of induction. The emf has a magnitude proportional to the rate of change of the primary magnetic field in the conductor. Therefore, a current is induced in the conductor like concentric horizontal eddy currents resembling smoke rings which run below the transmitter and diffuse through the medium (Nabighian, 1979). Over time the ground resistance weakens the current (generating heat) and shifting the maximum current density outwards and downwards, so that the current density is increasingly weaker. Therefore, currents decay over time and diffuse in depth,as function of ground conductivity, a process that occurs more slowly in highly conductive ground compared to poorly conductive ground (where currents diffuse and decay more quickly). A coil receiver sensor is used to detect the secondary magnetic field generated by the induced currents. The rate of change of the secondary magnetic field, induces a voltage in the Rx-coil which is measured as a function of time . The depth of the diffusion phenomenon is called the diffusion depth, and is calculated by relating time t (from the source impulse) to penetration depth d. Diffusion depth is defined as the distance over which a primary field amplitude is reduced by a factor of 1\e (Keller and Zhadanov, 1995).

The eddy current generated in the ground, immediately after the Tx-loop current is switched off, is effectively a ground image of the transmitter loop. It is close to the surface and the conductivity of the uppermost layers strongly influences the measured signal . As the current penetrates deeper into the ground the measured signal provide information on the conductivity of the lower layers. In this way, the receiver coil will therefore provides information on conductivity as a function of depth; this is a TEM sounding. The bandwidth of the system does not correlate directly with the system's base frequency (which is the time window applied for collecting data), and instead is largely determined by the frequency range of the primary EM field. The latter is not easy to establish, and to overcome this difficulty most TEM systems implement a linear shut-off ramp for the current (Raiche, 1984, Fitterman and Anderson, 1987). The length of the off-ramp is inversely proportional to the high frequency bandwidth. A long linear ramp has the effect of making early time responses resemble a step response. A short linear ramp instead retains the characteristics of an impulse response (West et al., 1984). However, instantaneously shutting down a current in a loop is highly problematic because a plethora of self inductance, back currents, and other phenomena occur with the result that the current is effectively not off. By implementing a short linear ramp it still provides a limited bandwidth, but the signal contains the highest frequency range for the shortest possible off time.

"*The sensitivity of the step response to the shallow resistivity distribution is inferior to that of the impulse response, indicating that a short ramp is preferable for environmental investigations"*(Sørensen et al., 2012). Transient systems must be capable of handling the great variety of the earth's responses and so they need a very wide dynamic range. A rapid ramp off of the transmitter current (waveform with a linear ramp off) induces high frequency harmonics in the primary EM field, resulting in early off-time gates, which is appropriate for mapping near surface resistivity. Conversely, an extended, gradual shut off of the transmitter current results in deeper ground penetration, inducing secondary currents mainly in any good conductors.

In the receiver coil, TEM measurements are taken at frequent time windows, referred to as "time gates". The early time gates are very narrow because they occur when the transient voltage is changing rapidly, especially for highly resistive ground with low τ values. The later gates occur when the transient voltage is changing more slowly and so they are much longer. The early time gates thus provide information about the near surface, while late time gates provide information about the deeper subsoil. The gates are spaced with a logarithmically increasing time period in order to minimize distortion of the transient voltage and improve the signal/noise (S/N) ratio at late times, a method called "log-gating" (Munkholm and Auken 1996).

Basic equations used in EM theory

To date, the mathematical expressions defining the components of the EM field are very elegant, but it is still extremely difficult to arrive at a numerical evaluation. A thorough treatment of the mathematical theory of EM induction is provided in Ward and Hohmann, 1988, and West and Macnae, 1991. There are two measurable components of the EM field: the electric field and magnetic field. These are not simple functions of spatial location but also involve time or frequency. An EM field is a manifestation of the distribution of electric charges within a medium and it can be expressed in the differential form of Coulomb's Law:

$$\nabla \cdot \varepsilon_0 \mathbf{E} = q$$

Electromagnetic phenomena are governed by Maxwell's equations. James Clerk Maxwell (1831-1879) managed to integrate the existing theories of electric, magnetic, and electromagnetic induction and defined an elegant set of differential equations. There are four fundamental constitutive relationships that define the response of a medium to a variety of electromagnetic inputs. The relationships between electric field E, current J, and electric displacement D are described in two of these, while a second pair describe the relationships between magnetic field H, magnetic induction B, and magnetic polarization M. In quantitative terms, these four constitutive relations are:

$J = \sigma E$

$D = \varepsilon E$

$B = \mu H$

$M = \chi H$

where σ is electric conductivity (Grant and West, 1965), ε dielectric permittivity, μ magnetic permeability, and χ magnetic susceptibility. The four parameters comprehensively describe the electromagnetic properties of a material. The first relation is effectively the well-established Ohm's law in a microscopic context. According to Maxwell's laws, an alternating current induces secondary currents in a conductive earth. These secondary currents in turn generate secondary magnetic fields, measurable using EM receivers. The primary field source can be compared with the secondary fields in order to quantify conductivity (i.e. frequency domain methods). Alternatively, the secondary field can be measured in the absence of a primary magnetic field (i.e. time domain methods, as described in the following section of this chapter).

The coupling between the E and H fields is described by Ampere's and Faraday's law.

$$\nabla \times H = -\frac{\partial D}{\partial t} + J \quad \text{(Ampere's law)} \quad \text{and} \quad \nabla \times E = -\frac{\partial B}{\partial t} \quad \text{(Faraday's law)}$$

The way in which an electric current can generate an induced magnetic field is described by Ampere's law. If the electric field E is unstable and varies over time then there will be an additional current in the medium known as the displacement current, proportional to the variation of the electric field E. This proportional factor is known as the dielectric permittivity ε. Consequently, an additional contribute, dD/dt, acts to induce the magnetic field H. Since the displacement current acts in exactly the same way as the conductive current J, the total current will be J+ dD/dt.

The Maxwell–Faraday equation is a generalization of Faraday's law, stating that any magnetic field that varies through time will be accompanied by a spatially-varying, non-conservative electric field, and vice-versa. The emf induced in a coil is equal to the negative of the rate of change of the magnetic flux.

AEM systems

A small exploration company called Stanmac collaborated with McPhar Engineering in 1946 to develop a portable ground EM system that was towed by a tractor over frozen lakes. A forward trailer carried a transmitter with a receiver on a rear trailer 60 m further behind. The following year a similar arrangement was designed for flight, with a transmitter mounted on a wooden Anson aircraft with the transmitter dipole axis horizontal and transverse to the direction of flight, referred to as the y transmitter axis. The receiver was towed behind on a sort of glider referred to as a "bird". The successful testing and implementation of this system represent the birth of airborne electromagnetic surveying (Fountain, 1998). An AEM survey was subsequently conducted in 1953 by Inco and led to the discovery of the Heath Steele zinc-lead-copper and silver deposits. This was the first discovery made directly from an AEM survey and the method was soon widely used and a variety of other related systems were developed.

Starting from 1997, various reviews have been published regarding airborne electromagnetic surveying (Fountain, 1998; Witherly, 2000; Fountain and Smith, 2003; Nabighian and Macnae, 2005, Fountain et al., 2005, Thomson et al., 2007, Allard 2007, Sattel 2009).

AEM systems vary by their features, sizes, and fields of application, but they can be divided into two main categories: fixed-wing plane and helicopter based, implementing both frequency and time domain systems. The primary magnetic field in frequency-domain airborne electromagnetic systems is generated by a sinusoidal current flowing through a transmitter coil at a specific frequency. The primary magnetic field induces eddy currents in the subsurface, which in turn generate a secondary magnetic field that varies according to the distribution of ground conductivity. The receiver coil picks up the secondary magnetic field and it is compared to the predicted primary magnetic field at the receiver coil. The primary field is much stronger than the secondary and so it is generally bucked out, with the secondary field measured in parts per million (ppm).

Time-domain airborne electromagnetic systems operate by abruptly shutting off a current flowing through a transmitter loop, causing a variation in the magnetic flux generated by the

current. This variation induces the flow of currents in the ground (according to Faraday's law). The currents diffuse outwards and downwards into the subsurface. The induced secondary magnetic field by these currents is measured using an induction coil, which is generally located near the transmitter.

The first fixed-wing airborne electromagnetic (AEM) system was put into operation in 1948, followed in 1955 by the first helicopter AEM system (Fountain, 1998). These early systems were nearly all frequency-domain based, but in the late 1970s, fixed-wing AEM systems mostly switched to time-domain systems, while helicopter systems remained mostly frequency-domain. The idea emerged among geophysicists of creating a hybrid combination of a fixed wing time domain AEM system and a HFEM systems to get the best of the two worlds: combine the high transmitter power of fixed wing systems depth penetration, while the slower speed and lower altitude of HFEM systems gives higher spatial and near surface resolution, and they are better for surveying more rugged topography. "*The dream was the same: update the time domain technology and mount the system onto a helicopter platform to create the helicopter time domain system (HTEM).*" (Allard 2007). The powerful fixed-wing systems were generally employed when there was a need for a large footprint and the capability for deep investigation of discrete conductors, typically for identifying base metal and uranium deposits for mining. Helicopter borne systems instead provided a high level of near surface resolution, which made then very effective for near surface mapping, but their depth penetration is limited especially in the presence of conductive overburden. Helicopters are also limited compared to fixed wing systems as regards the size and weight of equipment, which effectively also limits transmitting power.

In recent years these systems have seen considerable improvements in data quality, signal to noise ratio, investigation depth, and spatial resolution. Further technological improvements include more accurate GPS location, navigation systems, greater data storage capacity, and higher data processing speeds. All this helped in the emergence of HTEM systems, which can be considered the most important development in this field over the last 10 years. These new EM systems offer

important improvements for mineral exploration (Palacky and West, 1991, Fountain et al, 2005), but the impact of this enhanced tool extends into a wide range of applications, including groundwater mapping, environmental applications, and others. The key factors for the immediate success of HTEM are its excellent horizontal accuracy (especially with the coincident transmitter-receiver systems), good near surface resolution (in large part due to its wide high frequency contents), cost effective implementation, and significant depth of effective exploration. In the years 2000 to 2002, there were two different, independent HTEM systems available commercially: the AeroTEM (Boyko et al., 2001, Balch et al., 2002) by Aeroquest Ltd., and the VTEM (Witherly et al., 2004) by Geotech Ltd. Soon afterwards two more systems were developed: the SkyTEM (Sørensen and Auken, 2004) by SkyTEM ApS, and the HeliGEOTEM (Fountain et al., 2005) by Fugro Airborne Survey.

There are two basic configurations adopted by almost all the systems:

- the receiver coils are in, or very close to, the center of the horizontal transmitter loop. These are called central loop configurations and include the SkyTEM, VTEM, AeroTEM, and HoisTEM systems.
- the receiver coils are fitted on the towing cable at a height above the horizontal transmitter loop. These are called vertical separated loop configurations and include the NewTEM and HeliGEOTEM systems.

Concentric coil systems suffer from the strong primary field induced during on-time which can persist into off-time as a high system transient, overpowering the weaker secondary field. This problem is overcome using a bucking coil to reduce the primary field amplitude by over four orders of magnitude at the Z-axis receiver coil (Walker et al., 2008). Residual primary field variations are then eliminated from the Z-axis coil using an algorithm during post-processing, which also includes deconvolution of the system waveform. The SkyTEM system has its receiver Z coil located 1.5 m vertically above the edge of the transmitter loop in a null coupling position. The receiver X coil is

located 2 m behind the transmitter loop again in a null coupling position. The self-response of the system, generally called noise or bias, can be very clearly established by flying the system at very high altitudes where the response of the ground is negligible. It is generally sustained that system response must be lower by a factor of 50 to 100 than the signal levels detected at operational heights of about 30 m (Sørensen and Auken, 2004).

A limitation that most AEM systems suffer from is the impossibility of obtaining unbiased early-time voltage data, making it essential to apply timing and primary field removal (Macnae and Baron-Hay, 2010). The early-time data give information about near-surface sensitivity, which is essential for groundwater applications. AEM systems are also complex to design and the acquisition of AEM data can be impaired by a variety of noise sources from both inside and outside the system. For example, definition of an absolute time-zero can be problematic in addition (Christiansen et al., 2011). With the objective to improve near-surface resolution, advancements have been made in AEM system modeling (Christiansen et al., 2011), and AEM surveys calibration using ancillary information (Auken et al., 2009; Foged et al., 2013; Podgorski et al., 2013).

Over the years HTEM systems have evolved to satisfy different exploration goals, but adaptations to any one specific exploration environment can easily compromise the performance of the system in a different setting. One common adaptation is raising the transmitter dipole moment in order to increase the response amplitude and improve detection of deep conductors. HTEM systems have also undergone a variety of adaptations in loop sizes, number of loop turns, and transmitter current with the aim of increasing the dipole moment. Despite these improvements, the limitations in equipment size and weight always define a ceiling to the transmitting power achievable with helicopters compared to fixed wing systems, with a resulting limit to ground depth penetration (which is nevertheless always much greater than with any helicopter borne frequency domain system). If the aim of a survey is to map near surface conductivity, then a lower dipole moment combined with a faster switch off time represents a reasonable compromise. Over the last few years the SkyTEM (Sørensen and Auken, 2004) and VTEM (Legault et al., 2012) development teams

have strived to improve the performance of HTEM systems for very near surface resolution as much as possible (within the high frequency component). As a result, these systems have been successfully used for hydrogeological surveys when near surface information is crucial for groundwater mapping. Sedimentary environments exhibiting moderate to high resistivity in the shallow subsurface represent a particular challenge for achieving satisfactory near surface resolution using AEM measurements. As is well known, near-surface resolution is highly dependent on the specific instrument's capacity to measure the early time portion of the transient ground response. The receiver bandwidth and implemented current waveform also significantly influence the resulting near-surface resolution. An important role is also played by the transmitting current waveform and base frequency in the intensity of the induced EM ground response (Liu, 1998). Each system adopts a specific waveform at one or more base frequencies in order to fulfill precise objectives and strategies.

Sources of noise in TEM data

There are two main types of EM noise, which can be produced by natural sources or from cultural sources. The noise spectrum from natural sources has daily, annual and geographic variations. In the following a brief review of the sources is given and a more thorough discussion of the EM noise spectrum may be found in e.g. Macnae et al. (1984), McCracken et al. (1986) and Spies & Frischkneckt (1991), while the present discussion is limited to a brief review of the same. Natural EM noise below 1 Hz is mainly the result of interaction between the earth's magnetic field and solar plasma arriving from the sun. The spectrum above 1 Hz is of more influence in TEM soundings with the major source being lightning discharges during thunderstorms. This noise source can seriously compromise TEM data quality during summer or the rainy season when intense electrical storms are reasonably common on a continent scale. The amplitudes are generally 5 to 10 times greater than the vertical field, and when numerous spherical events are present, it is difficult to filter them out because their amplitude and time distribution are essentially random. Ground response varies most rapidly during early time measurement gates and so dense sampling is

required to define these variations, while at later gates the signal to noise ratio deteriorates requiring longer averaging intervals to extract the ground response (Nabighian and Macnae, 1991). One method for recording the response during later time is by acquiring transient decay with gates acting as windows equidistantly spaced in logarithmic time. A mean value within each of these logarithmically spaced time windows is calculated in a process called "log-gating" (Munkholm and Auken, 1996). Repeated ground response measurements are log-gated and subsequently the values for the same delay time are stacked (gate stacking), on the assumption that the noise has a Gaussian distribution. For white (Gaussian) noise, which is stochastic and has the same power through all frequencies, a factor N increase in stack size (where N is the number of measurements in the stack) will decrease the standard deviation of the noise by a factor $\sqrt{N}$. The increased integration time and increasing delay times, mean that log-gating has the effect of increasing the stack size for progressively later time gates and thus reducing the standard deviation of the noise through time by a factor of the square root of the gate length.

Signal quality can be greatly improved by data stacking. The distinct advantage of ground-based TEM surveys over HTEM surveys is the possibility of stacking data at the same position for a extended period. Similarly, the flight speeds of HTEM systems is around 30 m/s, which is much slower than most AEM systems, making it possible to collect and stack 2 to 3 times more data per km. Spatial and data resolution are strongly dependent on the stacking time window, with a small number of stacks offering good near surface horizontal spatial resolution, but a low signal to noise ratio at late time. A large number of stacks excessively smoothes the data and limits near surface resolution, while providing improved data quality at late time.

Cultural sources become a significant contribution to increase the noise level within populated areas. One of the main contributors in culturally noisy areas is the infrastructure distribution, resulting in spectral peaks at 50 or 60 Hz and the corresponding odd harmonics. Although the voltage waveform is maintained sinusoidal at 50 or 60 Hz, the current produces disturbing fields which fluctuates outside the sinusoidal waveform (i.e. due to the variable grid

loading), and high amplitude broadband transients sometimes occur. Cultural noise sources include buried pipelines, cables, fences, power lines, road networks, and others features around the area (Nekut and Eaton, 1990). Currents are induced in the earth by power lines and communication transmitters and give rise to a secondary field coherent with the ground response, which in turn is superimposed to the measured signal. Sørensen et al. (2000) and later Danielsen et al., (2003) differentiate two types of coupling: galvanic and capacitive, and reference may be made to these authors for a in-depth discussion of EM coupling. The safe distance from man-made conductors is a minimum of 100-150 m. The effects of coupling must be accurately removed from data to permit a reliable interpretation of TEM soundings and so any soundings conducted in proximity to pipelines, cables, power lines, railways, road guardrails, and metal fences cannot be correctly interpreted and should be culled. It is critical to know the level and nature of noise when processing transient electromagnetic sounding data. Inadequate noise estimation can easily result in erroneous interpretation of the data. The only way to adequately identify and remove distorted data, while retaining enough data for meaningful interpretation, is spatially dense sampling. This differentiates ground based TEM from HTEM surveys, because while TEM surveys offer a better signal to noise ratio due to enhanced stacking, HTEM surveys permit higher data density and consequently improved identification of coupling.

Inversion in applied geophysics

Inverse theory is a very extensive subject and a detailed description would be extremely onerous and beyond the scope of this short chapter. Instead the aim is to outline the basic elements required for solving practical inverse problems with airborne electromagnetic time domain data (AEM), concentrating on the inversion methodology applied in the present study. AEM geophysics serves to help solve practical environmental and geotechnical problems and, more in general, for subsoil exploration. The typical scenario involves firstly the identification of a physical property like electrical conductivity, density, seismic velocity, magnetic susceptibility, or otherwise that is considered diagnostic of a sought geological structure or buried object. Next, a geophysical survey

is designed and field data are acquired. The ground is characterized by its 3D distribution of physical properties, and responses might be fields measured above the surface of the ground or in boreholes. All energy propagation through the ground depends on the 3D distribution of one or more physical properties, and consequently each datum is sensitive to variation of properties within a volume. This is one of the things that differentiates geophysics from direct sampling in a borehole, which instead provides information for a specific point within a 3D space. Each geophysical datum is sensitive to processes within a volume, or may depend on the volumetric distribution of a physical propriety, and all this is encoded in the data in a complex way. The inversion is required to extract such information from the data. Geophysicists have known about the need for inverting data for many years, but the limitations of computer technology a few decades ago meant that even the best inversion algorithms were able to recover estimates for only a limited number of parameters. Since then, considerable advances in computer performance and improvements in the mathematics of inversion, have brought more realistic inversions within reach, enhancing the role of geophysics for solving practical problems. Nevertheless, while it is now easy to obtain an image of the earth from an inversion algorithm, it has also become clear that extracting information about the subsurface from geophysical data is still not a trivial operation. Data interpreters (i.e. end users) must understand the basic issues that render each solution non-unique, and how prior information is used to "regularize" each case, if they aim to achieve good quality interpretations. They must also know how well data needs to be fitted, in other words, how well the simulated data from a recovered model needs to match “real” observations. There is the quandary that for each model that “acceptably” fits the data there are an infinite number of other models that fit the data equally well, which is known as the non-uniqueness of the inverse problem (Ellis, 1998). The non-unique nature of the inverse problem also means that it is an ill-posed problem, as noted from Tikhonov and Arsenin, 1977. This implies that it is necessary to provide prior knowledge or additional information about the model. If the model information is characterized by known probabilities, then a statistical formulation could offer a useful framework for resolving the inverse problem

(Tarantola, 1987). This requires a probability density function for these quantities and Bayes' theorem is used to generate an *a posteriori* probability density function for the model parameters. In the deterministic approach the optimum ground model is identified according to the objective function, and this is considered to be the solution to the inverse problem. The aim of the deterministic approach is generally the identification of a single solution for the objective function, (in a process known as global optimization), solving the inverse problem by identifying the model that minimizes the model objective function and also "fits" the data within the noise level (Brodie, 2013). Noise is supposed to be the degree of uncertainty related to errors in the measured data, combined with other sources and errors arising from discrepancies between the mathematical representation of the ground and the actual ground (for example, representing the 3D ground with 1D or 2D approximations). None of the above mentioned errors are completely known in most cases, so this issue is dealt with by assuming data errors to be Gaussian (Butler, 2005 chap. 5, Munkholm and Auken, 1996).

Before dealing with the inverse problem, an understanding of how to describe and solve the forward problem is necessary. In this procedure the data sources and ground model are assumed to be known for the calculation of the responses (Tarantola and Valette, 1981). A generic geophysical survey dataset can be expressed as:

$$F_j[m] = dj_{obs} \equiv d_j + n_j \quad \text{and} \quad j = 1,2,3.., N,$$

where $\mathbf{F_j}$ is a forward modeling operator incorporating details of the survey design and the relevant physical equations, and **m** is a generic property distribution. $\mathbf{Dj_{obs}}$ is the observed datum which consist of the true datum ($\mathbf{d_j}$) plus noise $\mathbf{n_j}$.

1D or 3D Inversion ?

Numerous N data (d_{obs}) are acquired in AEM geophysical surveys. An inverse problem aims to identify the model m (i.e. recover the physical property distribution) that produces the

observations including noise. Several factors, many already mentioned above, make this task much more complicated than solving a forward problem.

As already noted, one of the main characteristics of AEM surveying is the capacity to collect extremely large datasets applicable to from mineral exploration to groundwater and geological mapping, which can be very time consuming to process and invert. Traditionally, transient soundings, collected over a 3D environment (the earth), were interpreted using 1D ground models but very slow ordinary 1D least squares iterative inversion programs on the computers were available at the time (Fittermann and Stewart, 1986, Macnae and Lamontagne, 1987). Today the availability of much faster modern computers makes inversion with 1D models easy, although inverting huge data sets can still be onerous in computation time. This technique is very demanding, with simultaneous inversion of numerous laterally constrained TEM soundings in order to assure lateral continuity of the concatenated 1D models. This includes a full non-linear damped least squares inversion based on an exact forward solution, modeling the instrumentation's system transfer function (STF). The solutions developed by Ward and Hohmann, 1988 are used as the basis for the forward modeling algorithm. Modeling the STF also includes the low-pass filters (Effersø et al., 1999), and turn-on / turn-off ramps (Fitterman and Anderson, 1987). These inversion techniques are referred to as Lateral Constrained Inversions (LCI, Auken and Christiansen 2004; Auken et al. 2005), and Spatial Constrained Inversions (SCI, Viezzoli et al., 2008), and they differ from the earlier stitched-together 1D models (Macnae and Lamontagne, 1987, Auken et al., 2003 and Huang and Fraser, 2003). The drawback of the latter is that the resulting models exhibited abrupt variations between adjacent models, "… *which is a non optimal result for sedimentary environments where the lateral variations are expected to be smooth* …" (cf. Viezoli et al., 2008). There are also a number of proposed methods for 3D forward modeling of the time domain EM response in literature: Arnason (1995), Best et al. (1995), Alumbaugh et al. (1996), Sugeng (1998), and various algorithms have been defined (Alumbaugh and Newman, 2000 and Haber et al., 2004). While these studies demonstrate that 3D inversion of TEM data is possible, it remains an

impractical solution due to the demands of computation power (very time consuming), and it is extremely challenging because the electric fields in the subsurface (cf. Maxwell's equations) must be solved for every source position. There have been recent attempts to develop and apply fast and effective 2D and 3D inversion schemes for AEM data (Wilson, Raiche and Sugeng 2006, Guillemoteau, Sailhac and Behaegel 2012). Nevertheless 3D inversions have not become established as routine practice, and in many contexts the benefits of current 3D over 1D methods are disputable (Viezzoli et al. 2010). The 1D inversion approach is perfectly viable in geological contexts of gradually varying 3D structures and moderate conductivity contrasts. Conversely, in geological contexts with pronounced 3D model characteristics, a 1D inversion will be strongly influenced by the 3D effects and might easily generate unreliable models. Literature includes a number of papers discussing the influence of 3D structures on 1D interpretations of TEM data, including Auken (1995), Hördt and Scholl (2004), Newman et al. (1987), and Goldman et al. (1994).

Smooth and/or layered resistivity model

Normally, AEM inversion codes based on 1D forward modeling apply lateral/spatial constraints to regularize the inversions so as to achieve solutions compliant with the predicted geological variations (Vallée and Smith 2009, Christensen and Tølbøll 2009, Brodie 2010, Auken et al., 2013, Kirkegaard and Auken 2013). Using local constrained 1D models in this way for inverting pseudo 2D/3D models has been found to be very effective for modeling quasi-layered structures when the 2D/3D effects are not particularly pronounced (Newman et al., 1987, Sengpiel and Siemon 2000, Auken et al. 2005). This type of algorithms normally offer support for two modeling approaches: "layered/discrete models or the L1 norm optimization method" inversions, which invert for a limited number of layers with variable layer boundaries; or "smooth models or the L2 norm based least-squares optimization method" inversions, which are based on a large number of stacked layers in a fixed vertical discretization. In the latter approach, the inversion problem is typically greatly over-determined, with vertical regularization required to stabilize the solution (Constable et

al., 1987). In the former approach the inversion can operate without additional regularization, due to the much smaller number of free model parameters in play. Both methods have pros and cons, with the smooth approach producing sections with formation boundaries smeared out by regularization, while the discrete approach can introduce artifacts if the geology is unexpectedly complex. Another advantage of the discrete model technique is its greater sensitivity to the specific choice of starting model, and consequently both types of inversion are often utilized as complementary tandem solutions. Smooth inversions can be parameterized by setting 19 or more fixed thickness layers, but free resistivity with vertically constrains. In layered or "blocky" models a small number of layers are selected as representative of the existing geological context, with lateral and vertical constraints applied for resistivity and layer thickness.

Blocky parameterized inversions are best for determining layer interfaces, resistivity, and depth of penetration; smooth inversions offer more independence from the starting model and gradual resistivity transitions are more obvious, which is helpful when tracing out complex geological structures. Vertical constraints are applied in the smooth models to generally stabilize the inversion, for example by removing fictitious layers, which is particularly important for models based on a relatively small number of data points. Blocky inversions also enable the application of lateral constraints for layer depth, corresponding to layer thickness and for resistivity to take into account lateral variability in layer resistivity. Smooth models are discretized down to a depth, which is supposed to be consistent with the penetration capability of the system, with layers of logarithmically increasing thickness, starting from few meters thickness for the shallower strata. As already noted, smooth models provide good definition for complex geological structures and are powerful tools for evaluating the complexity of the subsurface, but they also produce smooth structure models with blurring of sharp formation boundaries, making them difficult to define and resulting in excessively high or low resistivity values. An inversion scheme with relatively few layers instead tends to produce a more blocky model cross-section which can be helpful for quantitative evaluation of layer thicknesses.

Vignoli et al., 2013 recently developed a different algorithmic approach, known as sharp spatially constrained inversion (sSCI). This involves implementation of an extension of the pseudo 3D formalism Spatially Constrained Inversion (Viezzoli et al., 2008), as well as the pseudo 2D special case Laterally Constrained Inversion (Auken and Christiansen 2004). A new regularizing term supports the L2 norm of the spatial gradient of the solution (Zhdanov and Tolstaya 2004, Pagliara and Vignoli 2006, Zhdanov et al., 2006; Vignoli et al., 2012). This new regularization term helps generate solutions compatible with observed data, while retrieving the model characterized by the minimum number of vertical and lateral transitions. Using this technique eliminates the need to consider both the discrete and smooth inversions. Detailed information about the inversion algorithm is provided in Vignoli et al., 2013.

Laterally Constrained Inversion (LCI)

The inversion algorithm is described in detail in Auken and Christiansen (2004). In LCI, 1D models are concatenated along a profile to produce pseudo-2D images, providing a good approximation of the real distribution of conductivity. The inversion system can operate on very large data sets. The primary ground model parameters are resistivities and thicknesses. The models are laterally joined with the requirement of approximate matching of neighboring parameters, which are typically resistivity and depth, within a specified variance. The lateral constraints can be classed as *a priori* information about the geological variability within the measurement area. The lateral constraints act on the model parameters that have little influence on the data, and vice versa, allowing information from one model to spread into neighboring models. The smaller the predicted model parameter variation, the stricter the constraint should be. The resulting model is characterized by lateral smoothness with sharp layer interfaces. It is assumed that geological coherence is represented by the lateral constraints, effectively reducing the number of free parameters in the inversion. A series of soundings is inverted as a single system, providing layered and laterally smooth model sections.

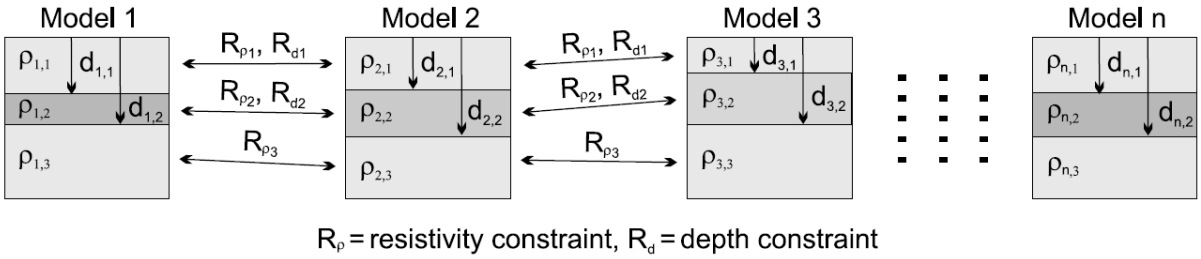

Figure 1.
Model parameters with vertical and lateral constraints (adapted from Auken and Christiansen, 2004)

The dependence of apparent resistivity on subsurface parameters is generally described as a non-linear differentiable forward mapping. Established practice in the inversion formulation is to apply linearized approximation with the first term of the Taylor expansion:

$$\mathbf{d_{obs} + e_{obs} < G(m_{true} - m_{ref}) + g\ (m_{ref})} \qquad \text{(a)}$$

where d_{obs} denotes the observed data, e_{obs} is the error in the observed data, and g is the non-linear mapping of the model to the data space. The linear approximation is only considered valid if the true model, m_{true}, sufficiently matches an arbitrary reference model, m_{ref}. The covariance matrix for the observation errors is C_{obs}. The partial derivatives of the mapping are contained in the Jacobian matrix G, and the constraints are connected to the true model as:

$$\mathbf{R\delta m_{true} = \delta r + er} \qquad \text{(b)}$$

where the roughening matrix R, contains 1s and −1s for the constrained parameters, with 0 in all other positions. In this approach, lateral constraints and vertical constraints can be used together. The predicted variation in the underlying geological model determines the strength or variance of the constraints (described in the covariance matrix CR). Minor constraints only permit small model changes, and vice versa, and so the constraints are ideally determined for each data set after assessing the stochastical properties of the underlying geological features. In approximate terms, a constraint value of 1.1 permits model parameters to vary by 10% between neighboring models. Combining (a) and (b), the inversion problem can be expressed as:

$$\begin{bmatrix} G \\ R \end{bmatrix} > \boldsymbol{\delta m_{true}} = \begin{bmatrix} \delta d_{obs} \\ \delta r \end{bmatrix} + \begin{bmatrix} e_{obs} \\ e_r \end{bmatrix} \qquad \boldsymbol{C'} = \begin{bmatrix} \boldsymbol{C_{obs}} & \underline{\mathbf{0}} \\ \underline{\mathbf{0}} & \boldsymbol{C_R} \end{bmatrix}$$

By simultaneously inverting all the data sets in this way, the common object function is minimized and the number of models generated is equal to the number of 1D soundings included. Since the lateral constraints and data are all part of the inversion, the output models are balanced between the constraints, physics, and data. A priori information is a means for including information independent of the resistivity data, and it helps resolve the non-uniqueness of the model. In line with Jackson (1979), a priori information on primary parameters is included as an extra data set m_{prior}, and the a priori model variance is described in the covariance matrix C_{prior}.

Spatially constrained inversion (SCI)

LCI inversion techniques are profile oriented because of the way they focus on producing a continuum along a line. Consequently, profile-oriented techniques work better for structures aligned with the flight path. This type of inversion algorithm is, however, not designed to establish any connections between neighboring lines, and so features that are perpendicular to flight lines benefit only partially from inline constraints or smoothing due to this lack of information exchange between adjacent lines in the model space. Spatially constrained inversion, or SCI (Viezzoli et al., 2008), was conceived with the aim of extending the idea of along-profile constrained inversion to spatially constrained inversion, for improvements both along and across profiles. The principles of SCI resemble those of LCI with the basic difference being the definition of constraints set laterally in two dimensions rather than just laterally along the flight path. SCI resembles the quasi-3D layered inversion methodology devised by Brodie and Sambridge 2006, with their algorithm specially designed for helicopter survey electromagnetic TEM data and allowing for the inversion of large data sets. The mathematical formulations of the SCI method and the LCI method described in Auken and Christiansen, 2004 are very similar. In both cases least-squares inversions of layered ground are regularized with spatial constraints, producing smooth lateral transitions. The forward 1D calculation is based on the solutions of Ward and Hohmann, 1988.

SCI and LCI differ primarily for the elements of the roughening matrix R. LCI only includes constraints on neighboring soundings along a flight line or profile, with R set to 1 and -1 for the constrained parameters. The first selects constraining points for Delaunay triangulation, which is conducted on the whole data set. The immediate nearest neighbors, to be used as model parameter constraints, are identified for each data point. Refer to Aurenhammer (1991) for a detailed description of Delaunay tessellation. Of the various different algorithms for calculating Delaunay triangulation, SCI adopts the Quickhull algorithm by Barber et al., (1996). Setting the constraints defines how many neighboring soundings each sounding will be constrained to, and it was decided to set the constraints to nearest neighbors, which are the ones between the soundings connected by Delaunay triangles. This produces a continuum of interconnected soundings, each one constrained only to its nearest neighbor. Model parameter information is dispersed horizontally between nearest neighbors into the whole data set. The Delaunay triangulation procedure ensures that the data points are well connected even with very irregular data density.

Depth of investigation for 1D (EM-DC) model

Ground-based and airborne EM are diffusive methods and there is no specific depth limit for information on the resistivity structure of the ground. It is thus of great importance to establish the depth limit within which a model can be considered reliable and any method for calculating depth of investigation (DOI) must at some point assign a depth limit for the information. In most cases this value is relative and might be, for example, 5% of total sensitivity. Various approaches for calculating DOI or penetration depth have been developed over the years. The simplest for EM purposes is based on the diffusion depth of a planar wave in full-space, at a time t within the time-domain, in full-space with conductivity σ (Ward and Hohmann, 1988). Empirical formulas have been used to formulate another set of methods (Banerjee and Pal, 1986; Huang, 2005; Szalai et al., 2009). Christiansen et al., (2012) proposed a method based on a recalculated Jacobian matrix of the final 1D model. It resembles the approach of Oldenburg and Li (1999) in the use of the full system transfer function and system geometry, the entire data set, and the data noise handling. Christiansen

et al., 2012 introduced a new concept for the calculation of DOI that is simple but robust, and valid for any 1D EM and DC geophysical model with an absolute global threshold value. Only the portion of the Jacobian regarding observed data is included in the DOI calculations. Any lateral or vertical model constraints or *a priori* information contributions to the model are not included.

Final remarks

It is not easy to understand electromagnetic theory which involve concepts and properties that are difficult to perceive, like lines of force and electromagnetic fields. This introductory chapter discussed how these fields and forces can be measured, providing a means for establishing the electrical properties of the ground. Time domain electromagnetic techniques are very useful for mineral exploration and a wide range of other geological, hydrogeological, and environmental applications. Thanks to its non-invasive nature, good resolution, and very extensive surveying potential, it is an optimal instrument for explorative geophysical mapping. The appropraiteness of any individual airborne system is determined by the signal to noise ratio, required resolution, type of survey, depth to target, and the physical properties of the study area.

References

Allard, M., 2007, On the origin of the HTEM species, In Proceedings of Exploration 07: Fifth Decennial International Conference on Mineral Exploration, Toronto, Canada.

Alumbaugh, D.L., Newman, G.A., Prevost, L., Shadid, J.N.,1996, Three-dimensional wideband electromagnetic modeling on massively parallel computers, *Radio Science* 31, 1–23.

Alumbaugh, D.L., Newman, G.A., 2000, Image appraisal for 2-D and 3-D electromagnetic inversion, *Geoph*., 65, 1455–1467.

Árnason, K., 1995, A consistent discretization of the electromagnetic field in conducting media and application to the TEM Problem, *In Proceeding* at International Symposium on Three-Dimensional Electromagnetics, 167–180.

Auken, E., 1995, 1D time domain electromagnetic interpretations over 2D and 3D structures, In *Proceedings* of the Symposium on the Application of Geophysics to Engineering and Environmental Problems, Orlando, USA, 329–338.

Auken, E., F. Jørgensen, and K. I. Sørensen, 2003, Large-scale TEM investigation for groundwater, *Expl. Geoph*., 33, 188–194.

Auken E., and A.V., Christiansen, 2004, Layered and laterally constrained 2D inversion of resistivity data, *Geoph*., 69, 752-761.

Auken, E., A. V. Christiansen, B. H. Jacobsen, N. Foged, and K. I. Sørensen, 2005a, Piecewise 1D laterally constrained inversion of resistivity data: *Geoph. Prosp*., 53, 497–506.

Auken E., Christiansen A.V., Jacobsen L., and Sørensen K.I. 2008. A resolution study of buried valleys using laterally constrained inversion of TEM data, *J. Appl. Geoph.,* 65, 10-20.

Auken, E., A. V., Christiansen, Westergaard, J.H., Kirkegaard, C., N., Foged, A., Viezzoli, 2009, An integrated processing scheme for high-resolution airborne electromagnetic surveys, the SkyTEM system, *Explor. Geophys*., 40, 184–192.

Auken E., Kirkegaard C., and Christiansen A.V. 2013. Inversion of electrical and electromagnetic

data: Comprehensive system forward modeling and arbitrary model constraints (Part I). *Geoph. Prosp*., in press.

Aurenhammer, F., 1991, Voronoi diagrams - A survey of a fundamental geometric data structure: *ACM Comp. Surv*., 23, 345–405.

Balch, S, Boyko, W, Paterson, N, 2003, The AeroTEM airborne electromagnetic system: *The Leading Edge*, 22, 562-566.

Banerjee, B., and B. P. Pal, 1986, A simple method for determination of depth of investigation characteristics in resistivity prospecting: Exploration Geophysics (USSR), 17, no. 2, 93–95,

Bannister, P. R., 1969, The image theory quasistatic fields of antennas above the earth's surface: Rep. 106 1, Navy Underwater Sound Lab., New London, C.

Barber, B., D. Dobkin, and H. Huhdanpaa, 1996, The Quickhull algorithm for convex hulls: *ACM Trans. on Math. Software*, 22, 469–483.

Behroozmand A.A., Auken E., Fiandaca G., and Christiansen A.V. 2012a. Improvement in MRS parameter estimation by joint and laterally constrained inversion of MRS and TEM data, *Geoph*., 74, 191-200.

Best, M.E., Duncan, P., Jacobs, F.J., Scheen, W.L., 1995, Numerical modeling of the electromagnetic response of three-dimensional conductors in a layered earth, *Geoph*., 50, 665–676.

Boyko, W., Paterson, N., and Kwan, K., 2001, AeroTEM: System characteristics and field results: *The Leading Edge*, 20, 1130-1138.

Brodie, R. S., and M. Sambridge, 2006, A holistic approach to inversion of frequency domain airborne EM data. *Geoph*., 71, 301–312.

Brodie R. 2010, Holistic Inversion of Airborne Electromagnetic Data. PhD thesis, The Australian National University, Canberra, Australia.

Brodie, R.C., 2013, Monte Carlo (stochastic) inversions - similarities and differences to gradient descent methods, In Extended Abstract at 23rd International Geophysical Conference & Exhibition, ASEG 2013, Melbourne, Australia.

Butler, D. K. (Ed.) 2005, Near-surface geophysics, , Society of Exploration Geophysicists (SEG), n. 13, chapter 5.

Christiansen, A. V., Auken, E., and Sørensen, K., 2009, The transient electromagnetic method, In Groundwater geophysics, Springer Berlin Heidelberg, 179-226.

Christiansen, A.V., E., Auken, and A., Viezzoli, 2011, Quantification of modeling errors in airborne TEM caused by inaccurate system description, *Geoph*., 76, 43-52.

Christensen N.B. and Tølbøll R.J. 2009, A lateral model parameter correlation procedure for one-dimensional inverse modeling, *Geoph. Prosp*., 57, 919-929.

Christiansen A.V., and E., Auken (2012), A global measure for depth of investigation, *Geoph.*, 77, 171-177, doi:10.1190/geo2011-0393.1.

Constable S.C., Parker R.L., and Constable C.G. 1987, Occam's inversion: A practical algorithm for generating smooth models from electromagnetic sounding data, *Geoph*., 52, 289-300.

Danielsen, J. E., Auken, E., Jørgensen, F., Søndergaard, V. H., and Sørensen, K. I., 2003, The application of the transient electromagnetic method in hydrogeophysical surveys, *J. of Appl. Geoph.*, 53, 181–198, doi: 10.1016/j.jappgeo.2003.08.004.

Effersø, F., E. Auken, and K. I. Sørensen, 1999, Inversion of band-limited TEM responses, Geoph. Prosp., 47, 551–564.

Ellis, R.G.,(1998), Inversion of airborne electromagnetic data, Expl. Geoph., 29(2) 121 – 127.

Fiandaca G., Auken E., Gazoty A., and Christiansen A.V. 2012a. Time-domain induced polarization: Full-decay forward modeling and 1D laterally constrained inversion of Cole-Cole parameters, Geoph., 77, 213-225.

Fiandaca G., Ramm J., Auken E., Binley A., and Christiansen A.V. 2012b. Layered and Laterally Constrained 2D Inversion of Time Domain Induced Polarization Data, Paris, France.

Fitterman D.V. and Stewart M.T. 1986, Transient electromagnetic sounding for groundwater, Geoph., 51, 995–1005.

Fitterman, D.V., Anderson, W.L., 1987, Effect of transmitter turn-off time on transient soundings. Geoexpl., 24, 131–146.

Foged, N., Auken, E., Christiansen, A. V. and Sørensen, K. I. 2013. Test site calibration and validation of airborne and ground based TEM systems. *Geoph*., 78, 95–106.

Fountain, D.K., 1998, Airborne Electromagnetic systems – 50 years of development: *Expl*. *Geoph*., 29, 1-11.

Fountain, D.K., and Smith, R.S., 2003, 55 years of AEM; 50 years of KEGS. KEGS 50th Anniversary Symposium, Toronto, Canada.

Fountain, D., Smith, R., Payne, T., and Lemieux, J., 2005, A helicopter time-domain EM system applied to mineral exploration: system and data. *First Break*, 23, 73-80.

Goldman, M., Tabarovsky, L., Rabinovich, M., 1994, On the influence of 3-D structures in the interpretation of transient electromagnetic sounding data, *Geophs*., 59, 889–901.

Grant, F. and West, G. (1965), Interpretation Theory in Applied Geophysics, Mc Graw-Hill.

Guillemoteau J., Sailhac P., and Behaegel M. 2012, Fast approximate 2D inversion of airborne

TEM data: Born approximation and empirical approach, *Geophs*. 77, 89-97.

Haber, E., Ascher, U.M., Oldenburg, D.W., 2004, Inversion of 3D electromagnetic data in frequency and time domain using an inexact all-at-once approach, *Geoph*., 69, 1216.

Hördt, A., Scholl, C., 2004, The effect of local distortions on time-domain electromagnetic measurements, *Geophs*., 68, 87–96.

Huang, H., and D. C. Fraser, 2003, Inversion of helicopter electromagnetic data to a magnetic conductive layered earth, *Geoph*., 68, 1211–1223.

Huang, H., 2005, Depth of investigation for small broadband electromagnetic sensors, Geophysics, 70, G135–G142.

Jackson, D.D., 1979, The use of a priori data to resolve non-uniqueness in linear inversion, *Geoph. J. Royal Astr. Soc*., 57, 137–157.

Keller, G.V., and Zhadanov, M.S., 1994, The geoectrical methods in geophysical exploration, Elseiver (Amsterdam, New York-Tokyo), 31, pp 873.

Kirkegaard C. and Auken E. 2013, Inversion of electrical and electromagnetic data: Parallel, scalable and memory efficient algorithms for very large airborne EM datasets (Part II). *Geoph. Prosp*., in press.

Legault, J. M., Prikhodko, A., Dodds, D. J., Macnae, J. C., Oldenborger, G.A., 2012, Results of recent VTEM helicopter system development testing over the Spiritwood Valley aquifer, Manitoba: *in Expanded Abstracts*: 25th SAGEEP Symposium on the Application of Geophysics to Engineering and Environmental Problems, Tucson, Arizona (USA).

Liu, G., 1998, Effect of transmitter current waveform on airborne TEM response: *Expl. Geophys*., 29, 35–41.

Macnae, J.C., Lamontagne, Y. and West, G.F., 1984, Noise processing techniques for time-domain EM systems, *Geophys.*, 49, 934-948.

Macnae, J., and Y. Lamontagne, 1987, Imaging quasi-layered conductive structures by simple processing of transient electromagnetic data, *Geoph.*, 52, 545–554.

Macnae, J., and S. Baron-Hay, 2010, Reprocessing strategy to obtain quantitative early-time data from historic VTEM surveys: *In Expanded Abstract* at 21st International Geophysical Conference & Exhibition, ASEG, Sydney, Australia.

McCracken, K.G, Oristalio, and Hohmann, G.W., 1986, Minimization of noise in electromagnetic exploration systems, *Geophys.*, 51, 819-832.

Monteiro Santos F.A. 2004. 1-D laterally constrained inversion of EM34 profiling data, *J. Appl. Geoph*., 56, 123-134.

Munkholm, M.S. and Auken, E. 1996, Electromagnetic Noise Contamination on Transient Electromagnetic Soundings in Culturally Disturbed Environments, J. Env. Eng. Geophs., 1, 119 – 127.

Nabighian, M.N. 1979, Quasi-static transient response of a conducting half-space. An approximation representation, Geophys., 44, 1700-1705.

Nabighian, M.N., Macnae, J.C., 1991, Appendix A: TEM systems, In Electromagnetic methods in applied geophysics, Nabighian, M.N., Ed., II, 479-483.

Nabighian, M. N. (1998a), Electromagnetic Methods in Applied Geophyics, vol. 2, SEG.

Nabighian, M. N. (1998b), Electromagnetic Methods: Theory, Vol. 1, SEG.

Nabighian, M. and Macnae, J., 2005, Electrical and EM methods 1980-2005, *The Leading Edge*, 24, 42-45.

Nekut, A.G. and Eaton, P.A., 1990, Effects of pipelines on EM soundings, 60th SEG meeting, 1990, Expanded Abstracts, 491-494.

Newman, G.A., Anderson W.L., and Hohmann G.W. 1987, Interpretation of transient electromagnetic soundings over three-dimensional structures for the central-loop configuration. *Geoph. J. Roy. Astr. Soc*., 89, 889-914.

Oldenburg, D. W., and Li, Y., 1999, Estimating depth of investigation in DC resistivity and IP surveys, Geophys., 64, 403–416.

Pagliara G. and Vignoli G. 2006, Focusing inversion techniques applied to electrical resistance

tomography in an experimental tank. International Association for Mathematical Geology XI International Congress Processing.

Palacky, G.J. and West, G.F., 1991, Airborne Electromagnetic methods: in Nabighian, M.N., Ed., Electromagnetic methods in applied geophysics - applications Part A and B: *Soc. Expl. Geophys*., Inv.in Geophys. 3, 811-879.

Podgorski, J.E., Auken, E., Schamper, C., Christiansen, A.V., Kalscheuer, T. and Green, A. G. 2013. Processing and inversion of commercial helicopter time-domain electromagnetic data for environmental assessments and geologic and hydrologic mapping. *Geoph*., 78, 149–159.

Raiche, A. P., 1984, The effect of ramp function turn-off on the TEM response of layered earth, *Expl. Geoph*., 15, 37–41.

Szalai, S., A. Novak, and L. Szarka, 2009, Depth of investigation and vertical resolution of surface geoelectric arrays, J. Env. Eng. Geophys., 14, 15–23.

Sattel D., 2009, An overview of helicopter time-domain EM systems. *in Extended Abstracts*: 20th Geophysical Conference ASEG, Sidney, Australia.

Sengpiel K.P. and Siemon B. 2000, Advanced inversion methods for airborne electromagnetic exploration. *Geoph*., 65, 1983-1992.

Sørensen, K.I., Auken, E., Thomsen, P., 2000. TDEM in groundwater mapping—a continuous approach, *In Proceedings* of the Symposium on the Application of Geophysics to Engineering and Environmental Problems, Arlington, Virginia, 485–491.

Sørensen, K.I. and Auken, E., 2004, SkyTEM – a new high-resolution helicopter transient electromagnetic system: *Exp. Geoph*., 35, 191-199.

Sørensen, K.I. and Nyboe, N. S., 2012, Near Surface Resolution and Turnoff Times in Airborne TEM Investigations, *In Proceedings*: 25th Symposium on the Application of Geophpysics to Engineering & Environmental Problems, Tucson, Arizona (USA)

Spies, B.R. and Frischkneckt, F.C., 1991, Electromagnetic sounding, In Electromagnetic methods in applied geophysics, Nabighian, M.N., Ed., II, 285-426.

Sugeng, F., 1998, Modelling the 3D TDEM response using the 3D full-domain finite element method based on the hexahedral edge-element technique, *Expl. Geoph*., 615–619.

Tarantola, A., 1987, Inverse problem theory, Elsevier Science Publishing Co., Inc.

Tarantola, A., and Valette, B., 1982, Inverse problems – Quest for information, J. of Phys, 50, 159-170.

Thomson, D. J., and Weaver, J. T., 1970, Image approximation for quasistatic fields over a 2-layer conductor, Elec. Letters, 6, p. 855-856

Thomson S., Fountain D., and Watts T., 2007, Airborne geophysics - Evolution and revolution. *In Proceedings* of Exploration 07: Fifth Decennial International Conference on Mineral Exploration, Toronto, Canada, 19-37.

Tikhonov, A.V., and Arsenin, V.Y., 1977, Solution of ill-posed problems, John Wiley & Sons, Inc.

Triantafilis J. and Monteiro Santos F.A. 2009. 2-dimensional soil and vadose zone representation using an EM38 and EM34 and a laterally constrained inversion model. *Austr. J. Soil Res*., 47, 809-820.

Vallée M.A. and Smith R.S. 2009, Inversion of airborne time-domain electromagnetic data to a 1D structure using lateral constraints, *Near Surf. Geoph*., 7, 63-71.

Viezzoli, A., Christiansen, A.V., Auken, E., and Sørensen, K., 2008, Quasi-3D modeling of airborne TEM data by spatially constrained inversion: *Geoph.*, 73, 105-113.

Viezzoli A., Munday T., Auken E., and Christiansen A.V. 2010, Accurate quasi 3D versus practical full 3D inversion of AEM data - the Bookpurnong case study. *Preview*, 149, 23-31.

Vignoli G., Cassiani G., and Deiana R. 2012, Focused inversion of vertical radar profile (VRP) traveltime data, *Geoph.*, 77, H9-H18.

Vignoli, G., F. Gianluca, F., Christiansen, A., Kirkegaard, C., Auken, E., 2013, Sharp Spatially Constrained Inversion (sSCI) with applications to transient electromagnetic data, *Geoph. Prosp*., in press.

Walker S. and Rudd J. 2008, Airborne resistivity mapping with helicopter TEM: An oil sands case study. *In Proceedings* of the 5th International Conference on Airborne Electromagnetics, Helsinki, Finland, 06-03.

Wait, J. R. (1982), Geo-Electromagnetism, Academic Press.

Wait, I. R., and Spies, K. P., 1969, On the image representation of the quasistatic fields of a line current source above the ground: Can. J. of Phys., v. 47, p. 2731-2733.

Ward, S. H., and G.W. Hohmann, 1988, Electromagnetic theory for geophysical applications, in M. N. Nabighian, ed., Electromagnetic methods in applied geophysics: SEG, 131–311.

West, G.F., Macnae, J.C., and Lamontagne, Y., 1984, a time domain EM system measuring the step response of the ground, Geophys., 49, 1010-1026.

West GF, Macnae J.C., 1991, Physics of the electromagnetic induction exploration method. In: Electromagnetic methods in applied geophysics, Nabighian M.N. and Corbett J.D. (eds.) Society of Exploration Geophysicists.

Wilson, G.A., Raiche A., and Sugeng F. 2006, 2.5D inversion of airborne electromagnetic data, *Expl. Geoph.*, 363-371.

Wisén R. and Christiansen A.V. 2005, Laterally and Mutually Constrained Inversion of Surface Wave Seismic Data and Resistivity Data, *J. Env.& Eng. Geoph.*, 10, 251-262.

Witherly K., 2000, The Quest for the Holy Grail in Mining Geophysics. *The Leading Edge*, 19, 270-274.

Witherly, K., Irvine, R., and Morrison, E., 2004, The Geotech VTEM Time Domain helicopter EM System, *In Expanded Abstract* of 74th Ann. International meeting SEG, Denver, Colorado (USA), 1217-1220.

Zhdanov M.S. and Tolstaya E. 2004, Minimum support nonlinear parameterization in the solution of a 3D magnetotelluric inverse problem, *Inv Probl.*, 20, 937-952.

Zhdanov M.S., Vignoli G., and Ueda T. 2006, Sharp boundary inversion in crosswell traveltime Tomography, *J. Geoph. Eng.*, 3, 122-134.

Chapter 2

Advanced processing and inversion of AEM data: the Spiritwood Valley Aquifer case study

Introduction

The aim of this chapter is to present new geophysical results based on advanced processing and inversion of airborne electromagnetic time domain data (HTEM). The airborne survey was performed in Manitoba, Canada, in an area known as Spiritwood Valley using a helicopter system called AeroTEM III (Aeroquest company) over an area of 1062 km^2, corresponding to 3000 linear km. Before considering the results obtained, previous geophysical studies and numerous fieldwork measurements by the Geological Survey of Canada in the Spiritwood area are introduced.

The essence of this chapter is presented in the processing paragraph. In this section the reader is conducted through the entire AEM data handling process, which involves data processing and inversion. Altitude data are processed using a specific filtering technique that efficiently removes any possible inappropriate reflections from the earth (canopy effect, spikes from navigation deflections, etc.). The processing of transient voltage data is also discussed in detail. As is known, completely raw data are always influenced by electromagnetic coupling to man-made structures. Such noisy data are carefully culled from the dataset to avoid uncoupled data being distorted by coupled data which would directly affect inversion results. A Spatially Constrained Inversion (SCI), using both the smooth and blocky models, is closely connected to the processing procedure which, in turn, can affect the output models if the procedure has not been performed correctly. Several resistivity maps derived from inversions are also presented. A comparison is made between smooth and blocky models in order to establish the main differences between these two output models. This chapter also presents a real life example to illustrate the difficulties associated with modeling and inversion of AEM data. Appropriate modeling of the waveform, time gates, transmitter area, number of turns, etc. (all part of the system transfer function) are of primary importance when attempting AEM data inversion. However, this example presents the possibility

(not rare) of misinformation directly from the contractor and\or misunderstanding of the survey report. If the system transfer function is not modeled accurately (see Christiansen et al. 2011 for details), the errors introduced may migrate to the model's earth or geometry related parameters. Different geometry files were applied to each flight. These files represent the system transfer function modeled for the inversions. The reason different geometry files were calculated is that, by analyzing the nominal timing of individual waveforms used during data acquisition, a marked difference of Rx (receiver coil) nominal time gates between adjacent survey flights was identified. This also involved the possibility of having striping or artifacts in the resistivity maps derived from the inversions, thus requiring additional post processing of data to try and remove them.

The survey area: previous study at Spiritwood Valley Aquifer

The GSC Groundwater Geoscience Program (2009-2014) includes an investigation of buried valley aquifers in Canada with the aim of complete mapping and characterization of key Canadian Aquifers. In Canada buried valley aquifers represent important hydrogeological sources of groundwater for drinking, agriculture and industrial use. The Spiritwood Valley Aquifer extends from southern Manitoba into South Dakota with an estimated length of at least 500 km. While it is an important water resource for North Dakota, it is not well analyzed in Manitoba and, despite some exploratory drilling, little progress has been made in mapping its extent in Manitoba.

A large area of southwestern Manitoba is short of high yield sources of groundwater from traditional bedrock or drift aquifers. In some areas substantial pipeline and farm water supplies have been developed by local government agencies, exploiting sand and gravel aquifers buried in Tertiary or Pleistocene valleys eroded into the underlying Cretaceous bedrock. These aquifers offer variable short-term yields and the long-term sustainability is seriously in doubt due to limited recharge. The valleys typically exhibit virtually no surface topographic expression. They are only partially traced out by boreholes (e.g., Klassen and Wyder 1970; Watermark Consulting 2004) and the hydrogeological fill properties and sedimentary architecture are poorly characterized. In

response to growing demand for groundwater in the local area, there is a renewed interest in evaluating the supply potential from sand and gravel deposits in buried valley features.

Geophysical and geological investigations were conducted with the aim of establishing a regional three-dimensional model of the complex aquifer geometries of Spiritwood Valley. This chapter describes a number of surveys that provided electromagnetic time domain data, seismic measurements, electrical tomography, and borehole logs.

The GSC started seismic investigation of the Spiritwood buried valley in 2007 using a vibrating source and a landstreamer receiver array. The resulting P- wave reflection profiles enabled definition of the profile of the broad buried valley and assessment of the properties of the materials filling a more incised valley at the base of the main broad valley, together with the overlying glacial sediments of up to 105 m in depth. Three seismic profiles along 18 linear km in the Killarney area revealed that the incised valley was approximately 800 m wide and 20 m deep near the Killarney township.

The GSC conducted an experimental airborne electromagnetic (AEM) survey in 2010. This covered the extension of the valley inferred from the results of the seismic surveys and geological data from existing boreholes and wells in the area. The survey aimed to investigate the potential for prairie buried valley mapping and characterization using commercially available AEM systems. The 1062 km^2 survey was defined using an AeroTEM III time-domain system with 400 m line spacing and control lines spaced at 5000 m (Oldenborger 2010a, b gives preliminary results). Additional simultaneous experimental geophysical surveys were conducted of the region. These included land-based resistivity and other high resolution seismic landstreamer surveys to investigate the location and architecture of the Spiritwood buried valley. Using the highly successful results, the collected datasets were combined to produce extremely valuable insights, enabling selection of a location for a deep cored borehole near Cartwright, Manitoba in order to characterize ground features, penetrating down to the groundwater-bearing gravel and sand sediments near the base of the buried valley (GSC-BH-07). The resulting borehole core, downhole geophysical logs, chemo-stratigraphic

analyses, and hydrogeological data are currently being used to improve understanding of the geological characteristics of prairie buried valleys (Crow et al. 2012). During the fall of 2011 a further airborne electromagnetic survey was conducted in the Spiritwood area in addition to the geophysical and ground measurements. The aim of the air survey was to test an innovative system called the "Full waveform VTEM system", representing a more advanced implementation of the original VTEM system (Legault et al. 2012). Spiritwood was chosen as a reference area due to the availability of previous airborne and ground EM surveys together with other ancillary data including electrical and seismic readings, together with borehole and well-logs recorded by the Geological Survey of Canada. Also in more general terms, the Spiritwood Valley Aquifer was selected for detailed investigation because:

1) The 2007 seismic reflection data and subsequent ground based geophysical measurements in 2010, had revealed the presence of a smaller incised valley within the broad buried valley. This encouraged further investigation since the data suggested the existence of an interesting and complex geological architecture.

2) The trans-boundary extension of this aquifer is of special interest to the Government of Canada, because it is also a significant groundwater resource for North Dakota (the Spiritwood Aquifer has been extensively exploited in North Dakota).

3) In order to assess the airborne electromagnetic data, high-quality supporting data are required (this will be considered in detail in Chapter 3).

The helicopter survey produced revealing imagery of the Spiritwood buried valley geometry with a complex nested structure of smaller incised valleys within the broader valley, and the continuity of inferred aquifer materials throughout the area of the study.

The AEM results motivated additional ground-based resistivity and seismic studies in 2010. These investigated the lateral and vertical matching of the land and airborne survey datasets (Figure 1). A further 42 linear km of landstreamer data were also collected over areas of particular interest, as well as resistivity and induced polarization measurements taken along a subset of the seismic

profiles of more than 10 km. It was found that overall the AEM data provided excellent spatial location of valley features, but ground-based geophysical surveys are sometimes necessary for improved estimates of deep incised valley depths, and for better resolution of features near to the surface. These data and relative discussions are presented in Oldenborger et al. (2013).

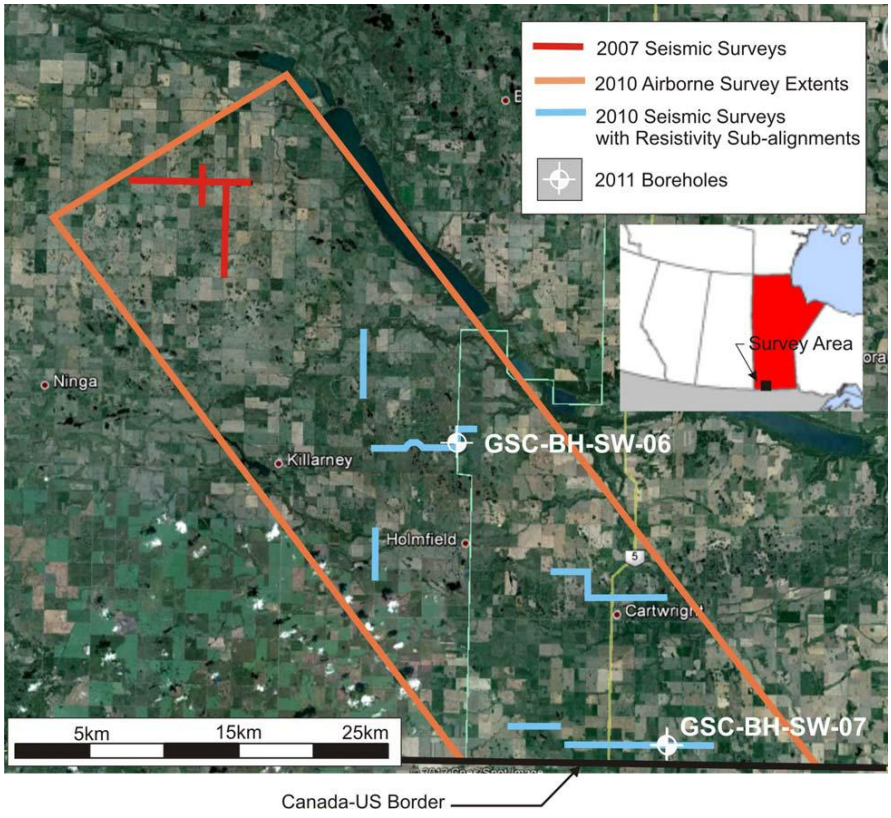

Figure 1.
Overview of geophysical surveys carried out by the GSC in the Spiritwood region since 2007 and locations of boreholes drilled in 2011. The solid orange line perimeter represents the AEM survey block extents (adapted from Crow et al. 2012).

The AeroTEM III survey in Spiritwood Valley

The Spiritwood Valley HTEM survey was flown during the period from February–March 2010. The survey required approximately 5 days of flying time to cover the entire survey block, although weather restrictions resulted in approximately 4 weeks of deployment time. The survey block was aligned in the general direction as illustrated in Figure 2. Given the linear nature of the survey target and the estimated axial direction, traverse line spacing was set relatively high at 400 m and control lines were spaced at 5000 m. The AeroTEM system is based on a rigid, concentric-loop geometry with the receiver coils positioned in the centre of the transmitter loop (Balch et al. 2003).

The system measures voltage in an induction coil sensor, which is equivalent to the time rate of change of the secondary magnetic field dB/dt.

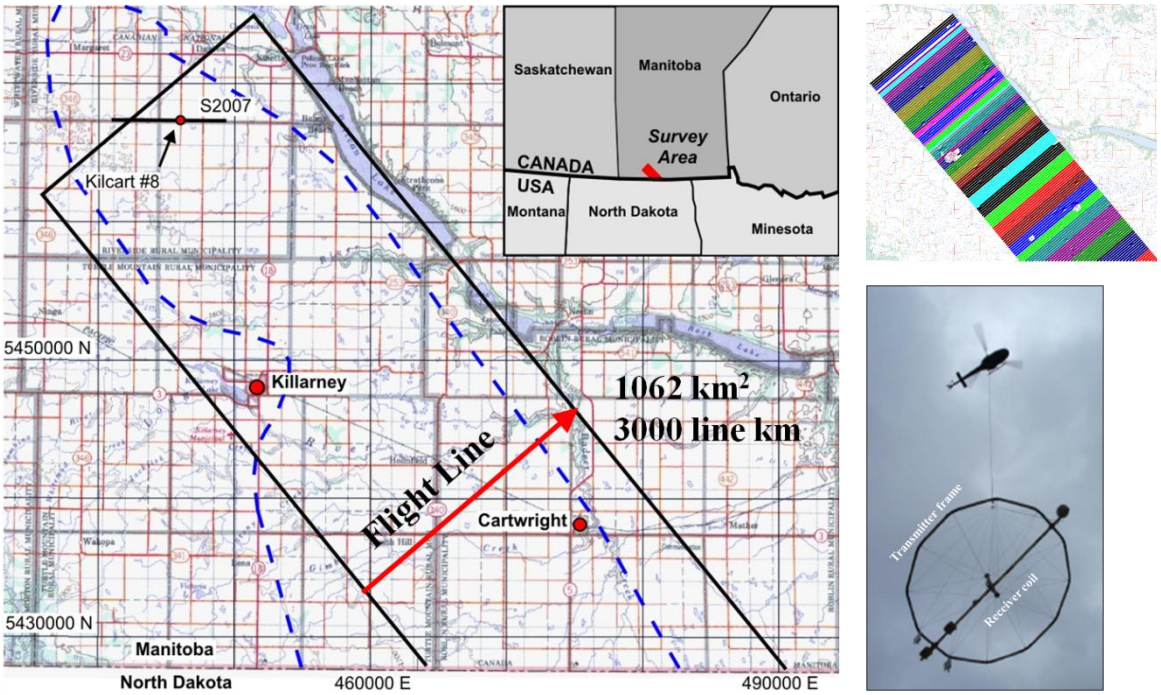

Figure 2.
Spiritwood Valley location map. The red arrow indicates the direction of HTEM flight lines within the entire survey block (black line).Two inset images show, respectively, the number of separate flights (36) covering 3000 linear km (above) and the AeroTEM III system (below, courtesy of Aeroqest ltd).

The transmitter waveform is a triangular current pulse of 1.75 ms duration operating at a base frequency of 90 Hz (Figure 3). The transmitter loop has an area of 78.5 m^2, with a maximum current of 480 A. The receiver coils are oriented one on a vertical plane (Z-axis), and one on an in-line horizontal plane (X-axis). The collected data consist of a series of 16 on-time gates and 17 variable width off-time gates (70 µs to 3 ms after time-off). The TEM decays were leveled for system drift using high-altitude corrections (Sørensen and Auken 2004). Then, raw collected data are stacked, compensated, drift corrected, and micro-leveled by the company (e.g. Aeroquest) before being supplied to geophysicists\geologists for further processing, inversion and interpretation.

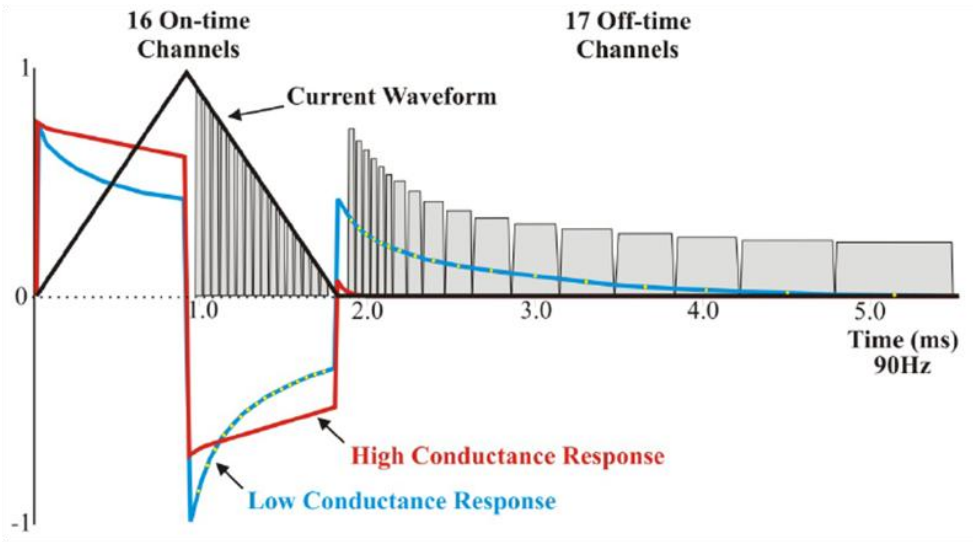

Figure 3.
Schematic AeroTEM III transmitter waveform and response (adapted from Aeroquest Spiritwood survey report). At 90 Hz, the triangular current pulse is approximately 1.7 ms in duration. The duration of off-time measurements is approximately 3.4 ms after transmitter turn off.

The "Full Waveform VTEM system" survey in Spiritwood Valley

In an effort to improve the shallow imaging capability of the VTEM helicopter EM system, by obtaining the most accurate early-time data possible, a full waveform system was developed and tested (Legault et al. 2012) during fall 2011, over the Spiritwood Valley area. The survey consists of three separated blocks of closely spaced lines (300 m relative distance) covering approximately 220 linear km (Figure 4). Forty-four time measurement gates were used for final data processing in the range from 0.018 to 9.977 ms. Results of the Full Waveform VTEM surveys led to improved accuracy of transient data at earlier times than previously achieved, as early as ~20 μs after current turn-off (versus ~100 μs for standard VTEM) and as late as ~10 ms. The pulse shape is trapezoidal with a base frequency of 30 Hz and 4.073 ms pulse width (Figure 4). The VTEM data strategically cover the Spiritwood area with a few lines over the northern, central, and southern parts of the AeroTEM survey block. These lines specifically followed 2 seismic profiles, one of which was also overlapped by an electrical tomography profile.

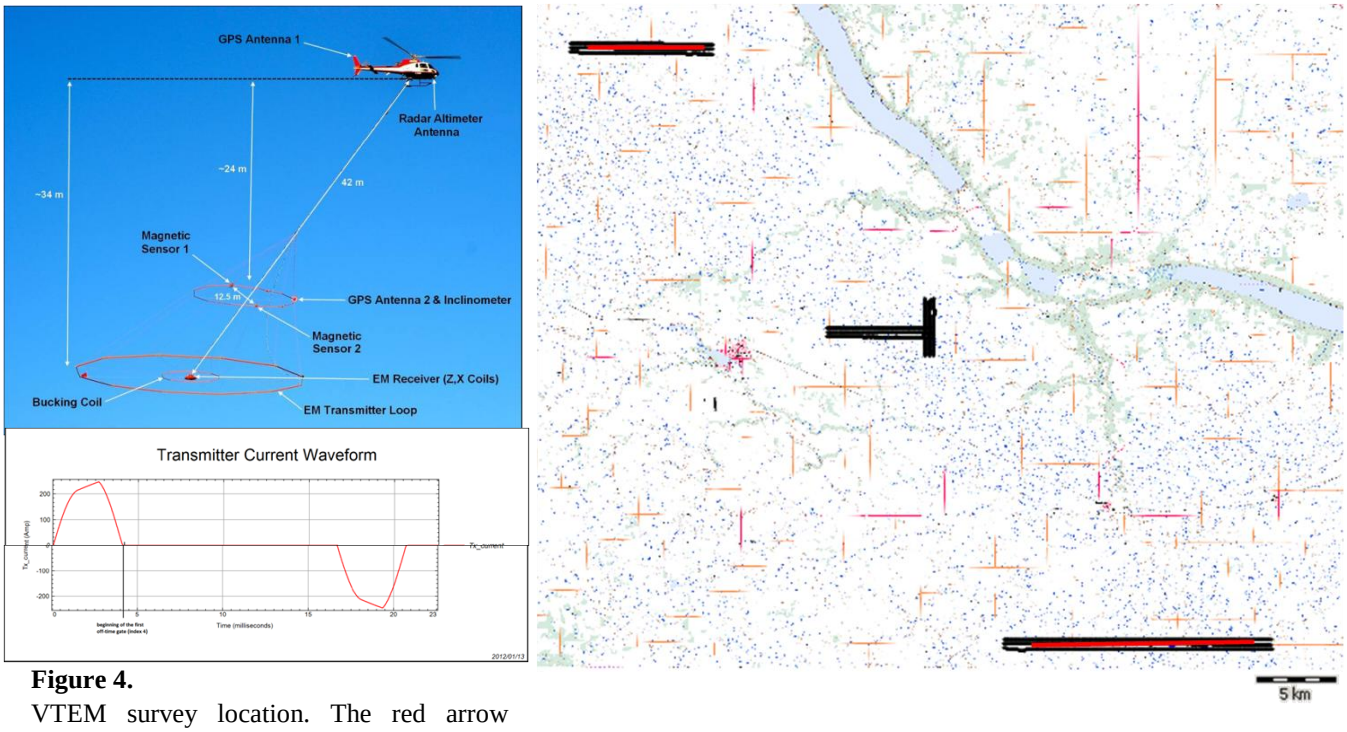

Figure 4.
VTEM survey location. The red arrow indicates the seismic profiles along which airborne EM data were collected (black line). Two inset images show, respectively, the VTEM system (above) and the trapezoidal waveform (below) (adapted from Geotech's survey report).

Seismic surveys in Spiritwood Valley

The Geological Survey of Canada (GSC) have been testing and developing landstreamer data acquisition systems for low depth P and S-wave seismic reflection surveys over the last few years. It has become routine for the GSC to collect ~1000 records per day or 1.5-6 linear km per day, using their Minivib/landstreamer data acquisition system. This brief section presents the seismic data recorded for different areas of glaciated terrain in Spiritwood Valley. The purpose for acquiring shallow seismic reflection data was principally to help calibrate the AEM survey for the delineation and characterization of Quaternary aquifers in hydrogeological investigations of regional scale. The GSC near-surface seismic reflection method is described in Pugin et al. (2009a; 2009b). Utilizing a vibrating seismic source coupled with a landstreamer provides very clear and adaptable seismic reflection data. The landstreamer in the present survey consisted of 48 3-C geophones spaced at 1.5 m intervals. The source input was a non linear (-2 dB/octave) sweep signal from 20-240 Hz. This design was intended to increase vibration time in the low frequency domain and improve generation of shear wave energy (Figure 5).

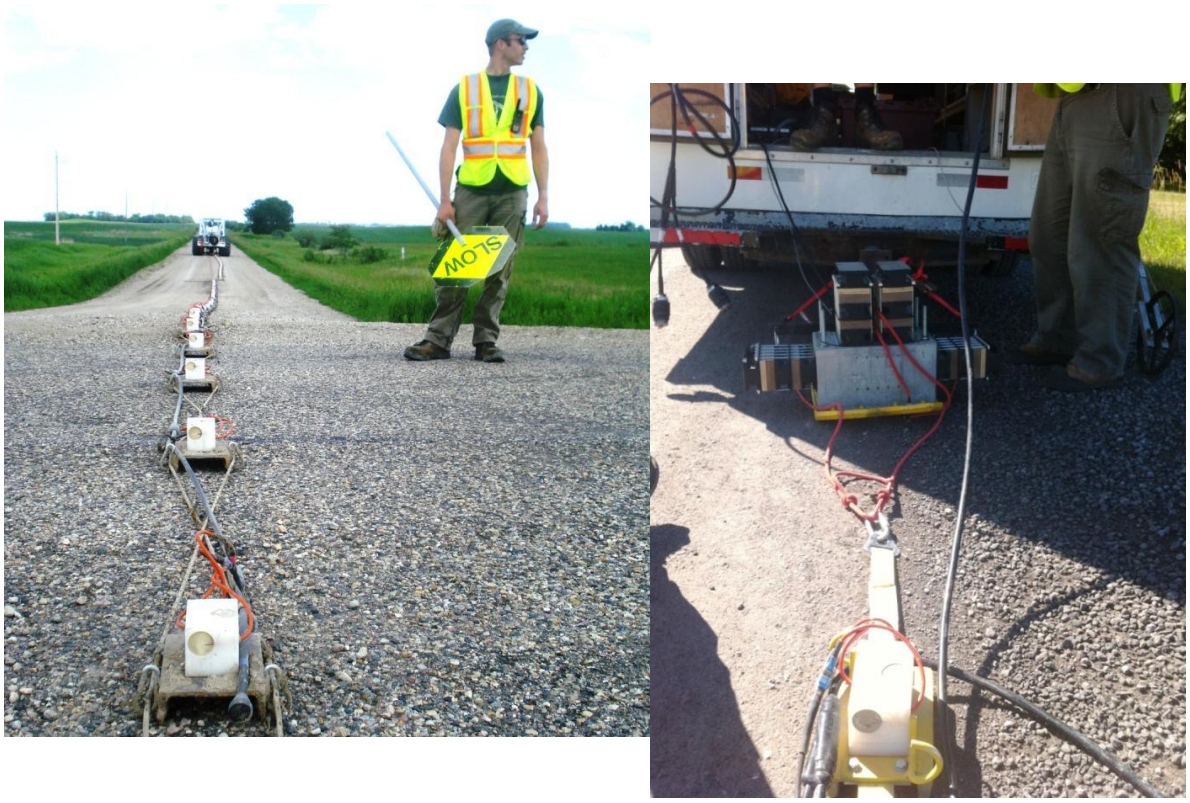

Figure 5.
The 3-C seismic landstreamer receiver array consists of 48 geophones with a spacing of 1.5 m (left panel, adapted from Pugin et al. 2011). The Minivib I vibratory seismic source, which pulls the landstreamer forward, can be seen in the right panel.

The principal focus here is on 2 seismic profiles which will be applied in turn to constrain AEM data inversion (as discussed in Chapter 3). Details of the channel features and the valley fill stratigraphy can be observed in the P-wave section of seismic 1 (Figure 6). Two main valleys can be seen as inset channels eroded into bedrock to depths of over 100 m below ground surface. Where the near-surface sediments are water-saturated or comprise dense materials (i.e. hard till), very pronounced P-wave reflections from overburden materials and bedrock can be observed. Consequently, it is deduced that coarse-grained material such as till, or sand and gravel will return high amplitude P-wave reflections. This can be seen in seismic 1, where the sedimentary fill of the channels produces multiple high amplitude reflections, suggesting the materials are coarse-grained sand and gravel deposits. The deeper hard interface is interpreted as the signature of the top of the bedrock, which consists of fractured siliceous shale. The GSC borehole was sunk on profile S1

following the ground geophysics campaign (Crow et al. 2012). The results for GSC-SW-07 are shown in the seismic section of figure 6 as a simplified stratigraphic log.

More seismic profiles (totaling 18 linear km) were collected in the Killarney area in the north-western portion of the Spiritwood Valley (Pugin et al. 2009) in 2007. The 2007 seismic reflection line delineates an incised channel (~800 m wide and 20 m deep), within the broader Spiritwood Valley system (Figure 7). A dense sequence of high-amplitude, coherent reflections are interpreted as produced by stratified deposits within and overfilling of this deepest section of the valley. The stratified channel fill deposits interpreted from the seismic section correlate with 15 m of sand and gravel (the productive aquifer zone) found above bedrock in a borehole located on the profile track (Kilcart #8). The deepest part of the channel is located 1–1.5 km west of the current production well, and the sand and gravel deposits here are estimated to be ~40 m thick and represent a target zone for a potential high-yield well (Pugin et al. 2009). Kilcart 8 is a logged Manitoba monitoring well, but not by the GSC, so the logs have to be classed as "un-calibrated".

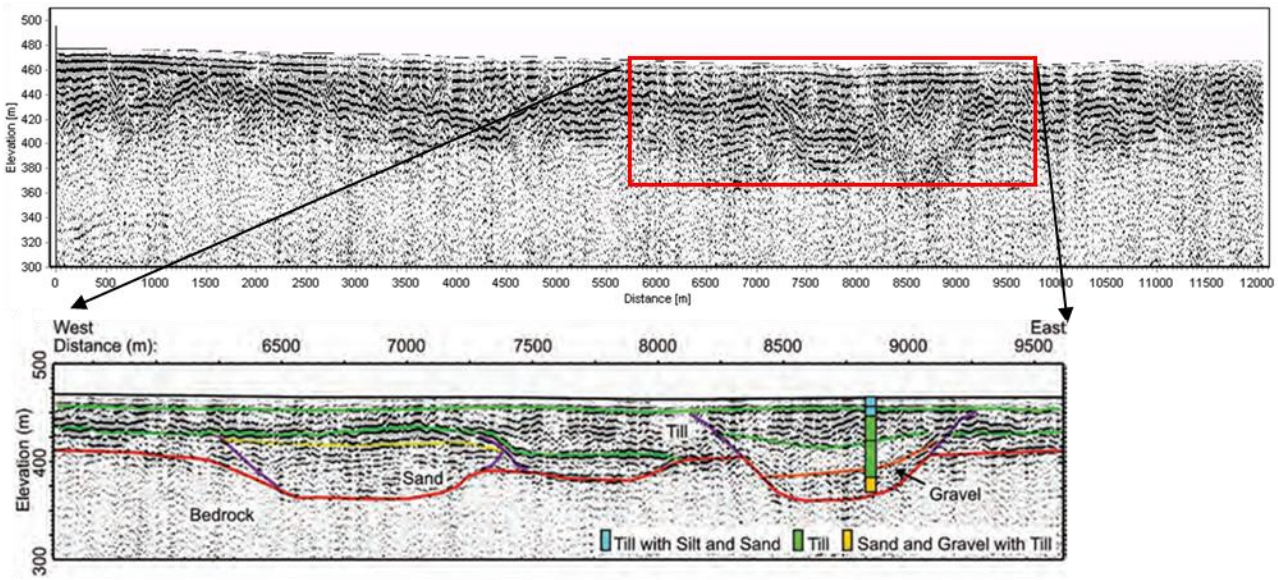

Figure 6.
Seismic results for profile S1. The red box is a close up zoom of the entire seismic profile. A simplified stratigraphic log for GSC-SW-07 is illustrated for correlation in the lower section. The interpreted P-wave seismic reflection section shows respectively, inter-till boundaries (green), gravel surfaces (orange), bedrock surface (red), and erosional surfaces in purple (adapted from Oldenborger et al. 2013).

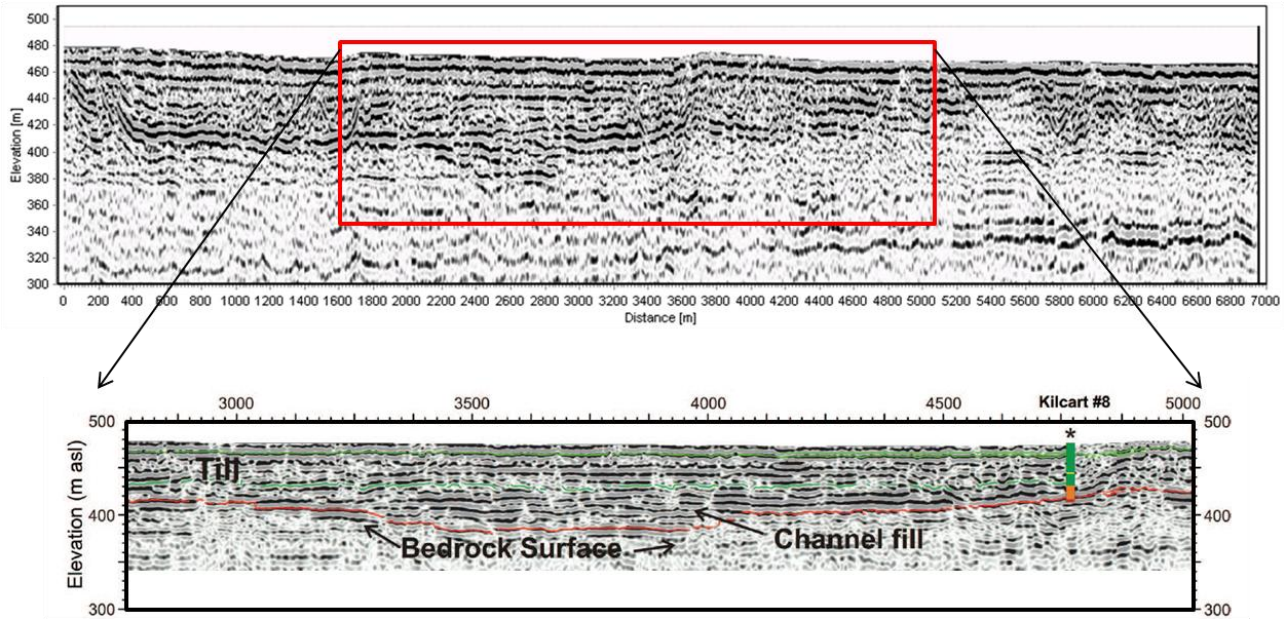

Figure 7.
Seismic results for profile S2007. The red box is a close up zoom of the entire seismic profile. A simplified stratigraphic log for Kilcart 8 is illustrated for correlation in the lower section. The interpreted P-wave seismic reflection section shows respectively, inter-till boundaries (green), and bedrock surface (red) (adapted from Pugin et al. 2009).

ERT surveys in Spiritwood Valley

In 2010 a ground electrical resistivity survey program was conducted (Oldenborger et al. 2013) in order to obtain further depth controls and, more specifically, some independent measurements of subsurface resistivity. The AEM results and seismic lines were used in order to establish the survey sites. Electrical resistivity data were collected over a total of 10 linear km and at 4 different locations inside the AEM survey area coinciding with the 2007 and 2010 3b, 3c, and 2d seismic lines (the seismic lines are not illustrated here). Electrical and time-domain IP data were collected using the Multi-Phase Technologies DAS-1 system. A 64-electrode array was deployed in both Wenner and dipole-dipole geometries, with dipole lengths from 10 to 90 m. Surveys were performed at 1 Hz using 2 stacks and full reciprocals (for the dipole-dipole array) and rolled in sections of 32 electrodes. The smoothness-constrained least-squares algorithm of Loke et al. (2003) was used to invert the data and produce resistivity models as a function of depth (Figure 8). The high resistivity resolution of the ERT data is very marked and the range of resistivity of the geological units varies across a very narrow range (5-45 Ohm-m). The ERT models enable dis-crimination of the conductive basement, resistive incised valley fill, moderately resistive broad

valley fill, overlying conductive till, and surface sediments as resistive materials, as shown in the schematic cross-section (Figure 9).

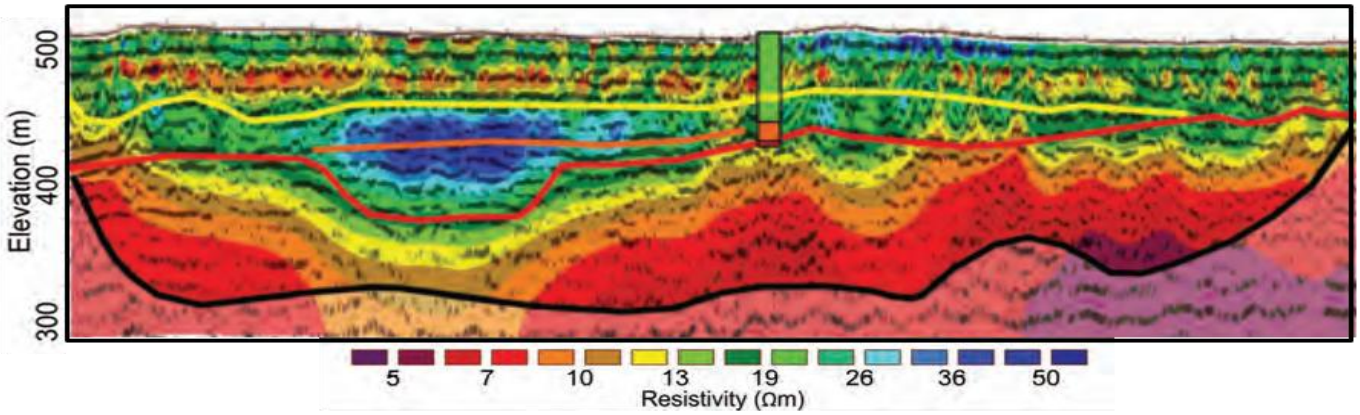

Figure 8.
ERT profile. The solid black line indicates the approximate depth of investigation.

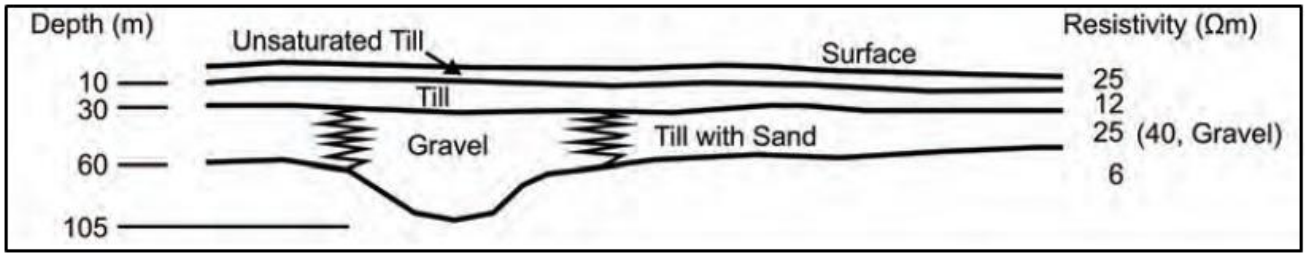

Figure 9.
Schematic interpretation of the ERT model (adapted from Oldenborger et al. 2013).

Boreholes in Spiritwood Valley

There are several water wells and borehole logs for the Spiritwood valley area. Most of the wells were drilled to supply water for agriculture, industry, farms, and domestic use. A direct comparison of well data with TEM results is complicated by two factors. Firstly, the wells are not high-quality geotechnical boreholes and the stratigraphic logs represent driller's observations which are subject to well-to-well inconsistency and observational errors. Useful geological information is available from the stratigraphic descriptions of the BH-07 borehole drilled by the Geological Survey of Canada in 2011 (located in the southern part of the survey area on seismic line 1, Crow et al. 2012). The depth of drilling was limited to about 97 m and did not reach bedrock (which is assumed to be deeper). The first 9 m shows very fine to fine sand embedded on sandy silt diamicton. These layers overlay clay till varying to hard clay diamicton sediments before drilling indicates relatively

uniform till and coarse grained sediments at the bottom of the borehole. A suite of downhole geophysical logs was also acquired for GSC-BH-07 consisting of several measurements including conductivity (see Table 3 from Crow et al. 2012 for logging details). The main focus here was on conductivity results with the aim of comparing this information with the AEM results (see Chapter 3 for details). These geophysical logs reveal a change in conductivity corresponding with changes in lithology. The surface appears more resistive (about 170 mS\m or 17 Ohm m) in the borehole down to 9 m. Subsequently the borehole penetrates till of relatively uniform conductivity (~110 mS/m, 9 Ohm m) from 15-80 m in depth. Several other boreholes were drilled by the GSC and geophysical logs collected, but this information was not used in the present thesis.

Processing AeroTEM data

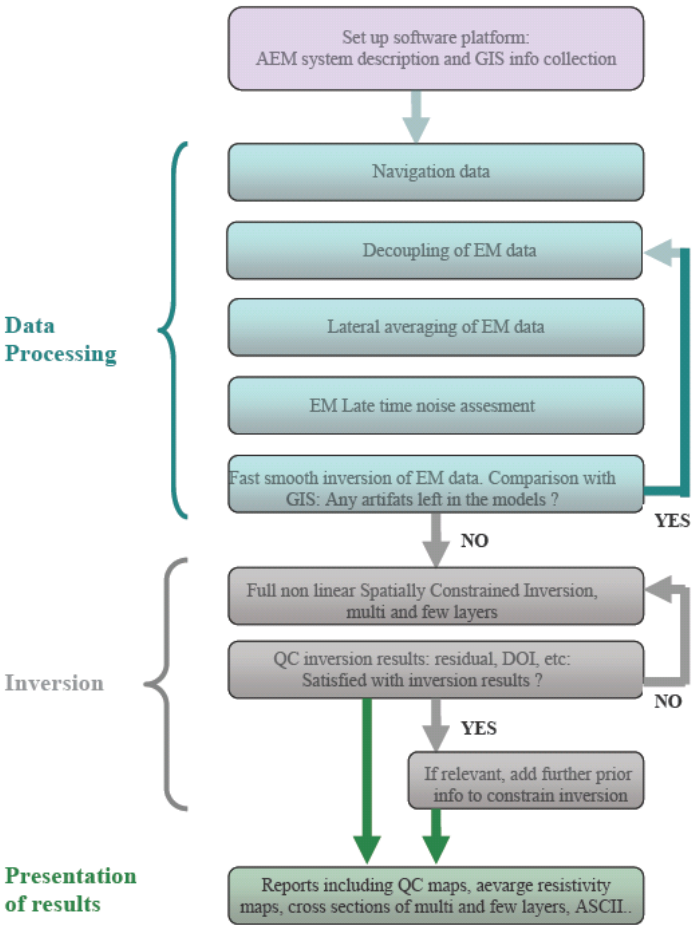

Figure 10.
Workflow scheme for data processing and inversion of AEM data carried out with the Aarhus Workbench (adapted from Aarhus University, Hydrogeophysics Group report).

High-quality data processing is essential in hydrogeophysical surveys. The aim of data processing is to prepare data before an inversion is run. Processing includes importing data, altitude corrections, filtering, and discarding of distorted or noisy data contaminated by culture. The data are then averaged spatially, which allows increasing signal to noise levels without compromising lateral resolution.

The AeroTEM III data consist of navigation data and voltage data (magnetic data were also collected by the AEM system but these are not of interest for this

PhD research). The AEM data were processed using the Aarhus Workbench software package (Aarhus Geophysics, 2009). The Aarhus Workbench is a common platform for working with geophysical, geological, and GIS data. It includes fully integrated modules for generating geophysical thematic maps, geo-statistic modeling, and visualizations on GIS maps. This is extremely important when working in densely inhabited areas where long data sequences often have to be culled because data are severely biased by coupling to manmade conductors (Danielsen et al. 2003). In general, data processing is a four-step process (see also figure 10):

1) Automatic filtering and averaging of navigation data; manual corrections may also have to be applied to altitude data after automatic filtering.

2) Automatic processing of voltage data i.e. removing or minimizing high frequency noise.

3) Voltage data are evaluated manually for further processing refinement (necessary in areas with cultural responses).

4) Finally, a fast inversion using a smooth model is used to fine-tune the processing of steps 1 to 3.

Altitude processing

The AeroTEM navigation system comprises a GPS receiver mounted on the instrument panel and an antenna fitted on the front of the bird. A series of ground reference stations are located across the USA and these monitor GPS satellite data, providing ground correction taking into account satellite orbit and clock drift, as well as signal delays (caused by the atmosphere and ionosphere). The differentially corrected GPS positional survey data are then recorded in real-time as 0.1s interval geodetic coordinates. In addition, a radar altimeter is used to measure terrain clearance. The antenna was mounted outside the helicopter below the cockpit and so the data were recorded at the height of the helicopter rather than that of the bird above the ground, with an accuracy of +\- 1.5 m in altitude.

As mentioned above, the navigation data were automatically filtered and averaged for processing purposes and then the altitude data was corrected manually if necessary. The automatic processing results were inspected, comparing flight time profile plots against data values (altitude, voltage readings, etc.), as illustrated in Figure 11. Various quality control parameters were also plotted, so that flight speed, topography, transmitter current, and other parameters can be displayed. A key processing element was an integrated interactive GIS map highlighting the location of the helicopter. When combined with proper GIS themes, this generally enables explanation of the majority of data features, for example a sudden increase in altitude and relatively coherent noise is caused by the helicopter crossing a power line, road, or railway, and poor reflections can be caused by the helicopter traveling over a forest. Helicopter speed is affected by both down and up wind conditions, which results in shifts in data density along adjacent flight lines. This phenomenon must be taken into account when averaging the raw data to maintain a coherent distribution of soundings along flight lines with consistent lateral resolution. Bird height is measured in order to distinguish the substratum from air, in particular in highly resistive areas. Accurate altitude estimates help to avoid false shallow highly resistive artifacts in the model. They also provide an accurate starting parameter and so help to stabilize and accelerate inversion (Auken et al. 2009). The AeroTEM III system is not equipped with laser altimeter and tilt devices, unlike the SkyTEM system frame (Sørensen et al. 2004).

Flight altitude is included as an inversion parameter with a prior value, set to compensate frame oscillations during flight. AeroTEM III altitude frame monitoring is not very accurate and highly uncertain, making it difficult to estimate a more precise standard deviation for this parameter. The frame has a mean terrain clearance of 35 meters, and as a precaution the standard deviation of this parameter was set to 4 m to avoid inversion, significantly shifting the altitude parameter to fit the data.

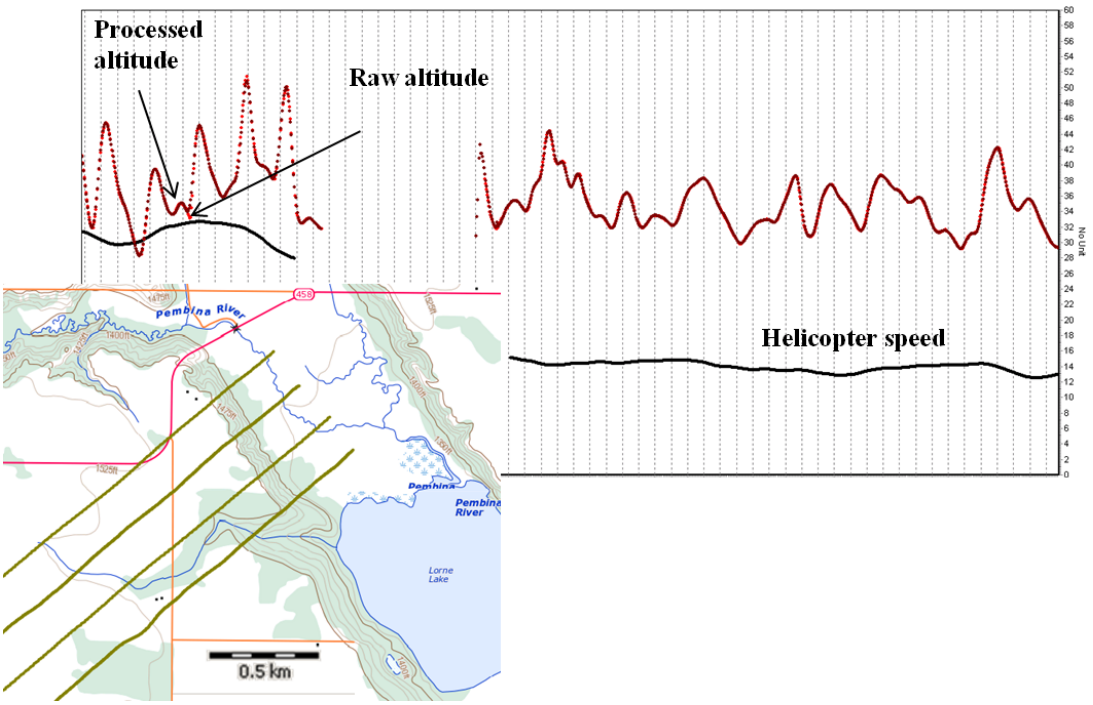

Figure 11.
The figure shows a typical integrated plot of navigation data. Raw altitude data from the altimeter are shown in red, the processed and transmitter altitude in brown. The helicopter speed is black and exhibits quite a significant shift in velocity between adjacent flight lines (the end of a flight line is indicated by a break in the black line).

Voltage data processing: raw and averaged data

The raw streaming data was initially processed using a proprietary software algorithm developed by Aeroquest Surveys, and involved compensating the z component data for the primary field waveform. Compensation coefficients were determined for the system transient and applied to the stream data. Stream data were then filtered, stacked, and binned to the 33 on-time, and 17 off-time channels. Next, the stacked data were leveled and split up into individual line segments. The stacked data filtering process is designed to remove or minimize any high frequency noise that fails to match the predicted geology. Drift corrections were also applied to the EM dataset and to assist this process the EM system was flown up to a height of about 500 m above ground level several times per flight, where the influence of the Earth's secondary magnetic field is assumed to be negligible. The typical EM noise level observed during the survey was 3-5 nT/s during off-time and no spheric events occurred during the survey.

Unfortunately, the data from areas with a substantial presence of infrastructure, like pipes, power lines, and metal fences, required a lot of manual processing, even though filters had been designed to help cull disturbed data (Figure 12).

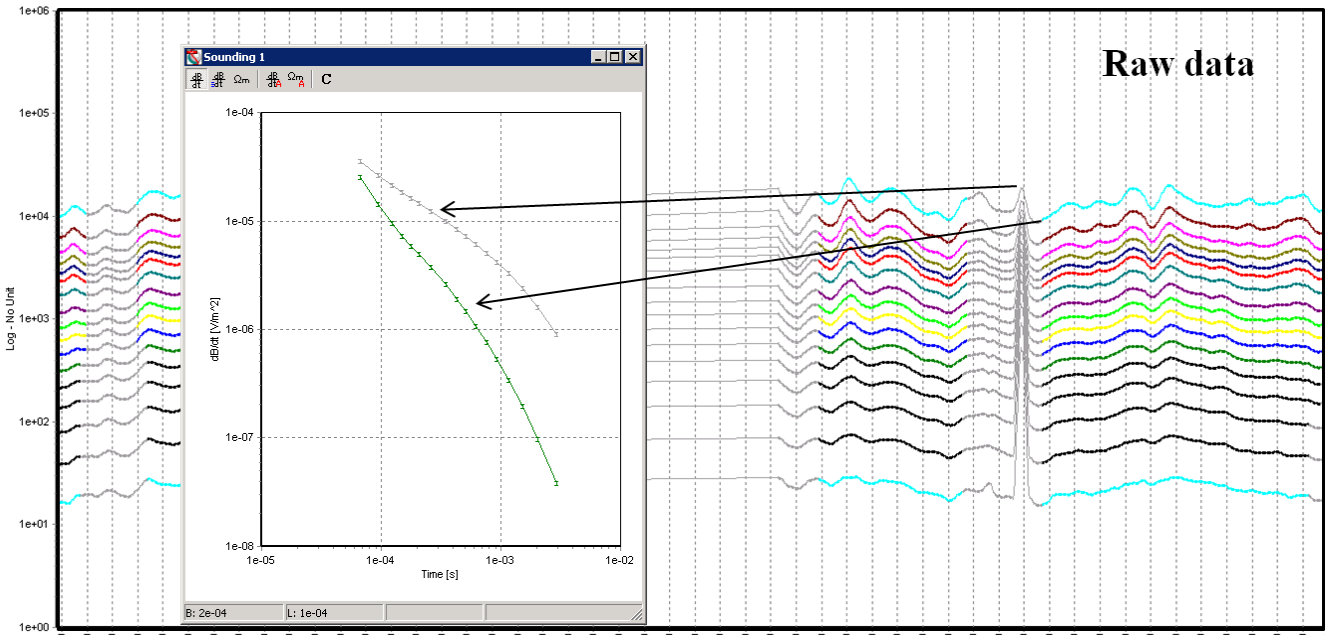

Figure 12.
The data processing window of the Aarhus Workbench, showing portions of data deleted because of coupling with man-made structures. The insert shows the corresponding transient in dB/dT.

The physics underlying the galvanic and capacitive coupling phenomena is discussed by Danielsen et al. (2003) . A filter for detecting capacitive coupling, showing oscillations and possible sign changes, is easier to design. The capacitive coupling detection filter operates by examining both the raw data stacks for changes in curve slopes, and searching for signs of changes in the time interval of the complete decay curve. Normally the filter is executed from the first sounding gate (for AeroTEM this is about 6.5x10-5^{s} as nominal time gate), or at worst it starts no later than the 3rd time gate up until the signal reaches the noise floor. It is not considered viable to design filters to detect galvanic coupling because the signal level is simply raised and does not show oscillation, or, in some cases only the late time gates are disturbed visually, with oscillations. In most cases of this type the entire data curve is deleted because often unrealistic increases in signal are observed, typical of the galvanic effect, before the late time oscillations arise (Figure 13).

It is necessary to intervene manually on the AeroTEM data to fine tune the results from the filters and achieve the most reliable results. As already stated, the raw data was intensely pre-processed (i.e. leveled) by contractors. This causes the data to appear extremely smooth with minimal data oscillations, suggesting data minimally affected by coupling, with the exception of powerful sources of e-m noise, like power lines, when coupling is obvious.

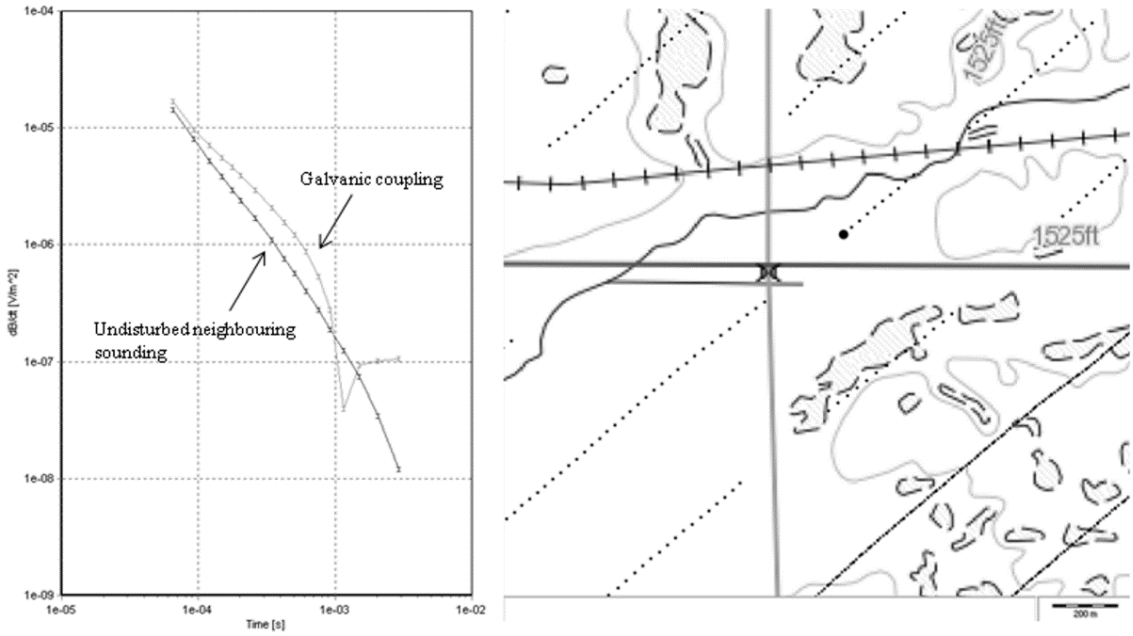

Figure 13.
Processing window example of a coupled TEM response compared to an undisturbed neighboring sounding. Galvanic coupling results from induced currents in man-made conductors such as power lines, cables, or fences through the transmitter loop. The insert to the right shows the corresponding location of the investigated sounding (see the bold dot).

This means that no automatic filters proved effective for detecting and eliminating man-made coupling, and all the de-coupling processing was performed manually, flight by flight, almost sounding by sounding.

Data averaging

It is standard practice in airborne TEM to average early and late data over the same distance. Early data generally provides shallow ground information and late data provides information from deeper underground (according to the depth of penetration of the system). The negative aspect of this approach is that high resolution cannot be maintained for early data (from near to the surface)

in which the signal-to-noise ratio is normally quite high, while also obtaining a reasonable signal-to-noise ratio for late data from greater depths. Furthermore, for quasi-layered environments it is important to note that a short sounding distance, for example 5 m, does not automatically produce high lateral resolution if the data are averaged over long time spans or distances like, for example, 150 m (the system footprint is in the order of 100 m on the ground, Beamish, 2003). The result is simply a high level of information redundancy. In the general averaging voltage data approach trapezoidal average windows are used so that early data are averaged less than late data, as illustrated in Figure 14.

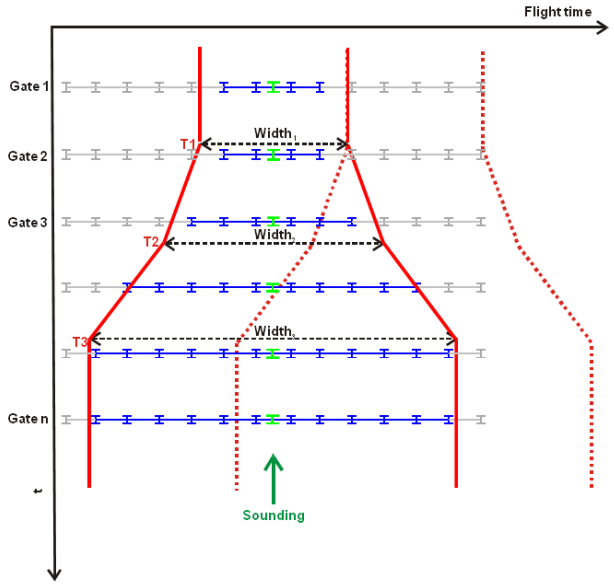

Figure 14.
The principle behind the trapezoid shaped averaging core, in which data are averaged over larger time spans at later times to maintain as much lateral resolution as possible at early times while maintaining a high penetration depth (Auken et al. 2009).

This approach actually reflects the nature of the electrical fields in the substratum itself. Immediately after the Tx-loop current is shut off, the ground current is close to the surface and the measured signal primarily indicates the conductivity of the upper layers. Later in time the current is deeper under the ground and the measured signal gives indications of the conductivity of the lower layers. If sounding is conducted every 30 m, the very early data in time is not averaged for more than 30 m, whereas late data may be averaged for 300 m since the eddy current footprint is much

greater at depth (Nabighian 1979, Reid et al. 2004). In this way optimal resolution of near-surface resistivity structures can be maintained, where the ground current system is relatively small and the signal-to-noise ratio good, while simultaneously providing a reasonable signal-to-noise ratio at late times, to maintain the desired penetration depth.

The trapezoidal average filter width was set as narrow as possible for the early-time gates, so as to achieve the best possible un-smeared resolution for near-surface resistivity structures. The same trapezoidal time window was also selected for the late-time gates to achieve the desired depth of penetration, while retaining the lateral resolution of the geological layers. However, the pre-processing of raw data with Aeroquest leveling clearly imposed a smoothness of voltage data and compromised existing lateral variability, and so in the present study the approach was to avoid automatic averaged filtering. Instead filtering was performed manually, flight by flight. Average initial core duration is 1 s at 70 μs (1^{st} nominal time gate) and was purposely maintained constant at depth, the last time gate being at 3 ms. This approximately represents averaging a stack of round 20 m at the surface and at depth (Figure 15).

All the data was assigned a minimum small uniform data uncertainty of 3%. On the basis of the helicopter speed of around 80 km/h, soundings were produced every 1.4 s corresponding to approximately 30 m (see also figure 15). Subsequently, the automatic stacking soundings were visually inspected in a number of different data plots. During this phase it was assessed whether late time data points should be ascribed higher uncertainty or eliminated entirely. It is normal to cull data when the background noise level reaches Earth response level. Assessing usability of data is achieved by inspecting the decay curves, noise measurements, and distance from potential noise sources. This process is required in order to establish reliable model parameters right across the data sections. Random noise declines proportional to $t^{-1/2}$ while effective noise after stacking normally varies between 0.1 and 10 nV/m^2. Clearly the early measurements are many times higher than the noise level.

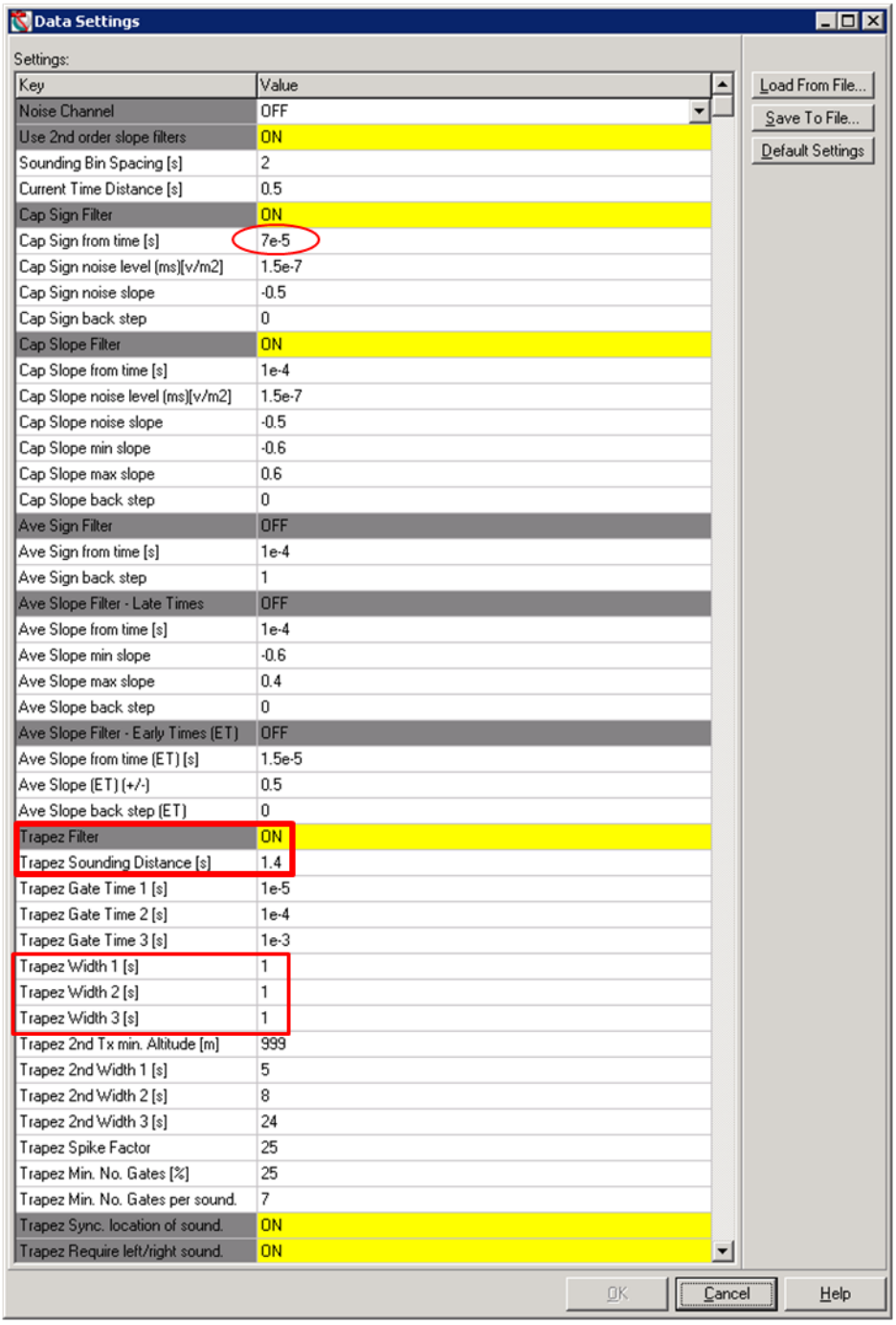

Figure 15.
Example of automated filter settings employed in the first part (automatic filtering) of processing. The red boxes outline respectively, 70 us as reference time for coupling detection at raw data (i.e. capacitive), 1.4 s as time distance to averaged soundings (corresponding to 30 m distance per sounding) and the applied trapezoidal time width.

Figure 16 shows an averaged sounding (transformed into late time apparent resistivity), with different time gates displaying different noise levels. The high early signal levels (gates 1,2) recorded during the entire survey are thought to be the effect of the system's high self response, in other words the primary field affecting early gate data, resulting in total omission before inversion.

This problem is typical of concentric coil systems (systems that are not null-coupled) in which the strong primary field present during on-time can extend into off-time as a high system transient, overpowering the weaker secondary field. Noise assessment was also performed for late time readings to maximize resolution at depth and eliminate raw data leveling effects from flight to flight. Despite primary field compensation and leveling, systemic self response was still identified for some late time readings. System bias might be expressed since it abruptly changes trend compared to a theoretical flat trend of apparent resistivity for a half-space. The first approach was to increase noise level at the last few gates in order to improve the data fit of the forward response after inversion had been run.

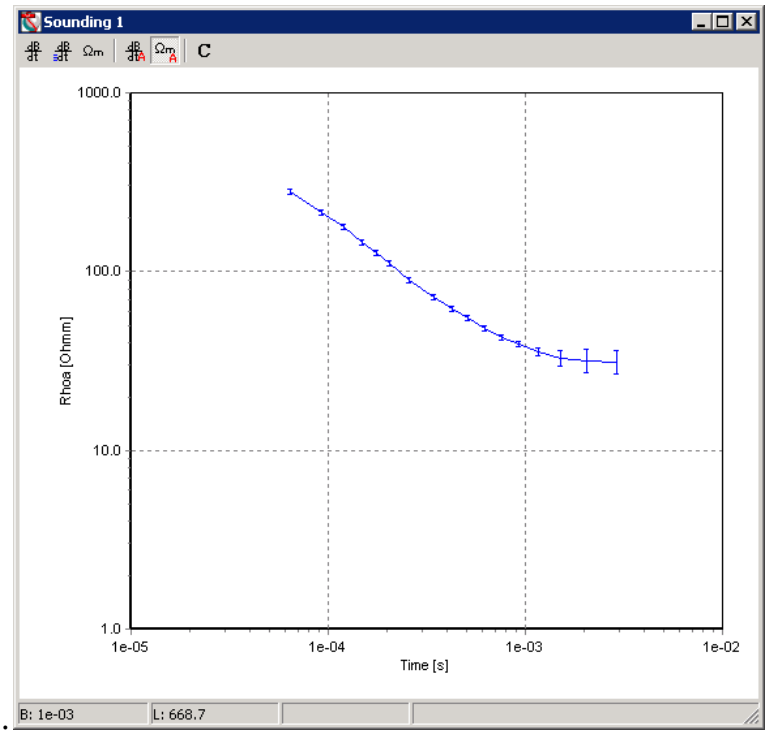

Figure 16.

Example of averaged sounding (transformed into late time apparent resistivity), with different time gates displaying different noise levels. This level increases from 10% at gate 14 to a level of 25% at gates 16 and 17.

Fast smooth LCI inversion for " post-processing assessments"

Before attempting a numerical inversion of data, the question should be posed as to whether the data was properly processed. When a large part of the data have been culled because of coupling, and when the main noise source is natural background noise, it is always useful to run a smooth inversion of data in order to evaluate whether further manual processing is required. This is essential if the aim is to obtain a reliable final resistivity model. In the present study the Laterally

Constrained Inversion (LCI) algorithm (Auken et al. 2004) was used for this "post-processing check". This inversion is used to identify and remove outlier data that, for some reason, have not been eliminated by the automatic filters or manual processing. It is also of a primary importance for identifying artifacts in the output model, i.e. unexpected conductive\resistive layers that can be attributed to the data or, much more importantly, to an inappropriate system description. Such "incidents" always occur both at early and late times, where, in turn, signal-to-noise level is low. Figure 17 shows an example of a resulting smooth LCI inversion for a flight line. The data residual, the misfit between the forward model and observed data, is also plotted on the section. It is not yet possible to describe or interpret the outcomes in terms of resistivity values of potential lithologies, or as evidence of erosional structures, etc. It is first necessary to characterize the inversion, remove potential outliers and, above all, observe whether the forward response fits the observed data within the noise level.

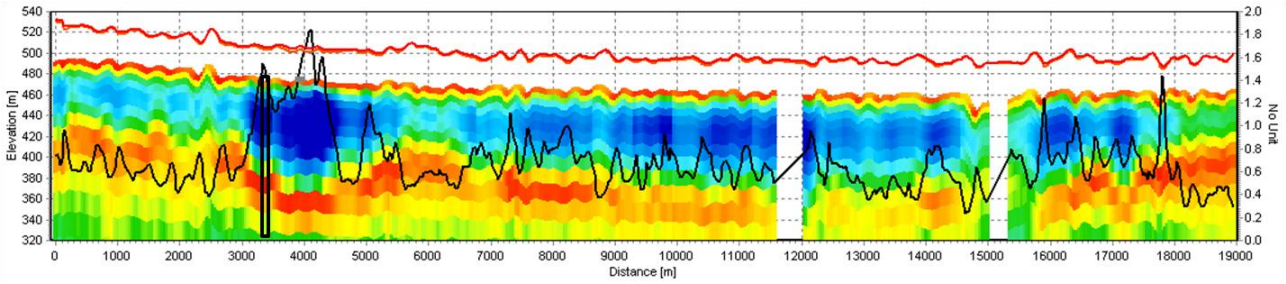

Figure 17.
The figure shows an inverted section of the data with a lateral constrained inversion (LCI, Auken et al. 2004). Inversion was run on data including biased gates. The removal of data was caused by crossing a road. The black line indicates the data residual (misfit between forward model and observed data) and the narrow black rectangle at kilometric 3500 m represents a reference sounding (see following figures).

As expected (there was already a hint), the measured data were not well fitted at early times. This is present systematically throughout the entire dataset, and for each flight the first two gates were completely off compared to the rest of the decay curve. This suggests the presence of a residual primary field on the off time gates (known as bias effect, already observed by Macnae et al. 1984). Too much signal (high voltage) was not derived from a transient secondary field (an "earth response") but rather from extra signal from the transmitter loop (on time), which is clearly represented as a thin, constant thickness, shallower conductive layer throughout the section (see

figure 17). Observing the decay curves (Figure 18), this immediately shows up as a significant change in curve inclination during very early times. The figures show the forward model respectively of the dB\dt and as rho data. The latter is more indicative to explain the presence of this conductive layer, while the dB\dt curve clearly indicates which gates are responsible for this marked misfit. The forward model, in order to fit the biased gates, also appears to over-fit other gates, the 3rd and 4th gates, which appear not to be affected by bias. Notwithstanding the presence of a bucking coil on the frame, primary field compensation, filtering and pre-leveling of the raw data, etc., nothing else can be done to recover those 2 gates. The alternative is to omit these early time gates from the subsequent inversions in order to eliminate this shallower conductive artifact from the output resistivity models. This can easily be done in the inversion setting window.

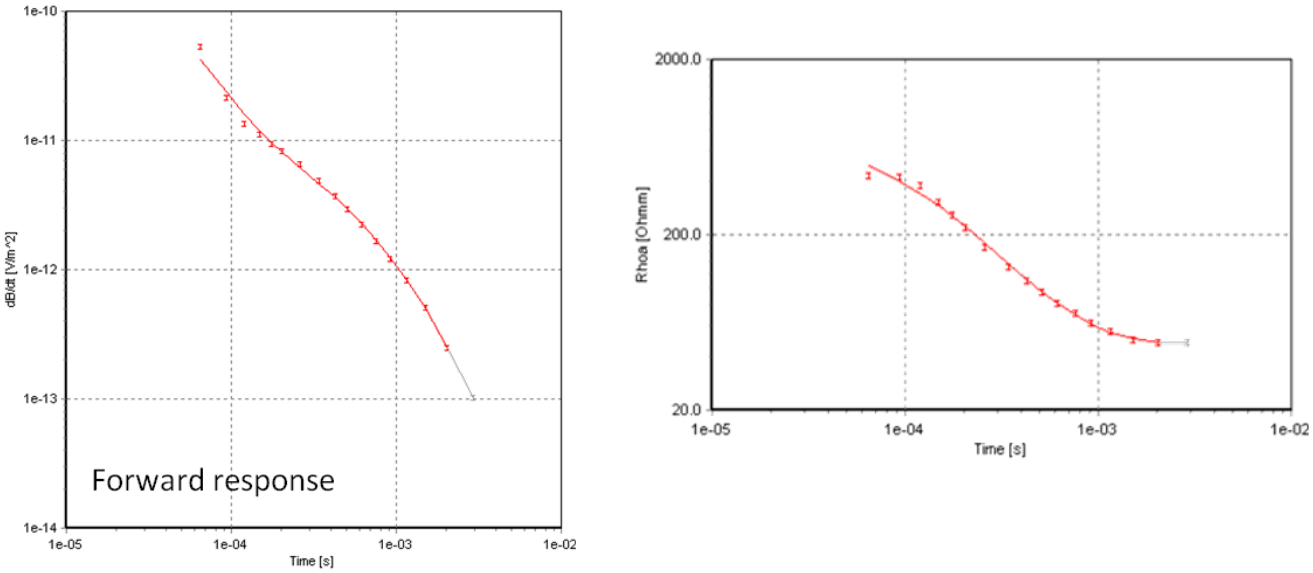

Figure 18.
Model curve showing the sounding from Figure 18 (black rectangle) along with the forward response (red line). As seen, the data are generally well fitted, but an evident discrepancy between the forward model (red line) and measured data (red error bars) is observable at an early time.

Inversion of AeroTEM data

Inversions are carried out using the quasi 3-D Spatially Constrained Inversion program (Viezzoli et al. 2008). SCI is a full non-linear damped least squares solution, in which the transfer function of the instrumentation is modeled. The system transfer function includes transmitter current, turn-on and turn-off ramps, gate times, low pass filters, and system altitude. The system

description is represented by a geometry file. This file contains all information inherent to the system used for the survey. This information includes the Tx current, loop area, number of gates, repetition frequency, waveform, and Rx time gates. Observing the nominal Rx time gates scaled to each of the nominal waveforms, flight by flight (for a total of 40 flights), a noticeable discrepancy was observed between the timing of Rx measurement time gates. In order to avoid any potential artifacts in the inversion (i.e. striping along adjacent flights), the entire set of waveforms (one for each survey flight) were modeled separately based on all available information (time on, time switch, and time off). Consequently, the Rx gates are scaled according to the waveform and applied as a different geometry file for each of the survey flights. Figure 19 shows the nominal time for gate 1 for the entire set of survey flights. This graph clearly shows how the differences (in time) between the 1st Rx gate are significant, in some cases exceeding 30μs.

In the SCI scheme the model parameters for different soundings are tied together spatially with a partially dependent covariance, which is scaled according to distance (Viezzoli et al. 2008). Models are constrained spatially to reflect the lateral homogeneity expected from the geology (either vertical and horizontal layer resistivity, boundary thickness, or depth). Constraints include boundary conditions and delimit changes in values within a defined deviation. Flight altitude is included as an inversion parameter, but with an a priori value (2 m) and standard deviation assigned (1.2). The depth of investigation (DOI), based on an analysis of the Jacobian matrix, was also calculated for the output models. The DOI represents the maximum depth at which there is sensitivity to the model parameters (Christiansen et al. 2012). This DOI, is presented superimposed to crop the average resistivity horizontal maps and as fading colors below the DOI on the vertical cross sections. This means that any model parameter lying significantly below the DOI should be disregarded. For example, the DOI often lies at, or close to, an interface between a conductive overburden and a resistive deeper layer. In this case it is assumed that the conductive layer does end at that interface, and lies above a significantly more resistive layer, whose absolute resistive value is poorly determined.

Inversion was started with a homogeneous half space (40 Ωm) and resistivity was calculated from the mean apparent resistivity of the soundings. Before data inversion, late time noise assessment was performed to maximize resolution at depth and to eliminate the effects of raw data leveling from flight to flight. The inversion is parameterized as a smooth model with several layers (19 or more), each having a fixed thickness, but free resistivity (with vertical constraints) and as a layered model (also called a blocky inversion) where only a few layers are selected as representative of the existing geological setting. Both schemes have advantages. The resistivities were scaled according to apparent resistivity. Layer interfaces, resistivities, and depth of penetration are best determined from the blocky parameterized inversion. Conversely, smooth inversion is more independent of the starting model and gradual transitions in resistivities are more conspicuous, facilitating the delineation of complex geological structures. The vertical constraints used in the smooth models are applied to stabilize the inversion, for example to remove fictitious layers especially in models based on a small number of data points. Moreover, the blocky inversion allows the use of lateral constraints, applied respectively to layer depth which, in turn, corresponds to layer thickness, and resistivity to account for lateral variability in layer resistivity. The smooth model is discretized up to a depth which is supposed to be consistent with the penetration capability of the system, with layers of logarithmically increasing thickness, starting from a few meters in thickness for shallower strata. This smooth model enhances complex geological structures and is a powerful tool for evaluating the complexity of the subsurface. These SCI algorithms produce smooth structure models in which sharp formation boundaries are blurred and often hard to recognize. In contrast, an inversion scheme with few layers tends to give a more blocky appearance to the model section possibly aiding quantitative evaluation of layer thicknesses.

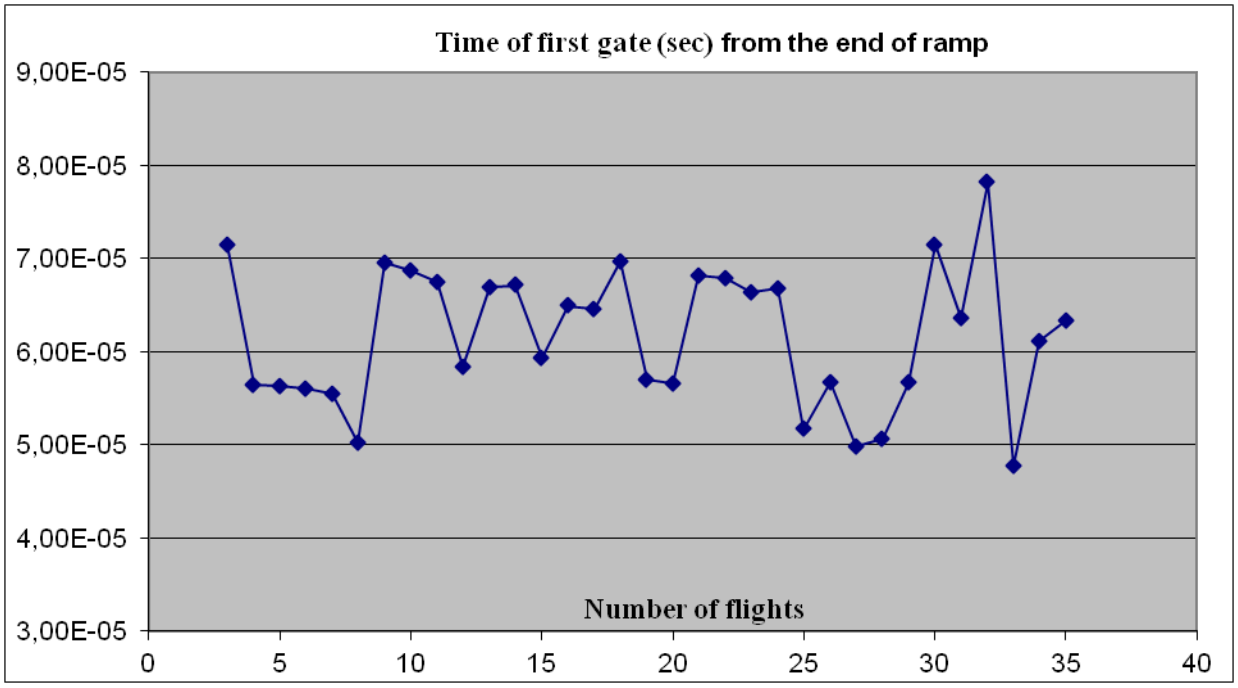

Figure 19.
Time (sec) of the first Rx gate for all the flights (40) of the AeroTEM system deployed in the survey.

Inaccurate description of the system transfer function

The effects in the predicted models of inaccurate system description in the 1D forward modeling of AEM data has already been studied and demonstrated in detail by Christiansen et al. (2011). Surprisingly, a situation was encountered in which the information reported in the Spiritwood survey report was somewhat different from a correct system description, the latter being required for correct inversion of AEM data and, above all, in order to derive a reliable resistivity model. The first system inverted turned out to be inaccurate and is referred to as the "wrong system" while the correct one is referred to as the "true system". The wrong system information consisted of a transmitter loop with an area of 63.5 m^2 (which corresponds to an equivalent square loop type of 7.9 m across) with a maximum current of 480 A and 8 turns (which generates a peak moment of 233 kAm^2). In contrast, the "true" system geometry corresponds to a Tx loop of 78.5 m^2 (corresponding to a square loop 8.86 m across) with the same input current but a different number of turns (5 instead of 8), generating a peak moment of 188 kAm^2. In general, a different peak moment results in different voltage which, in turn, corresponds to different ground conductivity. However, in the situation that arose the same data voltage was inverted using two different system

transfer functions, since the first was found to be simply wrong. So the question arises of how to deal with the output resistivity models.

The output model derived from the wrong system description (erroneous system transfer function in the inversion calculation) results in inappropriate resistivity values for good conductors (which appear to be higher) as well as inaccurate layer depth , i.e. the shale bedrock appeared to be deeper (Figure 20). Figure 21 shows the inversion result for the "correct" system description. As can be seen by comparing both sections (Figures 20 and 21), the conductive bedrock appears to be more conductive and not as deep as in the previous resistivity model in Figure 20. Obviously, if data is inverted taking into account this change from a high moment to a lower peak moment (which is the amount of energy diffusing in the ground), this results in a change in the range of resistivity values. In particular, what was already conductive (i.e. the bedrock) now appears to be more conductive since the lower peak moment, but with the same measured voltage (as for the highest moment), implies a more conductive layer in order to generate the same voltage data. Moreover, since the diffusion speed depends on the resistivity of the layers (i.e. the diffusion speed is high for high-resistivity layers and low for low-resistivity layers) this conductive layer also appears to be shallower.

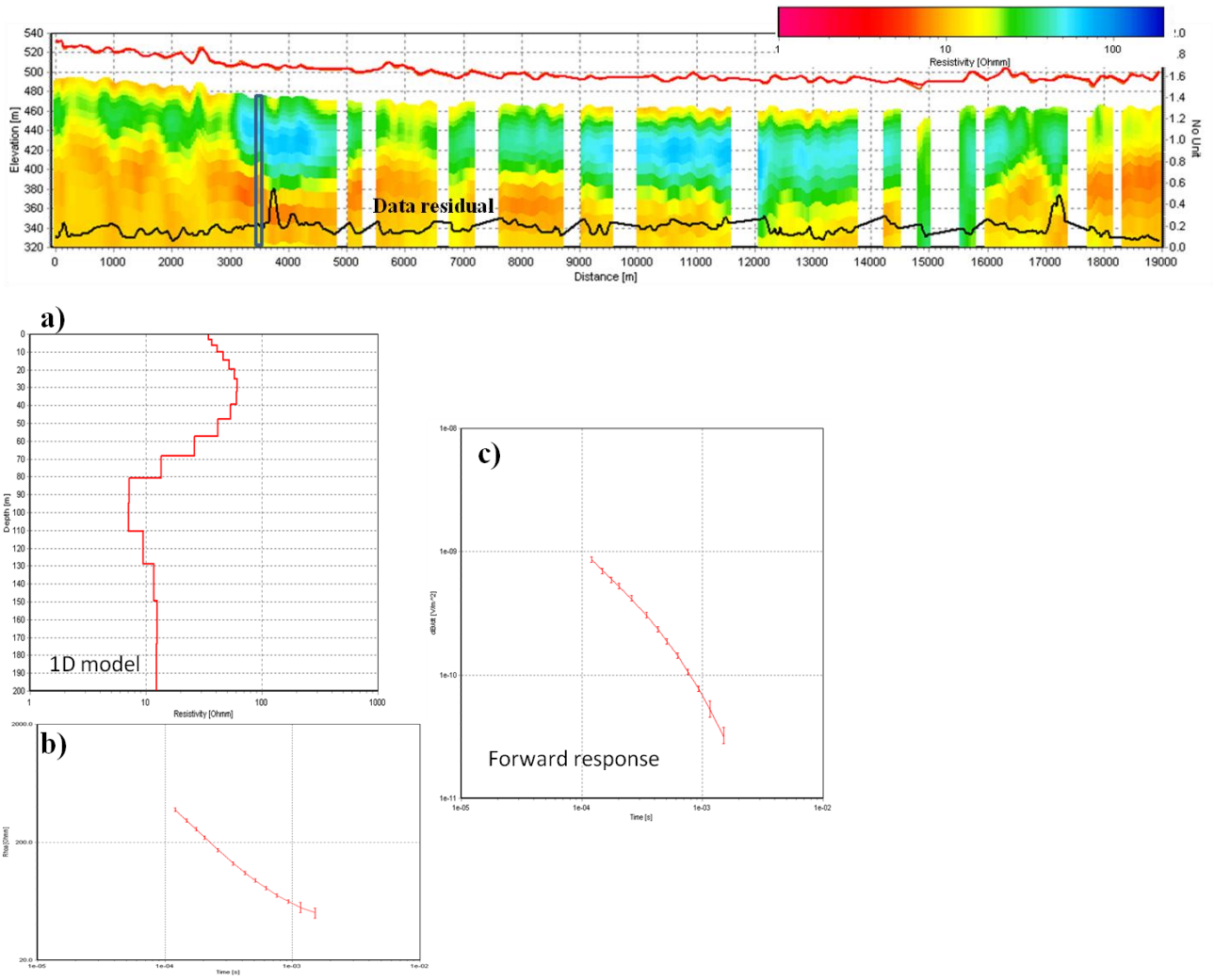

Figure 20.
Smooth inversion results along a flight line (above). a, b, and c) show respectively the 1D model, the rho curve, and the forward response relative to a reference sounding (grey rectangle).

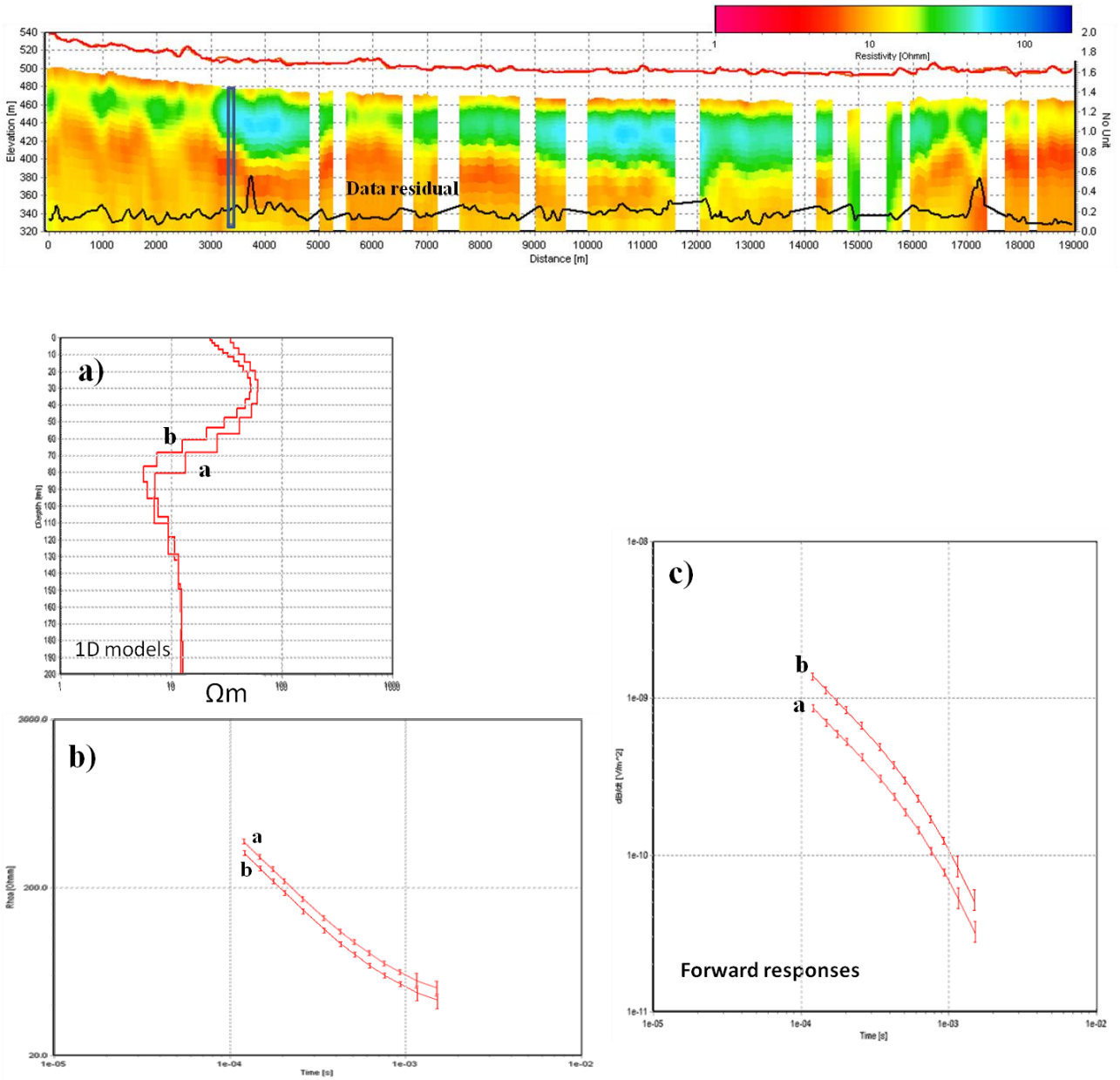

Figure 21.
Smooth inversion results along the same flight line as for figure xxx (above). a, b, and c) show respectively the 1D model, the rho curve, and the forward response relative to a reference sounding (grey rectangle). Model **a** corresponds to the wrong system transfer function (STF) while model **b** refers to the correct STF.

The phenomenon described above is also clearly evident (and perhaps more obvious) if we compare AEM inversion results, for both STF, with seismic data. Figure 22 (top) shows the AEM model derived from the wrong STF along seismic line 1 (the black line represents the depth of the bedrock derived from seismic bedrock reflector). The conductive shale bedrock derived from AEM data appears to be about 15-20 m deeper than the seismic bedrock reflector, and the resistivity value of the shale bedrock is around 15 ohm m. For the true system description a better match is observed

with ancillary seismic data (Figure 22, bottom). The shale bedrock appears to

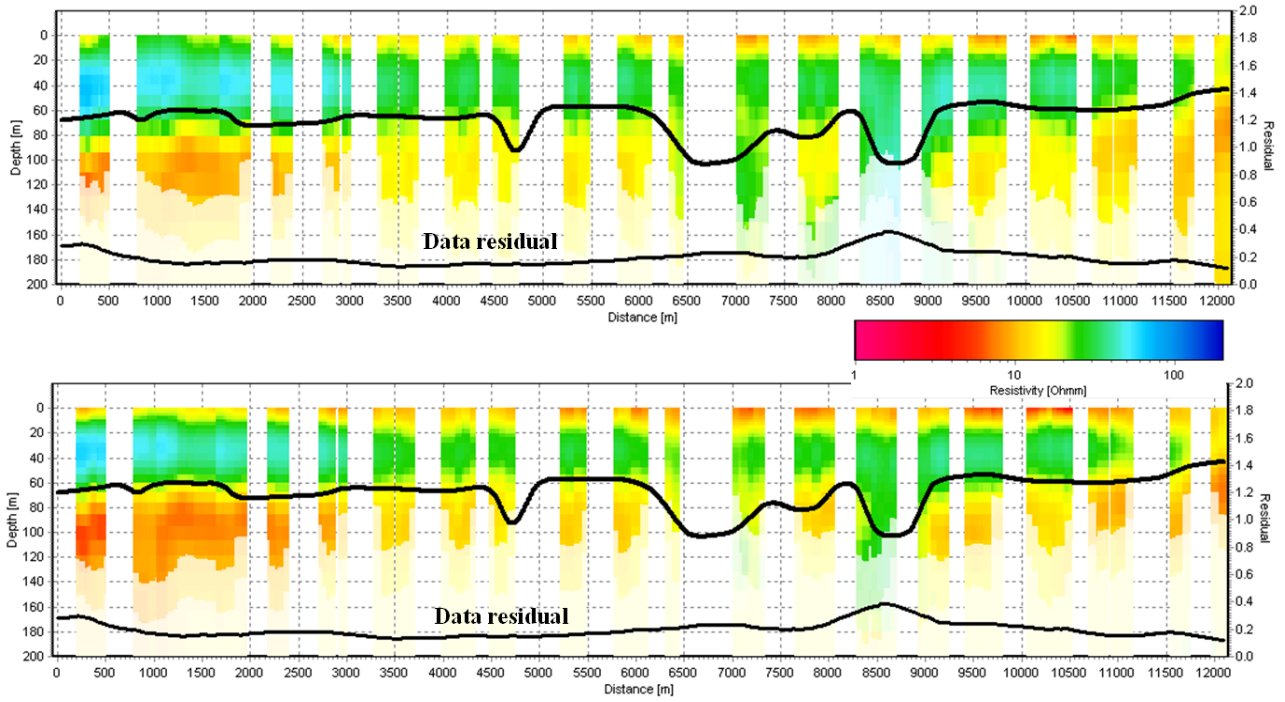

Figure 22.
Smooth inversion results along seismic line 1 located in the southern part of the area. The two profiles show respectively the inversion results derived from the wrong system transfer function (above), and from the correct STF (bottom).

be more conductive (as expected), with resistivity values ranging from 8 ohm m up to 12 ohm m. Moreover, layer depths from both AEM and seismic data are now largely comparable with an excellent depth match along the seismic bedrock reflector (black line). This is an independent confirmation that the newly applied system transfer function results in a more reliable resistivity model that fits with other sets of geophysical data. However, the data residual remains low, meaning that the forward response fits the observed data (within noise level) for both STF suggesting the non-uniqueness of the solution to the inverse problem.

Blocky inversion results

After analysis of the smooth model inversion results and multiple tests using different numbers of layers, led to the decision to present results from a 4 layer model. A conservative approach was adopted, using the smallest number of layers that satisfactorily fit the data for the entire survey. This ensures maximum sensitivity for each of the parameters modeled to the data, and therefore maximum reliability of models. However, it should be noted that in all cases the five-layer

model produced similar results to the four-layer model because the inversion algorithm tends to derive two consecutive layers, representing the conductive bedrock, with about the same resistivity if the model has numerous layers. By contrast, in a three-layer model there is loss of existing structures when more than three layers are required to correctly fit the data. Initially, while trying to choose the number of layers the complication emerged that the geology of the northern part of the Spiritwood area could be represented as a three layer model. However, this did not apply for the remainder of the survey area. The reason is because the geological setting of the northern area is significantly different and less complicated than the rest of the area. An individual structure of valley-like features is observed extending from south to north and the shale bedrock is relatively shallow. The number of layers was chosen as the smallest number that fitted the data while being indicative of the predicted main geologic units of the area. The effect of reducing (or increasing) the number of layers would simply be to increase (or reduce) the optimal number of soundings by the SCI cells for computation purposes (always aiming at about 1000 model parameters per cell). SCI is a parallel procedure and so the total inversion time depends on the number of available processors. In addition, the few layers inversion process was started with an enormous half space of 40 Ohm. The models are connected laterally and require approximate identity between the neighboring parameters of resistivity and depth to within a specified variance. The lateral constraints can be considered as a priori information regarding geological variability within the measuring zone. In general, it is assumed that the smaller the expected variation for a model parameter, the tighter the constraint should be. On the basis of known geological variability (resistivity and structure geometry derived from the smooth model) moderate or tight lateral constraints were applied, taking into account existing lateral variability (both for depth and lateral resistivity constraints). In response to the obvious variability of the resistivity values and the presence of narrow structures from the smooth model, moderate constraints were applied both for resistivity and depth. Furthermore, considering that most of the structures lie within a depth of 80 to 100 m and the geology is quite complex, the use of loose constraints allowed a single layer (the 4th

layer) to fit the same geological features (i.e. shale bedrock) for different elevations. Reference constraints of 1.5 were applied on the resistivities of the first two layers, and 1.3 on the last two layers (total of 4 layers as blocky model), and 1.5 applied on all depths. The reference distance is 25 m based on the sounding distance. This means that the models were allowed to vary by approximately 50% down to 30% in resistivity, and 50% in depths over 25 m on average.

Figure 23 shows a comparison between the smooth model and the blocky model along a coincident flight line. The models look similar (as expected) but some differences are also evident. The SCI-section in figure 23, b reveals the same overall characteristics as the SCI smooth inversions in panel a, but with a sharp boundary and a general increase in the resistivity value for the resistive layer. Applying the lateral constraints it is seen that the shale bedrock (with low resistive value) is found along the entire profile except beneath the deeper valley structures (as in the smooth model). The lateral constraints thus add sufficient information regarding the expected geological variability to extract from the data the sparse information on this layer at the bottom of the BVs. The high-resistivity layers above the conductive bedrock are well resolved but it is not possible to establish anything about their resistivity other than it being higher. The data residuals indicate that the forward models fit observed data mostly below a normalized residual of 1.

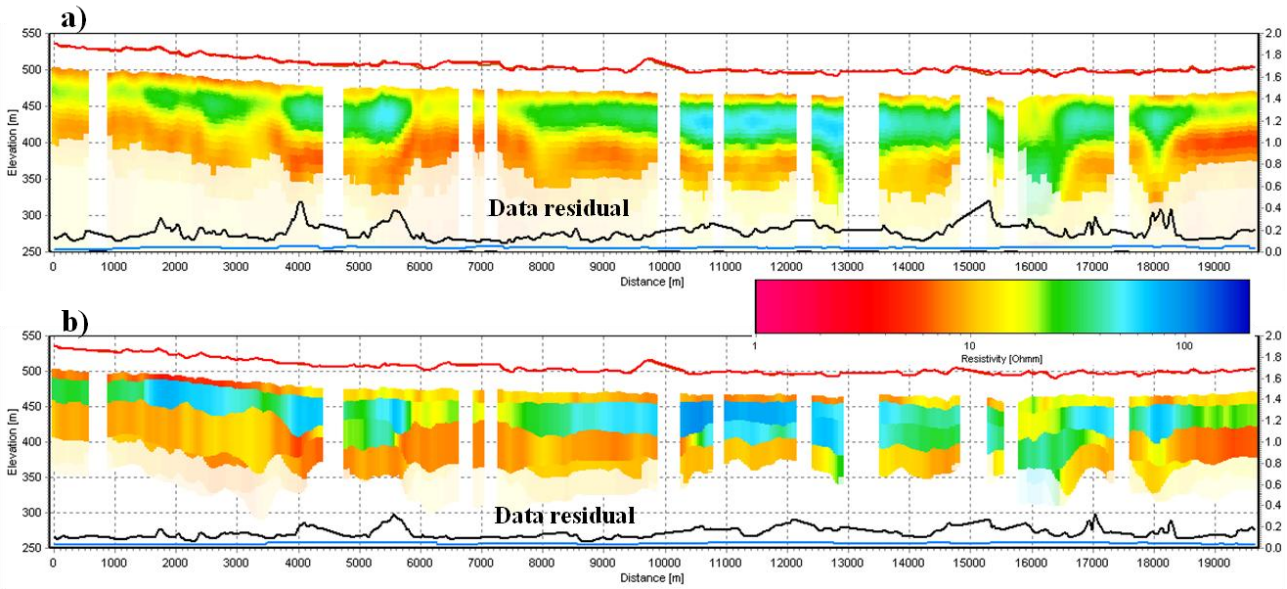

Figure 23.
Comparison between the a) smooth, and b) fewer layer (blocky) results for coincident flight lines.

Interpretation of AeroTEM smooth inversion results

To visualize the resistivity structures of the survey area, a number of geophysical theme maps and vertical sections are presented. The maps of average resistivity at different vertical intervals are shown for depth below ground surface. In a setting like Spiritwood Valley, with little topographic relief, inspecting results only in depth below ground surface is probably not misleading. The average resistivity maps in Figure 24 clearly show the existence of a valley as an elongated, resistive feature, known as the *Spiritwood Valley Aquifer*. It is approximately 10 km wide and has a conductive background which, according to boreholes, consists of Cretaceous shale bedrock. Along the middle of this valley a much narrower structure can be observed (1 km) and is interpreted as an inset valley that follows the main valley from north to south. In addition to the main incised valleys, multiple valley-like features outside of the main valley are observed (see also CDI results from Oldenborger et al. 2013). Some of the observed buried valleys are very narrow and reveal a complex glacial setting with many cross-cutting buried valleys of several generations, which are also documented in similar settings in Denmark (Jørgensen and Sandersen 2006).

In general, the electrical resistivities from the AEM model are normally below 10 Ωm for the Cretaceous shale layers, between 20 and 30 Ωm for clay till to silty-sandy till, and above 40 Ωm for sandy and gravely layers. To obtain this range of values, a statistical approach in the model space was adopted, in addition to the observed similarities with well stratigraphy information and, not shown in this chapter, direct comparison was made with electrical resistivity tomography surveys. AEM spatially constrained inversion results reveal, with good correlation of absolute values, the resistive and conductive structures imaged by the ERT electrical profile. However, AEM system limitations to resolve the near surface make it difficult to provide the same detail on the surface. The depths of the main buried valleys are recorded as exceeding 100 – 110 m, while most of the secondary valleys are between 40 and 80 m deep.

The resistive features attributable to sand and gravel filling the main buried valleys are well defined in the resistivity models obtained. However, it is obvious that the inversion results from the

AEM survey present high variability in resistivity values across the whole area (Fig. 24). This indicates that the resistive sediments, interpreted to be the response of sand and gravel, fill the main valley as well as partially covering the two inset valleys and the other small valleys. According to resistivity maps, another resistive body is found in the center of the survey area (Fig.). As noted by Wiecek (2009), inter-till sands are found down to a depth of approximately 30 m in this area, and the resistive body is likely to be these sands (Oldenborger et al. 2013).

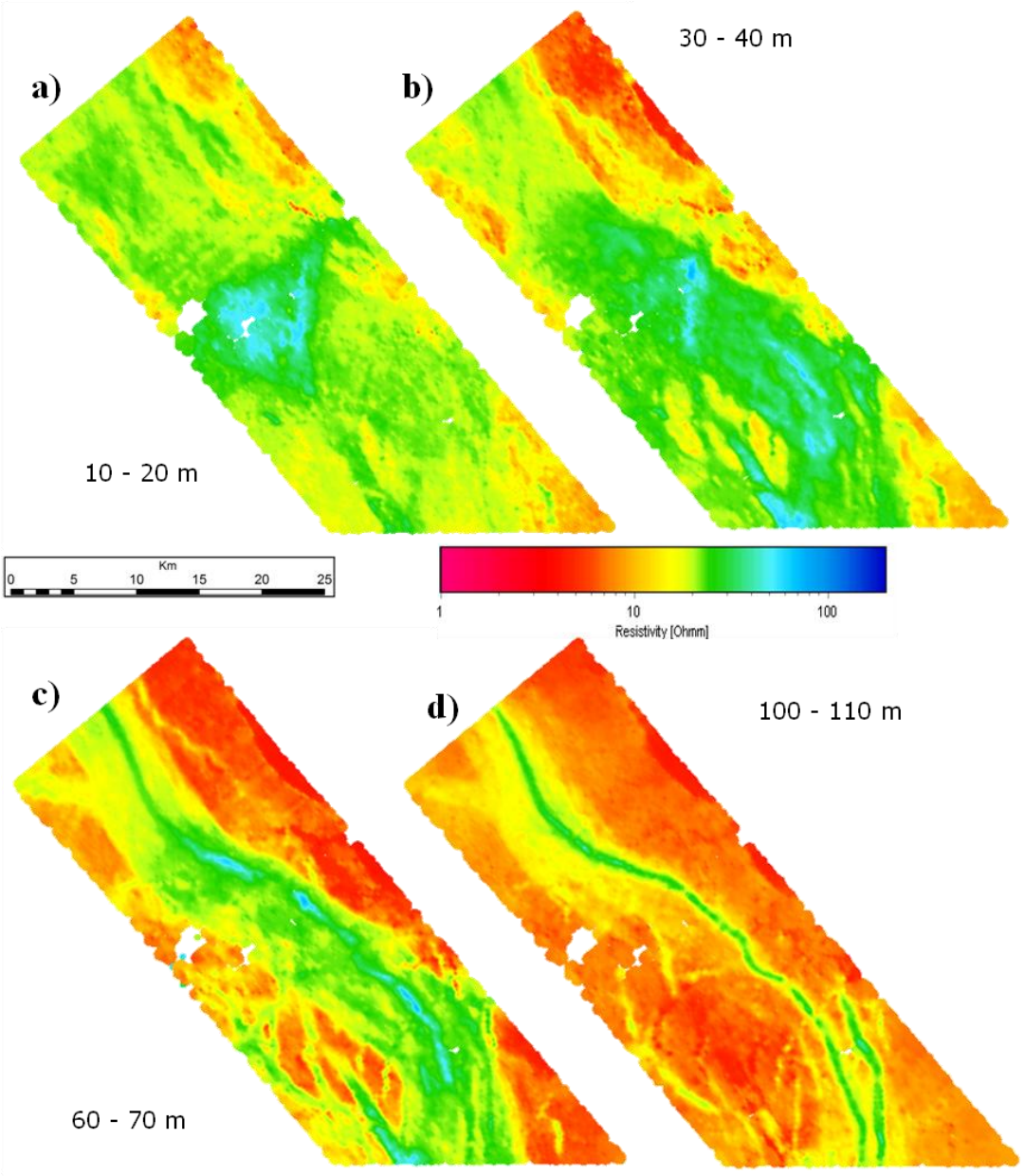

Figure 24.
Average resistivity maps for the (a) 10–20, (b) 30–40, (c) 60–70, and (d) 100–110 m depth intervals obtained from the AeroTEM III system data.

Final remarks

This chapter focused on several important aspects which are of primary importance when approaching the processing and inversion of AEM data. The entire processing workflow of AeroTEM III navigation and voltage data was discussed. Several steps were taken in order to obtain maximum data quality and so achieve the most detailed possible resolution of the resistivity structure of the subsurface. An examination was also made of how data are averaged using trapezoidal average filters. The filters are designed so that the lateral resolution of resistivity structures is blurred as little as possible. It was argued that data which are influenced by coupling to man-made installations on the ground surface must be culled before entering the averaging scheme as, otherwise, good data are degraded. This chapter also presented a real life example illustrating the difficulties associated with modeling and inverting AEM data. There is also the possibility (not rare) of misinformation directly from the contractor or misunderstanding of the survey report. If the system transfer function is not modeled accurately, the errors introduced may migrate to the model's earth or geometry related parameters. This shows that not only is it obviously important to model the system transfer function correctly, but it is also important always to analyze the output carefully, e.g. for systematic errors that might point to wrong settings. A potential problem was encountered because a wrong STF not only affects the output resistivity model but also has a negative effect on further data integration and/or joint interpretation.

All the things mentioned above are of fundamental importance since the aim of processing is to prepare data for inversion. A Spatially Constrained Inversion using smooth and blocky models was actively applied to evaluate processing, since the final inversion is closely linked to the processing procedures (data handling). Minor changes in data can transform the outcome of the investigation from success to failure. Therefore, the need not only for high precision unbiased data, but also high-quality processing, is inescapable.

The present study analyzed the smooth and blocky resistivity model derived from the spatially constraint inversion (SCI, Viezzoli et al. 2008) in detail. The Spiritwood AEM data show

significant geological structures and clearly indicate a complex valley morphology that can be used to significantly improve geological and hydrogeological knowledge on a regional scale. Inversion results reveal multiple resistive valley features inside a wider, more conductive valley structure. Furthermore, the models show the presence of resistive layers interpreted as interbedded sand and gravel above the shale in addition to resistive materials at the bottom of the buried valley which, in turn, represent potential aquifers for exploitation. Fidelity of electrical resistivity derived from the AEM inversion is of great significance when attempting to assess the hydrogeological importance of geological units.

Despite the early-time limitation of AeroTEM system and the fact that it is not designed for peak response over resistive materials such as those found in this survey area, the AeroTEM dataset provides rich information content in terms of lithological detail, identification, and bedrock morphology. The Spiritwood AEM survey successfully mapped valley locations that continue to be difficult to define using seismic, electrical resistivity, and borehole methods. In conclusion, buried valleys are important hydrogeological structures in Canada and other glaciated terrains, providing sources of groundwater for drinking, agriculture, and industrial applications. Hydrgeological exploration methods such as pumping tests, borehole coring, or ground-based geophysical methods (seismic and electrical resistivity tomography) provide limited spatial information and are inadequate to efficiently predict the sustainability of these aquifers on a regional scale. Airborne geophysics can be used to significantly improve geological and hydrogeological knowledge on a regional scale.

Additional key maps

Outlined below is a brief explanation of the various key maps, and their applications. All the maps were made using the Kriging method with a search radius of 500 m and 30 m node spacing.

- **Map A** displays the topography used in the processing and inversions. The DEM image is superimposed over the geo-referenced raster imagery available for the survey area.

In addition, several "processing" and "quality control" maps are also illustrated. In particular, SCI smooth derived maps related to the "uncoupled" data (including all nominal Rx time gates), and the final map, presenting entirely processed (de-coupled and with the biased Rx time gates omitted in the inversions) AeroTEM data from the Spiritwood Valley Aquifer survey area. The following maps are intended to illustrate the main end products in order to evaluate and assist concrete assessments of the entire processing workflow.

- **Map B** shows the difference between the AeroTEM soundings that entered the processing (upper), and those that were used for the inversion, after the processing (lower), due to infrastructures. It is useful to note how much of the EM data was culled during the processing due to coupling with infrastructure.
- **Map C** shows, color-coded, the number of time gates used for the inversion of individual soundings. The maximum number of gates possible in this case, if there had been no noise on any of them, was 17 gates. However, when the averaged late time gates fell into noise and contain no signal, they are deleted during processing and do not enter the inversion in order not to produce artifacts in the output models. For obvious reasons, this map is not presented for the uncoupled results (when no time gates are omitted from inversions and/or deleted during processing).
- **Map D** shows, color-coded, the spatial variation of the absolute value of the misfit between forward modeled data and measured data, normalized to the data noise for each

time gate (top panel refers to processed data and lower panel to unprocessed data). Values lower than 1 indicate that the modeled data fit the measured data within noise level, i.e. the inversion fitted the data. Values higher than one can be due either to strong 3D effects, or to noisier or less accurate data. In general, data residual is much closer to 1 for unprocessed data. In particular, data misfit gets higher near to infrastructures and clearly delineates the road and power line networks. This indicates how the forward model cannot fit observed data when affected by coupling.

- **Map E** shows average resistivity maps for the (a) 10–20, (b) 30–40, (c) 60–70, and (d) 100–110 m depth intervals (same as for figure xxx) obtained from unprocessed AeroTEM data (without any de-coupling and keeping all time gates, i.e. bias included). Detailed descriptions and interpretations based on these maps will be discussed in Chapter 4. The same resistivity maps at the same depth intervals are shown in figure xxx for comparison.
- **Map F** shows the variation between inversion input and output altitude. Unprocessed data show very high variability of this inversion parameter over the entire area. As expected, the inversion moved down the output altitude, which appears to be about 5 m up to 10-13 m lower than the input altitude, in order to fit the data. Note that the first two gates are affected by primary fields, which results in higher measured signals at the very near surface. This high signal consists in a thin conductive layer all over the survey area. To fit the early time (biased) gates the inversion lowers the altitude and puts a conductive layer on top of the surface to compensate the signal at early time. For the processed data, altitude difference is negligible, meaning that inversion does not move the altitude to fit observed data.
- **Map G** shows, color-coded, the spatial variability of the model-dependent DOI, presented in depth below surface. For a more conservative analysis of sensitivity at depth only the DOI upper is presented. Refer to section 2.4 for a detailed discussion on

the DOI. The color scale maximum is only indicative, and does not imply that this value was expected for the entire area. For the processed data the footprint of the roads in the DOI map can be misleading. This is due to the effect of the manual processing only over roads or other infrastructures. Average late time data were culled much more according to the footprint of the eddy currents, which is greater in depth (see section 2.3, average data processing for details). All soundings close to roads contain only early time gates which, in turn, give rise to a lower DOI. In general DOI is lower for the processed data due to late time gate omission in addition to the late time noise assessments. Moreover, the DOI is not expressed with higher values over the main buried valley. This is an alternative way to assess how the sensitivity at the bottom of the buried valley is rather low in this data.

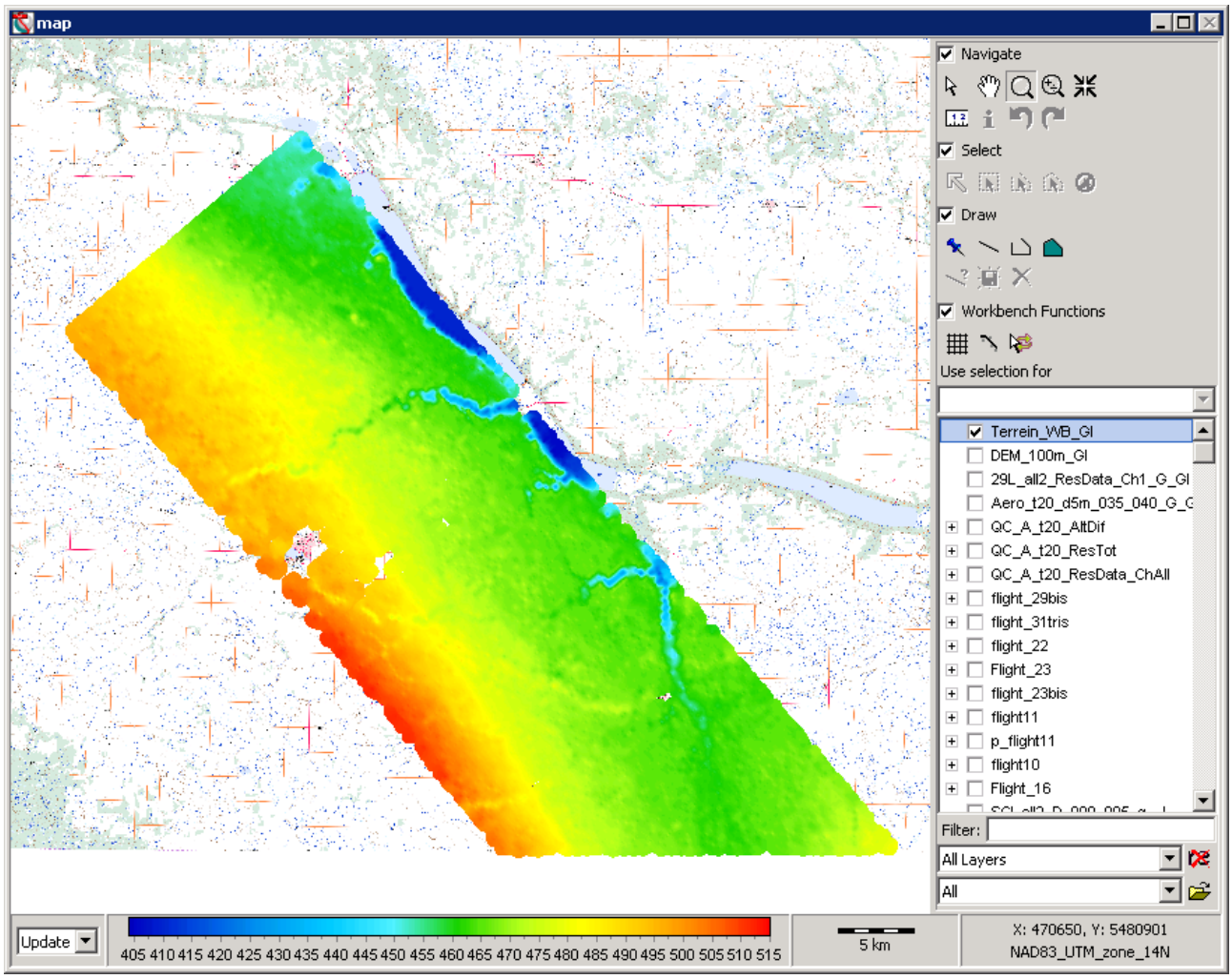
map
Navigate
Select
Draw
Workbench Functions
Use selection for
Terrein_WB_Gl
DEM_100m_Gl
29L_all2_ResData_Ch1_G_Gl
Aero_t20_d5m_035_040_G_G
QC_A_t20_AltDif
QC_A_t20_ResTot
QC_A_t20_ResData_ChAll
flight_29bis
flight_31tris
flight_22
Flight_23
flight_23bis
flight11
p_flight11
flight10
Flight_16
Filter:
All Layers
All
Update
405 410 415 420 425 430 435 440 445 450 455 460 465 470 475 480 485 490 495 500 505 510 515
5 km
X: 470650, Y: 5480901
NAD83_UTM_zone_14N

Map A

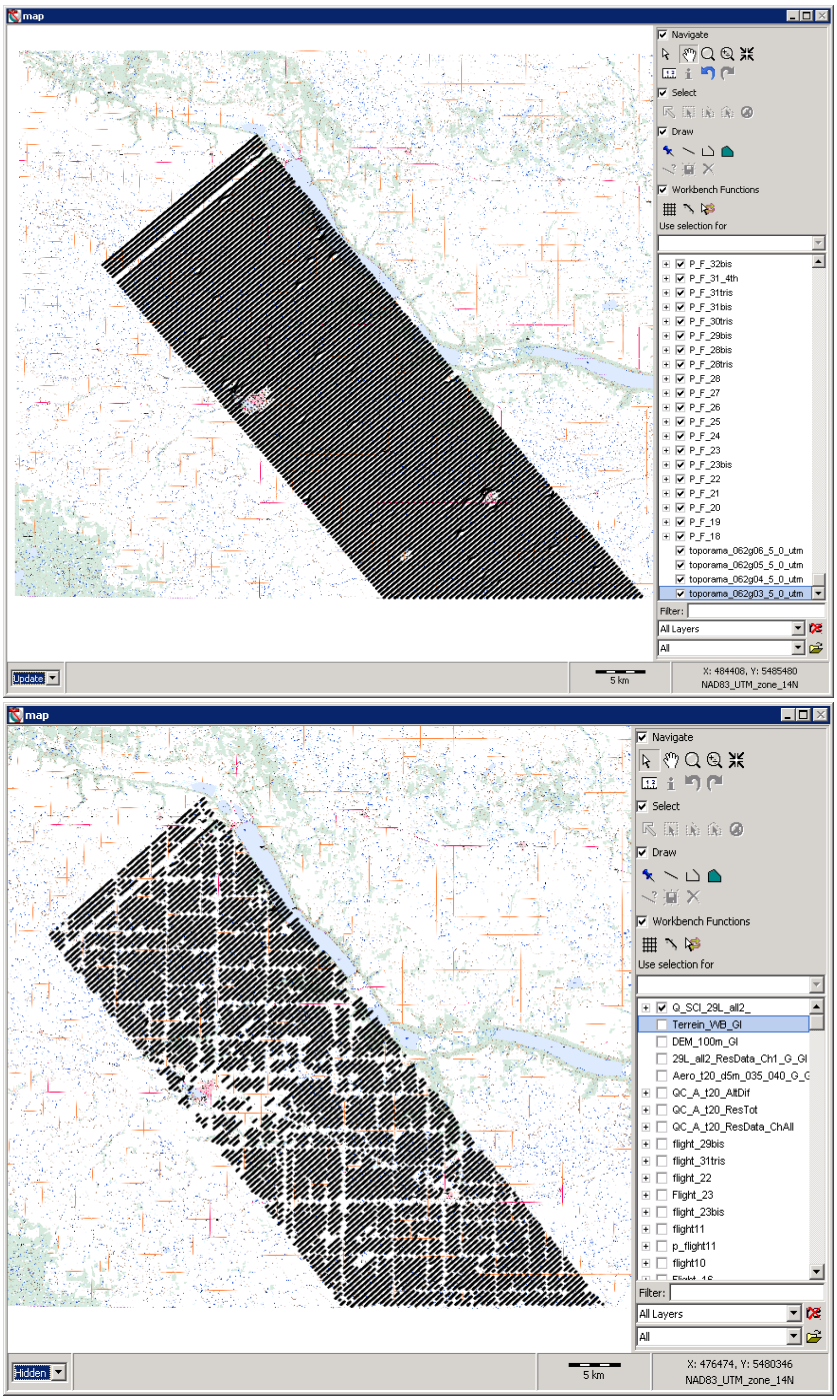
map
Navigate
Select
Draw
Workbench Functions
Use selection for
P_F_32bis
P_F_31_4th
P_F_31tris
P_F_31bis
P_F_30tris
P_F_29bis
P_F_28bis
P_F_28tris
P_F_28
P_F_27
P_F_26
P_F_25
P_F_24
P_F_23
P_F_23bis
P_F_22
P_F_21
P_F_20
P_F_19
P_F_18
toporama_062g06_5_0_utm
toporama_062g05_5_0_utm
toporama_062g04_5_0_utm
toporama_062g03_5_0_utm
Filter:
All Layers
All
Update
5 km
X: 484408, Y: 5485480
NAD83_UTM_zone_14N
map
Navigate
Select
Draw
Workbench Functions
Use selection for
Q_SCI_29L_all2_
Terrein_WB_GI
DEM_100m_GI
29L_all2_ResData_Ch1_G_GI
Aero_t20_d5m_035_040_G_G
QC_A_t20_AltDif
QC_A_t20_ResTot
QC_A_t20_ResData_ChAll
flight_29bis
flight_31tris
flight_22
Flight_23
flight_23bis
flight11
p_flight11
flight10
Filter:
All Layers
All
Hidden
5 km
X: 476474, Y: 5480346
NAD83_UTM_zone_14N

Map B

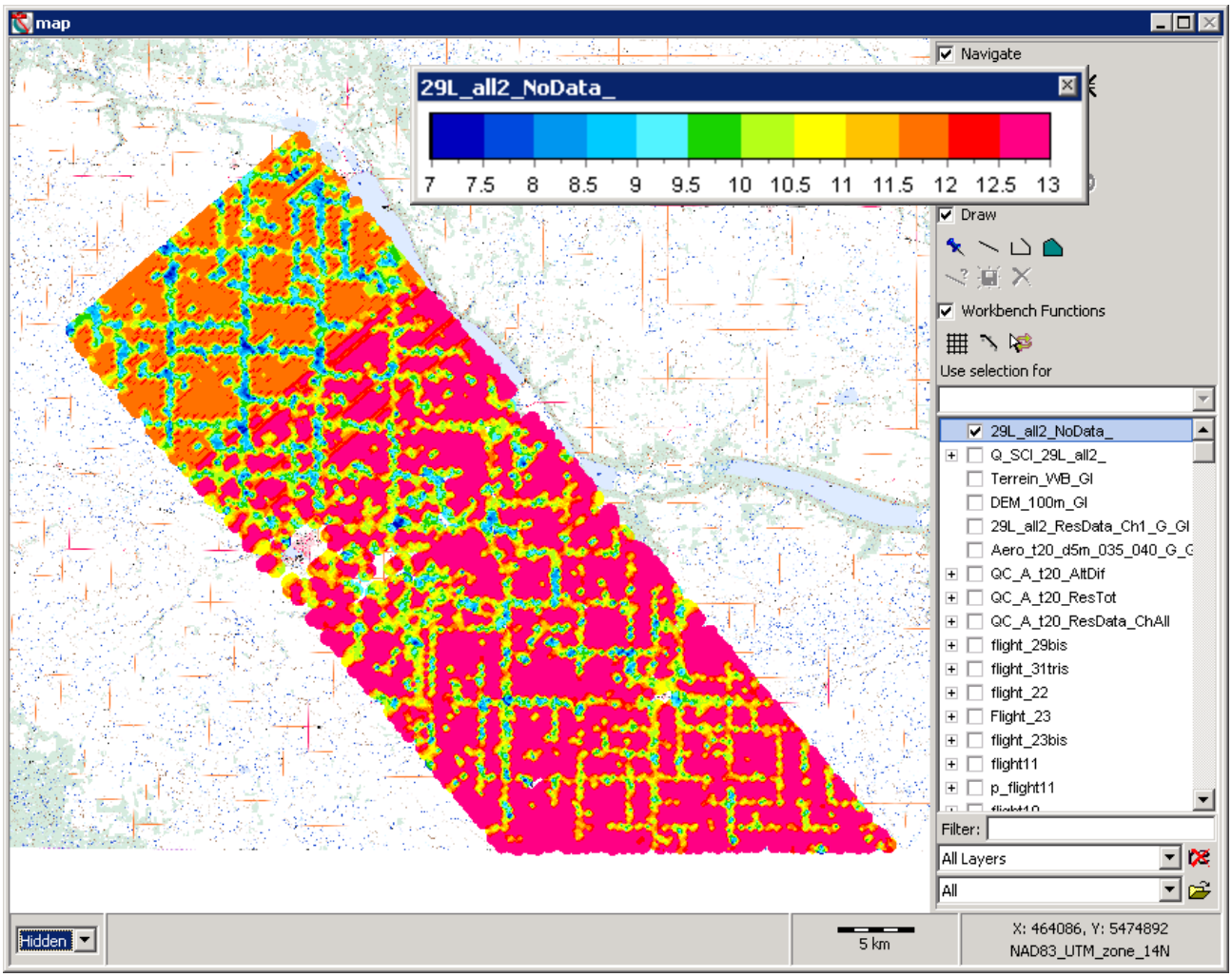
map
29L_all2_NoData_
7 7.5 8 8.5 9 9.5 10 10.5 11 11.5 12 12.5 13
Navigate
Draw
Workbench Functions
Use selection for
29L_all2_NoData_
Q_SCI_29L_all2_
Terrein_WB_GI
DEM_100m_GI
29L_all2_ResData_Ch1_G_GI
QC_A_t20_AltDif
QC_A_t20_ResTot
QC_A_t20_ResData_ChAll
flight_29bis
flight_31tris
flight_22
Flight_23
flight_23bis
flight11
p_flight11
Filter:
All Layers
All
Hidden
5 km
X: 464086, Y: 5474892
NAD83_UTM_zone_14N

Map C

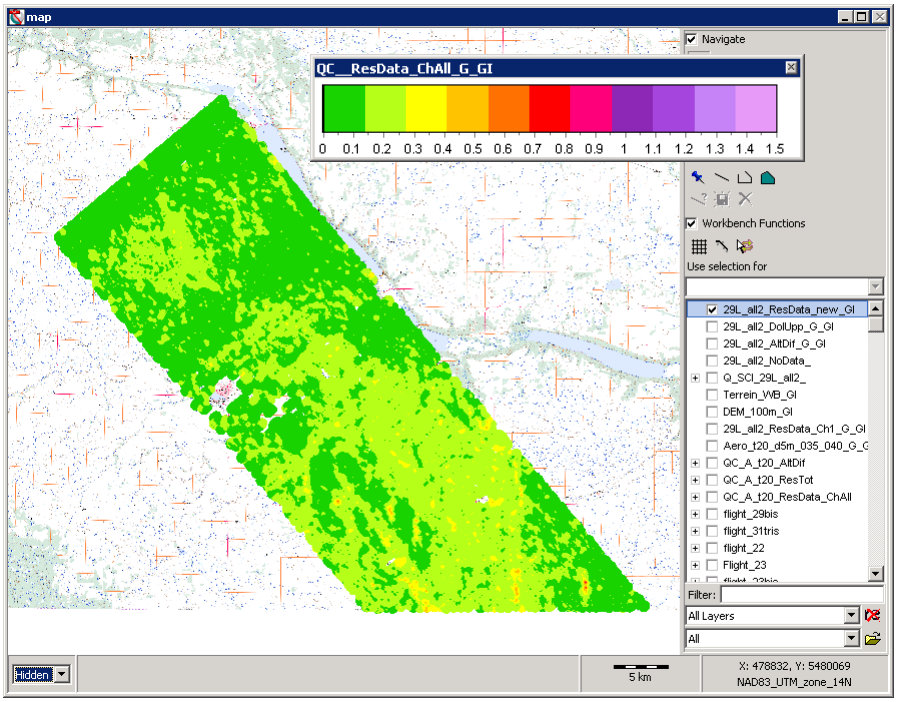
map
Navigate
QC__ResData_ChAll_G_GI
0 0.1 0.2 0.3 0.4 0.5 0.6 0.7 0.8 0.9 1 1.1 1.2 1.3 1.4 1.5
Workbench Functions
Use selection for
29L_all2_ResData_new_GI
29L_all2_DoIUpp_G_GI
29L_all2_AltDif_G_GI
29L_all2_NoData_
Q_SCI_29L_all2_
Terrein_WB_GI
DEM_100m_GI
29L_all2_ResData_Ch1_G_GI
Aero_t20_d5m_035_040_G_G
QC_A_t20_AltDif
QC_A_t20_ResTot
QC_A_t20_ResData_ChAll
flight_29bis
flight_31tris
flight_22
Flight_23
Filter:
All Layers
All
Hidden
5 km
X: 478832, Y: 5480069
NAD83_UTM_zone_14N

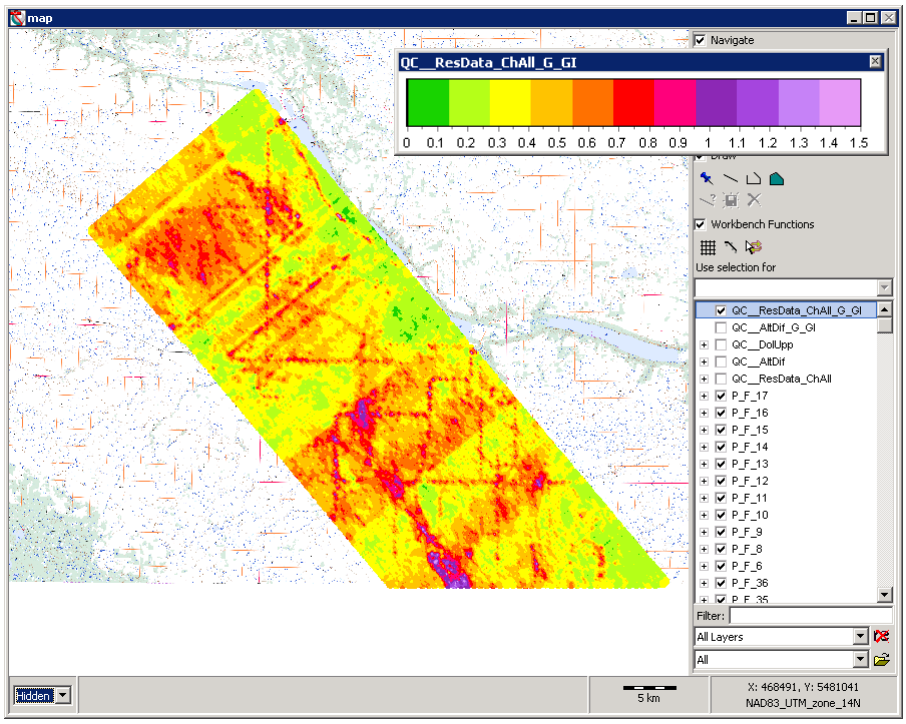
map
Navigate
QC__ResData_ChAll_G_GI
0 0.1 0.2 0.3 0.4 0.5 0.6 0.7 0.8 0.9 1 1.1 1.2 1.3 1.4 1.5
Workbench Functions
Use selection for
QC__ResData_ChAll_G_GI
QC__AltDif_G_GI
QC__DoIUpp
QC__AltDif
QC__ResData_ChAll
P_F_17
P_F_16
P_F_15
P_F_14
P_F_13
P_F_12
P_F_11
P_F_10
P_F_9
P_F_8
P_F_6
P_F_36
Filter:
All Layers
All
Hidden
5 km
X: 468491, Y: 5481041
NAD83_UTM_zone_14N

Map D

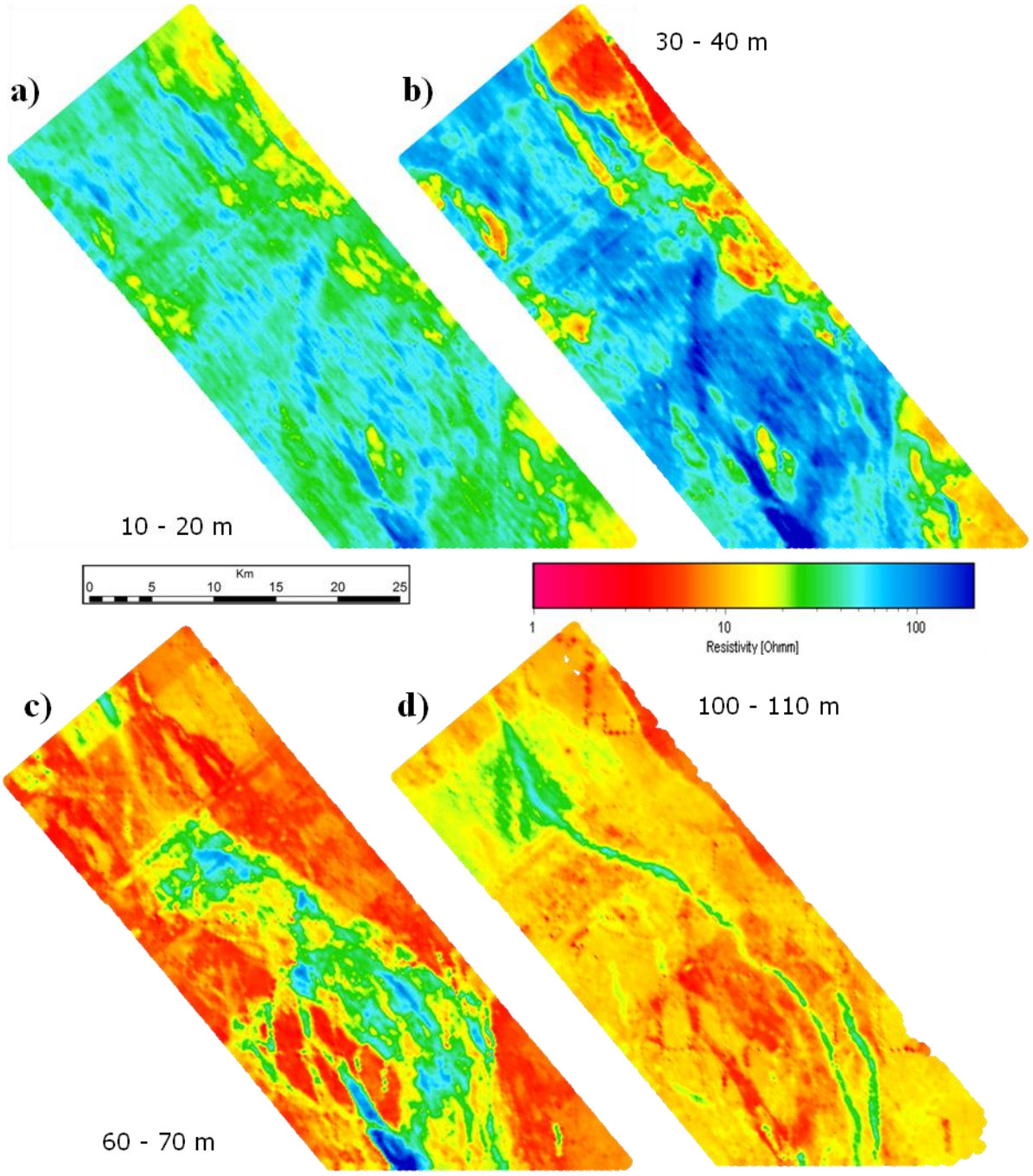
a)
b)
30 - 40 m
10 - 20 m
Km
0
5
10
15
20
25
1
10
100
Resistivity [Ohmm]
c)
d)
100 - 110 m
60 - 70 m

Map E

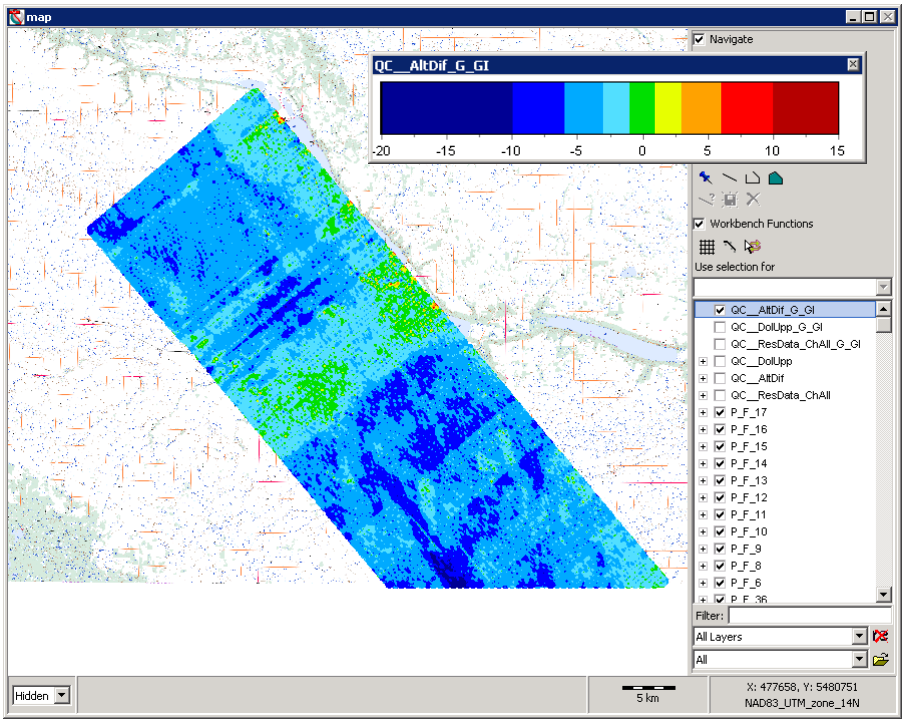
map
Navigate
QC__AltDif_G_GI
-20 -15 -10 -5 0 5 10 15
Workbench Functions
Use selection for
QC__AltDif_G_GI
QC__DolUpp_G_GI
QC__ResData_ChAll_G_GI
QC__DolUpp
QC__AltDif
QC__ResData_ChAll
P_F_17
P_F_16
P_F_15
P_F_14
P_F_13
P_F_12
P_F_11
P_F_10
P_F_9
P_F_8
P_F_6
Filter:
All Layers
All
Hidden
5 km
X: 477658, Y: 5480751
NAD83_UTM_zone_14N

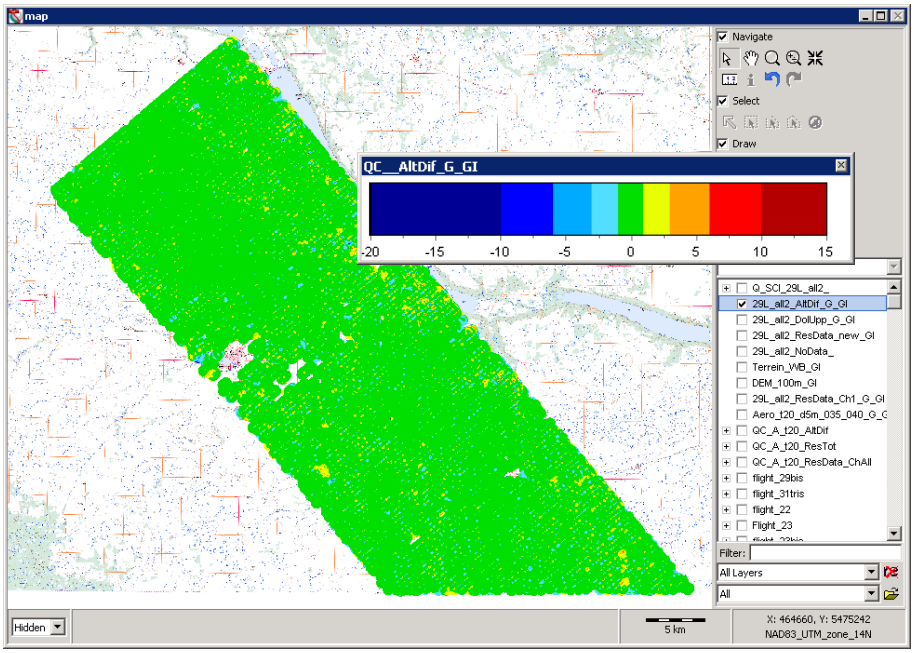
map
Navigate
Select
Draw
QC__AltDif_G_GI
-20 -15 -10 -5 0 5 10 15
Q_SCI_29L_all2_
29L_all2_AltDif_G_GI
29L_all2_DolUpp_G_GI
29L_all2_ResData_new_GI
29L_all2_NoData_
Terrein_WB_GI
DEM_100m_GI
29L_all2_ResData_Ch1_G_GI
QC_A_t20_AltDif
QC_A_t20_ResTot
QC_A_t20_ResData_ChAll
flight_29bis
flight_31tris
flight_22
Flight_23
Filter:
All Layers
All
Hidden
5 km
X: 464660, Y: 5475242
NAD83_UTM_zone_14N

Map F

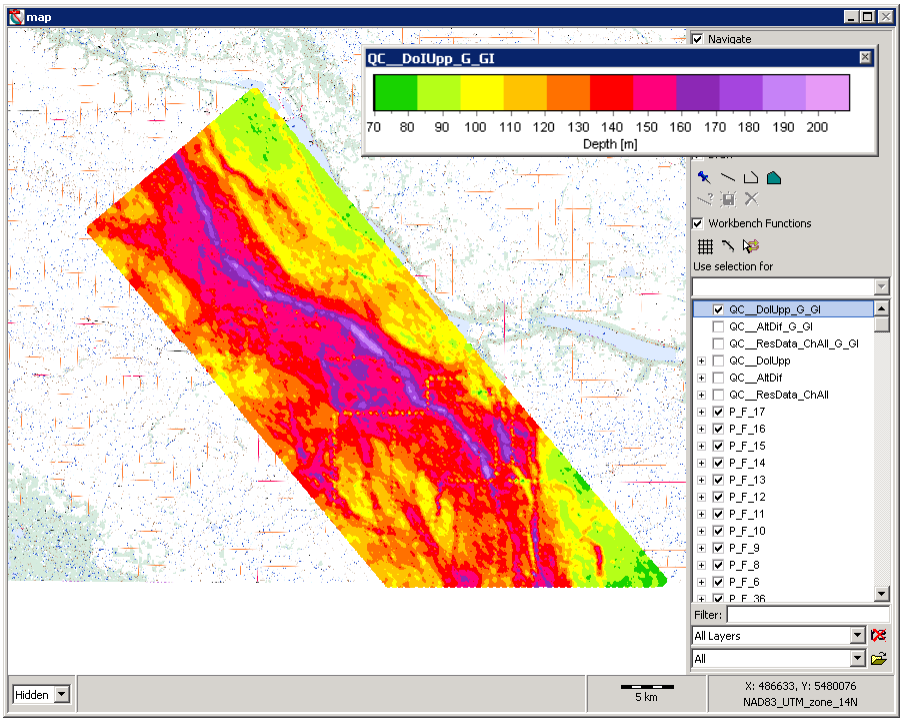
map
QC__DoIUpp_G_GI
70 80 90 100 110 120 130 140 150 160 170 180 190 200
Depth [m]
Navigate
Workbench Functions
Use selection for
QC__DoIUpp_G_GI
QC__AltDif_G_GI
QC__ResData_ChAll_G_GI
QC__DoIUpp
QC__AltDif
QC__ResData_ChAll
P_F_17
P_F_16
P_F_15
P_F_14
P_F_13
P_F_12
P_F_11
P_F_10
P_F_9
P_F_8
P_F_6
Filter:
All Layers
All
Hidden
5 km
X: 486633, Y: 5480076
NAD83_UTM_zone_14N

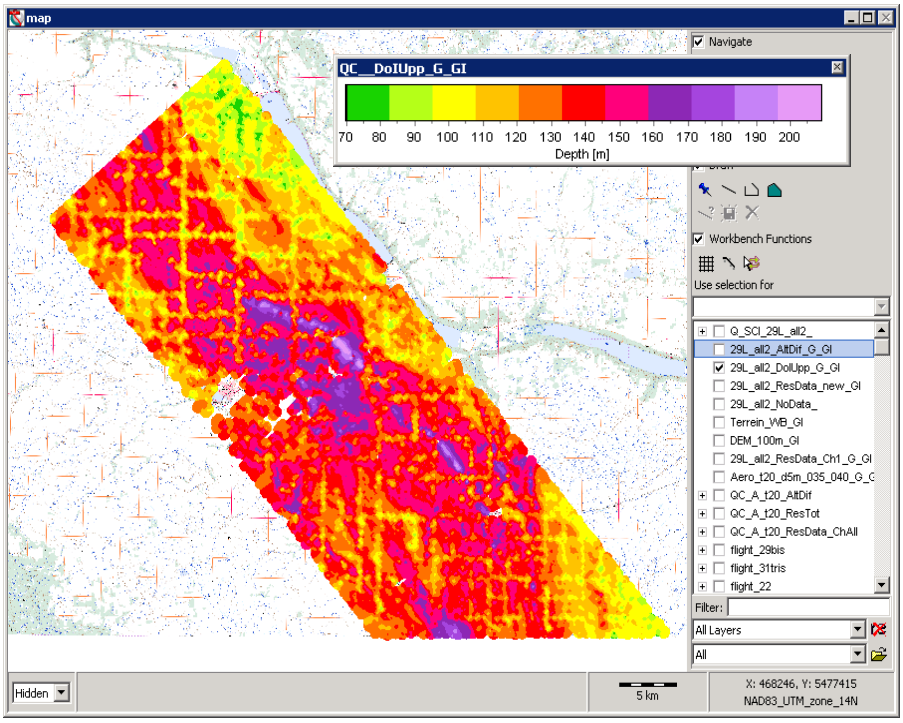
map
QC__DoIUpp_G_GI
70 80 90 100 110 120 130 140 150 160 170 180 190 200
Depth [m]
Navigate
Workbench Functions
Use selection for
Q_SCI_29L_all2_
29L_all2_AltDif_G_GI
29L_all2_DoIUpp_G_GI
29L_all2_ResData_new_GI
29L_all2_NoData_
Terrein_WB_GI
DEM_100m_GI
29L_all2_ResData_Ch1_G_GI
Aero_t20_d5m_035_040_G_G
QC_A_t20_AltDif
QC_A_t20_ResTot
QC_A_t20_ResData_ChAll
flight_29bis
flight_31tris
flight_22
Filter:
All Layers
All
Hidden
5 km
X: 468246, Y: 5477415
NAD83_UTM_zone_14N

Map G

References

Aarhus Geophysics, 2009, Aarhus Workbench. Available online at http://www.aarhusgeo.com/products/workbench.html (accessed 9 May, 2009).

Auken, E., Christiansen, A.V., Jacobsen, B. H., Foged, N., and Sørensen K. I. (2005), Piecewise 1D laterally constrained inversion of resistivity data, Geoph Prosp, 53, 497–506.

Auken, E., A. V., Christiansen, Westergaard, J.H., Kirkegaard, C., N., Foged, A., Viezzoli (2009), An integrated processing scheme for high-resolution airborne electromagnetic surveys, the SkyTEM system, Explor. Geophys., 2009, 40, 184–192, doi:10.1071/EG08128.

Balch S. J., W. P. Boyko and N. R., Paterson (2003), The AeroTEM airborne electromagnetic System, The Leading Edge, 22, 562-566.

Beamish, D., 2003. Airborne EM footprints. Geophysical Prospecting 51, 49–60.

Christiansen A.V., and E., Auken (2012), A global measure for depth of investigation, Geophysics, 77, 171-177, doi:10.1190/geo2011-0393.1.

Christiansen, A.V., E., Auken, and A., Viezzoli (2011), Quantification of modeling errors in airborne TEM caused by inaccurate system description, Geophysics, 76, 43-52, doi:10.1190/1.3511354.

Crow H.L., R.D., Knight, B.E., Medioli, M.J., Hinton, A., Plourde, A.J.-M., Pugin, K.D., Brewer, H.A.J., Russell and D.R., Sharpe (2012), Geological, hydrogeological, geophysical, and geochemistry data from a cored borehole in the Spiritwood buried valley, southwest Manitoba, Geological Survey of Canada, Open File 7079.

Danielsen, J. E., Auken, E., Jørgensen, F., Søndergaard, V. H., and Sørensen, K. I., (2003), The application of the transient electromagnetic method in hydrogeophysical surveys, J. of Appl. Geoph, 53, 181–198, doi: 10.1016/j.jappgeo.2003.08.004.

Groundwater Geoscience Program of the Geological Survey of Canada (2009-2014), http://ess.nrcan.gc.ca/gm-ces/index_e.php)

Jørgensen, F., and Sandersen, P.B.E., 2006, Buried and open tunnel valleys in Denmark – erosion beneath multiple ice sheets: Quaternary Science Reviews, 25, 1339-1363.

Klassen, R.W., and Wyder, J.E., 1970, Bedrock topography, buried valleys and nature of the drift, Virden map area, Manitoba. Geological Survey of Canada, Paper 70-56.

Legault, J. M., A., Prikhodko, D. J., Dodds, J. C., Macnae, G.A., Oldenborger (2012), Results of recent VTEM helicopter system development testing over the Spiritwood Valley aquifer, Manitoba, paper presented at 25th SAGEEP Symposium on the Application of Geophysics to Engineering and Environmental Problems, Tucson, Arizona, USA.

Loke M.H., I., Acworth, and T., Dahlin (2003). A comparison of smooth and blocky inversion methods in 2D electrical imaging surveys, Explor. Geophys., 34, 182–187, doi:10.1071/EG03182.

Macnae, J. C., Lamontagnei, Y., and West, G. F., (1984), Noise processing techniques for time-domain EM systems, Geophysics, 49, 934-948.

Nabighian M.N. 1979. Quasi-static transient response of a conducting half-space - An approximate representation. Geophysics 44, 1700–1705.

Oldenborger, G.A. (2010a), AeroTEM III Survey, Spiritwood Valley, Manitoba, parts of NTS 62G/3, 62G/4, Manitoba: In Geological Survey of Canada: Open File 6663.

Oldenborger, G.A. (2010b), AeroTEM III Survey, Spiritwood Valley, Manitoba, parts of NTS 62G/3, 62G/4, 62G/5, 62G/6, Manitoba. In Geological Survey of Canada: Open File 6664.

Oldenborger, G.A., A.J.-M., Pugin, and S.E., Pullan (2013), Airborne time-domain electromagnetics, electrical resistivity and seismic reflection for regional three-dimensional mapping and characterization of the Spiritwood Valley Aquifer, Manitoba, Canada, Near Surf. Geophys., 11, 63-74, doi:10.3997/1873-0604.2012023.

Pugin A.J.-M., Pullan S.E., Hinton M.J., Cartwright T., Douma M. and Burns R.A. 2009. Mapping buried valley aquifers in SW Manitoba using a vibrating source/landstreamer seismic reflection system, in Proceedings of the Symposium on the Application of Geophysics to

Engineering and Environmental Problems (SAGEEP'09), Fort Worth, Texas, USA, 29 March–1 April 2009, 586–595.

Pugin, A.J.-M., Pullan, S.E., Hunter, J.A., and Oldenborger, G.A., 2009b, Hydrogeological prospecting using P and S-wave landstreamer seismic reflection methods, Near Surf Geoph, 7, 315–327.

Reid J.E., and Vrbancich, J., (2004), A comparison of the inductive-limit footprints of airborne electromagnetic configurations, Geophysics, 69, 1229–1239.

Sørensen, K. I., and Auken, E., 2004, SkyTEM? A new high-resolution helicopter transient electromagnetic system, Expl Geoph, 35, 194–202. doi: 10.1071/EG04194.

Viezzoli, A., A.V., Christiansen, E., Auken, and K., Sørensen (2008), Quasi-3D modeling of airborne TEM data by spatially constrained inversion, Geophysics, 73, 105-113, doi:10.1190/1.2895521.

Watermark Consulting Ltd., 2004, Groundwater investigations, Southwestern Manitoba, Pierson, Tilston, Broomhill and Willen areas, WM124. Report to AAFC-Prairie Farm Rehabilitation Administration, Regina, Saskatchewan.

Wiecek, S., (2009), Municipality of Killarney, Turtle Mountain groundwater assessment study: W.L. Gibbons & Associates Inc.

Chapter 3

Investigate the role of a priori information into the inversion of AEM data: the case study of Spiritwood Valley Aquifer

Introduction

In this chapter we investigate the general assumption that data integration, or combination of several complimentary types of geophysical data collected over the same survey area, can improve inversions, reduce ambiguity and deliver high resolution results for the very near-surface.

Data integration is a loose term in the geophysical literature. Existing examples in literature where knowledge from high resolution reflection seismic data is used to improve airborne time-domain electromagnetic data inversion are few and far between. Joint interpretation of high resolution seismic data and AEM inversions have been performed to enhance AEM results by many authors with different levels of detail (Gabriel et al., 2003, Hoyer et al., 2011, Jorgensen et al., 2003c, Oldenborger et al., 2013). Such a pure comparison between different data results, in effort to support the geological interpretation, is not the same as to integrate data in one inversion process. Seismic and ERT data are usually performed independently, and no attempt has ever been made to integrate their results with AEM. Electrical resistivity tomography (ERT) results have been used to support AEM interpretations in a few case studies. For example, Hammack 2010 presented an example where electrical data contributes as "ground confirmation activities" which, in turn, support HEM survey interpretations and provide an accurate representation of the conductivity distribution within a coal-waste impoundments. Other examples come from Smith et al., 2011, for uranium deposits and Viezzoli et al., 2010 for coastland investigations. Example of ground follow-up geophysical surveys using DC geoelectrical methods were conducted in areas where significant conductivity anomalies were identified first by the airborne survey (Siemon et al., 2012). However, such comparisons of results from different survey types, in effort to support the geological interpretation, is not the same as integrating different data types in a single inversion process.

One interesting example of integration between seismic and AEM come from Burschil et al., 2012. The author present a study where picked horizons from several seismic lines give a-priori information to layer boundaries, leading new inversion output to more reliable resistivity-depth models of the subsurface. There are a number of concurring factors that promote the use of a priori information in inversion of geophysical data. The first one is probably the desire to cross check the geophysical derived model against ancillary information. The second is the inherent non uniqueness of the results of inversion of geophysical data, which is due to the fact that the problem is usually ill posed. The third is the ever higher level of accuracy of the output sought after by end users that, rightly so, demand results (either direct or derived) they can use directly for management. Last, but not least, is the drive to incorporate different physical parameters originating from different sources into one inversion problem, in order to derive directly, e.g., geological or hydrogeological models that fit all data sets at once. When we talk about ancillary information as other available set of data in the same survey area, there might be several ways of using this data as a priori to constrain the inversion. It's important to underline when a priori information can be applied as a reference data to guide AEM data modelling for example. This way of cross-check "a posteriori" of the two applied geophysical methods not only entails about the consistency between the two dataset, also determines a more robust inversion result perhaps reflecting better with the geological knowledge. For this purpose, electrical data have been used as a posteriori information to improve AEM inversion output by mean several processing step-adjustments.

Ground based data exist in the survey area and make it possible to provide some additional information on subsurface resistivity values. Over 10 line-km of electrical resistivity data were collected and supply a simplified electrical model relative to the geological layers. In this paper we also demonstrate how ancillary electrical resistivity data can be significantly used to "post-calibrate" AEM inversion results in order to obtain a reliable resistivity output model that match considerably better with electrical data, first, and knowed geology.

To add a-priori information to the AEM data, and to have it migrate throughout the dataset, we use the framework of the Spatially Constrained Inversion (SCI, Viezzoli et al., 2008). In the SCI the resistivity model is constrained spatially to make use of the inherent geological spatial coherency present, in different degrees, in every environment. These constraints represent, per se, a priori information, that are fitted, together with the AEM data, during the inversion. However, we now want to add a-priori, from seismic reflectors, into the inversion calculation, as a completely independent source of data. The a-priori information is treated as nothing but an extra data set, carrying location, values, uncertainty, and expected lateral variability. The information it contains is carried by the spatial constraints to the location of the neighbouring AEM soundings.

We examine the benefit of incorporating ancillary seismic data and ERT results into inversion of two helicopter time-domain electromagnetic (HTEM) data collected over the Spiritwood Valley Aquifer in Manitoba, Canada. Reflection surfaces picked from high-resolution seismic reflection data are used as a-priori information that defines layer depths in the inversion of HTEM data. This results in consistency between the data sets, but does not necessarily yield an inversion result that is in agreement with geological knowledge. To this end, we also incorporate a calibration of the HTEM data using ERT results as constraint information. This calibration is a pre-inversion processing step that involves applying small time shifts to data gates that are required to match the post-inversion HTEM and ERT resistivities. The result is a model that matches considerably better with ERT and known geology and a methodology that can be a applied to the entire survey area.

Survey area and methods

The Spiritwood Valley Aquifer is a Canada-USA trans-border buried valley aquifer that runs approximately NW–SE and extends 500 km from Manitoba, across North Dakota and into South Dakota (Winter et al., 1984). The Spiritwood aquifer system consists of glacially deposited silt and clay diamicton with sand and gravel bodies, infilling a broad north-south trending shale bedrock valley and a series of narrow incised buried valleys (Oldenborger et al., 2013). Numerous data sets

have been collected over the Spiritwood (Oldenborger, 2010a, 2010b; Crow et al., 2012) making it a good candidate for survey comparisons. To this end, In 2010, the Geological Survey of Canada conducted an airborne electromagnetic (AeroTEM III) survey over a 1062 km2 area along the Spiritwood Valley, north of the US border (Oldenborger 2010a; 2010b). During Fall, 2011, Geotech conducted a helicopter-borne geophysical survey over the same area chosen as a "test area" based on the availability of previous airborne EM (AeroTem survey), electrical and seismic data (Legault et al., 2013). VTEM data were collected over the Spiritwood using a newly-developed full waveform system designed for obtaining improved early-time data and shallow imaging capability (Legault et al., 2012). The VTEM survey consists of three separate blocks of closely spaced lines (300 m separation) that cover approximately 220 line km in regions of existing seismic, electrical and borehole data. As part of its Groundwater Geoscience Program, the Geological Survey of Canada (GSC) has been investigating buried valley aquifers in Canada using airborne and ground-based geophysical techniques. To obtain a regional three-dimensional assessment of complex aquifer geometries for the Spiritwood, both geophysical and geological investigations were performed with the aim to develop an integrated conceptual model for a quantitative description of the aquifer system.

As described in chapter 2, ground based data were collected in the Spiritwood area and make it possible to provide some constraints on the AEM resistivity model. Downhole resistivity logs were collected and provide information on the electrical model relative to the geological layers (Crow et al., 2012). In addition, over 10 line-km of electrical resistivity data and 42 km of high resolution landstreamer seismic reflection data were collected at selected sites (Oldenborger et al.,

2013). We focus on two profiles in the north and the south of the survey area (Figure 1).

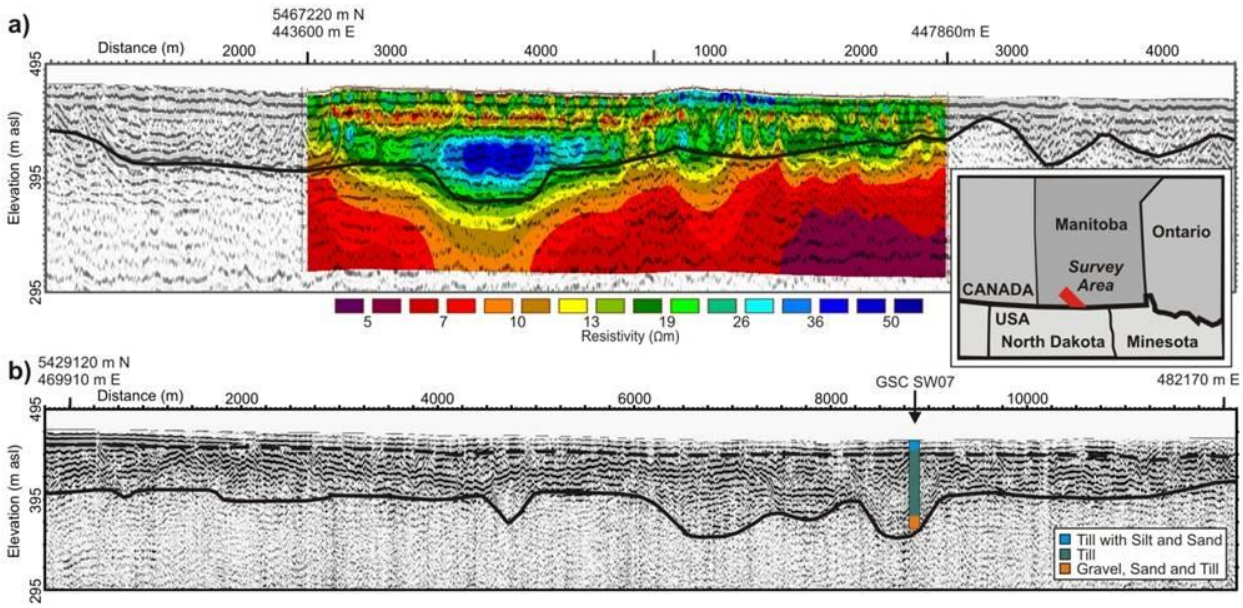

Figure 1.
Seismic and electrical data for the Spiritwood Valley aquifer. A) Northern profile S2007 with P-wave reflection section and ERT model. Solid black line represents interpreted bedrock reflection surface. b) Southern profile S1 with P-wave reflection section and cored borehole GSC-SW-07. Solid black line represents interpreted bedrock reflection surface; dashed black line represents interpreted inter-till reflection surface. Inset map shows survey location.

Section S2007 in the north has P-wave seismic reflection data and ERT data; section S1 in the south has P-wave reflection data and a cored borehole (Oldenborger et al., 2013; Crow et al; 2012). Structures observed in the seismic data include incised valleys cut into the shale bedrock to depths of about 100 m below ground surface. Two solid black lines identify the bedrock signature, as interpreted by seismic data processing, while the red dashed line represents another reflector attributed to a shallow inter-till reflection (Figure 1b, dashed black line).

Inversions of both HTEM dataset along S2007 and S1 are carried out using the quasi 3-D Spatially Constrained Inversion (SCI, Viezzoli et al., 2008). Prior to inversion, navigation data are filtered and averaged automatically, and manual corrections are applied to the altitude data if needed (see chapter 2 for details). Data are filtered for coupling or noise due to the presence of culture. Data are then averaged spatially using trapezoid filters of the optimum size that allow increasing signal to noise levels without compromising lateral resolution (*Auken et al*., 2009).

Soundings were taken each 1.5 s which corresponds to approximately 30m. During inversion, the flight altitude is treated as an inversion parameter and the depth of investigation (DOI) is calculated for the output models (*Christiansen et al*., 2012). The inversion is parameterized with 29 layers, each having a thickness logarithmically increasing down to a depth of 200m with an homogeneous half space of 40 Ωm as a starting model.

AeroTEM system

We remind to chapter 2 for a full and more detailed discussion about processing and inversion of AeroTEM data . Additional details of AeroTEM III system are described below. This system is based on a concentric-loop geometry with the receiver coils placed in the centre of the transmitter loop (Balch et al. 2003). A disadvantage of concentric coil systems is that the strong primary field present during the on-time can extend into the off-time as a high system transient and overpower the weaker secondary field. The AeroTEM system overcomes the primary field problem by means of a bucking coil that reduces the amplitude of the primary field at the Z-axis receiver coil greater than four orders of magnitude (Walker et al., 2008). Variations in the residual primary field are then removed from the Z-axis coil by a post-processing algorithm that includes deconvolution of the system's current waveform. The transmitter waveform is a triangular current pulse of 1.75 ms duration operating at a base frequency of 90 Hz. The use of a triangular rather than a square waveform energizes lower decay time-constants in the subsurface, which makes the system more responsive to high-conductance bodies (Sattel, 2009). The transmitter loop has an area of 78.5 m^2, with a maximum current of 480 A. The collected data consist of 17 variable width off-time gates with gates center approximately from 70 μs to 3 ms after time-off. Raw collected data are stacked, compensated, drift corrected and mircolevelled.

Inversion results

To visualize the existing resistivity structures in the survey area, a number of resistivity maps at different depth intervals are presented (see figures 23 of chapter 2). The smooth model enhances complex geological structures and is a powerful tool for evaluating the complexity of the

subsurface. The main Spiritwood Valley is readily apparent as a moderate conductivity feature set amongst a conductive background interpreted to be the response of the shale bedrock. In the centre of the main valley, we observe a resistive linear feature that is interpreted as an inset valley within the Spiritwood (Oldenborger et al., 2013). In general, most of the features observed in the SCI model are recovered without any a-priori information. The resistive signature of the incised valley is persistent with depth to over 100 m. In addition to the main and incised valleys, multiple valley-like features outside of the main valley are also observed. Furthermore, the models show the presence of resistive layers interpreted as interbedded sand and gravel above the shale in addition to resistive materials at the bottom of the main buried valley.

AeroTEM data: comparison with seismic 1 and seismic 2007

In the seismic data the main incised valleys appear to be filled with coarse-grained materials and cut into the bedrock to a depth of approximately 100 m below the ground surface (figures 2 and 3, a). The black line traces the bedrock surface (conductive shale) extrapolated from seismic processing data. Selected bedrock reflection values are interpolated as a grid and plotted on top of the SCI resistivity model to directly compare the two results.

Using the inversion results, the upper shale surface can clearly be identified as a conductive boundary overlaid with more resistive materials (figures 2, a and 3, b). The resistivity model also reveals that the main incised valleys are infilled with sand and gravels. A significant presence of inter-till sand is evident along S1 on the edge of the eastern buried valley and on the western side of the profile.

The AEM results overall agree closely with the seismic data regarding the depth of the conductive bedrock. However, in some areas the AEM results appear to overestimate the shale depth to some extent, and there is insufficient information from AEM data at the buried valley bottoms (figure 2b, from 6.3 to 9 km), where the seismic data instead reveals very marked reflections at that depth (see solid black line). The 2007 seismic data include a slight signature trace of a conductive layer lying somewhat deeper than the seismic bedrock reflector readings. It is

possible that the conductive bedrock of the buried valley base is deeper than the system's maximum depth capacity, or the overestimation of depth to bedrock might have other causes. Reflection surfaces are expressed in seismic data as changes in density and seismic velocity. However, the interface between sediment and bedrock might not be precisely defined as regards seismic parameters or electrical resistivity, and resistivity could vary gradually through the sediment to bedrock interface. Clearly there is a degree of ambiguity, making it difficult to correctly interpret the depth of a geological layer, especially in a smooth model.

A number of concurrent factors contribute to the result that the pre-processing and leveling of raw data by contractors, prior to actual data processing and inversion, induces significant lateral smoothing of the measured signal, especially at late time gates, masking the lateral variability of the geology in the data.

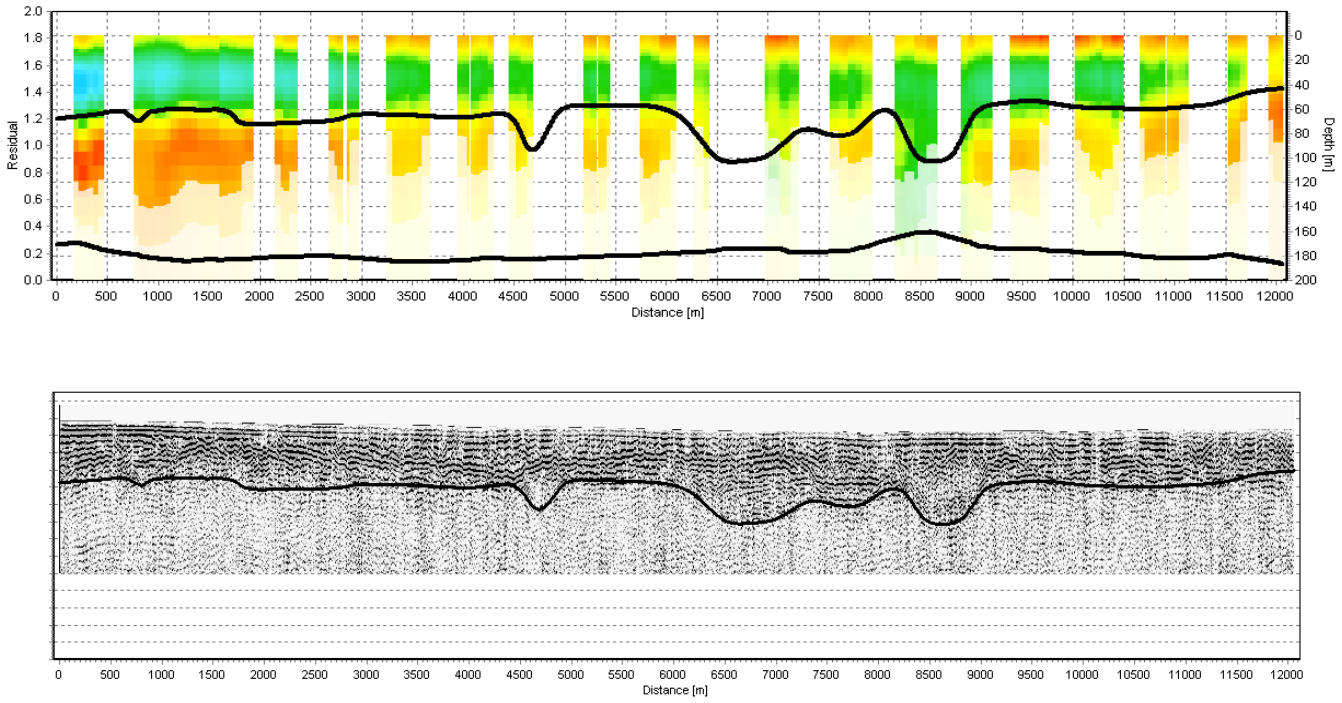

Figure 2.
a) S1 section and b) AEM inv results (no a priori..) along S1

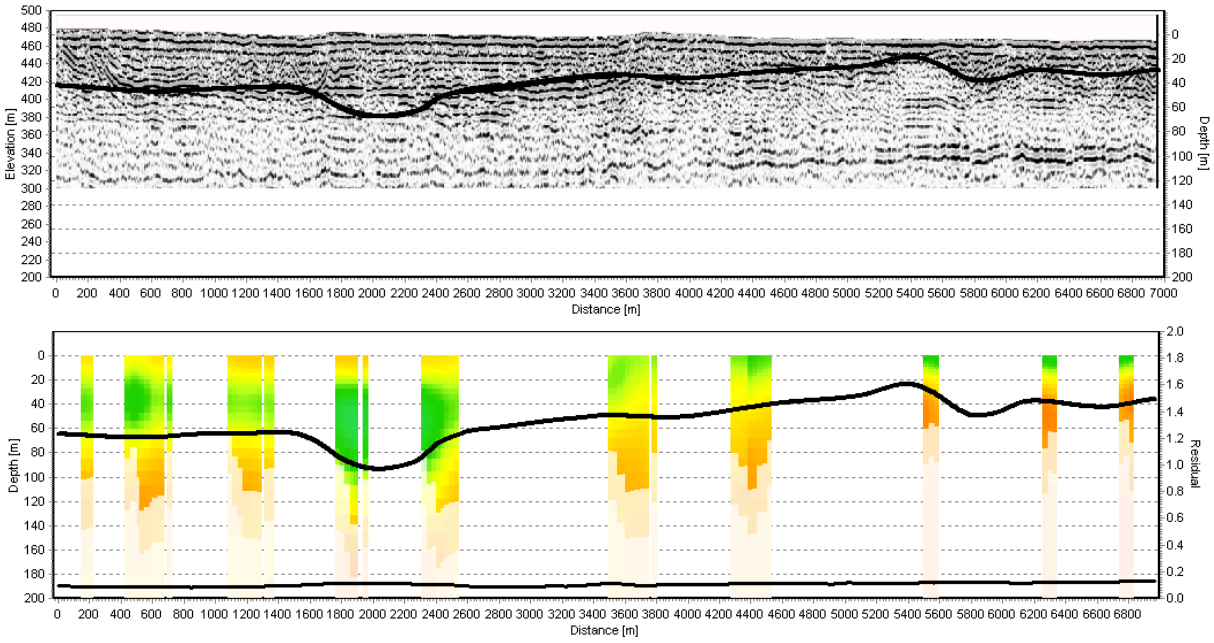

Figure 3.
S2007 section and b) AEM inv results (no a priori..) along S2007.

AeroTEM data: comparison with ERT

If the ground ERT and AeroTEM resistivity sections are compared in figure 4a and b respectively, is the ERT data that clearly exhibits high resistivity resolution, with the resistivities of the geological units changing across a very narrow range (5 to 45 Ohm-m). Both methods measure the subsurface electrical conductivity but the sample volumes and sensitivities differ significantly. The TEM method is an inductive technique with an investigation area dependent on the descending and expanding range of the transmitted current, typically 50 m by 50 m for ground TEM, more extensive for AEM. The resistivity method is a galvanic technique and samples a linear portion of terrain within the area of flow of an electrical current. High-resistivity structures are difficult to resolve using time domain electromagnetic methods, but are easily resolved using direct current methods. AEM is also highly sensitive to low-resistivity structures. An AEM spatially constrained inversion reveals the same resistive structures identified in an ERT electrical profile (figure 4a, b) with close correlation of the absolute resistivity values. The inverted AeroTEM data accurately define the resistive layer lying above the shale bedrock and below the more conductive layer of till in the higher sections of the inset valley. These resistivity features agree closely with ground ERT sounding readings.

The AeroTEM resistivity section provides clear definition of the uppermost conductive bedrock and as such compares favorably with the ground ERT and seismic results. However, the AEM system suffers from limitations in the resolution of the near surface (the first usable gate centers around 90 μs) and this compromises the level of near surface detail. As can be seen, the ERT data indicate a thin conductive layer, interpreted as an intra-clay till layer, with a highly resistive sub surface response (close to the Kilcart 8 borehole) while in contrast the AEM data exhibit no sensitivity to this variability in resistivity.

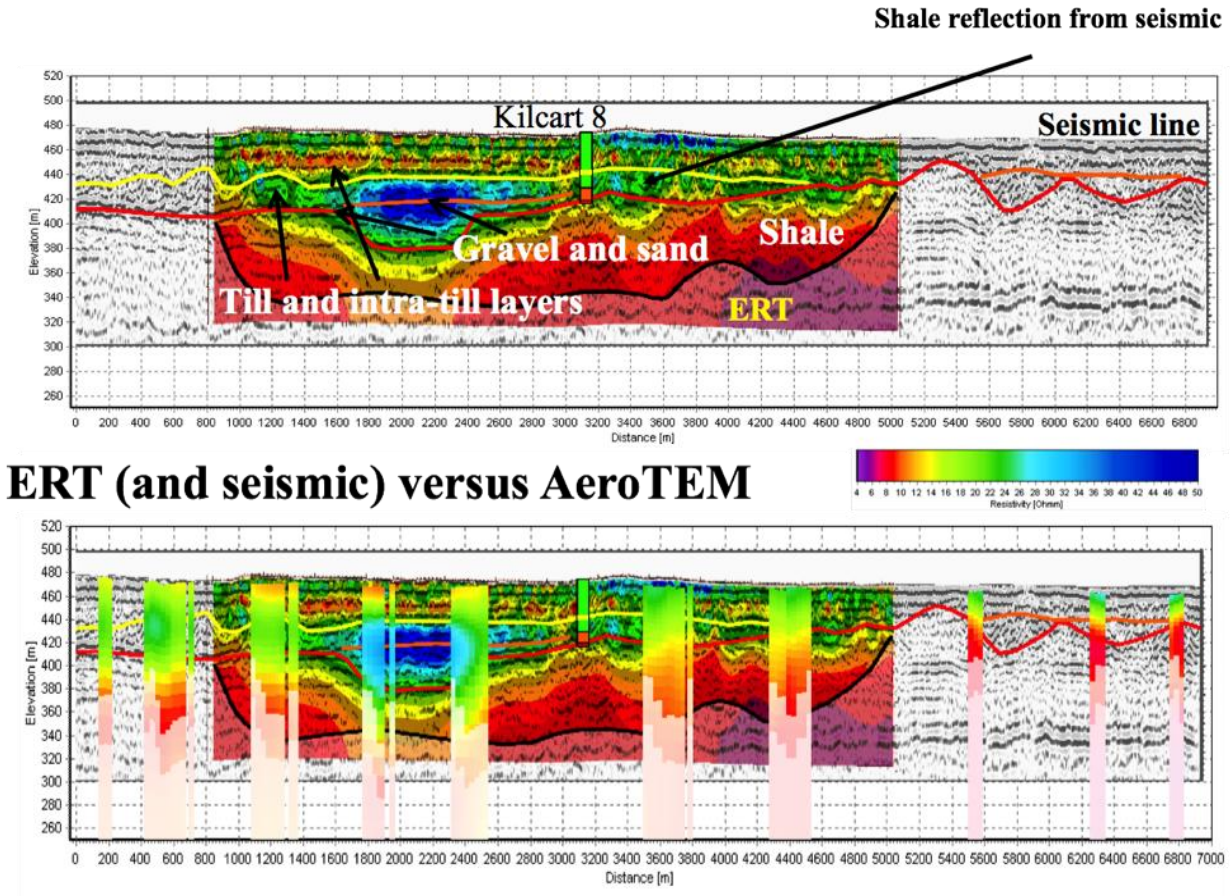

Figure 4.
Inverted resistivity models for ERI data acquired at the northern end of the survey area, compared to the seismic reflection data for line S2007.

AeroTem data: using the seismic as a priori data

The SCI formulations are integrated with a priori information as an additional data set, taking into account location, values, uncertainty, and expected lateral variability. Due to spatial constraints the a priori information is extended to the neighboring AEM sounding sites. For the

present purposes, the a priori information comprises seismic derived elevations of the conductive bedrock. It is integrated into the inversion as two parameters: 1) a grid of the bedrock surface elevations derived from seismic data (the shale basement), and 2) a resistivity value (together with standard deviation) for the bedrock elevations used. The seismic data were acquired along roads and so a large part of the data for the surroundings was removed due to coupling effects. The seismic data elevation grid was interpolated to a distance of 250 m in order to constrain the 1D models around the seismic lines. Histogram analysis of the relative frequency of values in the unconstrained smooth model (figure 5a and b) reveals a general bi-modal distribution (figure 5,c). The high resistivity peak is attributed to the valley fill materials (till), and the low resistivity peak is attributed to the more conductive shale bedrock. These values are applied as a guide for the SCI inversion with a priori data by applying resistivity values for the bedrock layer, but with differing standard deviations. It can be observed that the bedrock signature in the unconstrained AEM model exhibits a variable range of resistivity values along the seismic profile (see fig. 5a). The conductive shale bedrock appears to be markedly more conductive on the western and eastern sides compared to the central portion of the section. This indicates that 8 ohm m is the highest predicted data value, but is not a unique and ubiquitous bedrock resistivity signature value within the model space. In order to allow for this range of variability, an a priori resistivity value with two different associated standard deviation was applied, respectively 1.1 and 1.5 (representing 10% and 50% resistivity freedom).

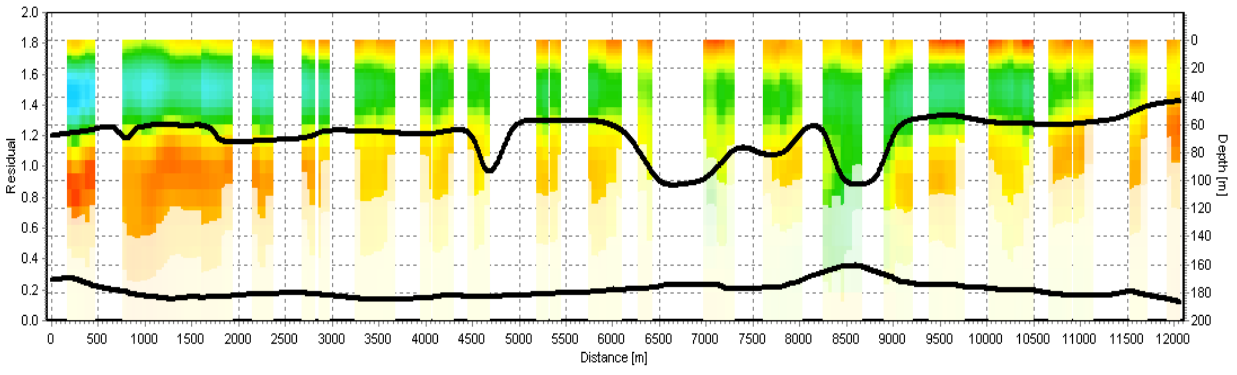

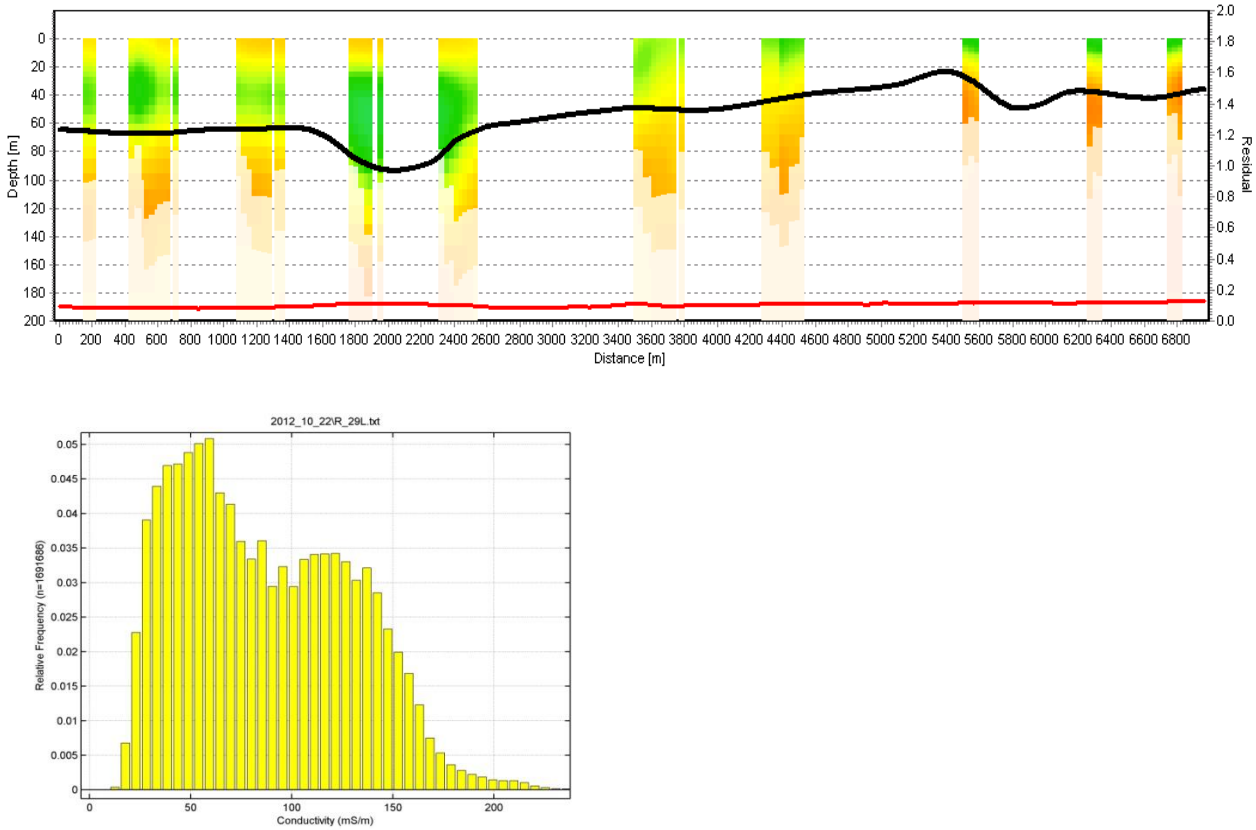

Figure 5.
SCI smooth results along a) s1, b) s2007. c) Histogram analysis. Units are in mS/m which corresponds to a factor of approximately 1000 to convert units to ohm m

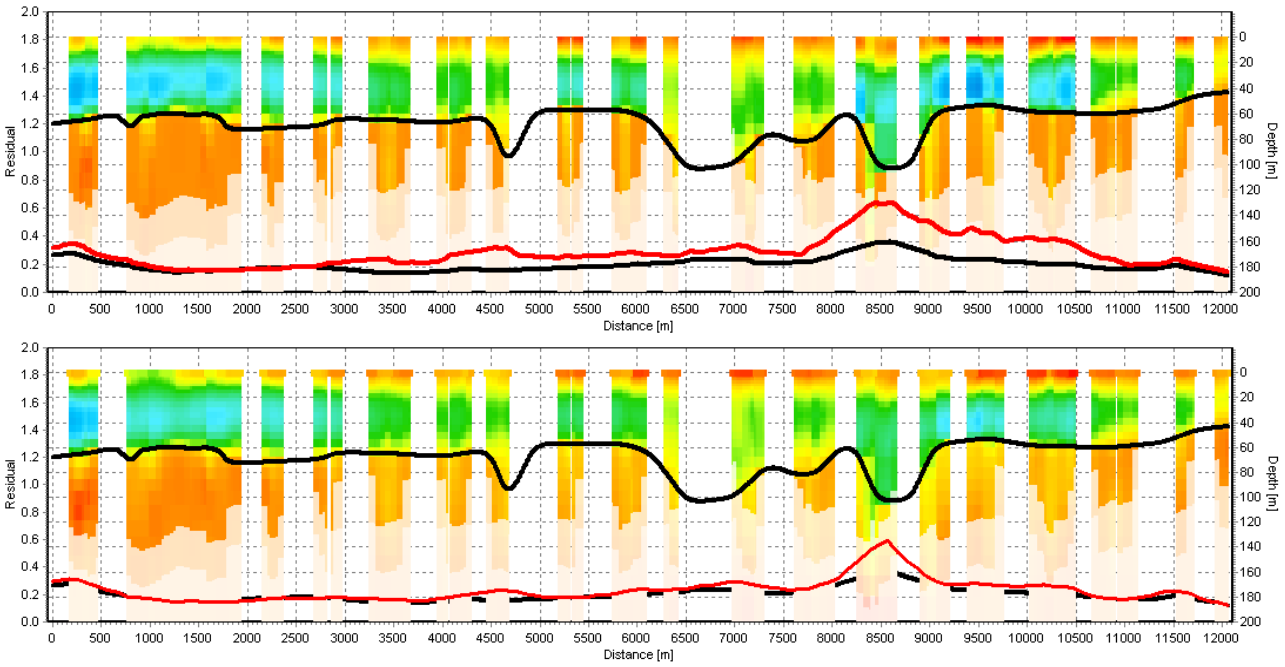

Figure 6.
AeroTEM inversion results a) with s1 as tight a priori with resistance value of 8 ohm m and 1.1 std, and b) s1 as tight a priori with resistance value of 8 ohm m and 1.5 std.

Another AEM data inversion was performed with the seismic data as “tight” a priori constraints (STD 1.1), which permits a maximum of 10% variability in inverted depth to bedrock. When 8 Ωm is used as bedrock resistivity with the same STD as the seismic depth to bedrock (figure 6 and 7 a), the residual is clearly higher than when applying 8 Ωm as the bedrock resistivity with associated standard deviation of 1.5. The misfit between forward modeled data and measured data represents the residual. It is also noticeable how the data residual remains low with the 1.5 STD a priori test, showing that this test does not conflict with the measured AEM data (figure 6 and 7 b).

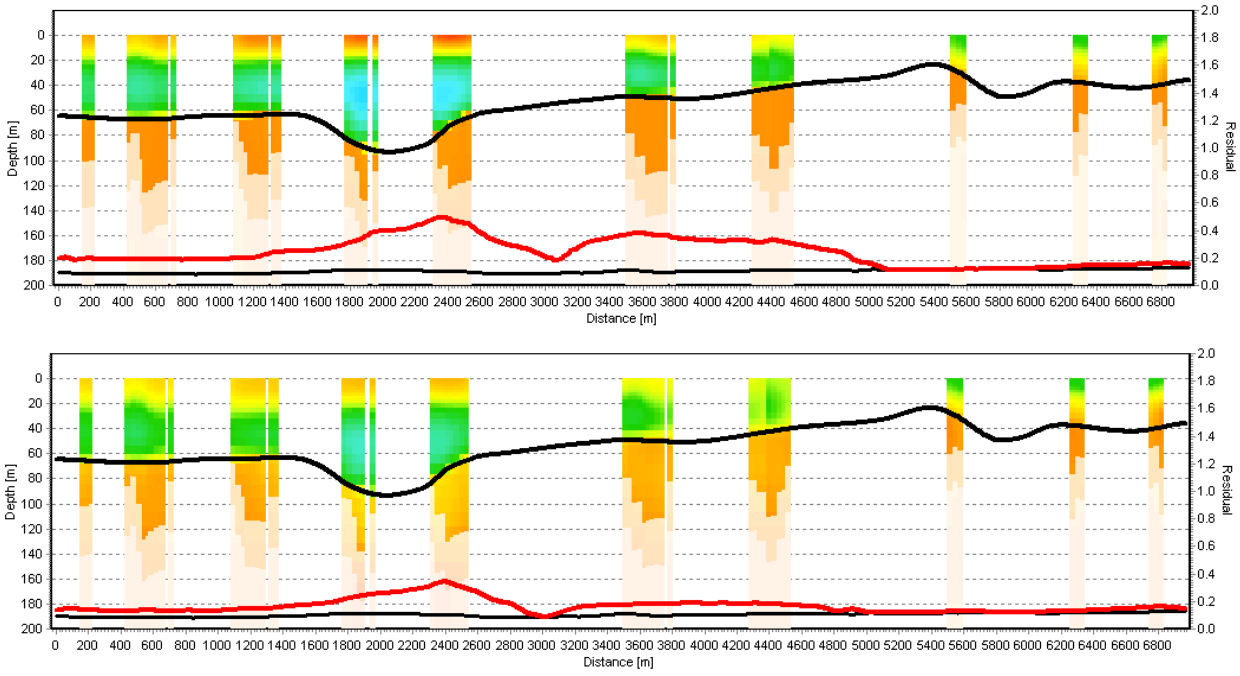

Figure 7.
AeroTEM inversion results a) with s2007 as tight a priori and resistivity value of 8 ohm m (1.1 std), and b) with s1 as tight a priori with resistance value of 8 ohm m and 1.5 std.

The seismic data defines the depth of the shale at the bottom of the BV down to the inversion, thereby reducing the number of unknown model parameters. This provides a general improvement in the sensitivity of the other model parameters, which applies both to parameters with added a priori data, and the overlying layers of higher resistivity relative to the model without a priori data. In addition, the inclusion of the seismic reflection depth to bedrock resulted in the conductive bedrock being more homogeneous and continuous, for a more structurally revealing geological result. In hydrogeological contexts like the present one, in which potential aquifers

appear to be relatively small and complex, an accurate picture of aquifer geometry is fundamental for groundwater resource mapping.

AeroTem data: using water wells as a priori data

In addition to seismic data, water well data was also used as a priori inversion information, in order to constrain the bedrock elevation. The water well data comprises an XYZ file listing bedrock contact points for each of the existing boreholes. The number of available boreholes is quite large, most having been drilled for agricultural, industrial, and domestic water supplies. However, not all the boreholes reach the shale bedrock and while they provide some information regarding sediments they cannot provide an absolute bedrock elevation value. Nevertheless, the sediments identified at the bottom of these boreholes could be used to establish a maximum bedrock elevation, in that the bedrock must occur somewhere below this elevation and not above it. For the purposes of the present study it was decided not to use this information to constrain the inversion because of the risk of seriously deteriorating the output model. Only boreholes that reached bedrock were used initially as a priori information to constrain the layer depth. This a priori information was integrated into the inversion as a grid of the bedrock surface elevation, and a resistivity value (with associated standard deviation) assigned to the elevations. The water well data are widely distributed (and not homogeneously spaced) over the survey area, and so the water well shale elevation grid required considerable interpolation, with a 5 km search radius (Figure 8a). Figure 8b shows the shale bedrock elevation derived from the unconstrained AEM data.

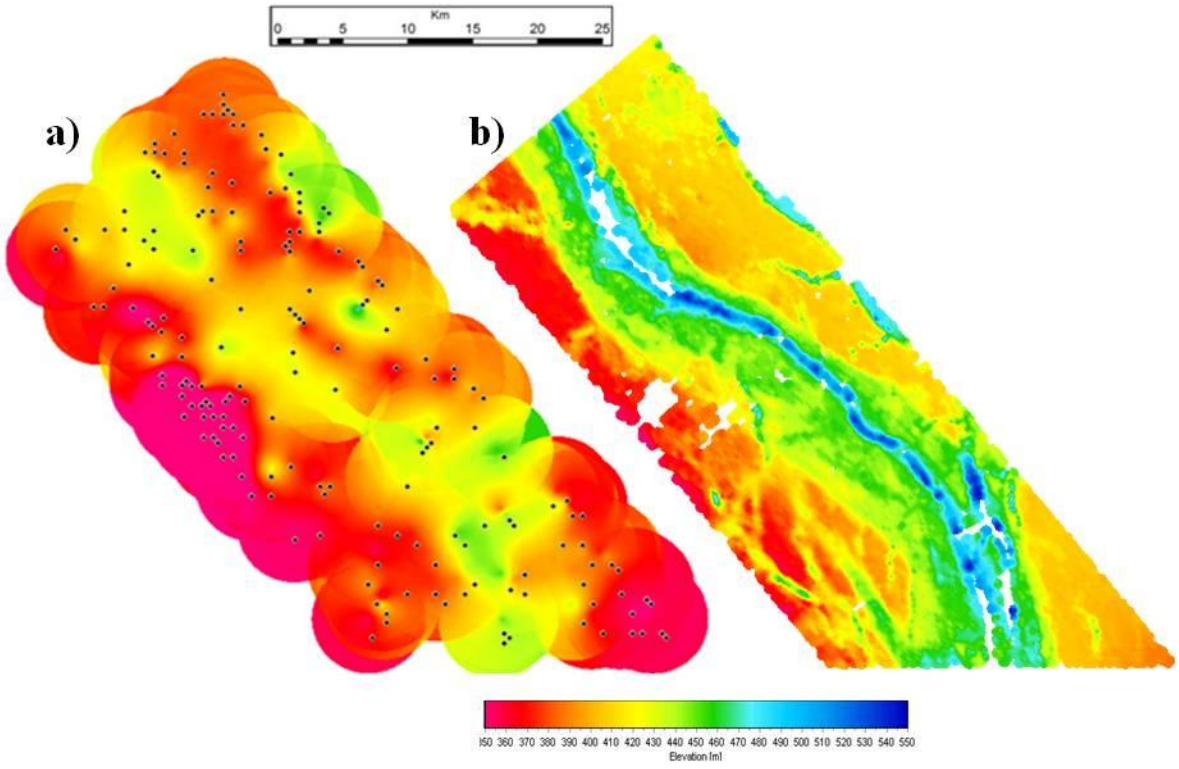

Figure 8.
Shale elevation surface derived from a) water well data, and b) AeroTEM data. The low density of the wells results in a limited estimation of the bedrock topography compared to the high resolution AEM data.

The resistivity value chosen for association to the grid was 8 Ωm with an assigned standard deviation of 1.5 (50 % variability across the model) on the basis of previous histogram analysis (as shown at the bottom of figure 5).

Figure 9 shows the results of smooth inversion using the water well bedrock elevations as a priori data. The correlation between the deepest conductor (i.e. shale bedrock) in AeroTEM inversion and the elevation to bedrock of boreholes is extremely low (as predicted). Using the a priori information dramatically smoothes the output resistivity model (fig. 9a compared to 9b, and figure 9c compared to 9d). The misfit is much greater compared to the unconstrained smooth model. This emerges again in two examples of soundings selected along the sections. The forward model is unable to fit the observed data from both the early and late time gates within the noise level (Fig. 9e compared to 9f). The water well data set must be carefully evaluated and interpreted before use. The spatial density of the wells is too low to characterize the lateral spatial structuring of the alluvial sediments and buried valleys. Consequently, another grid of bedrock elevation was

interpolated using a reduced search radius of 300 m. This eliminated all the problems caused by a large interpolation grid derived from low distribution data (boreholes) compared to the much higher AEM data density.

Further inversions were conducted using this new elevation grid as a priori data to constrain the bedrock layer. The new output resistivity model, based on both the smooth and the blocky inversion results from a flight line, are shown in Figure 10. If the unconstrained smooth model is compared with the well data, it is observed that some boreholes indicate the presence of shale bedrock, while the AEM model instead indicates the presence of a resistive body, interpreted as the infill materials of the buried valley, as can be seen in figure 10a, c. This becomes even more evident when this information is added as a priori data (Fig. 10b and 10d). The data residual clearly increases up to a value above 1. Forward models are unable to fit observed data within the noise level (figure 11, 12). Such a high misfit also suggests that this information contradicts the observed data. The interpretation of a specific layer in a borehole is affected by an uncertainty proportional to the quality of the borehole data in question, bearing in mind that these wells are not high-quality geotechnical boreholes. The stratigraphic logs are derived from the drillers' observations, and there is a risk of well-to-well inconsistency and observational errors.

However, even if the ancillary data is assumed to be reliable for the selected bedrock elevation values, another very serious problem affects the well data: *considerable uncertainty about their locations.* Incredibly, the true locations of the wells are not known! Furthermore, in a complex geological setting like Spiritwood Valley, including several narrow valley features, the use of imprecise water well observations as a priori data in order to better resolve these small structures is also conceptually wrong, considering that the water well locations have an uncertainty in the order of ±600 m. In the Spiritwood Valley Aquifer the inset valleys exhibit considerable spatial heterogeneity (particularly in the southern sector), which makes this a very problematic situation. Boreholes were found to indicate the top of the shale at a depth where instead the AEM data revealed a completely different bedrock depth, or some other structure (for example see figure 13).

If this issue was not addressed then numerous errors might have been induced in the output resistivity model. Several strategies were developed to improve the quality of the well data. First, all boreholes with high to very high stratigraphic description uncertainty (concentrating on bedrock detection) were eliminated from the database and so not considered as a-priori information. The shale bedrock is shallower and much more homogeneous in the eastern and the western parts of the survey area. Furthermore, the majority of the buried valleys lie within the main Spiritwood Valley, which runs approximately through the center of the survey area (figure 14, left panel). Using the previous inversion results with the a priori data (figure 10), the water well data was divided up according to position relative to the main Spiritwood Valley (figure 14, right). The boreholes located in the central portion of the survey area (the main Spiritwood Valley) were removed from the water well database. This eliminated the risk of introducing errors in the output models like those seen in figures 10 and 13. Two different grids with a search radius of 300 m were interpolated for the western and eastern portions of the survey area. In this way the ancillary information could be used as an independent data source and added into the inversion as separate a priori grids. Two grids were added as a priori information into a smooth inversion: 1) a bedrock elevation grid derived from data from water wells located on the eastern side of the survey area (1.5 STD and an assigned resistivity value of 8 Ωm relative to the predicted bedrock resistivity value), and 2) a bedrock elevation grid derived from data from water wells on the western side of the area (same settings for STD and resistivity). As a consequence, all the wells located within Spiritwood Valley were omitted from the database and not used as a priori information. Figure 15 shows the unconstrained smooth model in profile (see figure 16 for profile positioning). The bedrock elevations derived from water well data generally agree with the bedrock elevations obtained from AEM inversion results (only when data overlapped locally). This was further corroborated by the smooth inversion results using the water wells as a priori data (Figure 10b). The data residual remains low across the profile and does not increase when the a priori data were integrated into the

inversion, indicating that the data do not conflict. The smooth model's vertical resolution also increases when a priori data is added.

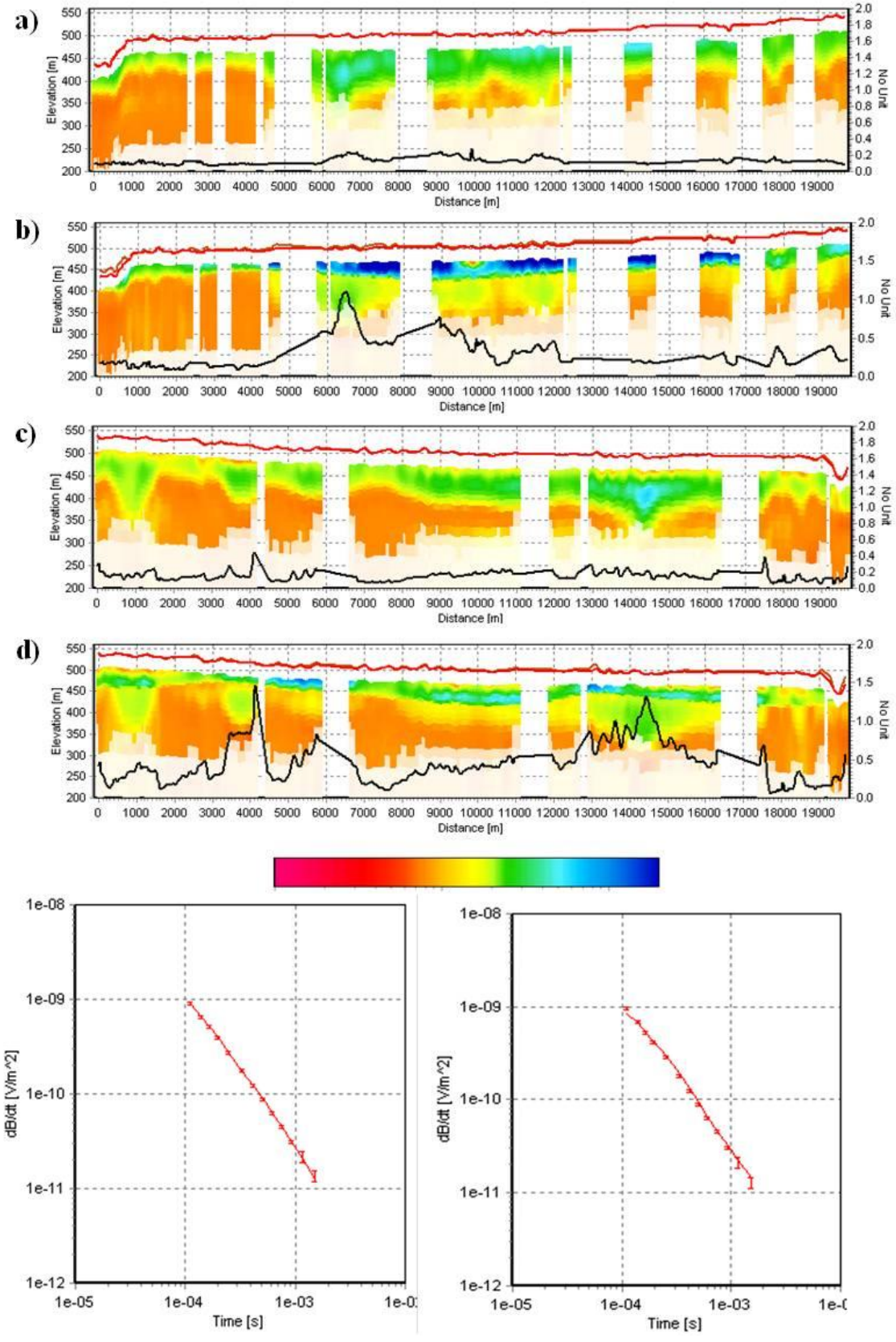

Figure 9.
Smooth inversion results respectively from the a,c) unconstrained smooth inversion, and b,d) constrained inversion, using a priori information (1.5 STD) derived from water wells. The forward responses of two selected soundings show the resulting data fit.

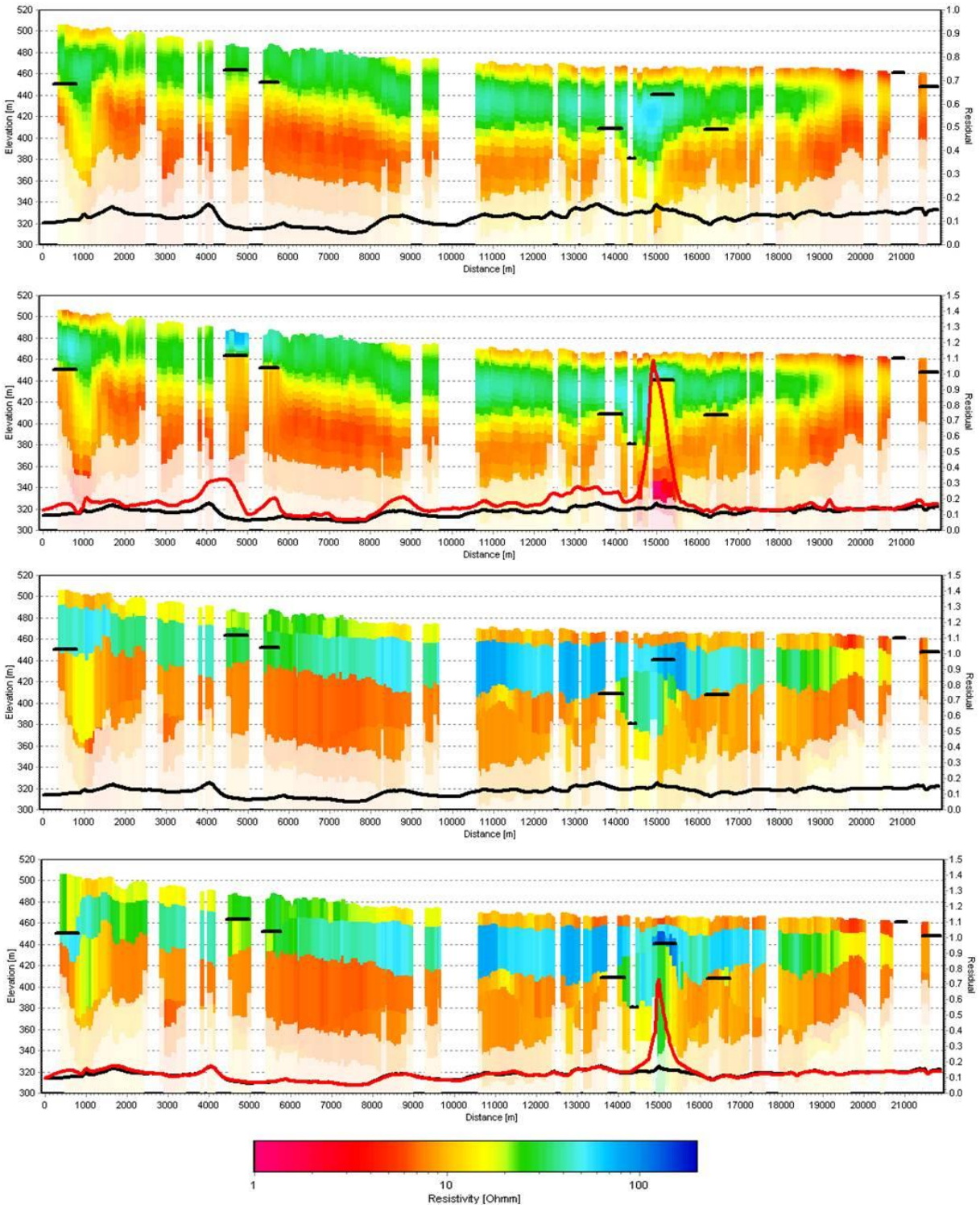

Figure 10.
a) Unconstrained smooth inversion results, and b) constrained smooth inversion results, using water wells as a priori data. c and d show respectively the unconstrained and constrained blocky inversion results. A significant increase in data residual is obvious in relation to certain water well data (particularly when the wells are close to **a buried valley**

structure), which explains the contrast between AEM and water well data, likely to result simply from inaccurate input coordinates on the map.

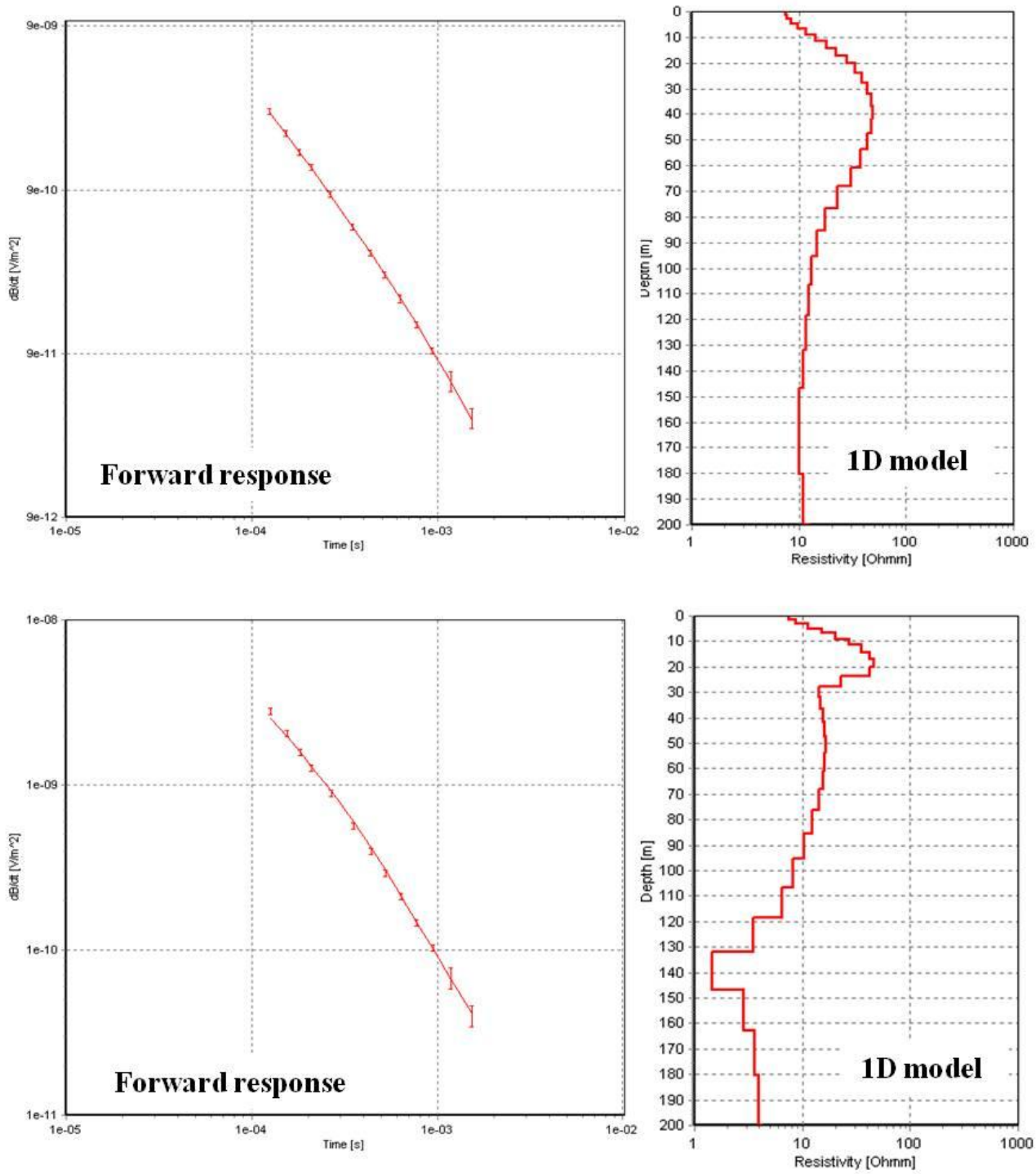

Figure 11.
Forward responses respectively for unconstrained smooth model (top) and constrained smooth model with water well data (bottom). The increase in data misfit in figure 10 is reflected in the forward response, which is unable to fit early time and late time gates (despite the increased noise level of the last two time gates).

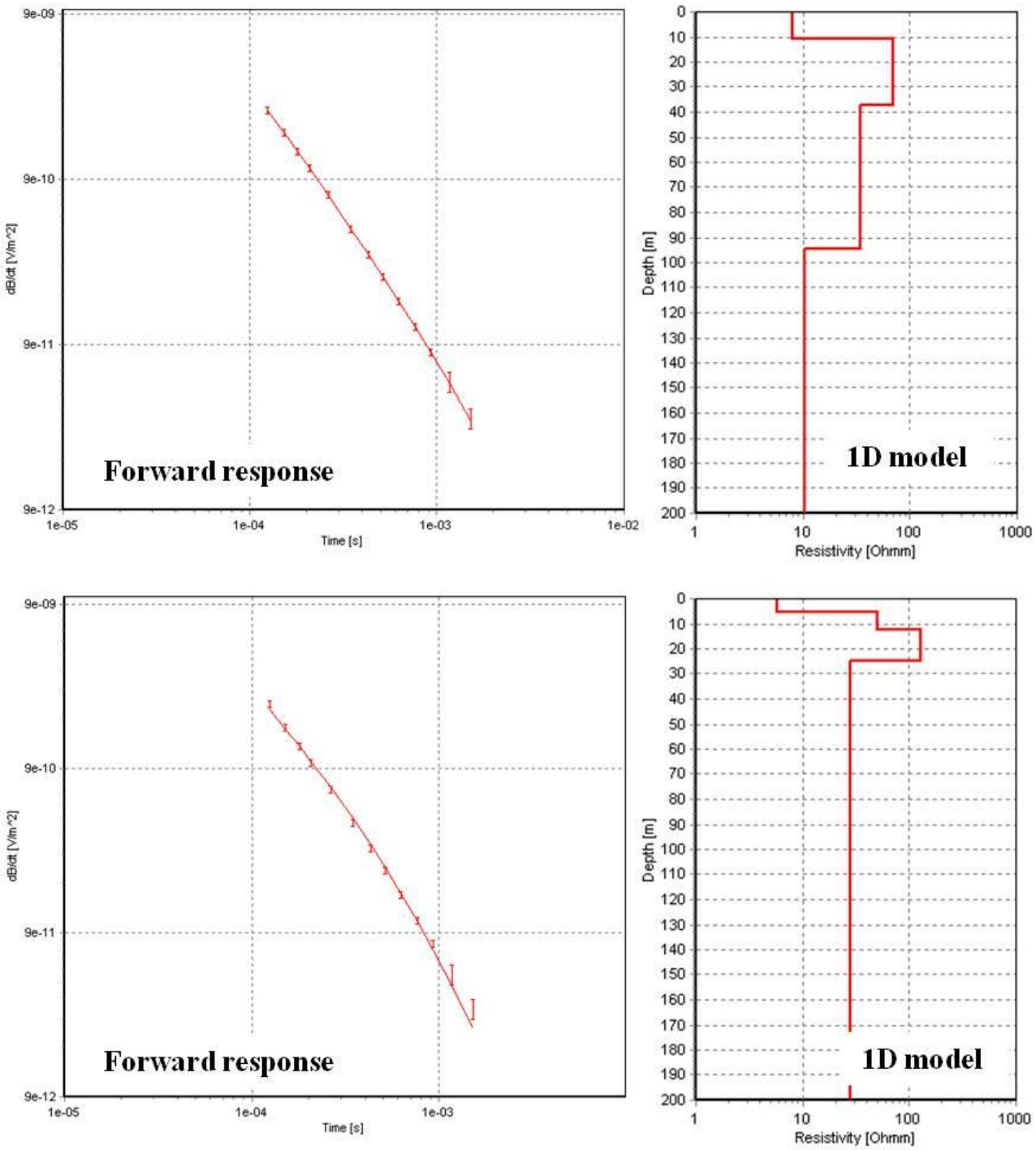

Figure 12.
Forward responses respectively for unconstrained blocky model (top) and constrained blocky model with water well data (bottom). The increase in data misfit in figure 10 is reflected in the forward response, which is unable to fit early time and late time gates (despite the increased noise level of the last two time gates).

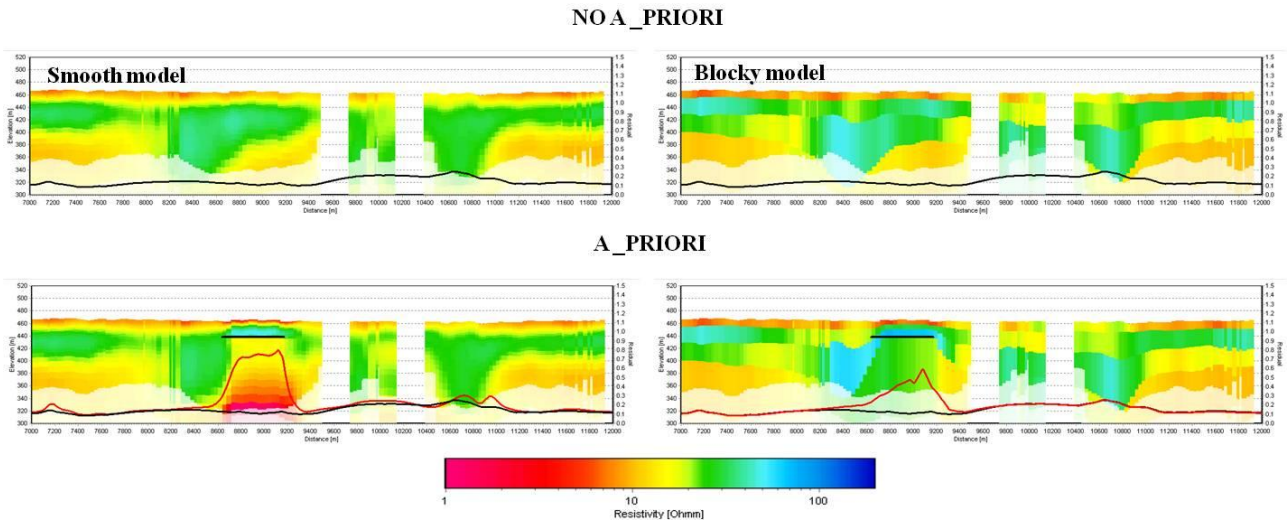

Figure 13.
Examples of a smooth and blocky inversion results without a priori (top) and with a priori (bottom) of a small portion of the Spiritwood Area close up to the two main buried valleys. The constrained inversion results clearly show the high contrast as well as the high inaccuracies of the water wells data as a priori information to constrain AEM data.

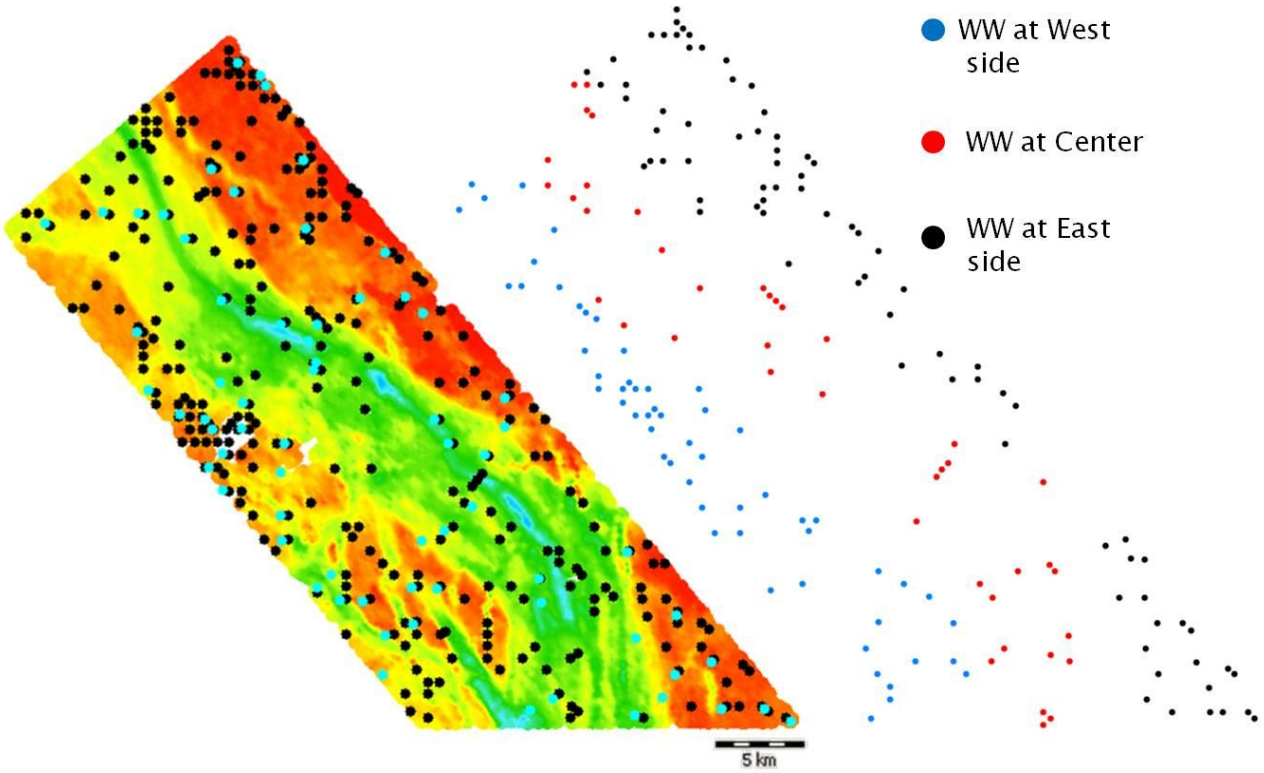

Figure 14.
New assessment of water well dataset (left) subdivided into three distinct areas in relation to their location in Spiritwood Valley (right). This subdivision reflect the main morphological form of the shale bedrock, which appears to be shallower in the eastern and western portions of the survey area and deeper in the central portion (due to the presence of Spiritwood valley set within the shale bedrock).

The resistive layer increases in resistivity as can be seen at the 1000 and 8500 m points along the profile. The boundary is well defined and sharper between the shale bedrock and the overlying resistive layers (assumed to be the till sequence). A few outliers remain in the water well data and at a distance of 11000 m along the section a well, added as a priori data into the smooth model, contradicts the AEM output model. This is also highlighted by a significant increase in data residual (Figure 10b). The misfit (data residual) increases significantly in relation to these "conflicting" a priori data throughout the survey area (figure 16).

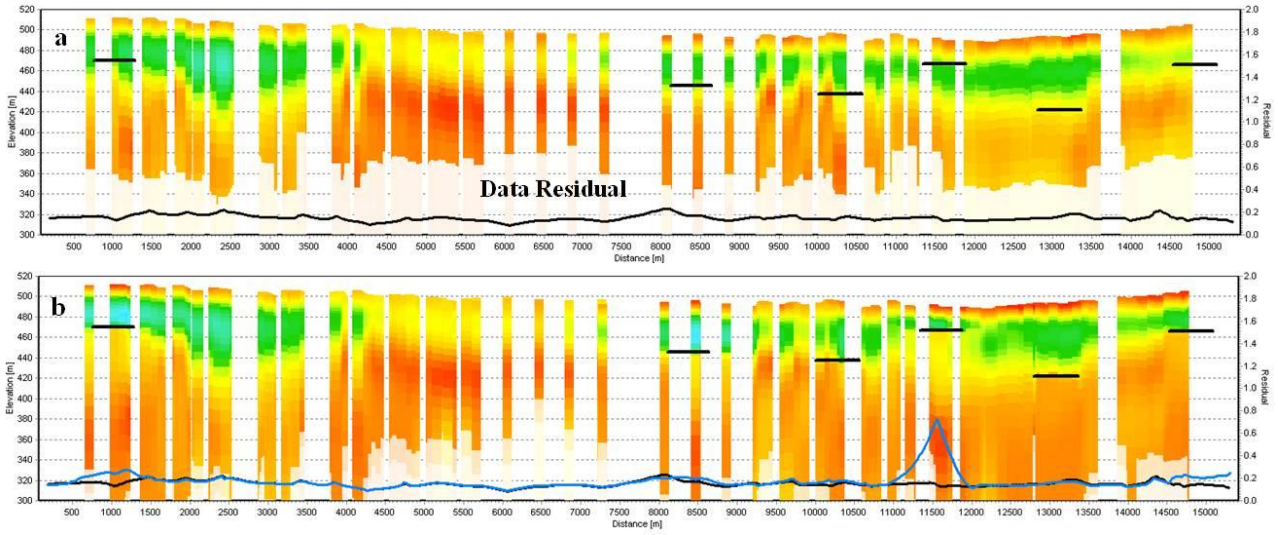

Figure 15.
Smooth inversion results without a priori data (top) and with updated water well data as a priori data in the inversion.

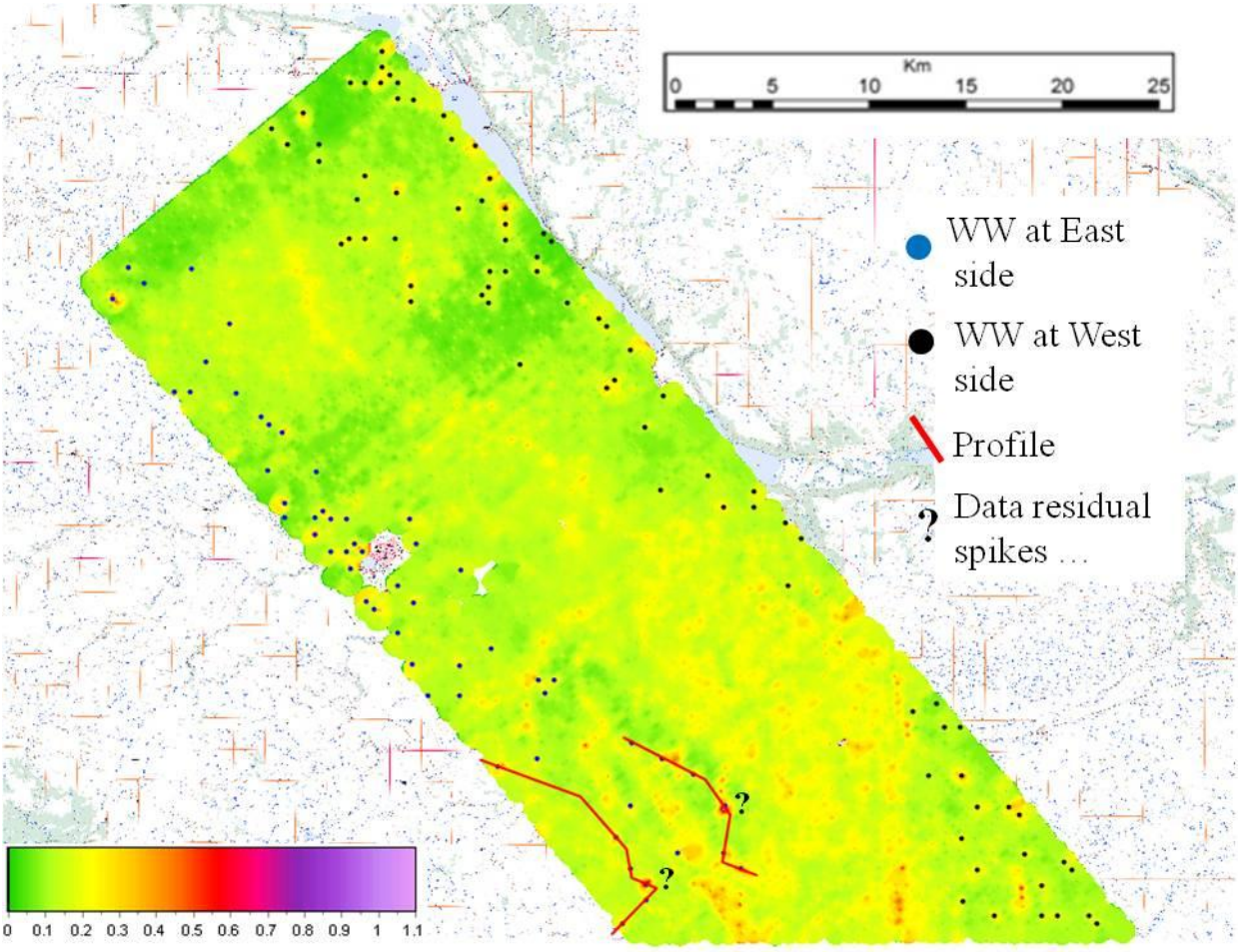

Figure 16.
Map of the data residual of the entire Spiritwood Valley area. It should be noted that in general data residual increases in relation to highly resistive shallow materials (in the central part of Spiritwood area). However, the persistence of a few outliers among the water well data also show up as high data residual (see question marks for examples).

General conclusion on AeroTEM results with a priori.

The Spiritwood AEM data show significant geological structures and clearly indicate a complex valley morphology that can be used to significantly improve geological and hydrogeological knowledge on a regional scale. Inversion results reveal multiple resistive valley features inside a wider, more conductive valley structure. Furthermore, the models show the presence of resistive layers interpreted as interbedded sand and gravel above the shale in addition to resistive materials at the bottom of the buried valley. Despite the early-time limitation of AeroTEM system and the fact that it is not designed for peak response over resistive materials such as those found in this survey area, the AeroTEM dataset provides rich information content in terms of lithological detail, identification and bedrock morphology. The Spiritwood AEM survey

successfully maps valley locations that continue to be difficult to define using seismic, electrical resistivity and borehole methods.

In general, most of the features observed in the SCI model are recovered without any a-priori information. However, adding a-priori information to the inversion in form of elevation to layers from seismic measurements can help increase resolution across a model of otherwise poorly determined parameters as well as return a better or more credible result in terms of expected geological setting. For the Spiritwood, inclusion of the depth to bedrock from seismic reflection data allowed the conductive basement layer to be more homogeneous and continuous providing a more structural geological result. Adding a-priori also reduced uncertainty in the resistivity values of the overlying layers which become more resistive although no a-priori information was added directly to those layers. Fidelity of electrical resistivity derived from the AEM inversion is of great importance when attempting to assess the hydrogeologic importance of geological units.

Focusing on water wells data, we found that the use of water wells information in addition to geophysical data is clearly complicated since the first often provide inaccurate information in terms of poorly described stratigraphy and due to the fact that their location is not correctly recorded. Therefore it makes them unusable and not comparable with the other available dataset in order to generate a reliable geological model. In addition, the lithological information contained in individual water wells ranges in quality, from highly detailed borings that can provide reliable information on both stratigraphic units and facies, to clearly erroneous records. This could be a problem since the goal of using a priori information directly from water wells data is to add a specific lithological layer (in terms of depth or elevation) to constrain the bedrock response derived from AEM model. Hence, if the lithological description at some borehole is wrong (or highly inaccurate) then it'll strongly affect the output resistivity model as well! As matter of the fact, huge editing of water wells data has been performed in order to remove those water wells of a low quality. In addition, subdividing the water wells database in 3 different part we also mitigate for those boreholes that are wrongly located, mainly in areas where several buried valleys occur.

Therefore, it was decided to use only those water wells information located in areas where the bedrock is more homogeneous and less articulated. Despite water wells editing, the main issue related to the wrong coordinates of each single water well is still an unresolved problem (figure 15b). Therefore, we assume that those particular water wells have to be removed from the database and they can't be used as a priori information to constrain bedrock layer. We also claim that the data residual map can also be potentially used as guide to visualize the water wells which completely disagree with AEM data in order to remove them (figure 16). It also means that the AEM data could be used, in this particular case, as a means to evaluate the reliability (or not) of the water wells data at Spiritwood Valley area. It has to be noted also how water wells data and AEM data considerably differ in terms of spatial distribution and lateral resolution (see also figure 8a and 8b). It is always a challenge to integrate such different set of data for every purposes, i.e geological and hydrogeological mapping. AEM data provide high data density (in the order of 1 soundings each 30m) to support high resolution hydrogeological mapping at large scale (regional scale). On the contrary, water wells data can be part of a large databases (hundreds of water wells data) but sparse information With this simple, yet rigorous, example we demonstrated the importance of determining the reliability of a given ancillary data before integrating it as a priori information into AEM data. Geological Surveys around the globe (like GSC), Universities, etc .. often have large databases of water wells data. We claim for a careful and scrupulous analysis when dealing with this specific source of data, particularly when the goal is to use those information to constrain other data sources for hydrogeological mapping, etcc A priori information, per se, should be used to improve the degree of accuracy and resolution of a predicted model. As matter of the fact, inaccurate a priori information give rise to a model with many uncertainties!!

VTEM system

The helicopter-borne Versatile Time Domain Electromagnetic (VTEM) system (Witherly et al., 2004; Witherly and Irvine, 2006) has been in continuous development since its inception in 2002. In an effort to improve the shallow imaging capability of the VTEM helicopter EM system, by obtaining the most accurate early-time data possible, a full waveform system has been developed (Legault et al., 2012) and tested (Legault et al., 2012, 2013) over the Spiritwood Valley Aquifer. At Spiritwood, system configuration consists of 3 axis induction EM receiver coils (with Z as vertical axis) deployed in the middle of the transmitter coil. Transmitter loop has a 26 m diameter, 4 turn and a peak current of 250 A that produced over 531,000 NIA of dipole-moment. The VTEM transmitter pulse shape is trapezoidal with a base frequency of 30 Hz and nominal 4.073 ms pulse width; data recording rates at output were 0.1 second. Forty-four time measurement gates were used for the final data in the range of 0.018–9.977 ms. Results of the Full waveform VTEM surveys have led to improved accuracy of transient data at earlier times than previously achieved - as early as ~20 μs after the current turn-off (versus ~100 μs for standard VTEM) and as late as ~10 ms as early as 18 μs after the current turn-off and as late as 9.977 ms.

The receiving secondary EM signal comprises effects of induction, capacitive leakage and band-pass filtering applied through the receiver. All these factors distort early time (after the primary field turn – off) TEM data and make it inapplicable. The Full Waveform technology consists of a combination of streamed half-cycle recording of transmitter and receiver waveform data, as well as continuous system calibration and parasitic-noise and transmitter-drift corrections (Legault et al., 2012, Prikhodko et al., 2013). Pre-processing included streamed half-cycle system calibration, drift corrections, parasitic noise corrections and ideal waveform deconvolution (*Macnae and Baron-Hay*, 2010). Deconvolution is a procedure that corrects one complete period for linear system imperfections including transmitter current drift. After calibration and deconvolution, digital filtering was used to reject major sferic events and to reduce noise levels.

Modelling of VTEM data

Despite drift corrections, waveform deconvolution, parasitic-noise removal, minor calibration issues are observable in the earliest time gates of the data. This can be attributed to a number of reasons, from small hardware (e.g, small primary filed left in the data), to data modeling (e.g, use of a transfer function for the forward response of the AEM system that does not represent the actual one), and their combination. Christiansen et al., (2011) describe in detail the effect of inaccurate modeling of the system transfer function in model space. Errors in the description of the transfer function influence the inverted model differently both at the early and late time; the output model can differ quite dramatically from the true model the measured data are sometimes not fit within the noise level. After preliminary inversion, the first two gates appeared inconsistent with expected forward responses and resulted in a strong, unexpected persistent conductor at the surface of the model (Figure 17). The results hinted at the fact that there was too much signal in the early times in the measured transient. Therefore, the first two gates (with gate centers earlier than 30 μs) were omitted from all subsequent inversions, early-time noise levels were increased to 20%, and the starting model has been modified to be resistive to a depth of 10 m. Things get better increasing noise level and applying a-priori information to the near surface layers. In addition to other issues (small current leaks, small primary field effect left, possibly small inaccuracies in the modeling of other high frequency effects), part of the problem that leads to extra signal in the early times can also be the degree in subjectivity embedded in choosing to use the end of ramp as time reference for the Rx gates (ref..Christiansen et al., 2011).

VTEM results with a priori: s2007

As mentioned above, using all measured off time gates results to an inconsistent output model according to ancillary electrical data. In particular, VTEM data overestimate the conductivity of the near surface layers. Things point toward the idea to remove first two gates and, farther, force the shallower layers of the smooth model to be resistive. Therefore, the starting model has been modified up to a depth of 10m to be resistive. Moreover, by increase noise level (20% error bars

respect to a standard of 5%) at early time allowed forward model to fit of the observed data at the price of a lower convergence which directly results in loss of shallower resolution in the predicted data. In general, the VTEM result shows good agreement with the S2007 information in terms of depth of the conductive shale bedrock (Figure 17a). However, in some areas, the SCI overestimates the depth of the shale. According to ground DC data, VTEM model clearly resolves the resistive body filling the incised valley as well as the conductive shale bedrock, but remarkable discrepancies lies primarily at surface level (figure 17a). To directly add the seismic data to the inversion, we use the SCI framework for which constraints represent a-priori information that are fit together with the AEM data during the inversion. The seismic data are used as a source of ancillary information on the elevation of the conductive bedrock. As for AeroTEM example before, the a-priori constraints include a resistivity value (and standard deviation) associated with the bedrock layer. Simple frequency histogram analysis of the unconstrained model indicates a peak resistivity of approximately 7 Ωm which we assign to the bedrock layer along with a factor of 1.5 standard deviation. Since the seismic data were acquired along roads, much of the surrounding data have been removed because of coupling effects. In order to constrain the 1D models around the seismic lines, the grid related to the seismic data elevation has been interpolated to a distance of 250 m. Constrained inversion results are shown in Figure 17b. The data residual (mean squared difference, weighed against noise level) doubles, but remains well within the gate dependent noise level associated to the soundings (i.e., below the value of 1), indicating that the a –priori information are consistent with the observations. We see that the bedrock contact is sharper and a resistive surface layer is more apparent. However, the very near surface structure still has a level of inconsistency with the ERT (Figure 17c). In particular, the first transition from resistive to conductive occurs at too shallow a depth and the incised valley fill is not a as well-distinguished from the surrounding overburden. Despite increased noise level at first 5 gates, when we examine the soundings, we see that the predicted data are consistently lower than the observed data for times less than approximately 80 μs (Figure 17d). As affect of the a-priori, the inset channel (sets amongst the

conductive bedrock) is better defined while the resistive body, filling the valley, appears as elongated higher resistive feature throughout the profile.

In the ground DC resistivity data there is a localized conductive feature at depth of 15m below the surface corresponding to embedded hard clay-till in the diamicton sequence. This is also seen in the VTEM data and is resolved much more sharply with depth to layer clearly shallower respect to ERT data. Although constrained inversion hints to a resistive surface layer (which is consistent with ERT), VTEM results seems to underestimate the depth of this layer which appear to be about 10 m off respect to electrical data (Figure 17c). The reasons for this discrepancy can be many, but should not be the lack of sensitivity of this AEM system.

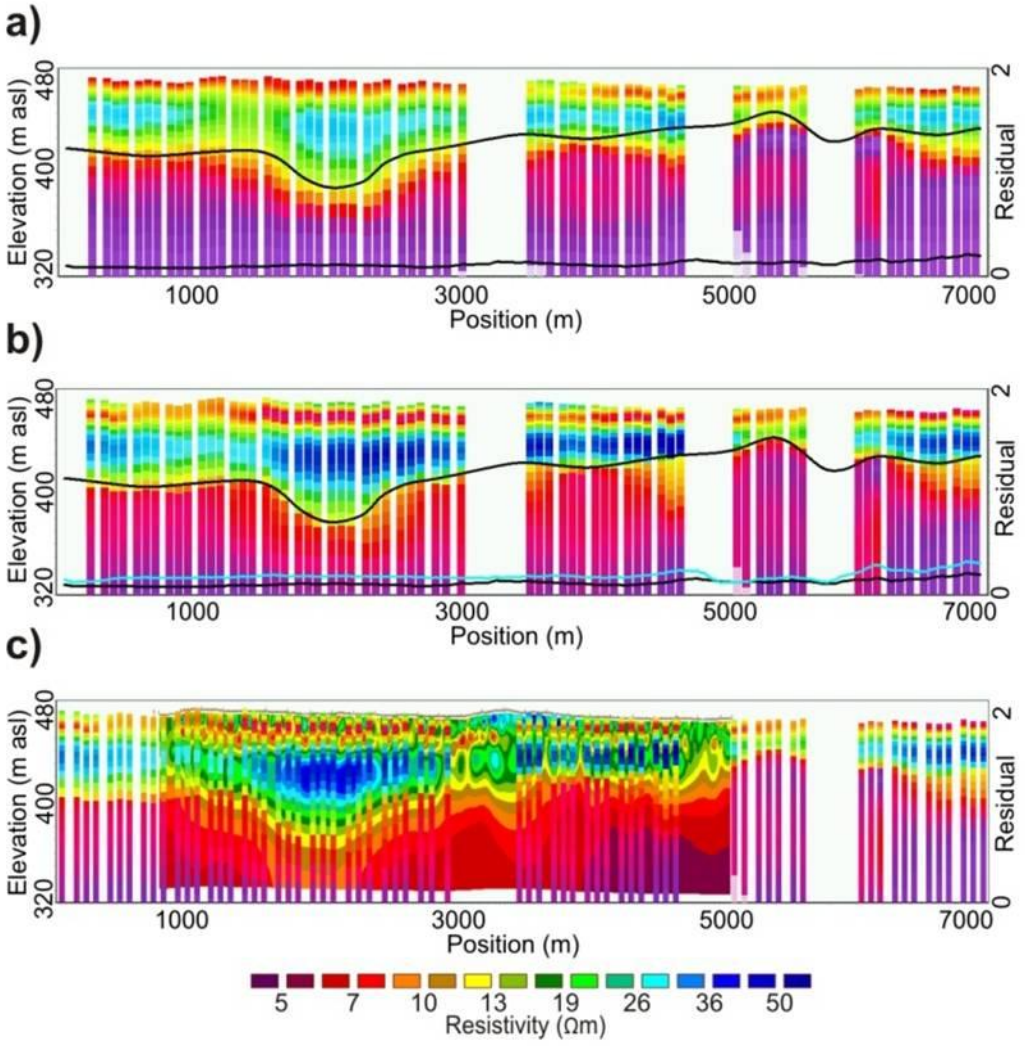

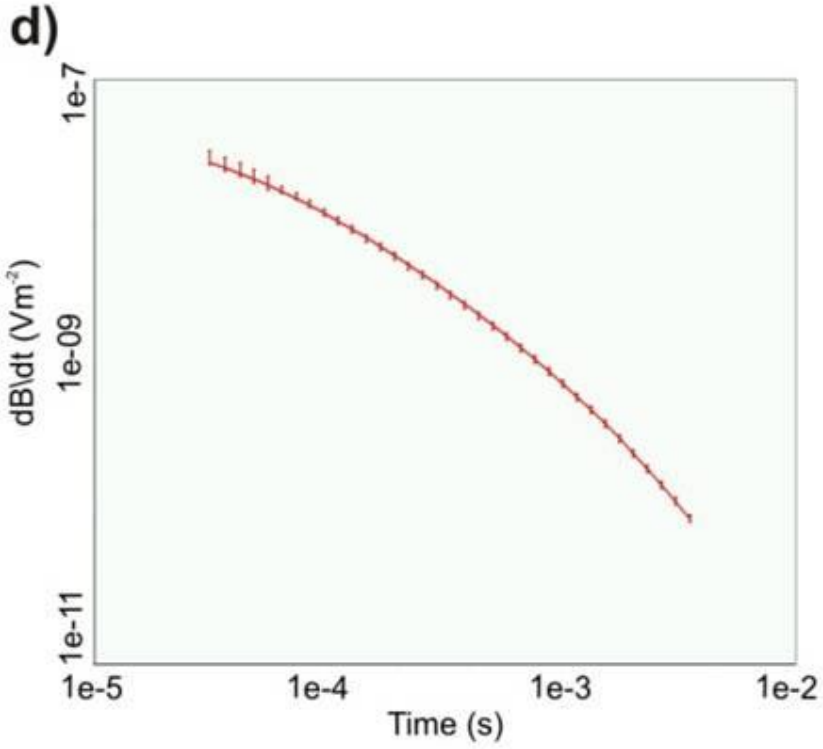

Figure 17.
S2007 VTEM inversion results. VTEM gates 1 and 2 at 21 µs and 26 µs after ramp off have been removed for all inversions. a) Unconstrained. Upper solid black line is the bedrock reflection surface. Lower solid black line is the unconstrained data residual or misfit. b) Constrained with bedrock reflection surface and bedrock conductivity of 7 Ωm (standard deviation factor of 1.5). Solid blue line is the constrained data residual. c) Comparison of ERT model with the constrained VTEM model. The VTEM model underestimates the depth to the shallow conductive layer by approximately 10 m. d) Example VTEM decay curve and data fit. Despite increased noise levels for the first 5 gates (vertical bars), the forward response (solid line) fits poorly the observed data at early time.

VTEM results with a priori: ERT

To reduce the data misfit at early time, we calibrate the VTEM data using the ERT ancillary information as a reference model (Figure 18a). We apply incremental negative time shifts to the VTEM data gates, and invert the shifted data until we obtain an optimum level of fit between the resulting VTEM model resistivity and the ERT model resistivity (Figure 18c). This procedure is similar to the data space calibrations described by Foged et al (2013) and Podgorski et al. (2013) that may be applicable when high-quality ground TEM data are available. However, ground TEM surveys and AEM surveys represent compatible data types that can be directly compared. This is not the case for AEM and ERT data, although the models should be directly comparable provided that effects of anisotropy and scale are negligible.

A small time shift is applied to all VTEM time gates which brings the first usable data gate (corresponding to the nominal 3rd gate) to a time of 10μs after the end of the ramp off . Note that the nominal gate 1 and 2 respectively at 21μs and 26 μs, after ramp off, were omitted from all run inversion. Results of the S2007 calibrated inversion are shown in Figure 3a using an optimal time shift of -21 μs. This calibration factor compensates for a number of possible sources of inaccuracies at early times, both in the data and in the modeling. The calibrated VTEM model is considerably more consistent with the ERT throughout the section, and simultaneously results in improved data fit at early time. The near surface shows up as a resistive layer and the resistive anomaly associated with the valley fill is well-delineated. These features are of significant hydrogeological influence in terms of governing the recharge pathway from the surface and the aquifer potential of the buried valley. The excellent agreement is also corroborated by a significant improvement on early time data fit. To guide the forward to fit the observed data which, in turn, implies to drive the AEM to reproduce the ERT accurately, we carried out those systematic adjustments in the data space. This "*iterative calibration procedure*" allows the near surface AEM output to be considerably more consistent with electrical data. The surface shows up as a resistive layer overlaying a thin conductive clay till layer which was exactly how the ERT data suggested. In addition, the existing resistive body, interpreted to be the response of coarse-grained sediments, is now well constrained within the valley eroded into the conductive shale bedrock but small discrepancy still lies at bedrock interface (figure 18a). Inversion of the calibrated data can also be constrained with depth to bedrock in the model space (Figure 18b). The outcome is a sharp bedrock surface and more subtle changes in the resistivity structure of the valley fill that match the ERT (figure 18c).

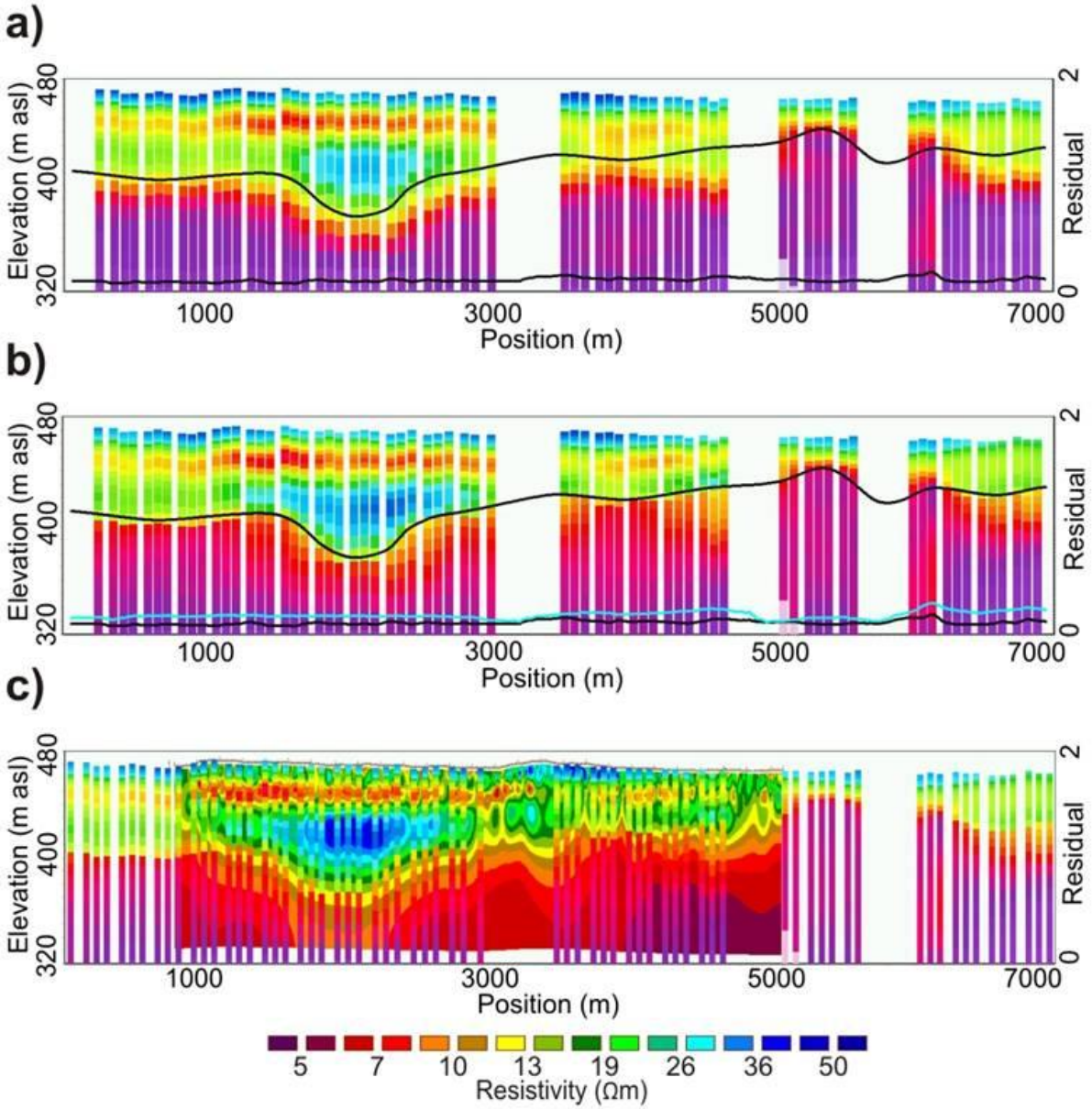

Figure 18.
S2007 calibrated VTEM inversion results. a) Calibrated and unconstrained. Upper solid black line is the bedrock reflection surface. Lower solid black line is the unconstrained data residual or misfit after a 21 µs shift of the data gates. b) Calibrated and constrained with bedrock reflection surface. Solid blue line is the constrained data residual. c) Comparison of ERT model with the calibrated and constrained VTEM model showing significantly improved agreement.

VTEM results with a priori: S1

We perform the same procedure for seismic S1 in the south part of the survey block. Inversion of the S1 VTEM data indicates a conductive surface over resistive materials over conductive bedrock (Figure 19a). Problems with this model include that we expect the surface to be resistive (Crow et al. 2012) and the two main incised valley down to the shale appear to be deeper

respect to seismic bedrock reflector. Seismic interpretation is corroborated by stratigraphic descriptions of a cored borehole along S1 (Crow et al., 2012). The depth of drilling was limited to about 97 m and didn't catch the bedrock at the bottom (supposed to be deeper). First 9m reveal very fine to fine sand embedded to sandy silt diamicton. This layers overlay clay till to hard clay diamicton sediments before drilling indicates a relative uniform till down to the bottom of the borehole. In addition, electromagnetic log also shows a change in conductivity. The surface looks more resistive (~17 Ohm m) in the borehole up to 9m. Then, measurements indicates a transition to till layer with relatively uniform conductivity (~9 Ohm m) from 15-80 depth (Crow et al., 2012).

The overestimation of the depth to bedrock might be due to several factors. Since those buried valley are significantly narrow structures eroded into the bedrock we do not exclude the possibility to have a 3D effect to the output resistivity model (Goldman et al., 1994). Furthermore, the seismic data depict reflection surfaces in terms of changes in elastic moduli. However, the sediment/bedrock interface may not be precisely defined in terms of either seismic parameters or electrical resistivity, or the resistivity may vary gradually across the sediment/bedrock interface All this illustrates the known ambiguity in interpreting correctly the depth of a geological layer, especially for a smooth model. Therefore, we applied bedrock depth derived from the seismic interpretation directly to constrain the inversion and to reduce such ambiguity. This constraint allowed mapping the bottom of the buried valleys more consistently with the seismic data (as expected), but also resulted in a resistive surface layer (consistent with GSC-SW-07 borehole) and an increase in the resistivity of the sediments above the bedrock from approximately 30-40 Ohm m to more than 50 Ohm m (Figure 19b). However, discrepancies are still observable if we compare the AEM results to borehole information and the shallow inter-till seismic reflector illustrated in figure 19b. This seismic reflector is interpreted to represent an interface between hard, compact till below and heterogeneous less-compact sandy till above. The inter-till reflector can be added to constrain the inversion which results in a match to the seismic information at surface. Although the near surface becomes resistive, the thin conductive layer below the inter-till reflection is inconsistent

with the borehole records and the data residual clearly indicates the presence of high misfit especially at early gates which indicates that the ancillary seismic information is in conflict with those observed data.

Guided by previous results for S2007, we apply the same calibration time shift to the S1 VTEM data. Figure 19c shows that inversion of the "calibrated" VTEM data (without any seismic constraint) provides a significantly improved match in the near surface with the seismic reflections and the borehole record. Calibrated VTEM inversion results clearly show the transition between a resistive shallower layer, with ρ ~20 Ω m and 10 m deep (representing the sandy silt diamicton in the borehole) to a more conductive (~9 Ωm) hard clay till layer. In fact, for the calibrated result, a shallow resistive layer corresponds remarkably well to the inter-till reflector. However, we lack good discrimination of the valley-fill sediments and there is discrepancy between the deep conductive layer and the bedrock contact as interpreted for the seismic data. To address these issues, we constrain the inversion of the calibrated data with the seismic bedrock reflector. We obtain more structure in the valley-fill sediments and increase consistency on the bedrock contact, although there is still some discrepancy between the VTEM model and seismic bedrock perhaps due to reason already discussed (Figure 19d). We further constrain the "calibrated" VTEM model with the shallower till reflector to account for all available information derived from seismic data (Figure 19e). The obtained smooth model matches considerably better with all available information along seismic s1, not only in terms of depth to layer (where we already have an excellent agreement with seismic), but also it fits with the very near surface resistivity which is also reflecting by the geophysical log.

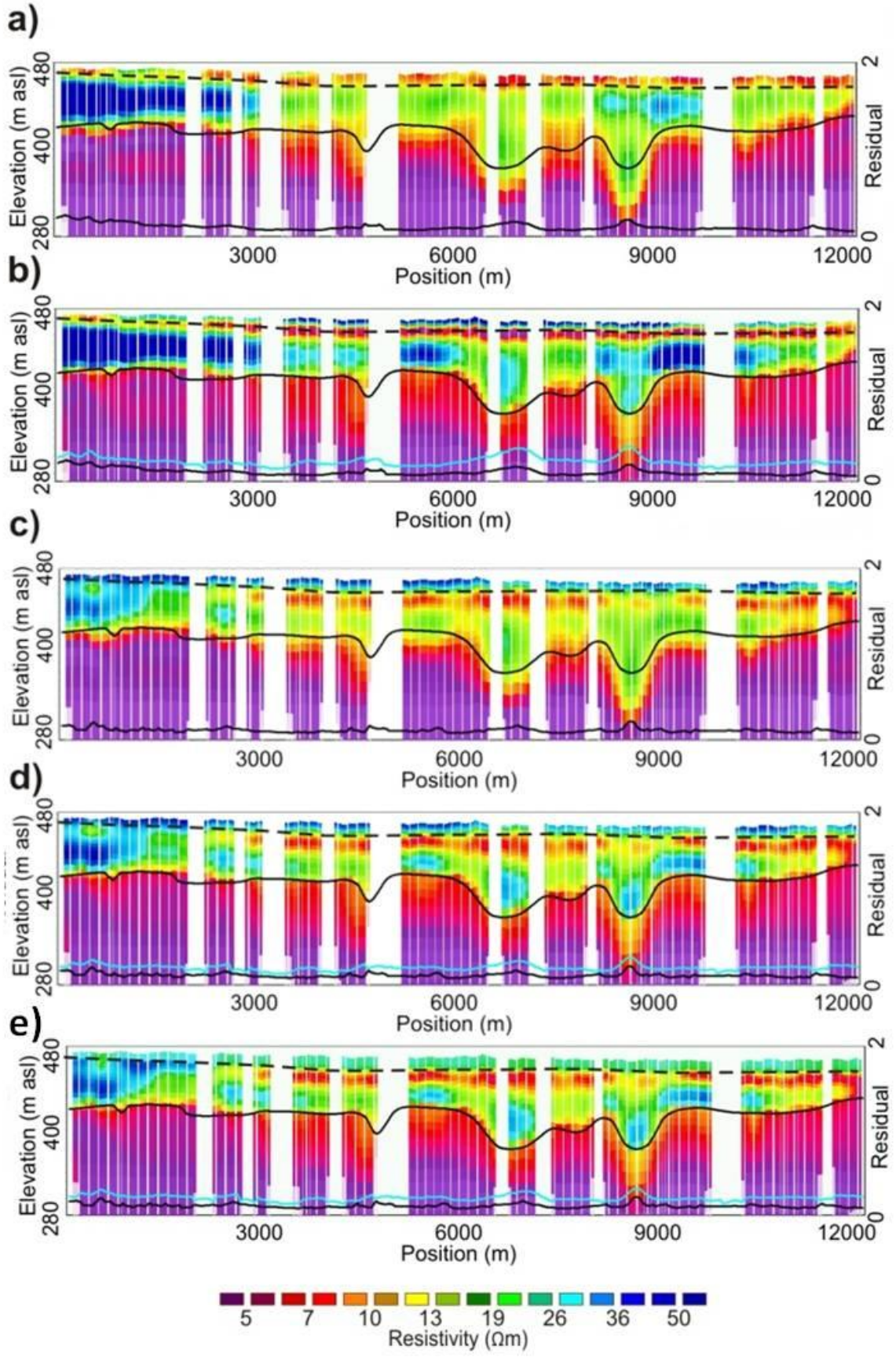

Figure 19.
S1 VTEM inversion results. a) Unconstrained. Dashed black line is the inter-till reflection surface. Upper solid black line is the bedrock reflection surface. Lower solid black line is the unconstrained data residual or misfit. b) Constrained with bedrock reflection surface. Solid blue line is the

constrained data residual. c) Calibrated and unconstrained. Lower solid black line is the unconstrained data residual or misfit after a 21 μs shift of the data gates. d) Calibrated and constrained with bedrock reflection surface. Solid blue line is the constrained data residual. e) Constrained with bedrock and inter-till reflection surfaces. Lower solid black line is the unconstrained data residual. Solid blue line is the constrained data residual. f) Calibrated and constrained with bedrock and inter-till reflection surfaces. Lower solid black line is the calibrated and unconstrained data residual. Solid blue line is the constrained data residual.

Disussion

Inversion of noisy, band-limited AEM data is inherently ill-posed and results are notoriously non-unique (Ellis, 1998). Nevertheless, we would like to use VTEM inversion results to build geological and hydrogeological models including the near surface. To this effect, we have utilized ancillary information to impose a-priori constraints in model space and to perform calibration of VTEM data such that inversion results are consistent with other information and data types. Seismic data provide high-resolution information regarding changes in seismic velocity that are used to derive an independent measure of depth to model layers such as the conductive shale bedrock. For the Spiritwood VTEM data, seismic constraints provide improved results, particularly in resolving depth to bedrock at the bottom of buried valleys. Results are further improved via calibration of the VTEM resistivity model against an electrical resistivity model derived from ERT and borehole data. In this way, we leverage the higher resolution and complimentary sensitivities of the seismic and electrical data to achieve a final VTEM model with a higher degree of confidence. Our time-shift calibration is similar to that applied for ground-based TEM data and HTEM data by *Foged et al*. (2013) and Podgorski et al. (2013), but is more generally applicable to ancillary information that is not directly comparable in data space. Our calibration focuses on the 2D cognitive comparison of resistivity magnitude, structures and features in model space for an entire flight profile. This approach ameliorates some issues associated with discrepancies in support volume and resolution/regularization between data types and model derivations that may be variable across a test section. We consider the model-space calibration an appropriate way to integrate electrical and AEM methods or other reference information that is not directly transferable to AEM data space. However, it is of utmost importance to honor the quality of the calibration reference information

and the validity of the model-to-model comparison since any errors may be propagated to the calibrated AEM.

For ERT and AEM models, we have inherent differences in the survey methods, acquisition procedures, measured data, noise levels, and support volume of measurement. Although both methods respond to the electrical conductivity of the subsurface, they sample significantly different volumes and have different sensitivities (geometry-based versus frequency-based). AEM has an area of investigation that is a function of the descending and expanding image of the transmitted current. The ERT method samples a portion of the ground defined by the region of galvanic current injection. Moreover, high-resistivity structures cannot be resolved easily using inductive methods, whereas they are better resolved by ERT. In theory, the inversion acts to remove differences between data types and data geometry (i.e. current patterns and sensitivity) to the limit of macro-anisotropy (Christensen 2000) such that output models can be taken to be the representations of the physical parameter within some limitations such as resolution and regularization. Even a joint inversion should not require any corrections for anisotropy of scale – that is, anisotropy that is due to features of resolvable size (e.g, Raiche et al., 1985; Monteiro Santos and El-Kaliouby, 2011).

The surficial sediments in the Spiritwood region are largely carbonate-rich silty-to-sandy diamicton (till) with localized glaciofluvial deposits. Given the unsorted nature of the diamicton, we do not expect anisotropy associated with large-scale clay fabric. However, discrete clay layers, sand lenses or till fabric may influence the electrical anisotropy (Sutinen et al., 2010). The borehole GSCSW07 along section S1 (Fig. 3) intercepts the surficial sandy-till layer that we attribute to be the source of the resistive surface layer observed in ERT profiles across the survey area (Oldenborger et al., 2013). From the electromagnetic log of GSCSW07 (Crow et al., 2012) we extract an estimate of horizontal resistivity for this 10m-thick surficial layer of $\rho_H \approx 15$ Ωm. From the ERT models, we estimate a bulk resistivity of $\rho \approx 18–23$ Ωm, although there is a significant degree of heterogeneity. These approximate resistivities suggest at least some degree of anisotropy with vertical resistivities of $\rho_V \approx 21–35$ Ωm. While significant, this degree of anisotropy would not

significantly affect our calibration due to the cognitive nature of the model comparison that involves visually observing the degree of match between models in terms of both resistivity magnitude and structure over the entire 2D profile. Our calibration will be robust with respect to relatively small differences in model resolution, model errors or artefacts, but it can also be performed to different levels of stringency in the face of uncertainty. For example, a minimum requirement for calibration of the Spiritwood VTEM data might be that it results in the structure of resistor over conductor over resistor over bedrock, as opposed to the structure observed with no calibration of conductor over resistor over bedrock.

Our calibration procedure was designed to reconcile early-time signal bias observed in the VTEM soundings that could not be accounted for in our forward modeling, but it does not require identification of the source of this bias. We hypothesize that signal bias most likely results from a large amount of primary field impacting the received signal at early times as a result of imprecision in timing, turn-off and establishment of time zero with respect to the transmitter waveform. However, neither the fact that our calibration empirically improves the fit between the observed data and our 1D forward model, or the observation that inversion results are in better agreement with ancillary information are conclusive evidence of a "timing error" in the data. We may have additional system effects such as current leaks or parasitic capacitance that contribute to enhanced signal strength at early time, or we may have modelling deficiencies (such as anisotropy) that result in under-prediction of the true signal strength. Of particular note is that the time shift calibration established for one part of our survey region is successfully applied to another in terms of agreement with other available data. This may not always be the case and the appropriate time shift is likely different for other systems and may be different for different datasets or flights with the same system.

Final remarks

Hydrogeological models often require near-surface resolution. However, helicopter time-domain electromagnetic (HTEM) data often suffer from system bias in the early time – a problem that leads to errors in the inverse model or limited near-surface resolution resulting from the discard of early-time data gates. In a hydrogeological applications with multi-scale and complex aquifer systems such as glacial buried valleys, aquifer mapping requires the ability to accurately resolve aquifer geometry and to distinguish physical properties or aquifer materials. For example, bedrock or aquitard depth is an important starting point for a variety of hydrogeological investigations such as groundwater modeling or exploitation drilling. However, an aquifer is also characterized by permeable sediments which may have a distinct signature in terms of electrical conductivity. Moreover, glaciated areas are typically complex, and detailed information and models are essential if the goal is to predict groundwater pathways. Especially with the presence of buried-valley geology such predictions are challenging and require high resolution models, where the individual valleys must be resolved. This work highlights a pioneering\pragmatic\experimental application of ancillary information into the inversion of airborne electromagnetic data. ERT data have been used as reference model to calibrate the whole AEM dataset. Furthermore, inclusion of the depth to bedrock from seismic reflection data allowed the conductive basement layer to be more homogeneous and continuous providing a more structural geological result. As a matter of fact, AEM are particularly well suited for integration with other data thanks to their high spatial data density. It has been demonstrated that there are several strategies for integrating ancillary information with AEM data. This approach uses both model-space constraints and data-space calibration based on ancillary information from other survey types. In this fashion we are able to enforce consistency, leverage the benefits of other data types such as high resolution seismic and ERT and reduce uncertainty in the HTEM derived model. Our holistic calibration approach is pragmatic in that sources of noise need not be identified. By applying calibration to an entire data set, the advantages of the regional extent and high spatial density of AEM can be fully utilized.

Provided that the involved ancillary information are relevant, of a good quality, they can be usefully treated as another data point or a reference model and directly applied to the AEM data in order to obtain a model with lower uncertainty, fitting all data and, at the end, a recalibrated dataset. Lower uncertainty in addition to an increased confidence in the near surface model is required for groundwater mapping which, in turn, allow better management decisions. An important corollary is that the constrained and calibrated HTEM results will be of a quality commensurate with the ancillary information. Those results offer new insights into the use of ancillary information and will be a critical baseline for future approach in AEM data processing.

References

Auken, E., A. V., Christiansen, Westergaard, J.H., Kirkegaard, C., N., Foged, A., Viezzoli (2009), An integrated processing scheme for high-resolution airborne electromagnetic surveys, the SkyTEM system, Explor. Geophys., 2009, 40, 184–192, doi:10.1071/EG08128.

Burschil, T., H., Wiederholda, E., Auken (2012), Seismic results as a-priori knowledge for airborne TEM data inversion - A case study, J. Appl. Geophys, 80, 121–128, doi:10.1016/j.jappgeo.2012.02.003.

Christensen, N. B., 2000, Difficulties in determining electrical anisotropy in subsurface investigations: Geoph. Prosp., 48, 1-19.

Christiansen A.V., and E., Auken (2012), A global measure for depth of investigation, Geophysics, 77, 171-177, doi:10.1190/geo2011-0393.1.

Christiansen, A.V., E., Auken, and A., Viezzoli (2011), Quantification of modeling errors in airborne TEM caused by inaccurate system description, Geophysics, 76, 43-52, doi:10.1190/1.3511354.

Crow H.L., R.D., Knight, B.E., Medioli, M.J., Hinton, A., Plourde, A.J.-M., Pugin, K.D., Brewer, H.A.J., Russell and D.R., Sharpe (2012), Geological, hydrogeological, geophysical, and geochemistry data from a cored borehole in the Spiritwood buried valley, southwest Manitoba, Geological Survey of Canada, Open File 7079.

Foged, N., E., Auken, A.V., Christiansen, K.I., Sørensen (2013), Test site calibration and validation of airborne and ground based TEM-systems, Geophysics, 78, 95-106, doi:10.1190/geo2012-0244.1.

Gabriel G., R., Kirsch, B., Siemon, and H., Wiederhold (2003), Geophysical investigation of buried Pleistocene subglacial valleys in Northern Germany, J. Appl. Geophys., 53, 159–180, doi:10.1016/j.jappgeo.2003.08.005.

Hammack, R., V., Kaminski, W., Harbert, G., Veloski, and B., Lipinski (2010), Using helicopter electromagnetic (HEM) surveys to identify potential hazards at coal-waste impoundments: Examples from West Virginia, Geophysics, 75, 221-229, doi:10.1190/1.3505764.

Hoyer A. S., H., Lykke-Andersen, F., Jorgensen, and E., Auken (2011), Combined interpretation of SkyTEM and high-resolution seismic data. Physics and Chemistry of the Earth, 36, 1386–1397, doi:10.1016/j.pce.2011.01.001.

Ellis, R.G.,(1998), Inversion of airborne electromagnetic data, Expl. Geoph., 29(2) 121 – 127, doi:10.1071/EG998121.

Jørgensen, F., P. B.E., Sandersen, E., Auken (2003), Imaging buried Quaternary valleys using the transient electromagnetic method, J. Appl. Geophys., 53, 199- 213, doi:10.1016/j.jappgeo.2003.08.016.

Jørgensen, F., E., Auken, H., Lykke-Andersen, K., Sørensen (2003c), Groundwater exploration by use of TEM, reflection seismic surveys and drillings, paper presented at 9th Annual Meeting, EEGS-ES, Prague, Czech Republic.

Legault, J. M., A., Prikhodko, D. J., Dodds, J. C., Macnae, G.A., Oldenborger (2012), Results of recent VTEM helicopter system development testing over the Spiritwood Valley aquifer, Manitoba, paper presented at 25th SAGEEP Symposium on the Application of Geophysics to Engineering and Environmental Problems, Tucson, Arizona, USA.

Loke M.H., I., Acworth, and T., Dahlin (2003). A comparison of smooth and blocky inversion methods in 2D electrical imaging surveys, Explor. Geophys., 34, 182–187, doi:10.1071/EG03182.

Macnae, J., and S. Baron-Hay (2010), Reprocessing strategy to obtain quantitative early-time data from historic VTEM surveys: paper presented at 21st International Geophysical Conference & Exhibition, ASEG, Sydney, Australia.

Møller, I., V.H., Søndergaard, F., Jørgensen, E., Auken, and A.V., Christiansen (2009), Integrated management and utilization of hydrogeophysical data on a national scale, Near Surf. Geophys., 7, 647-659, doi:10.3997/1873-0604.2009031.

Monteiro Santos, F. A., and El-Kaliouby, H. M., (2011), Quasi-2D inversion of DCR and TDEM data for shallow investigations, Geoph., 76, 239–250, doi: 10.1190/1.3587218.

Oldenborger, G.A. (2010a), AeroTEM III Survey, Spiritwood Valley, Manitoba, parts of NTS 62G/3, 62G/4, Manitoba: In Geological Survey of Canada: Open File 6663.

Oldenborger, G.A. (2010b), AeroTEM III Survey, Spiritwood Valley, Manitoba, parts of NTS 62G/3, 62G/4, 62G/5, 62G/6, Manitoba. In Geological Survey of Canada: Open File 6664.

Oldenborger, G.A., A.J.-M., Pugin, and S.E., Pullan (2013), Airborne time-domain electromagnetics, electrical resistivity and seismic reflection for regional three-dimensional mapping and characterization of the Spiritwood Valley Aquifer, Manitoba, Canada, Near Surf. Geophys., 11, 63-74, doi:10.3997/1873-0604.2012023.

Paine, J.G., and B.R.S., Minty (2005), Airborne hydrogeophysics, Hydrogeophysics, 50, 333-357, doi:10.1007/1-4020-3102-5_11.

Podgorski, J.E., Auken, E., Schamper, C., Christiansen, A.V., Kalscheuer, T. and Green, A. G. 2013. Processing and inversion of commercial helicopter time-domain electromagnetic data for environmental assessments and geologic and hydrologic mapping. Geoph., 78, 149–159. doi:10.1190/GEO2012-0452.1.

Raiche, A.P., Jupp, D.L.B., Rutter H. and Vozoff, K. 1985. The joint use of coincident loop transient electromagnetic and Schlumberger sounding to resolve layered structures. Geoph., 50, 1618–1627. doi: 10.1190/1.1441851

Siemon, B., T., Kerner, Y., Krause, and U., Noell (2012), Airborne and ground geophysical investigation of the abandoned salt mine environment along the Stassfurt-Egeln Anticline, Germany, First Break, 30, 43-53, doi:10.3997/1365-2397.2011038.

Smith, R.S., R., Koch, G., Hodges, and J., Lemieux (2011), A comparison of airborne electromagnetic data with ground resistivity data over the Midwest deposit in the Athabasca basin, Near Surf. Geophys., 9, 319-330, doi:10.3997/1873-0604.2011002.

Sutinen, R., Jakonen, M., Piekkari, M., Haavikko, P., Närhi, P., Middleton, M., 2010. Electrical-sedimentary anisotropy of Rogen moraine, Lake Rogen area, Sweden. Sedimentary Geology 232, 181–189.

Viezzoli, A., A.V., Christiansen, E., Auken, and K., Sørensen (2008), Quasi-3D modeling of airborne TEM data by spatially constrained inversion, Geophysics, 73, 105-113, doi:10.1190/1.2895521.

Viezzoli, A., L. Tosi, P. Teatini, and S. Silvestri (2010), Surface water–groundwater exchange in transitional coastal environments by airborne electromagnetics: The Venice Lagoon example, Geophys. Res. Lett., 37, L01402, doi:10.1029/2009GL041572.

Wiecek, S. (2009), Municipality of Killarney, Turtle Mountain groundwater assessment study: W.L. Gibbons & Associates Inc.

Winter T.C., R.D., Benson, R.A., Engberg, G.J., Wiche, D.G., Emerson, O.A., Crosby, and J.E., Miller (1984), Synopsis of ground-water and surface-water resources of North Dakota. United States Geological Survey, Open File Report 84-732.

Wynn, J. (2002), Evaluating groundwater in arid lands using airborne magnetic/EM methods. An example in the southwestern U.S. and northern Mexico, The Leading Edge, 21, 62-64, doi:10.1190/1.1445851.

Chapter 4

The impact on geological and hydrogeological mapping results of moving from ground to Airborne TEM.

Introduction

The transient electromagnetic (TEM) technique has been applied for hydrogeological mapping in numerous cases, in very different parts of the world, and with different levels of success. The technique owes its popularity to its relative ease of operation, its cost efficiency, and a strong affinity between its output and key geological and hydrogeological parameters. The ground-based TEM method has been used extensively in Denmark in the past decade and has proven to be a powerful tool in hydrogeophysical investigations as well as groundwater exploitation management (Auken *et al*., 2003).

The logisitcal simplicity of the TEM methods results from the inductive energization of the subsurface over a relatively small area of the Earth's surface while at the same time obtaining significant penetration depths; the TEM ratio of penetration depth to coil size can be much greater than 1, as opposed to geoelectrics, where deep penetration always comes at a cost of much longer electrode arrays. An experienced crew can acquire 5-10 ground-based TEM soundings in different locations per day, covering large areas in a relatively short time and hence, at low cost.

In terms of data processing, 1D inversions for electrical resistivity can provide a very good representation of the "true" geometry of the subsurface, particularly for layered sedimentary environments. In some cases, resistivity models can then be directly transformed into representations of aquifers and aquitards.

In this chapter we focus on the improvements to the geophysical and geological modeling and mapping and the hydrogeological management that can be obtained by moving from ground-based to airborne TEM data. The application of airborne TEM to hydrogeological mapping of large areas has been on the rise over the last decade (Wynn, 2002, Jørgensen *et al*., 2003, Paine *et al*., 2005, Møller *et al*., 2009 and Oldenborger *et al*., 2013). Geological survey organizations across the

globe have promoted (Australia, Canada), carried out (e.g., Germany) and/or supervised (e.g., Denmark, US) large AEM surveys. Private enterprises dealing with large scale hydrogeological mapping have also turned to AEM, integrated with other sources of information. The most important reasons for its popularity are the time and cost efficiency in producing high quality, spatially-extensive datasets that can be applied to multiple purposes. Here we carry out a simple, yet rigorous, simulation showing the impact of an AEM dataset towards hydrogeological mapping and management, compared to having only a ground-based TEM dataset, as well as to having only borehole data. We will investigate the differences between airborne and ground TEM surveys not only in terms of spatial resolution of the output resistivity model, but also in terms of the level of accuracy of the geological interpretation, keeping always in mind the consequent uncertainty in groundwater resources evaluation and management. We carry out the simulation by down-sampling an AEM dataset over the Spiritwood Valley Aquifer in Manitoba, Canada, down to the data density characteristic of high resolution large scale ground TEM surveys. AEM and ground based TEM can also have a complementary role in an hydrogeophysics survey. In addition we address the importance of the complementarity of AEM and ground TEM measurements. Ground TEM can provide extra depth of investigation in areas where the AEM might fail to reach the target. Perhaps an even more important contribution would be to deploy a calibrated ground based TEM system to check and post-calibrate, if necessary and possible, the Spiritwood AEM dataset. For this reason, during fall 2012, a ground TEM digital Protem has been calibrated over the Danish national test site of Lyngby following the calibration procedure and guidelines for configuration setup and measuring scheme for standard 40x40m loop (Foged et al., 2013). The test site was established in 2001, to ensure that any TEM system used in the Danish groundwater mapping campaign is capable of reproducing the reference model at the test site, so that soundings made with different instruments would end up with the same geophysical model and thereby the same geological model. The calibration procedure involved time-shifts and offsets of recorded transients of individual TEM systems. Data and 1D forward models are also presented in this chapter. Provided a ground TEM

system had been calibrated, then it can be used to acquire data over a series of diverse locations within the AEM Spiritwood survey area. Then, collecting a series of local 1D resistivity reference models, to be used to compare against the AEM data and derived models, it'll be possible to re-calibrate the AEM data.

Geology of the Spiritwood Valley Aquifer

Buried valleys are a common feature in glacial terrains of the Canadian Prairies. Particularly where the underlying bedrock consists of easily eroded sediments, such as shale, numerous valleys were cut into Cretaceous and Tertiary bedrock units prior to the initiation of continental glaciations (Batcher *et al*., 2005). Alluvial deposits, in particular sands and gravels, are generally thought to have been transported from the Rocky Mountains to the west and rest on the underlying bedrock in parts of many of these valleys. During the Pleistocene, considerable modification occurred to many of the older valleys and new valleys were formed by meltwater erosion most likely during glacial retreats. By the end of the Pleistocene many of the valleys had been partially or completely infilled with glacial sediment (Russel *et al*., 2004, Cummings *et al*., 2012). Cummings *et al*. (2012) presented a conceptual geological model for Prairie buried-valley incision pointing out "clasts provenance" as one of the main criterion used to interpret buried valley origin. Preglacial fluvial incision driven by tectonic uplift and tilting is typically invoked to explain buried valleys lined with Rocky Mountain clasts (Andriashek, 2003). Buried valleys that cross bedrock slope, stratigraphically overlie till, and contain Precambrian Shield clasts along their bases are commonly inferred to have been incised by proglacial meltwater streams (Kehew *et al*., 1986). A subglacial origin has been inferred for some buried valleys that stratigraphically overlie till and contain Precambrian Shield clasts (Andriashek, 2003).

The Spiritwood valley aquifer system lies within a till plain with little topographic relief. The underlying bedrock is the electrically conductive, fractured silicious shale related to the Odanah Member of the Pierre Formation (Randich and Kuzniar 1984). The stratigraphy within the valley is

variable and includes a basal shaly sand and gravel overlying by clay-rich and silty till units. Where coarse-grained sediments fill the eroded valleys, the potential for significant aquifers exists.

The simulated ground TEM survey at Spiritwood Valley Aquifer

As largely discussed on previous chapters, in 2010 the Geological Survey of Canada contracted an airborne electromagnetic (AeroTEM III) survey covering 1062 km^2 (3000 line km) over the Spiritwood Valley Aquifer. Refer to Figure 1 for the location of the survey. This survey required approximately 5 days of flight time to cover the entire survey block (although, weather restrictions resulted in approximately 4 weeks of deployment time). A thorough re-processing and inversion of the AeroTEM data with SCI, including different iterations to fine tune the results, took approximately 3 months. The total number of 1D models extracted from this dataset is in the order of 100000, equal to a spatial density of approximately 100 soundings/km^2.

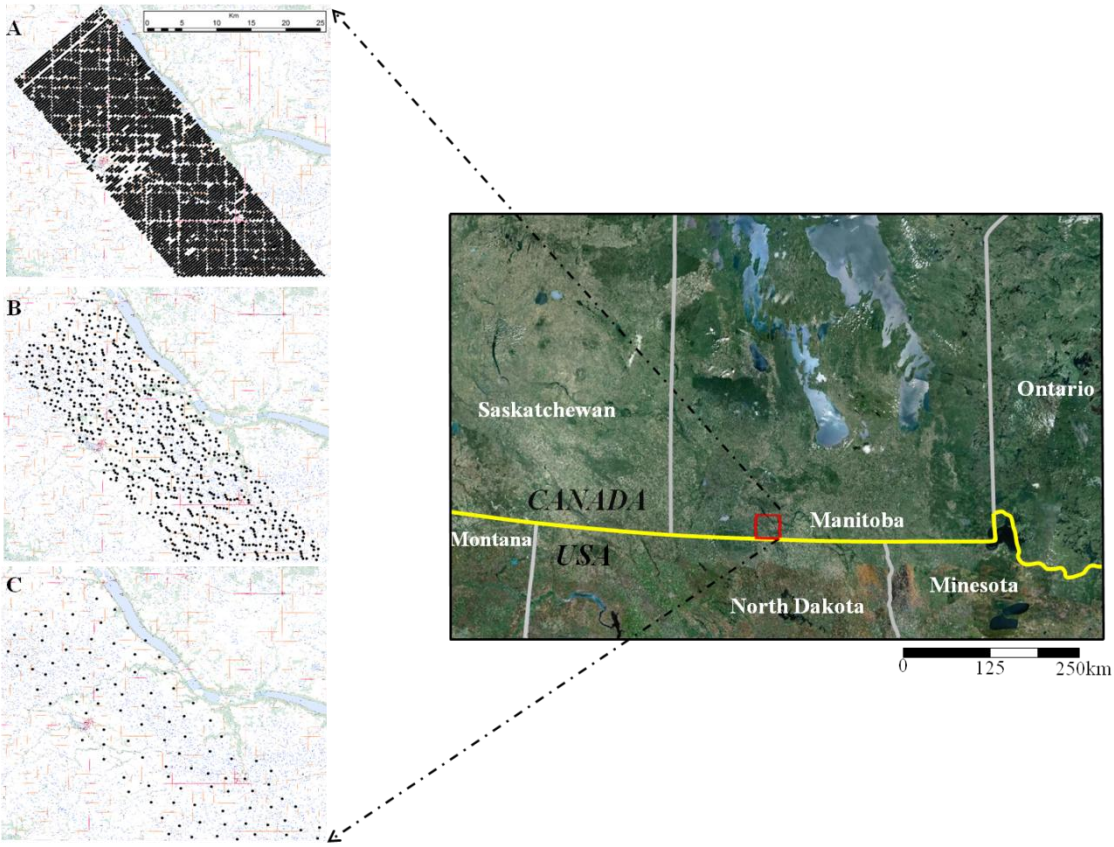

Figure 1.
Spiritwood Valley Aquifer location map (adapted from Google Earth satellite image). The red box indicates the survey area. A) Black dots indicates the 1062 km2 HTEM survey block. B) Simulated high resolution ground TEM survey. The AEM data have been averaged spatially using a trapezoid filters of 100 second resulting in approximately 1

sounding km^2. C) Simulated reconnaissance survey. 100 soundings have been picked manually all over the area in order to obtain a data density of about 1 sounding each 3km^2.

A typical AEM survey measures on the order of 1000 line km of data, with cross line spacing ranging from 100 m for very high resolution mapping, to greater than 1 km for regional mapping. As a consequence, the surface covered ranges typically from 100 km^2 to greater than 1000 km^2, with data density on the order of tens to hundreds of soundings/km^2.

AEM systems have a distinct advantage over ground-based methods in that they can be deployed in transition zones such as rivers (Fitzpatrick *et al*., 2007), lakes, lagoons (Kirkegaard *et al*., 2011), wetlands, coasts and the open sea (shallow bathymetry).

In order to simulate the ground TEM dataset we start from the AEM dataset. These data are then spatially down-sampled to a uniform sounding density over the entire survey block. Two versions of the ground TEM survey were simulated. The "*high resolution*" survey has less than 1 sounding/km^2 and a total of 700 soundings (Figure 1B). The "*reconnaissance*" survey has ~0.1sounding/km^2 and a total of 100 soundings (Figure 1C). Recall that the AEM survey provided approximately 100000 soundings, and 100 soundings/km^2.

The simulated ground TEM soundings were obtained with an energizing moment of 250000 Am^2 equal to that of the AeroTEM system. Given that a standard ground TEM system outputs up to 10 Amps, but more often less, a ground loop of greater than 100m x 100m sides, or multiple turns is required to achieve this moment. To carry out both the high resolution and reconnaissance ground-based TEM surveys would be lengthy and logistically demanding. We estimate that the high resolution survey (700 ground soundings) would require no less than 15 weeks of continuous acquisition for a crew with 3 operators in conditions of clean paddocks and crop fields. Similarly, the reconnaissance survey (100 soundings) would require 3-5 weeks.

Weather constraints, temporary limitations to site accessibility (e.g., un-walkability of the ground due to thawing or presence of crops) invariably add a significant amount of time to complete the survey. Another relevant, time consuming, at times unsurpassable obstacle to a ground survey

aiming at obtaining an even data density throughout the area are the permits needed to access the station sites, even in periods when no crops are on the fields. Beside data acquisition, approximately 2-4 weeks would be needed to carry out the detailed processing and inversion of the data, for hydrogeological applications.

Simulated & true ground TEM measurements

Before deriving geological interpretations from the geophysical results and comparing the results between those of the actual AEM survey and the simulated ground TEM surveys, we elaborate further on the representativeness of the simulated ground TEM data of a true ground TEM survey in terms of depth of investigation and lateral resolution. Arguably, while having the same Tx moment, a ground TEM system can obtain better signal to noise ratio than an airborne system. This is due to significantly greater stacking, the absence of motion induced noise in the receiver, and better coupling between the ground and the Tx coil. One might therefore argue that in the simulated ground soundings the signal falls into noise faster as compared to true ground TEM soundings. However, in this particular case, this bears very little influence, as the conductive bedrock (the Cretaceous shale) is shallow enough to be resolved by the simulated soundings, and conductive and thick enough to make any deeper layer unresolvable by virtually any TEM system. This can be readily seen by comparing the AeroTEM results to the VTEM data from coinciding lines (Figure 2).

Despite its significantly better signal to noise ratio, the VTEM system does not penetrate below the shale. The only exception to the argument above could be in areas where tunnel valleys erode deep into the shale where a true ground TEM sounding might have reached the shale in places where the simulated one does not. On a sounding by sounding base, the foot print of the simulated soundings in the near surface is slightly lower (i.e., higher lateral resolution) than that of an actual 100m x100m loop. In the deeper parts of the models, they are almost equivalent. It is worth noticing also that, in general, ground based soundings are less affected by system bias (primary field not completely removed) than airborne soundings. This is due to the decreasing level of secondary signal resulting from the vertical displacement of the Tx with respect to the ground. Some AEM

systems are more effective than others in the removal of primary field, with the AeroTEM III deployed in the Spiritwood being one of the worse. The simulated ground TEM survey might therefore reveal less near surface resolution than an actual one. We contend that the individual simulated TEM soundings are a good representation of actual ones, especially in the contest of deeper features, and that the illustrative purpose of this exercise remains valid.

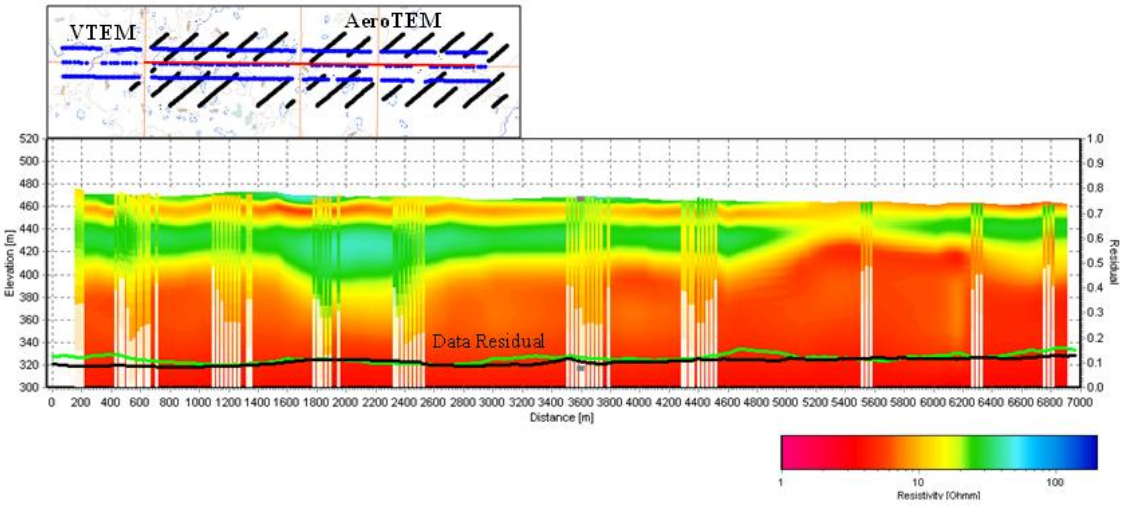

Figure 2.
SCI inversion result of AEM data related to AeroTem and VTEM surveys over coinciding lines at the north subset of the Spiritwood area. The inset box shows both, VTEM and AeroTEM flight lines in blue and black color respectively. AeroTEM dataset provides rich information content in terms of lithological detail and detection of bedrock morphology. As expected, earlier time gates from "Full Waveform" VTEM system, provide a better resolution in terms of shallower geological layers and resistive infilling sediments. In general, models show consistent agreement in terms of main resistive structures detection set amongst the conductive bedrock.

Description of processing and inversion methodology

For both ground-based and airborne EM data, data processing includeed data import, altitude corrections (for airborne only), filtering and discarding of distorted or noisy data contaminated by culture. Data are then averaged spatially using trapezoid filters that allow increasing signal to noise levels without compromising lateral resolution. Inversions are carried out using the quasi 3-D Spatially Constrained Inversion (Viezzoli *et al*., 2008). Oldenborger et al (2013) presented a resistivity model for the Spiritwood area from conductive depth image technique (CDI, Hunag and Rudd, 2008) and noted that the recovered resistivities appeared to be underestimated and of reduced range, with respect to ground ERT measurements. The author

attributes much of the reduced range to the CDI algorithm, concluding that "discrimination of aquifer material is hampered."

As opposed to the CDI, the SCI is a full non-linear damped least squares inversion based on exact forward solution, in which the transfer function of the instrumentation is modeled. The SCI is therefore expected to provide a better agreement with the ERT than the CDI. In the SCI scheme, models are constrained spatially to reflect the lateral homogeneity expected from the geology (either vertical or horizontal layer resistivity, boundary thickness or depth). Constraints include boundary conditions and delimit changes of values within a defined deviation. The inversions are started with a homogeneous half space of 20 Ωm and the model was discretized to 200 m depth, with layers of logarithmically increasing thickness.

We have treated the simulated ground TEM data as if they really had been acquired with a ground TEM system. They were processed for noise and coupling individually. No lateral averaging was carried out. Even the leveling that is usually carried out on the EM data as preprocessing by the AEM contractors before they are delivered has insignificant effect over kilometric distances between soundings. The inversions were carried out with the same forward and inversion algorithms used for the AEM data (Viezzoli et al., 2008), the only difference being that no spatial constraints were applied to the model parameters, as a consequence of the significant distance between soundings. The derived resistivity maps from the 1D models were then interpolated with a kriging algorithm applying a search radius of 5000 m and a node spacing of 100 m for the simulated TEM survey.

Geophysical results and derived geological interpretations

Average resistivity maps at different depth intervals are produce to visualize the results of the inversion of the different datasets (Figure 3). Figure 4 shows the average resistivity maps in a close up where particularly interesting features are in focus. The average resistivity maps in Fig. 3B clearly show the existence of a valley as an elongate, resistive feature (known as the Spiritwood Valley Aquifer). It is approximately 10 km wide and has a conductive background, which according

to boreholes consists of the Cretaceous shale bedrock. Along the middle of this valley we observe a much more narrow structure (1 km) interpreted to be an inset valley that follows the main valley

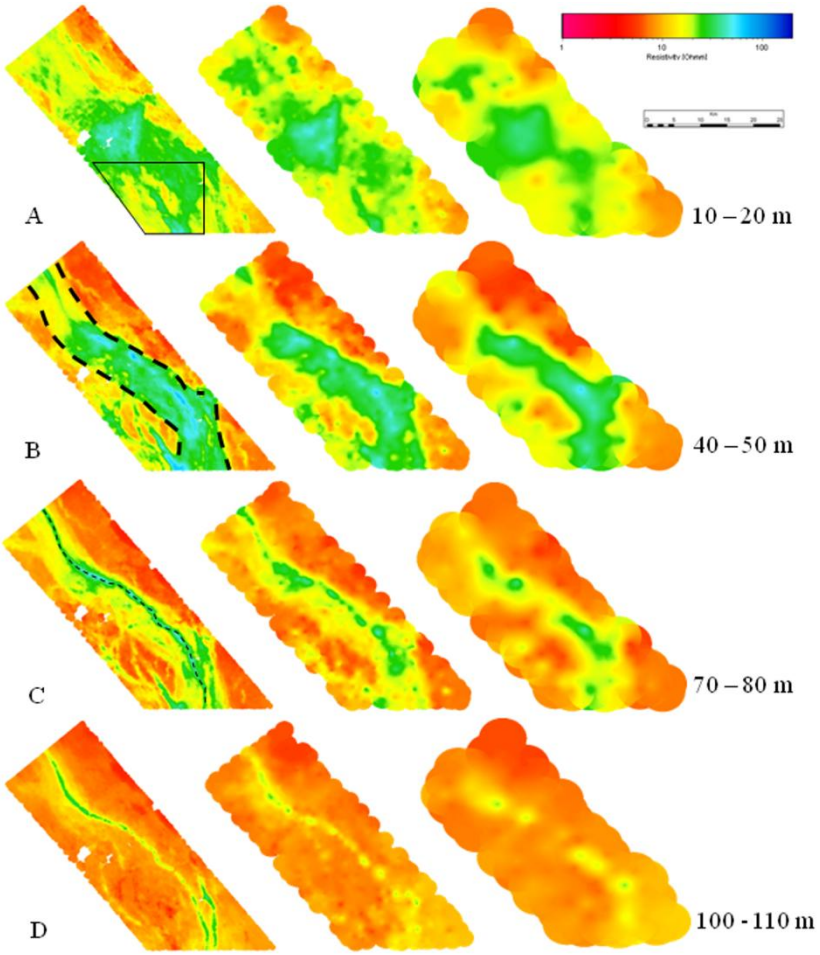

Figure 3.
Average resistivity maps at A) 10-20m B) 40-50m C) 70-80m and D) 100-110m depth, calculated from AeroTEM data for the Spiritwood Valley survey block. Kriging with 600m search distance and 50m cell spacing is used for contouring AEM data, while 2km and 5km search distance with 100m node spacing respectively for high resolution and the reconnaissance ground TEM simulated survey. From the left to the right side of the figure results from the "true" AEM, the simulated high resolution ground TEM and the reconnaissance survey are shown. The black box indicates the subset represented in figure 6. The dashed black lines outline the main Spiritwood Valley Aquifer (B, left side) and the inset valley (C, left side) respectively.

from the north to the south (Fig. 3C, D, left). In addition to the main incised valleys, multiple valley-like features outside of the main valley are observed (Fig. 4B, C, left) (see also Oldenborger *et al*., 2013). Some of the observed buried valleys are very narrow and reveal a complex glacial setting with many cross-cutting buried valleys of several generations (Fig. 3C, left and 4C, left), which are also documented in similar settings in Denmark (Jørgensen and Sandersen 2006).

In general, the electrical resistivities from the AEM model are normally below 10 Ωm for the Cretaceous shale layers, between 20 and 30 Ωm for clay till to silty\sandy till and above 40 Ωm for sandy and gravely layers. To obtain this range of values, a statistical approach in the model space in addition to the observed similarities with water well stratigraphy information and, not

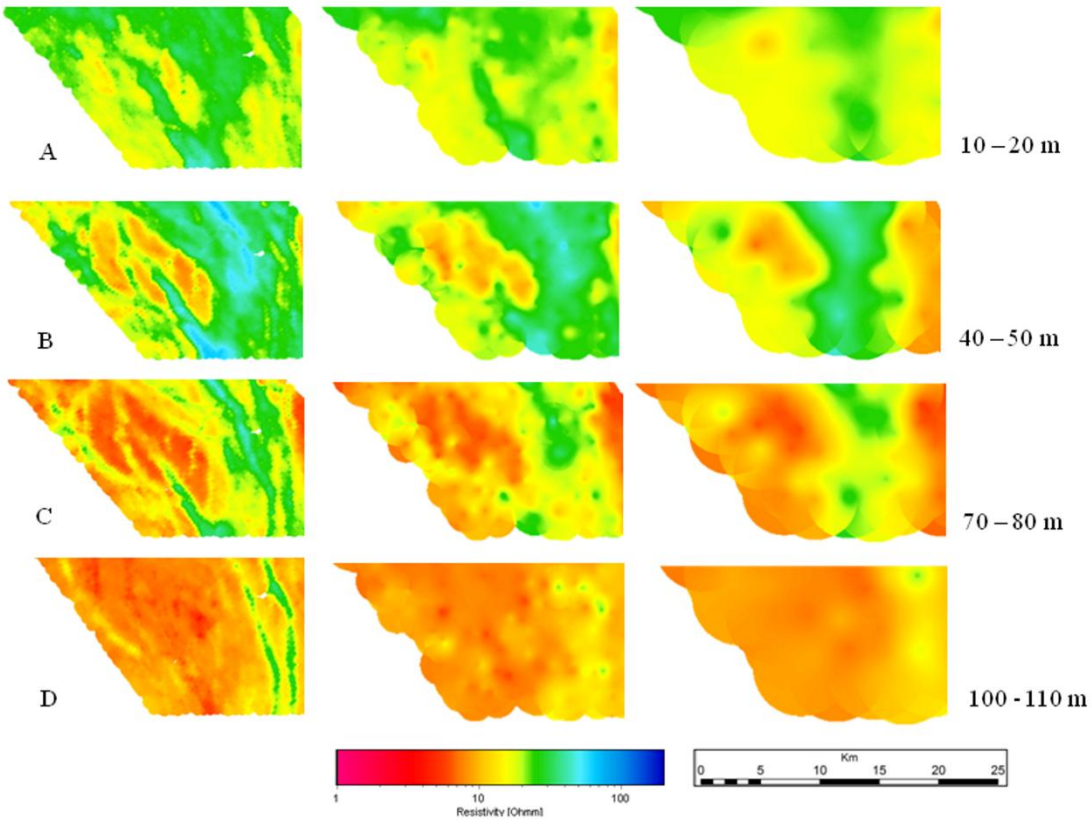

Figure 4.
Average resistivity maps at A) 10-20m B) 40-50m C) 70-80m and D) 100-110m in depth of a small subset in the south westward side of the survey area. The "true " AEM, on the left, show in detail a network of interconnected tributary valleys and the two inset channels into the main, resistive, Spiritwood valley set amongst the conductive bedrock. The high resolution ground TEM survey, in the center, poorly shows those features as long as reveals the main Spiritwood valley as a resistive structure without any evidence of the inset channels. At the right side of the figure, the simulated reconnaissance TEM survey has no evidence of any of the existing morphology that come in the first 50m depth and also clearly underestimates the main Spiritwood Valley structure.

shown here, direct comparison between electrical resistivity tomography has been performed. AEM spatially constrained inversion results reveal, with good correlation of absolute values, the resistive and conductive structures imaged by the ERT electrical profile However, AEM system limitations to resolve the near surface make difficult to provide same detail in surface. The depths of the main

buried valleys are recorded to exceed 100 – 110 m, while most of the secondary valleys are between 40 and 80 m deep (Fig. 3C, D and 4C, D).

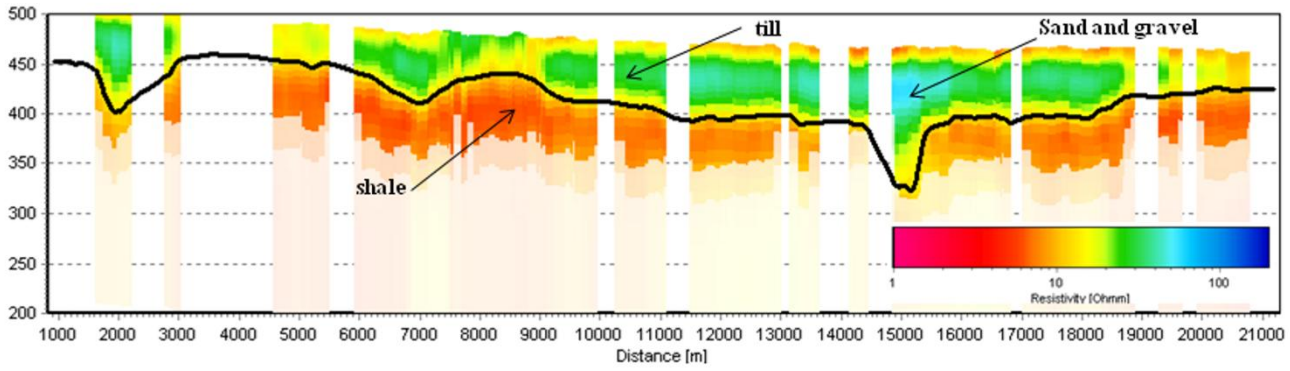

Figure 5.
Example of an AEM flight line SCI inversion result. We interpret the high resistivity range to be attributable to the valley fill materials (till, sand and gravel) and the low resistivity peak to be attributable to the conductive shale bedrock. The black solid line represents the obtained elevation for the conductive shale bedrock.

The resistive features attributable to sand and gravel filling the main buried valleys are well defined in the obtained resistivity models. However, it is evident how inversion result of the AEM survey provides a high variability of the resistivity values across the whole area (Fig. 3, left). Therefore, it indicates that those resistive sediments, interpreted to be the response of sand and gravel, fill the main valley as well as partially cover the two inset valleys and the other small valleys. According to resistivity maps, another resistive body is found in the center of the survey area (Fig. 3A, left). As noted by Wiecek (2009) inter-till sands are found down to a depth of approximately 30 m in this area, and the resistive body could likely be corresponding to these sands (Oldenborger *et al*., 2013).

In the following we will describe how a first approximation of hydrogeological units can be derived directly from the geophysical datasets with semi-automated procedures. As an example, we can produce a map of elevation of (or depth to) the shale, applying given search criteria so as to query the model space. See for example figure 5, where the solid line represents the elevation of the bedrock (as a surface) obtained searching through the resistivity model for a deep conductor (resistivity < 15 Ohm m). In particular, a statistical analysis of the relative frequency of model

values indicates a general bi-modal distribution. We interpret the low resistivity peak in the histogram (around 8-9 Ωm) to be attributable to the shale bedrock and we use this parameters to guide the search criteria to draw out this surface. It is obvious that similar derived products, which

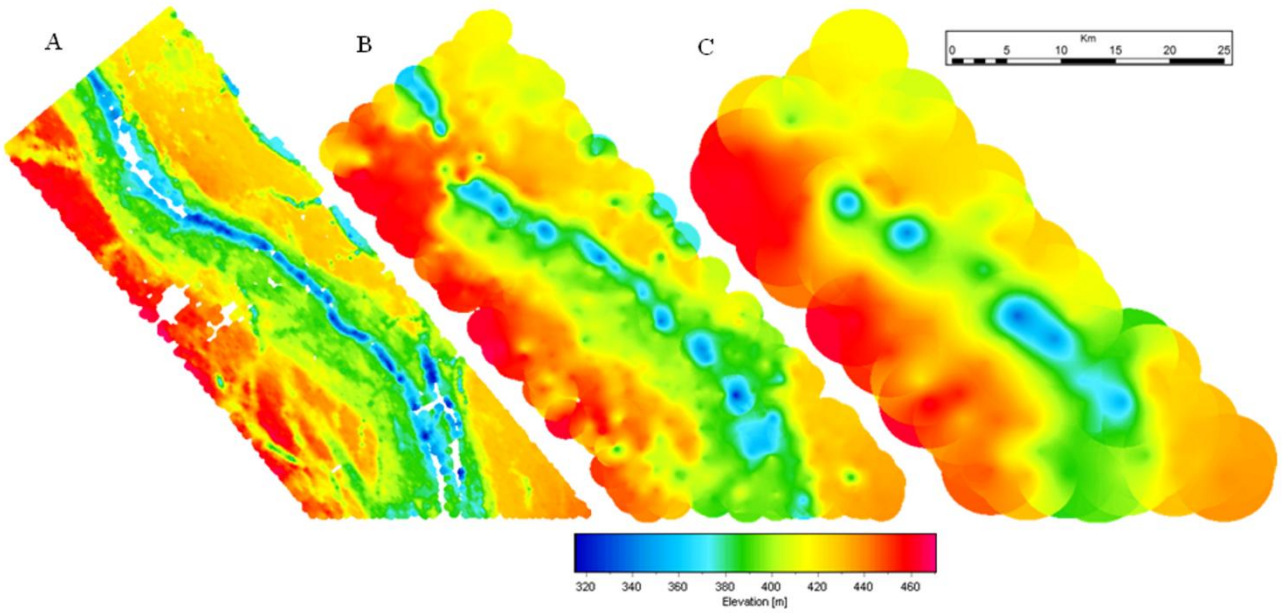

Figure 6.
Maps represent the derived elevation surfaces of the bedrock (conductive shale) from AEM results, on the left, and the two simulated ground TEM survey respectively the high resolution, to the center, and the reconnaissance survey to the right side.

are based on empirical correlation of different parameters, are more robust the higher the statistical population. Beyond that, applying spatial constraints in the inversion over dense datasets, like AEM, improve the lateral coherence of the resistivity models, and hence of the derived products. Figure 6 shows the surface of the resulting elevation of the shale over the entire area for the AEM, the high resolution and the reconnaissance survey. For reference we also present the shale elevation map derived from water wells data alone, which has required extensive interpolation with a 3 km wide search radius (as the same for the reconnaissance survey) since the boreholes are not homogeneously spaced (Figure 7).

In terms of water well data, the direct comparison of water well data to TEM results is complicated by two factors. Firstly, the water wells are not high-quality geotechnical boreholes and the stratigraphic logs represent driller's observations which are subject to well-to-well inconsistency

and observational errors. Secondly, provincial water well locations are reported on a quarter-section basis such that the true well location is not known and several wells from different locations may be assigned to the centre of the same quarter section. In effect, the water well locations have an

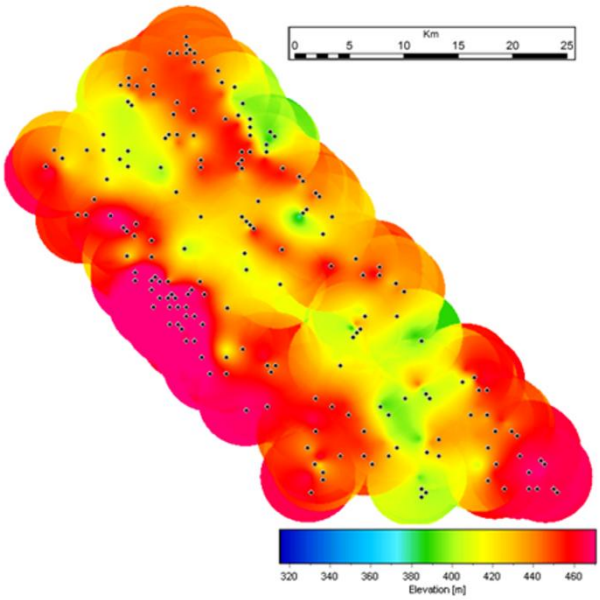

Figure 7.
Shale elevation surface derived from water well information. The low density of wells results in a limited estimation of the bedrock topography.

uncertainty of approxaimtely ±600 m in the case of the Spiritwood. Figure 8 shows a profile, along the longest inset valley, that includes all the water wells located above the thalweg of the valley. Out of the eight wells encountered, four wells indicate the presence of shale bedrock where the AEM model suggests the presence of a resistive body interpreted to represent the infilling materials of the buried valley. From a geological perspective, we could assume that this bedrock contact should be easily recognized due to the significant lithological contrast (although, this may not always be the case for hard tills, fractured shales and water well logs that are based on cutting observations and drill resistance). Therefore, we attribute this discrepancy to the combination of low resolution of the water well locations, and high degree of spatial heterogeneity associated with the inset valley. As a consequence, even large-scale geological structures like the main Spiritwood Valley are difficult to map in detail using existing water wells alone. This also implies the difficulty

to compare well data with the other available geophysical data in order to generate a reliable geological model. However, the well data seem generally to agree with the geophysical data on a

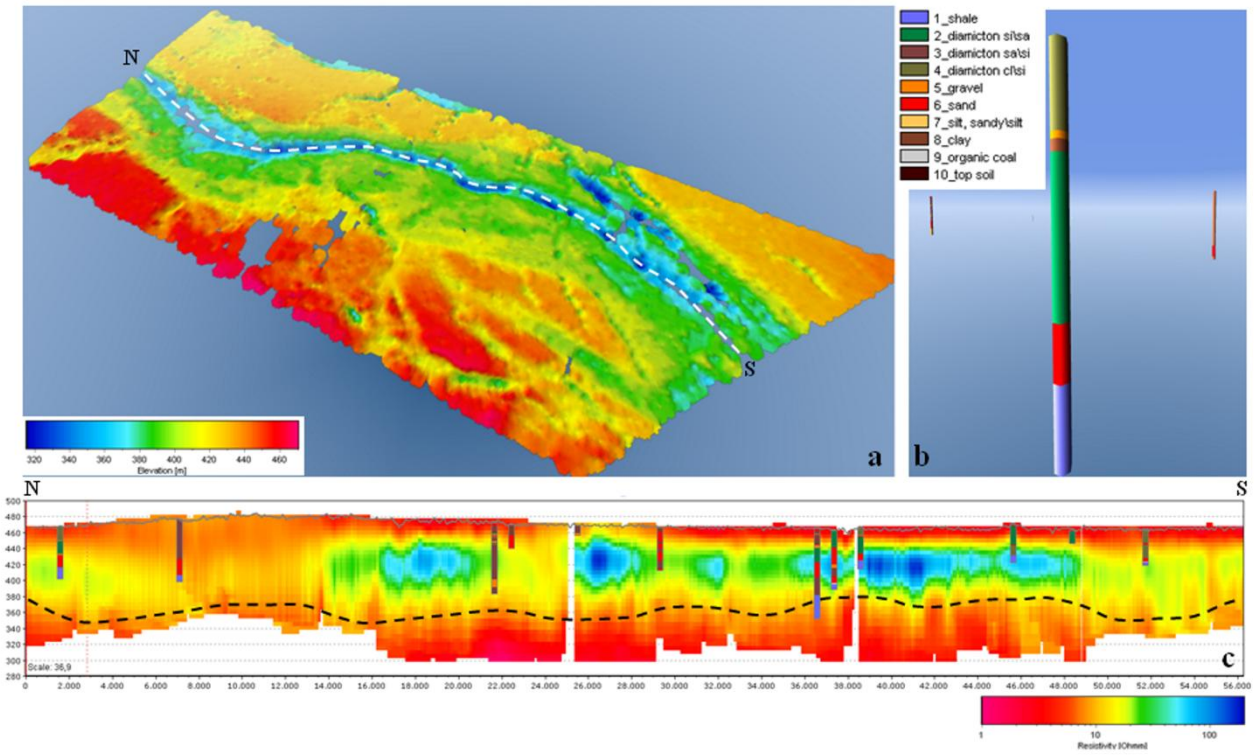

Figure 8.
A profile section N – S oriented, through the longest inset valley observed in the survey area, is plotted below the contour map. a) the conductive bedrock surface and the location of the profile are shown (dashed white line). B) Example of a water well data with associated stratigraphic information (see the legend on the left side for lithology detail). c) The profile connects all the boreholes that come across the buried valley. We also applied a small buffer zone in order to take into account only the boreholes that are located within the inset valley.

more regional scale, for example with regard to the presence of a sloping bedrock towards the East, Northeast and Southeast (Fig. 6). Compared to the full AEM survey, the results of the simulated ground survey (both data density levels) show much less details in terms of structural geometry of features; the clear network of secondary valley features disappears completely. For the reconnaissance survey (Figure 3, right side) we still observe the bulk of the main Spiritwood valley as a resistive signature that crosses the entire area, but with diffuse boundaries and uncertain total extent and geometry. The same picture is seen in figure 6 in terms of bedrock elevation where the valley incision into the bedrock gets very diffuse and difficult to follow for the reconnaissance survey. The high resolution ground survey (Figure 3, central panels) images more sharply than the

reconnaissance survey the long, resistive middle feature, and also hints towards the presence of possible secondary elements of the valley network.

The above observations are more evident in figure 4. It is here obvious, particularly for the reconnaissance survey, that there is no evidence of the detailed valley network filled with resistive materials. In the derived maps of the elevation of the shale (Fig. 6) the difference in the resolution of the valley network between the surveys is even more pronounced than in the resistivity maps.

The near-surface inter-till area in the central part of the area (Fig. 3A) is seen in all surveys, but its appearance loses a lot of detail in the ground TEM surveys. The overall scale of this geological structure is large enough to be captured by the limited spacing of the TEM soundings, but it appears that the scale length of detailed features related to the structure is not rendered adequately.

In general, the spatial variability of the resistive sediments within the valleys, both large and small, as well as within the inter-till formation, is captured by the true AEM survey, but much less by the ground surveys. A very high data density is required for delineating the detail in the inter-till formation and to outline and orientation of the buried valleys in complicated systems like the Spiritwood Valley. It is difficult to establish the connection between individual buried valleys if the only geophysical contribution comes from sparse ground TEM measurements.

Implications for hydrogeological interpretations and management - discussion

As mentioned above, the ground TEM surveys would take approximately 3-5 months and 1/2 months, for the HR and the Reconnaissance survey respectively. Even though such difference in time will be reflected in the costing, we estimate the cost of such undertakings to be in the order of hundred thousand USD. In comparison, the AEM survey took approximately 4 weeks to acquire, and a couple of months for accurate re-processing and inversions, with a total investment that can be estimated to be 2 to 3 times higher than the simulated ground based surveys. However, the unit cost of one sounding drops 2 order of magnitudes from the ground surveys (a few hundred USD/sounding) to the airborne survey (few USD/sounding). In our opinion, the extra bulk

budgetary investment required for an AEM survey is to be taken in serious consideration, given the added value in large scale groundwater programs.

In general terms, we will discuss the issue of general hydrogeological mapping of aquifers geometry, of aquifer vulnerability, and of flow models for sustainable development of GW resources. As demonstrated, AEM provides high resolution results and detailed geological interpretations, which result in a more connected (and hopefully more accurate) description of the whole set of existing structures. On the contrary, a low density dataset based on ground TEM surveys (i.e. reconnaissance survey) results in a low resolution resistivity model and a less detailed and disconnected description of the geological setting; small-scale but potentially important structures are lost and these omissions can propagate into hydrogeological models. For example, bedrock elevation or aquitard elevation is often an important starting point for a variety of hydrogeological investigations such as groundwater modelling or siting exploitation drilling. However, the elevation maps of the conductive bedrock derived from insufficient data, would result in an incorrect contribution to this crucial part of the hydrogeological understanding (compare figure 6C with 6A).

In a hydrogeological context like this, where potential aquifers appear to be relatively small and complex, the most relevant implication for groundwater resource mapping and management is the ability to resolve the aquifer geometry. If we only consider a ground TEM result, e.g. the reconnaissance survey, any mapping of aquifers is almost impossible due to the low density of collected data. Most of the deep aquifer targets in the area are situated within relatively small valley structures and without the detailed AEM data these aquifers are very difficult to map and target for drilling. Given only the ground based surveys, drill targets for finding high potential aquifers would be sporadic along the long inset valley (Fig. 3C, middle and right), but the uncertainty related to putting the boreholes at most optimized locations is high. Establishing locations for new groundwater exploration drillings or well fields is much safer with the maps generated from the AEM data at hand, i.e. location of a lot of small aquifers are indicated by the scattered resistive

bodies within the valley structures, and optimized positions for drilling can be determined by locating the exact position of the valley thalwegs from the shale elevation map (Fig. 6A). This turns out as an important aspect since the presence of resistive material enhance permeability into the valleys and may result in potential groundwater reservoir. Despite the obvious advantage in using AEM for mapping GW resources at high resolution, it must also be pointed that ground TEM data alone did produce results that allowed better hydrogeological mapping than the one based solely on boreholes.

According to the AEM data, the valley aquifers are often covered by clayey to silty\sandy sediments (i.e. till) giving them some kind of natural protection against pollution from the surface. However, where the valleys are cut by younger valleys filled by sandy material they can be exposed and vulnerable. Thus, vulnerability assessments of important deep aquifers in the area would also be impossible to perform solely based on the ground based surveys. In the area where extensive inter till sands are interpreted to cover the deeper setting including aquifer-hosting valleys, a detailed knowledge of the spatial extension and internal composition of this sand formation is important. Like the buried valley-geology this formation is much better resolved by the true AEM survey than by the ground survey.

Glaciated areas are typically complex and detailed information and models are essential if the goal is to predict groundwater pathways to well fields based on flow modeling (Troldborg *et al*., 2008; Troldborg *et al*., 2007). Especially with the presence of buried-valley geology such predictions are challenging and require high resolution models, where the individual valleys must be resolved (Shaver and Pusc, 1992; Jørgensen *et al*., 2008; Andersen *et al*., in press). Groundwater flow will tend to follow the often coarse-grained sediments in the valleys, but in cases where clay-filled valleys cut such pathways they can constitute effective barriers. So, the groundwater flow in our area is extremely connected to the existing geometry of the valley aquifer. The true AEM survey maps the valley network in detail, whereas the ground based does not at all. On this

background we evaluate, that only a flow model based on the true AEM survey would be able to produce useful results for groundwater management, i.e. catchment area calculation.

By resulting in the effective mapping of aquifer location and giving the potential for detailed groundwater flow prediction, the performed true AEM survey leads to a possibility for virgin aquifers to be exploited as local resources of pure water Last but not least, an accurate, large, high resolution model obtained from AEM can also help the managing body identifying and assessing issues linked to the varying quality of ancillary information. For example, it can serve as a base to screen for outliers existing databases of e.g., borehole stratigraphy.

Complementarity of AEM and ground based TEM

AEM and ground based TEM can be applied in a complementary way in hydrogeophysical surveys (i.e. Jorgensen et al., 2003, 2006, Podgorski et al., 2013,). In areas in which AEM sometimes fails to reach the target, ground TEM can provide readings for greater depths. An alternative and possibly more important approach might be the use, when useful and feasible, of a calibrated ground based TEM system to check and post-calibrate an AEM dataset (i.e. Podgorski et al., 2013). As an experiment, the authors calibrated a ground TEM Geonics system at the Danish test site. The calibration procedure developed by the Hydrogeophysics Group at Aarhus University was applied (Foged et al., 2013, "*guidelines for configuration setup and measuring scheme for standard 40x40 m ground based TEM-measurements*" report 2002). The Danish TEM test site is at Lyngby near Aarhus and was set up in 2001. The purpose of the test site is to check that all the TEM systems used in the Danish groundwater mapping program are capable of identifying the test site reference model. This ensures that measurements taken with different instruments can be referred to the same geophysical and thus geological model. The test site has been over the years used to calibrate TEM instruments from Denmark as well as France, Germany, Switzerland, Australia, the USA, and now also Italy. Originally the test site used a point with a single reference model, but in 2009 this was extended to include two intersecting lines. This made the site applicable for the calibration, validation, and testing of airborne TEM survey system. A number of ERT

measurements were performed in 2011 in to increase resolution of the first 15 m in terms of resistivity structure several ERT measurements were performed in 2011 (total of 11 profiles were measured with a profile length of 160 to 800 m.). ERT measurements were supplemented with an EC-log to clarify any electrical anisotropy in the geological layers (HGG report 2011,2012).

Ground TEM calibration procedure

Guidelines for configuration and measuring schemes were as noted above, followed by development of a calibration procedure. The calibration results showed that nine Geonics PROTEM47 system instruments from five consulting companies, returned the same TEM-response for the same site. TEM readings were taken in a circular configuration using a 40 x 40 m transmitter loop. In calibration unique time-shifts and data level shifts are assigned to each individual TEM systems. The nine measured responses were used to calculate an average which was adopted as the test site *reference response* (figure 9).

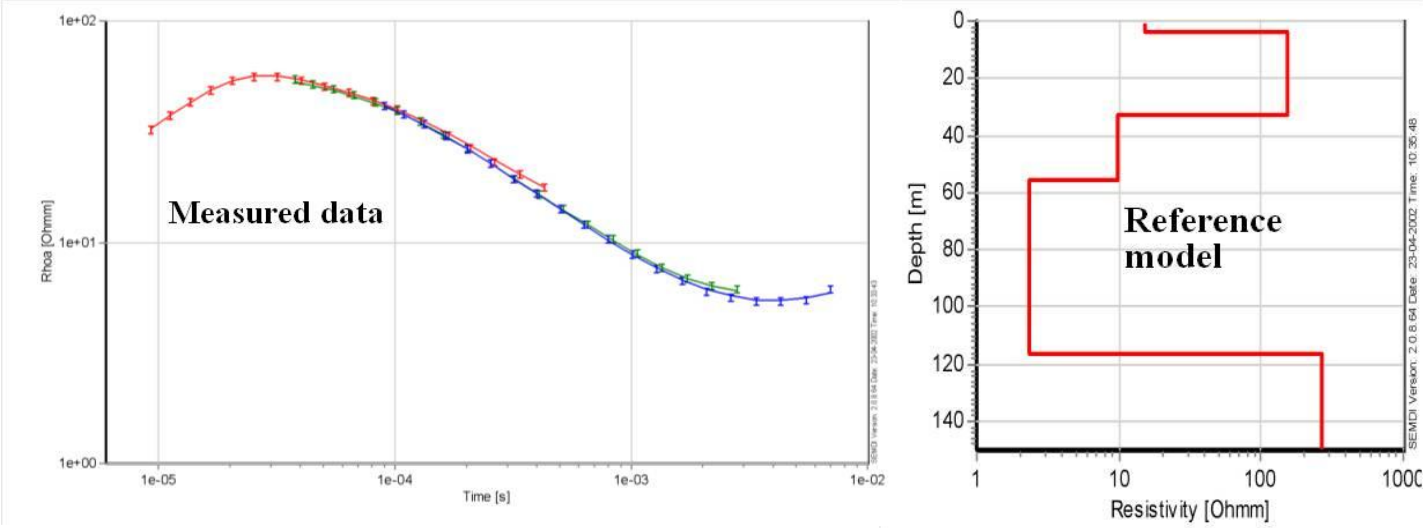

Figure 9.
The 2011 reference model of the TEM test site (right). Error bars are the data, solid line the forward response from the reference model. Left panel shows the typical ground-based forward response of the reference model (central loop configuration, 40 × 40 m^2 transmitter loop) plotted as Ω *f*(t) for the entire dynamic range (UH, VH, and HI repetition frequencies).

Following calibration the various systems return the reference response to within 3% at all time gate readings. In the first test, however, most of the instruments returned significantly different sounding curves. The explanation for these discrepancies was in part the result of using different generations of the PROTEM47-system, and in part caused by electronic malfunctions. Following

instrument repairs, upgrades, and minor time and data adjustments (calculated correction factors), consistent TEM responses were achieved from all nine TEM-systems roughly within the 3% deviation threshold. The nine individual systems were then continuously monitored and calibrated using the reference response. The calibration scheme presented here for TEM instruments resembles the GCM data calibration procedure described by Lavoue et al. (2010). In both cases, known resistivity models are used to calculate system specific forward responses, and measured data is matched to forward responses in order to define calibration constants. The system specific reference response can be compared directly with the measurement data. Calibration is completed with minor uniform level and time adjustments to the data-curve measurements until the best possible fit is achieved with the reference response (repeated for all the soundings on the basis of a gate-by-gate correlation with the resistivity model forward response).

Geonics ground TEM instrument and specifications

This section presents the equipment, instrument specifications, along with some measurement technique notes. The main function of time domain electromagnetic receivers is to record the transient signals that are generated during the decay of induced subsurface eddy currents. The transients are first divided into time windows by the PROTEM Receiver, and then the voltage in each window is converted into a digital value. A Geonics digital Protem combined with a TEM 47 transmitter and high frequency 1D induction coil were used at the Danish reference site to gather ground TEM data (figure 10). The high-frequency coil offered adequate bandwidth to capture the earliest portion of transient decay with minimal distortion. Measurements were taken in a central loop configuration with a loop size of 50x50m.

The receiver coils respond to the rate of variation in the magnetic flux. This generates an induced voltage proportional to the flux variation rate. Since magnetic flux is measured in nano Teslas (nT), the rate of variation is in units of nT/s. Conveniently (and not accidentally), 1 nT/s = 1 nV/m^2 of induced coil voltage per unit of effective area. Given a flux variation rate of dB/dt = dV/dA, and a coil area of A, then the resulting coil output voltage is: Vc = dV/dA * A

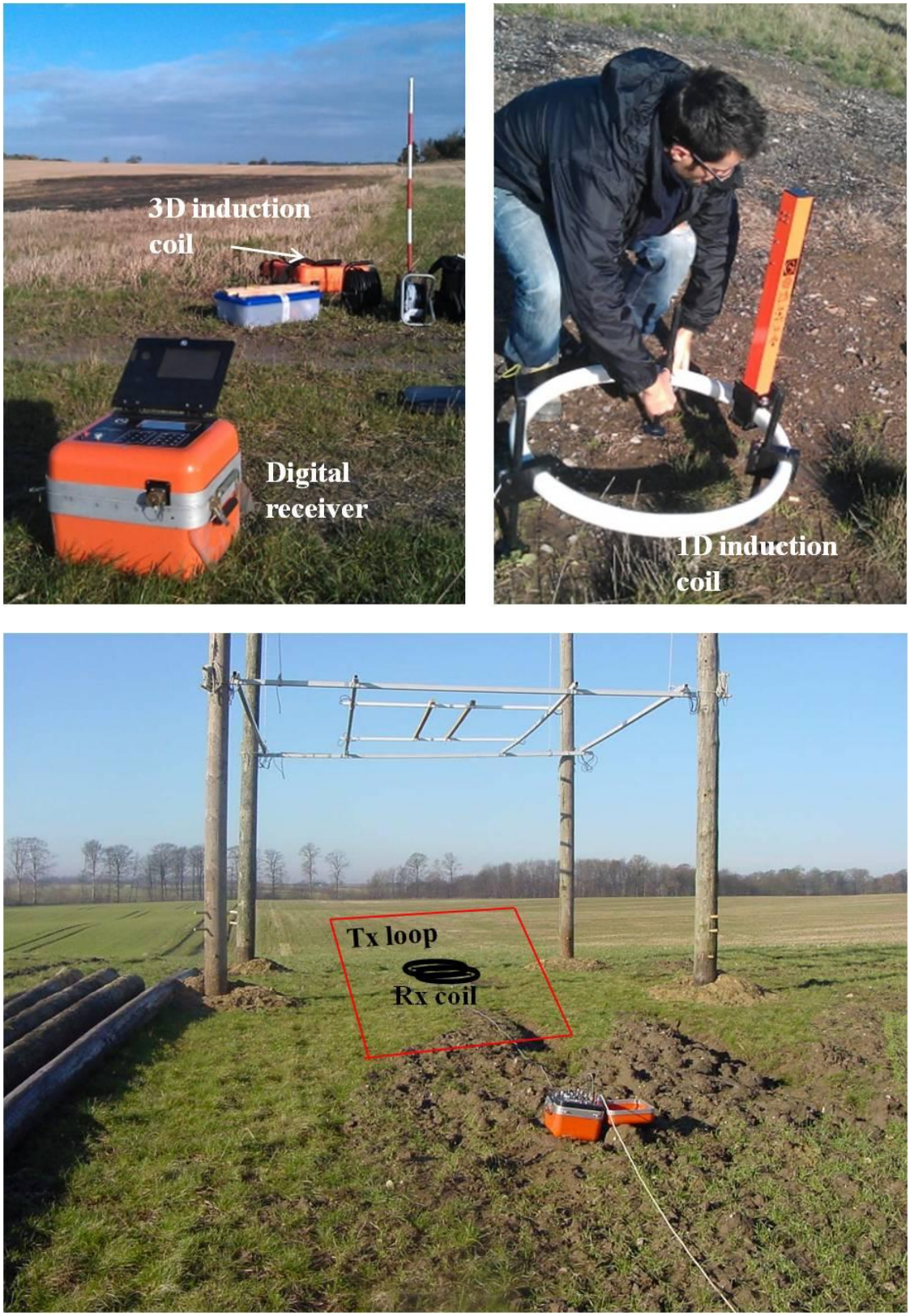

Figure 10.
Ground-based Geonics TEM47/PROTEM systems (Geonics Limited) operating at the Danish Test site (top). Field setup for a central loop configuration arranged at the test site (bottom).

Induced ground currents produce only very small secondary magnetic fields. The early receiver coil voltage readings per unit area are in the order of 0.1 mV to 1 mV, with generally around 1 nV or less in late readings. Accurate measurement of this response would be impossible without amplification because internal electronic noise would mask the signal. Amplification is achieved in three stages: coil effective area (all "copper area", or copper area combined with coil preamplifier), receiver preamplifier fixed gain, and user-selected gain (also see Geonics specifications). When using a TEM47 and 1D high frequency (1D HF) coil, the dB/dt response generally ranges from a 100 nT/s high, to a 1 nT/s low. The effective area of the HF coil (a combination of copper area and preamplifier) is 31.4 m2. User could be tempted to use gain 7 to amplify the late time high frequency coil signal, but as a result the early time response will obviously become too high with probable saturation of the signal at gates 1 or 2. Generally speaking, the optimum gain setting is the highest gain value that can be implemented without causing saturation or non-linearity of the readings. Several preliminary tests should be conducted in the survey area before the appropriate gain setting can be established. If moving into an areas with more numerous sources of noise or if the noise level in readings is seen to rise, the gain tests should be repeated. The modified symmetrical square wave transmitter current is abruptly reduced to zero after every second quarter-period for the duration of a quarter period, after which the flow direction is inverted. The total time of one cycle is referred to as the Tx period. At the start the Tx loop current is raised from 0 up to the value set for the specific sounding. The current is maintained at this value in the Tx loop for one quarter of the Tx period, then terminated so that the current falls back to 0 during the Tx turn-off time. The turn-off trend follows an almost linear ramp of duration determined by the Tx loop geometry. This duration is referred to as the "measurement period" and represents a quarter (T\4) of the complete cycle, terminating when the current returns to 0. The second half cycle begins after the end of the measurement period, following an identical sequence but with inverted current flow. The receiver has 20 narrow time gates designed to accurately

measure the voltage decay characteristics, with each gate opening in sequence and measuring the amplitude of the decaying voltage in 20 sequential time windows (Rx time gates).

Ground conductivity influences the amplitude, shape and duration of sampled signal pulses, and so different repetition rates are implemented in order to compensate for different transient durations over a wide time range. The repetition frequencies are: ultra high (235 Hz), very high (62.5 Hz), and hi frequency (25 Hz). Lower frequencies can also be implemented for readings from the last few Rx time gates (in which the noise level is close to zero). The ultra high frequency segment samples signals from the 7μs to 800μs recording times, the very high frequency segment samples the 35μs to 2.8 ms time interval, and the hi frequency segment samples the 88μs to 7 ms interval. Any changes in base frequency will affect the period T and so also the measurement period (T\4). The first measurement is normally taken at the highest repetition frequency (235 Hz), which also produces the shortest measurement period (0.8 ms). This provides measurements for the very early time gates, thus collecting data on near surface terrain. For deep sounding the response must be measured at very late times, and so the measurement period is extended (lower base frequency) to accurately measure the late time transient amplitudes (and also "*to avoid transient response run-on to the next primary field cycle",* McNeill, 1994).

The early time gates are very narrow because they are located in the sector in which the transient voltage varies rapidly. The later time gates are much wider since they are located where the transient voltage varies more slowly. Consequently*, "after the current in the Tx-loop is turned off, the current will be close to the surface, and the recorded data reflects the conductivity of the top layers (early time gates). At later times the current will run deeper in the ground, and the measured signal contains information about the conductivity of the lower layers"* (late time gates) (Christiansen et al., 2009).

4.6.3 Field work: ground TEM data collected at the test site

Field measurements were conducted by positioning a loop (wire) inside a square loop on the ground with an area of 50 x 50 m^2. The wire was connected to the transmitter (Geonics Tx 47), and the

receiving coil (1D high frequency induction coil) was positioned in the center of the loop. The induction coil was connected to a digital receiver (Protem receiver), this being connected in turn to the transmitter using a reference cable in order to enable synchronization between the transmitter and digital receiver. The output current for the on time phase was set on the transmitter. Several setting adjustments were required on the receiver before a measuring cycle could be run. The most important parameters that need to be accurately set are: loop size, turn-off time (derived from the loop geometry), input current (from the Tx), repetition frequency (first UH, then VH, then HI), integration time (stack number), and gain. The receiver induction coil was located at exactly the same position as all the other TEM instruments being calibrated (according to the 1D reference model). This avoided discrepancies relative to the reference model caused by variations in coil position. The system turn-off time for the transmitter current was set to 3 μs. This interval is the time during which the transmitter current is gradually turned off with an approximately linear ramp. This relatively short turn-off time makes it possible to achieve accurate readings for the resistivity properties of the uppermost portion of the subsurface. Transmitter currents of respectively 1 A and 3 A were used for the UH base frequency, and the VH and HI base frequencies. Given that the data was collected on a test site, it could be assumed that there were no local sources of significant electromagnetic noise, like for example power lines (50 Hz), metal structures (pipes, fences, etc.), or marked electrochemical effects (induced polarization, i.e. Flis et al., 1989). Nevertheless, background noise data was recorded before any test measurements in order to asses late time noise levels in the measurement data. Several records were acquired with short integration times (total measurement times) for each set of measurements in order to improve the signal to noise ratio, in particular for the UH an VH frequencies (HI frequency integration times are longer). Figure 11 presents the recorded data. The noise model was assumed to follow a power law distribution (Munkholm and Auken, 1996). The "background noise" (or "white noise") level is proportional to $t^{-1/2}$. It should be noted that the signal response is generally significantly stronger than the background noise, an only the latest time windows covered by the high frequency segment appear

mildly influenced by the noise. This typically high signal to-noise ratio is interpreted as arising from the combination of very few cultural noise sources in the measurement areas and the presence of shallow geological features with high electrical conductivity.

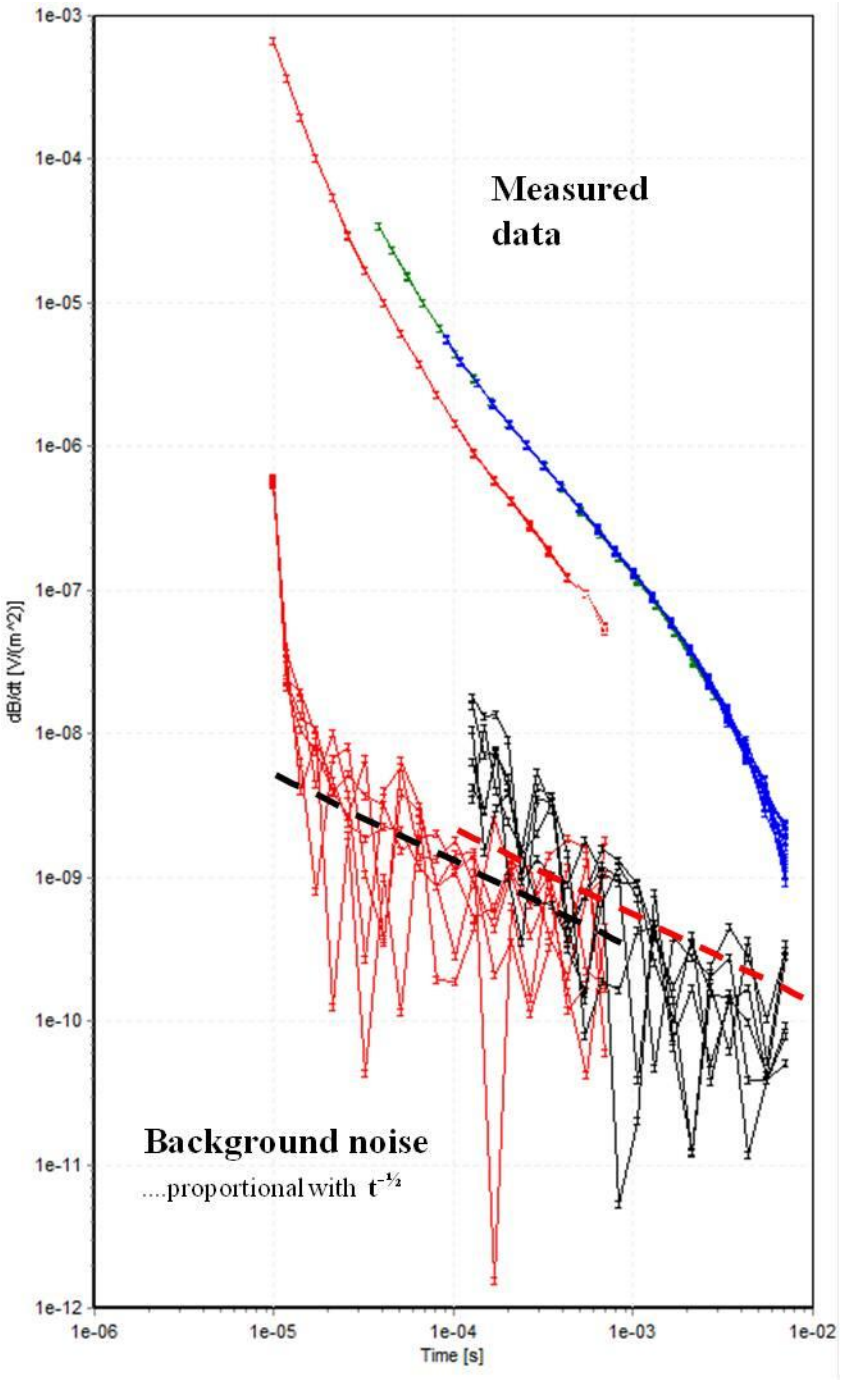

Figure 11.
TEM sounding and noise measurements for the ultra high (UH), very high (VH), and high (HI) segments. Error bars are 3%. Noise values were measured in the same time segment as for the transient data (but not for the VH frequency, which was just outside range). Theoretical curves for "background" noise with the $t^{-1/2}$ trend are shown with dashed lines.

Data calibration: time shift and amplitude shift correction factors

Initial processing of the TEM data included editing and definition of a priori uncertainties using the SiTEM program. The data were assigned a uniform STD of 3 % (in db/dt). The TEM data were then inverted in order to define 1-D resistivity models of the subsurface using the SEMDI program. Both the SiTEM and SEMDI programs were developed by the HydroGeophysics Group, Aarhus University (Munkholm and Auken, 1996; Effersø et al., 1999). The iterative least squares algorithm used to achieve inversion (modeling the complete system response) requires a starting model. One of the major advantages of using least squares-based inverse methods is that they provide as assessment of model resolution (Auken et al., 2002). The model resolution estimates for individual model parameters are presented here in relative numbers. A model parameter should, ideally, exhibit a resolution value of 1.00, while a resolution value of 1.05 indicates an estimated 5% uncertainty of the relevant model parameter. Low resistivity layers can generally be clearly resolved using the TEM method, while high resistivity layers (with resistivities of 100Ω m and above) are poorly resolved. An a priori model is defined for each inversion. Deciding the number of layers to be included is a crucial step when defining the starting model because this cannot be automatically changed by the inversion algorithm. It is normally advisable to opt for the model with the smallest number of layers in order to satisfactorily fit the observed data. The data were first inverted using a 5 layer starting model (figure 12). By observing the 1D model generated from the "uncalibrated ground TEM" data, several discrepancies emerge as regards thicknesses (and thus relative depths to layers) between layers when compared to the reference 1D model (1D model in figure 9 compared to figure 12). It is also clear that the reference model (see rho data of figure ddd, top) amplitude and time factor data differ from the measured data , in particular for the early time gates from around 9 to 40 μs. The reference model has relatively earlier time gates, and so the newly collected data require application of correction factors (amplitude and time shift) in order to reproduce the reference model. For further details regarding the calibration scheme, calculation of correction factors, etc., refer to Foged et al., 2013.

The reference model was therefore used to forward model the response of the uncalibrated ground TEM. Each TEM recording was referred to the relevant repetition frequencies, and then matched to the respective reference model within a set tolerance of 3%. This enabled evaluation of two variables: a time shift to be subtracted from the time of each gate for the UH and VH repetition frequencies and added to the time of each gate for HI frequencies, together with an amplitude factor by which the dB/dt value of each gate is multiplied. A simple MATLAB script (elaborated from Cyril, Hydrogeophysics Group, Aarhus University) was used to minimize the least-squares misfit between the reference TEM and the test TEM recordings by adjusting these two variables. Figure 13 shows the correction factors achieved after calibration.

A good fit for the early time gate as regards the reference response for the UH measurement period was achieved by applying a time shift factor of -0.6μs and a factor of 0.95 to get. These apparently small shift factors explain the marked discrepancy observed for the early time gate, in turn generating incorrect very near surface resolution. Factors of 1.03 and 0.94 were applied for VH to HI repetition frequency data, respectively, in combination with time shift factors of –2.7 μs and 13 μs. As measurement periods increase (and so the Rx time gates are later compared to the higher repetition frequency) the effects of minor early time shift factors generally decrease (see also Christiansen et al., 2011 for further details). This means that a time shift of for example 5\10 μs does not have any effect on the near surface output model when the nominal 1st gate (to be shifted) is in the order of tens of μs. The effects of a given time shift become less or even negligible at later time gates. Following the calculation of calibration factors based on the test site reference response, a calibrated System Transfer Function was defined for use in a second inversion of the collected data. Figure 14 shows these new (calibrated) inversion results. The same number of layer as the reference model were used in this case, using a 6 layer starting model for the inversion. An excellent data fit was achieved (within the noise level) together with a perfect match between the 1D reference model and the new 1D calibrated model (see figure 14, top). In relation to the deeper portion of the reference model, the present model produced no representation of the deep

conductive layer (at 260 m in depth). The instrumentation used in the present study did not acquire any data for such long time gates as those measured by the Hydrogeophysics Group using the WalkTEM instrumentation (see HGG report 2011).

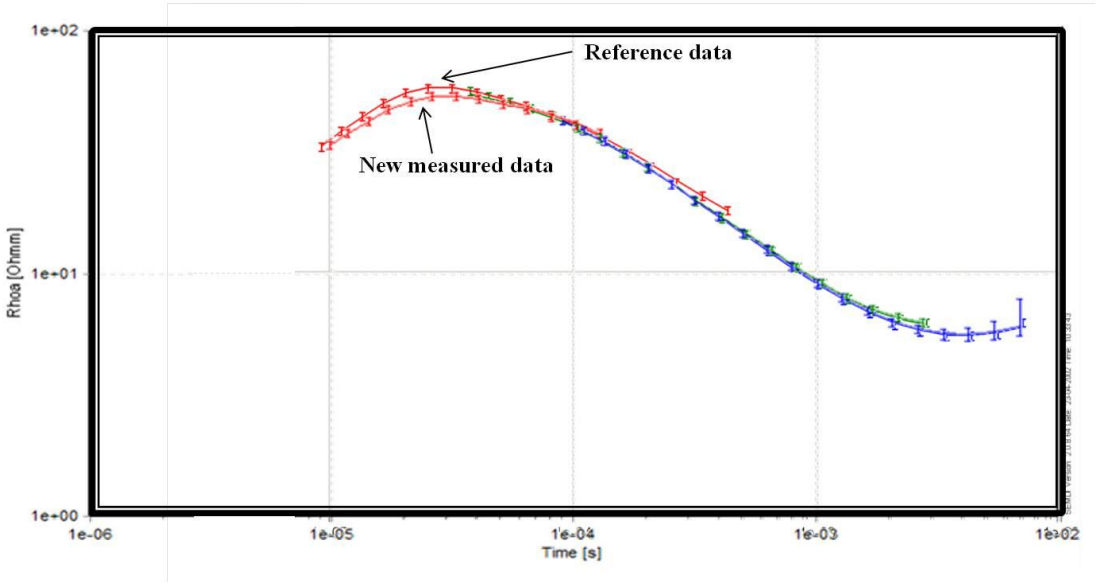

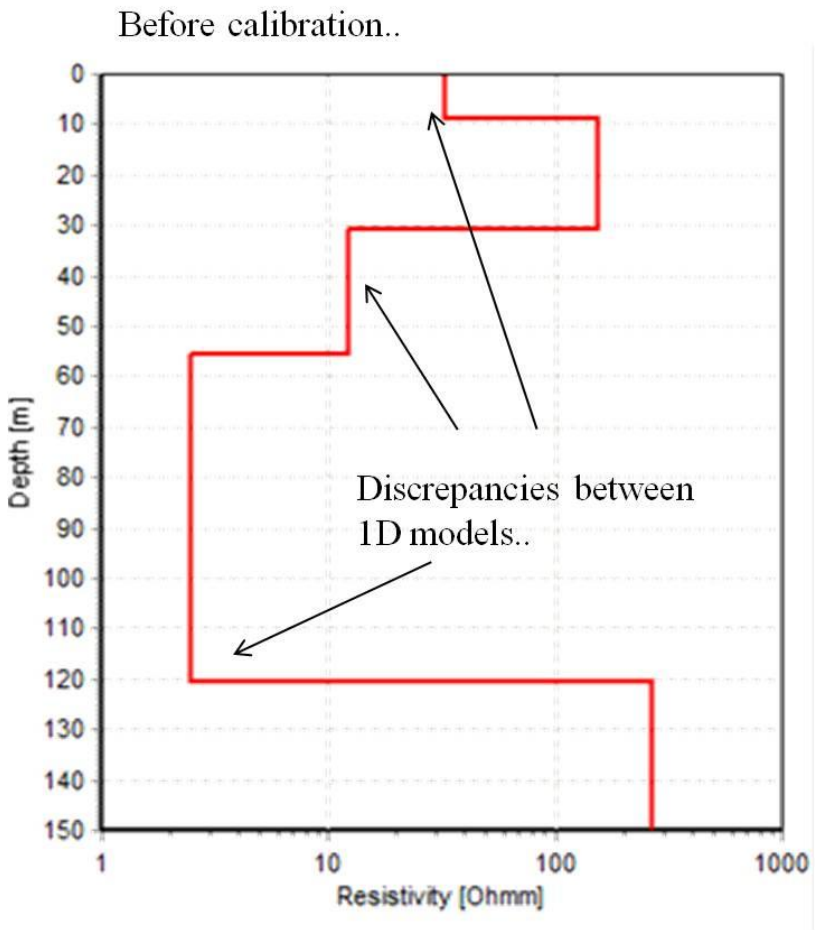

Figure 12
Comparison between the reference data and the new (uncalibrated) measured data. Error bars are the recorded data, the line is the forward response from the reference model Red, green, and colors indicate the ultra high, very high, and high segment of the sounding curve (top). 1D reference model before calibration (to better analyze differences compare it to figure 10, right or 15, top).

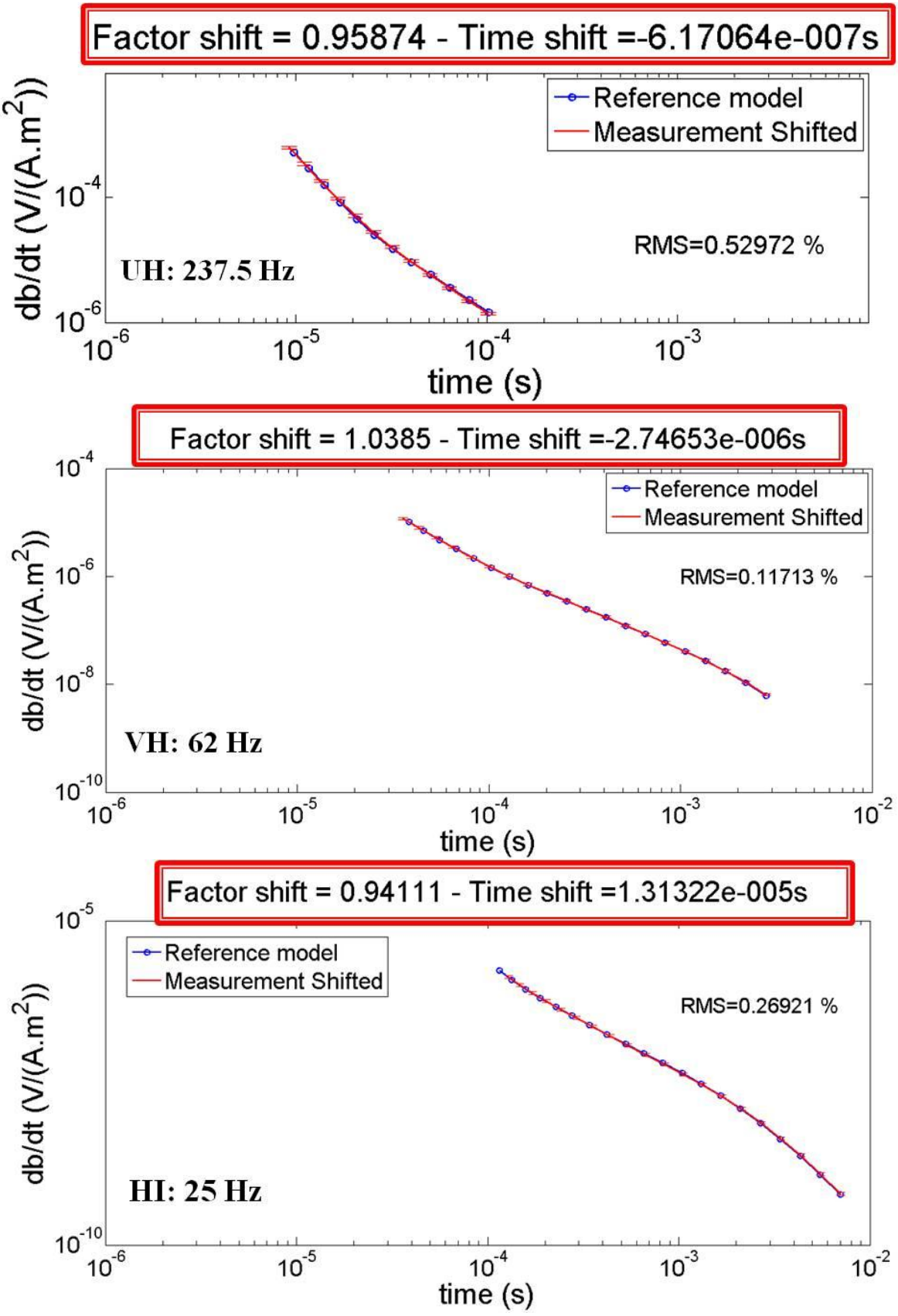

Figure 13.
The defined correction factors used to calibrate the new ground TEM recordings for each of the repetition frequencies. Late time noise assessments were performed and noisy late time gates were omitted to increase calibration accuracy. The calculated time shift factors were added (and subtracted, if negative) to all time gates and the dB/dt values were multiplied by the shift factor to complete calibration.

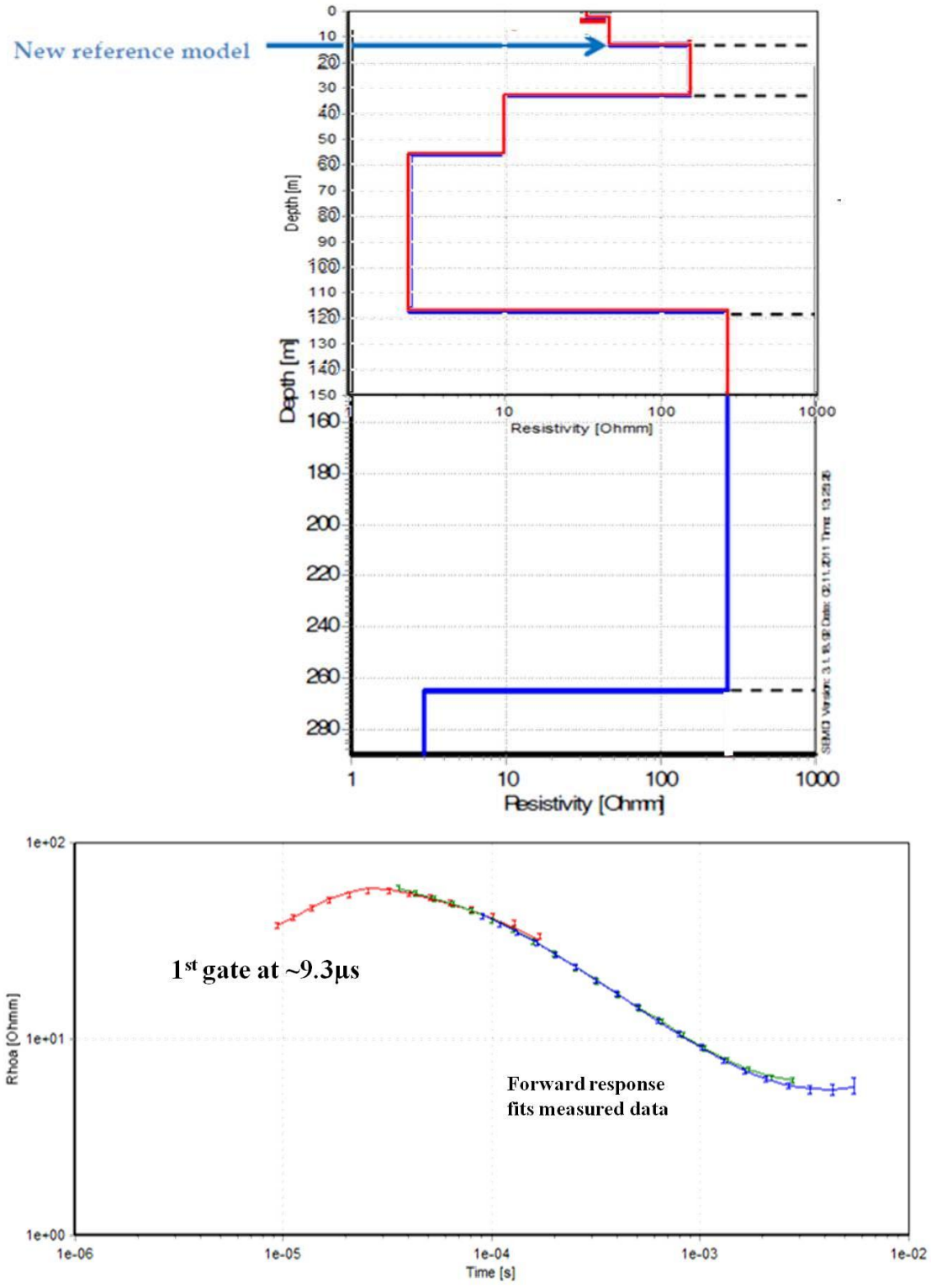

Figure 14.
Comparison between the new refined reference models at the national TEM test site (HGG report, 2011) and the calibrated 1D model from newly collected data at the same survey area (top). Calibrated TEM response over the test site after correction of the uncalibrated data with the defined calibration factors (time and amplitude shift as in figure 13).

Final remarks

In this chapter has been described the shortcomings in hydrogeological interpretation and management that could have arisen if the AEM survey had been substituted by a ground TEM survey in the same area. Output resistivity models clearly reveal how the mapping of hydrogeological features of great relevance, like main buried valleys as well as minor valley networks, could be inaccurate and poorly detailed in terms of structures morphology Furthermore, derived products of high density AEM inversion results, i.e. elevation of bedrock can be readily integrated and compared successfully with other available data, either geophysical or geological. Integrated with ancillary information, AEM provides, rapidly and cost effectively, robust results in terms of aquifer geometry and vulnerability mapping, and solid basis for subsequent flow modeling.

In the last three decades, airborne electromagnetic (AEM) systems have been used for many groundwater exploration purposes. This contribution of airborne geophysics for both groundwater resource mapping and water quality evaluations and management has increased dramatically over the last 10 years proving how those systems are appropriate for large-scale and efficient groundwater surveying. One of the major reasons for its popularity are the time and cost efficiency in producing spatially extensive datasets that can be applied to multiple purposes. In this chapter has been carried out a simple, yet rigorous, simulation showing the impact of an AEM dataset towards hydrogeological mapping, comparing it to having only a ground based TEM dataset (even if large and dense), and to having only boreholes. We started from an AEM survey and then we simulate two different ground TEM data sets: a high resolution survey and a reconnaissance survey. The electrical resistivity model, which is the final geophysical product after data processing and inversion, changes with different levels of data density. We then extended the study to describe the impact on the geological and hydrogeological output models, which can be derived from those different geophysical results and the potential consequences for groundwater management. Different data density results in significant differences not only in the spatial resolution of the output resistivity model, but also in the model uncertainty, the accuracy of geological

interpretations and, in turn, the appropriateness of groundwater management decisions. The AEM dataset provides high resolution results and well-connected geological interpretations, which result in a more detailed and confident description of all of the existing geological structures. In contrast, a low density dataset ground-based TEM survey yields low resolution resistivity models, and an uncertain description of the geological setting.

The AEM survey successfully maps valley locations that continue to be difficult to define using seismic, electrical resistivity and borehole methods. To further asses the AEM system response over the Spiritwood, the author performed the new calibration procedures for a ground based PROTEM 47 system on the Danish National Test Site for TEM systems. The calibration procedure involved small time-shifts and offsets of recorded transients of individual TEM systems. Given this calibrated ground system, ground TEM surveys can be conducted for the Spiritwood Valley in order to assess the possibility of re-calibrating the existing AEM dataset, thereby reducing the uncertainty of the hydrogeological models derived from non-calibrated AEM data (i.e. Podgorski et al., 2013).

References

Abraham, J.D., Cannia, J.C., Bedrosian, P.A., Johnson, M.R., Ball, L.B., and Sibray, S.S., 2012, Airborne Electromagnetic Mapping of the Base of Aquifer in Areas of Western Nebraska: USGS, North Platte Natural Resources District, the South Platte Natural Resources District, and the Nebraska Environmental Trust Scientific Investigations Report 2011–5219.

Allard M., 2007, On the origin of the HTEM species. in Proceedings: Fifth Decennial International Conference on Mineral Exploration, 355-374.

Andersen, T.S., Poulsen, S.E., Christensen, S., and Jørgensen, F., 2013, A synthetic study of geophysics-based modelling of groundwater flow in catchments with a buried valley: Hydrogeological Journal, in press.

Andriashek, L.D., 2003, Quaternary geological setting of the Athabasca Oil Sands (in situ) area, northeast Alberta: Alberta Energy and Utilities Board/Alberta Geological Survey, Earth Sciences report 2002-2003.

Auken, E., Nebel, L., Sørensen, K., Breiner, M., Pellerin, L.,Christensen, N.B., 2002. EMMA—a geophysical training and education tool for electromagnetic modeling and analysis. Journal of Environmental and Engineering Geophysics 7, 57–68.

Auken, E. Jørgensen, F., Sørensen, K.I., 2003, Large-scale TEM investigation for groundwater: Exploration Geophysics, 33, 188-194.

Balch, S.J., Boyko, W.P., and Paterson, N.R., 2003, The AeroTEM airborne electromagnetic system: The Leading Edge, 22, 562-566.

Betcher, R.N., Matille, G., and Keller G., 2005, Yes Virginia, there are buried valley aquifers in Manitoba: in Proceedings: 58th Canadian Geotechnical Conference, 6E-519.

Cannia, J.C., Abraham, J.D., and Peterson, S.M., 2012, Using Geophysical Data to Improve an Optimization Groundwater Model Evaluating the Effectiveness of Intentional Recharge in the North Platte River Valley, Western Nebraska, USA: in Symposium of Water: Science, Practice and Policy, Lincoln, Nebraska, USA

Christiansen A.V., and Auken E., 2012, A global measure for depth of investigation: Geophysics, 77, 171-177.

Crow H.L., Knight R.D., Medioli B.E., Hinton M.J., Plourde A., Pugin A.J.-M., Brewer K.D., Russell H.A.J., and Sharpe D.R., 2012, Geological, hydrogeological, geophysical, and geochemistry data from a cored borehole in the Spiritwood buried valley, southwest Manitoba: Geological Survey of Canada, Open File 7079.

Cummings, D.I., Russell, H.A.J., and Sharpe, D., 2012. Buried-Valleys in the Canadian Prairies: geology, hydrogeology, and origin: Canadian Journal of Earth Sciences, 49, 987-1004.

Effersø, F., Auken, E., Sørensen, K.I., 1999. Inversion of band-limited TEM responses. Geophysical Prospecting 47, 551–564.

Fitzpatrick, A., and Munday, T., 2007, The application of airborne geophysical data as a means of better understanding the efficacy of disposal basins along the Murray River: An example from Stockyard Plains, South Australia. in Extended Abstracts: ASEG, 2007.

Flis, M.F., Newman, G. A., and Hohmann, G. W., 1989, Induced-polarization effects in time-domain electromagnetic measurements,Geophysics, 54, 514-523.

Foged, N., Auken, E., Christiansen, A.V. Sørensen, K.I., 2013, Test site calibration and validation of airborne and ground based TEM-systems: Geophysics, in press.

Fountain D., 2008, 60 years of airborne EM - Focus on the last decade. in Proceedings: 5th International Conference on Airborne Electromagnetics, Haikko Manor, Finland.

Huang H., and Rudd J., 2008, Conductivity-depth imaging of helicopter-borne TEM data based on a pseudolayer half-space model: Geophysics 73, 115-120.

Jørgensen, F., Sandersen, Peter B.E., Auken, E., 2003, Imaging buried Quaternary valleys using the transient electromagnetic method: Journal of Applied Geophysics, 53, 199- 213.

Jørgensen, F., and Sandersen, P.B.E., 2006, Buried and open tunnel valleys in Denmark – erosion beneath multiple ice sheets: Quaternary Science Reviews, 25, 1339-1363.

Kehew, A.E., and Boettger, W.M., 1986, Depositional environments of buried-valley aquifers in North Dakota: Ground Water, 24, 728-734.

Jørgensen, F., Damgaard, J., and Olesen, H., 2008, Impact of geological modelling on groundwater models – a case study from an area with distributed, isolated aquifers: in Calibration and reliability in groundwater modeling, Refsgaard, J.C., Kovar, K., Haarder, E. & Nygaard, E., (eds.), IAHS Publication, Wallingford (Int. Assoc. Hydrol. Sci.) 320, 337-344.

Kirkegaard, C., Sonnenborg, T., Auken, E. and Jørgensen, F., 2011, Salinity distribution in heterogeneous coastal aquifers mapped by airborne electromagnetic: Vadose Zone Journal, 10, 125-135.

Lavoue, F., Van Der Kruk, J., Rings, J., Andre, F., Moghadas, D., Huisman, J.A., Lambot, S., Weihermüller, L., Vanderborght, J. and Vereecken, H., 2010, Electromagnetic induction calibration using apparent electrical conductivity modelling based on electrical resistivity tomography: Near Surface Geophysics, 8, 553-561.

Legault, J. M., Prikhodko, A., Dodds, D. J., Macnae, J. C., Oldenborger, G.A., 2012, Results of recent VTEM helicopter system devel. opment testing over the Spiritwood Valley aquifer, Manitoba: in Expanded Abstracts: 25th SAGEEP Symposium on the Application of Geophysics to Engineering and Environmental Problems, 17 pp.

Møller, I., Søndergaard, V.H., Jørgensen, F., Auken, E., and Christiansen, A.V., 2009, Integrated management and utilization of hydrogeophysical data on a national scale: Near Surface Geophysics, 7, 647-659.

Munkholm, M.S., Auken, E., 1996. Electromagnetic noise contamination on transient electromagnetic soundings in culturally disturbed environments. Journal of Environmental and Engineering Geophysics 1, 119–127.

Oldenborger, G.A., 2010a, AeroTEM III Survey, Spiritwood Valley, Manitoba, parts of NTS 62G/3, 62G/4, Manitoba: In Geological Survey of Canada: Open File 6663.

Oldenborger, G.A., 2010b, AeroTEM III Survey, Spiritwood Valley, Manitoba, parts of NTS 62G/3, 62G/4, 62G/5, 62G/6, Manitoba. In Geological Survey of Canada: Open File 6664.

Oldenborger G.A., Pugin A.J.-M., and Pullan S.E, 2013, Airborne time-domain electromagnetics, electrical resistivity and seismic reflection for regional three-dimensional mapping and characterization of the Spiritwood Valley Aquifer, Manitoba, Canada: Near Surface Geophysics, 11, 63-74.

Paine, J.G., and B.R.S. Minty, 2005, Airborne hydrogeophysics: Hydrogeophysics, 50, 333-357.

Podgorski, J.E., Auken, E., Schamper, C., Christiansen, A.V., Kalscheuer, T. and Green, A. G. 2013. Processing and inversion of commercial helicopter time-domain electromagnetic data for environmental assessments and geologic and hydrologic mapping. Geophysics, 78, 149–159.

Pugin, A.J.-M., Pullan, S.E., Hunter, J.A., and Oldenborger, G.A., 2009b, Hydrogeological prospecting using P and S-wave landstreamer seismic reflection methods: Near Surface Geophysics 7, 315–327.

Randich P.G., and Kuzniar R.L., 1984. Geology of Towner County, North Dakota: North Dakota State Water Commission, County Groundwater Studies, 36, Part III.

Russell, H.A.J., Hinton, M.J., van der Kamp, G., and Sharpe, D., 2004, An overview of the architecture, sedimentology and hydrogeology of buried-valley aquifers in Canada: in Proceedings: 57th Canadian Geotechnical Conference, 26-33.

Sattel D., 2009, An overview of helicopter time-domain EM systems. in Extended Abstracts: ASEG, 2009.

Sattel, D., and Kgotlhang, L., 2004, Groundwater exploration with AEM in the Boteti area, Botswana: Exploration Geophysics, 35(2), 147-156.

Shaver, R.B., Pusc, S.W., 1992, Hydraulic Barriers in Pleistocene Buried-Valley Aquifers: Ground Water, 30(1), 21-28.

Thomson S., Fountain D., and Watts T., 2007, Airborne geophysics - Evolution and revolution. In Proceedings of Exploration 07: Fifth Decennial International Conference on Mineral Exploration, 19-37.

Troldborg, L., Refsgaard, J., Jensen, K., Engesgaard, P., 2007, The importance of alternative conceptual models for simulation of concentrations in multi-aquifer system: Hydrogeology Journal, 15, 843-860.

Troldborg, L., Jensen, K., Engesgaard, P., Refsgaard, J., Hinsby, K., 2008, Using Environmental Tracers in Modeling Flow in a Complex Shallow Aquifer System: Journal of Hydrologic Engineering, 12 (11),1037-1048.

Viezzoli, A., Christiansen, A.V., Auken, E., and Sørensen, K., 2008, Quasi-3D modeling of airborne TEM data by spatially constrained inversion: Geophysics, 73, 105-113.

Walker, S., and Rudd, J., 2008, Airborne resistivity mapping with helicopter TEM: An oil sands case study. in Proceedings: 5th International Conference on Airborne Electromagnetics, 06-03.

Wiecek S., 2009, Municipality of Killarney, Turtle Mountain groundwater assessment study: W.L. Gibbons & Associates Inc.

Wynn, J., 2002, Evaluating groundwater in arid lands using airborne magnetic/EM methods. An example in the southwestern U.S. and northern Mexico: The Leading Edge, 21, 62-64.

Chapter 5

3D modelling of buried valley hydrogeology using airborne electromagnetic data

Introduction

The importance of buried valleys as groundwater resources is well known to geologists, hydrogeologists and geophysicists dealing with glaciated terrain. As water demand is largely increasing, several countries around the world has been promoting hydrogeological studies to adequately map buried valleys aquifers (Gunnik et al., 2012, Pugin et al., 2014). A thorough knowledge of their occurrence, depth, architecture and fill sequence require relevant geophysical as well as lithological data. The latter usually derive from drilled boreholes records while the former widely consists of time domain electromagnetic (TEM) data both ground-based (Jørgensen et al., 2003, 2005, Auken et al., 2003, Danielsen et al., 2003) and airborne (Auken et al., 2008, Oldenborger et al 2013, Siemon et al., 2009). Many authors have also demonstrated the use of seismic method as an effective tool for buried valley mapping in addition to TEM data (Gabriel et al., 2003, Jørgensen et al., 2003, Hoyer et al., 2011, Sapia et al., 2012, Oldenborger et al., 2013, Pugin et al., 2014).

Buried valleys often result in a complex aquifer architecture with numerous cross cutting features of several generations (Jørgensen and Sandersen 2006). As such, high data density and high model resolution is crucial for their exhaustive representation. This cannot be achieved with widely-spaced geophysical data such as sparse ground TEM data or localized reflection seismic profiles alone (Jørgensen et al., 2009, chapter 4 of this thesis). Moreover, low data density, combined with a frequently low sample quality, description and interpretation, makes water wells difficult to use for mapping buried valleys and inadequate for 3D hydrogeological model building (Jørgensen et al., 2009). On the contrary, HTEM surveys cover large areas and provide high density information at a regional scale. Helicopter systems were initially employed for mineral exploration activity (Fountain 1998). This method is very suitable for mineral exploration, due to the high conductivity contrast between host rocks and the mineral deposit. Conversely, the resistivity contrast between

aquitards and aquicludes is relatively small compared to the mineralization compromising the applicability of the method to adequately map potential groundwater resources.

The AEM systems have been constantly improved in the last 60 years (Allard, 2007; Fountain et al., 2008; Sattel, 2009) and increasingly applied for quantitative hydrogeological investigations in recent years also due to enhanced near surface resolution (Paine and Minty, 2005, Thomson et al., 2007). At the same time, the necessity to pay particular attention to the raw data processing (Viezzoli et al., 2012) as well as the importance of a truly calibrated dataset (Podgorsky et al., 2013, Foged et al., 2013) is mandatory if the aim is to derive reliable 3D hydro\geological interpretation through inversion of large voltage dataset. The latter also implies the relevance to properly modeling the system transfer function in order to avoid errors, both shallow and deep artifacts in the predicted model (Christiansen et al., 2011).

These approaches combined to a comprehensive understanding of the regional geological setting in which buried valleys occur, significantly contribute to build accurate and reliable 3D model of the buried valleys structures. 3D hydrogeological model building aims at create a model that reproduce the geological reality, at a certain scale, as close as possible (Bosh et al., 2009). Generally, hydrogeological models can be based on borehole data only (Venteris 2007) or based on borehole data combined with geological cross-sections (Kaufmann et al., 2007, Raiber et al., 2011, Royse 2009) or lithostratigraphic data combined to seismic profiles (Scharling et al., 2009). Borehole based 3D hydrogeological models often suffer of lack of sufficient data to build detailed 3D models due to wide interpolation between wells records (Tuner 2005). On the contrary, AEM data in addition to other ground geophysical data and reliable boreholes represent an effective tool for accurate 3D geo-modelling (i.e. Jørgensen 2013). Consequently, accurate hydrogeological models can farther help authorities in charge to more appropriate groundwater management (Berg et al., 2011). AEM based 3D hydrogeological model in recent literature arise from semi-automated geostatistical approaches (Gunnink et al., 2009, 2012) to cognitive geological knowledge-driven approaches (Jørgensen et al., 2010,2013). In both cases, the role of proper data handling combined

with appropriate system calibration is a key element to obtain a reliable 3D hydrogeological model for land use purposes and groundwater modeling. Geological Surveys or other Research Institutes around the world are (often) proprietary of large databases of every type of data (i.e. geophysical data, borehole data, etc.) and need to adopt "right strategies" as "correct approaches" which should involve accurate data processing, inversion and 3D hydro\geological model building. This chapter aims at giving a quantitative contribution to these outlined conditions. In this chapter a 3D hydro\geological voxel-based model of the Spiritwood Valley Aquifer, Manitoba, Canada is illustrated. The AeroTEM has been processed and inverted in order to obtain a resistivity model of the subsurface (see chapter 2). We build a 3D voxel-based lithlogical model of the buried valleys imaged by the HTEM survey. Seismic data and a borehole log have been used to constrain geometries and infill lithologies of the buried valleys revealed by the HTEM inversion results. Since the AeroTEM system shows limited resolution at the very near surface, a high near surface resolution HTEM resistivity model over the same survey area is presented as an example in order to stress the weakness of the AeroTEM lithological model. However, the resistivity model itself does not provide univocal information about lithology of the subsurface layers. Then, the challenge for the modeler is to convert resistivity value into lithology which can be done using a cognitive approach (Jørgensen et al.,2013). To solve most of the "groundwater" unknowns, several aspects are important: determination of the depth to bedrock, location high-porosity resistive materials (associated with fresh water) and determination of aquifer lithology and geometry. The output lithological voxel model allows resolution of the high geological heterogeneity which characterizes the Spiritwood Valley Aquifer area.

Transient electromagnetic airborne system (short review)

Since 1997, various reviews have been published regarding airborne electromagnetic surveying (Fountain, 1998; Witherly, 2000; Fountain and Smith, 2003; Nabighian and Macnae, 2005, Fountain et al., 2005, Thomson et al., 2007, Allard 2007, Sattel 2009) as also reported in chapter 1 of this thesis. In recent years these systems have seen considerable improvements in data

quality, signal to noise ratio, investigation depth, and spatial resolution. Further technological improvements include more accurate GPS location, navigation systems, greater data storage capacity, and higher data processing speeds. All this helped in the emergence of HTEM systems, which can be considered the most important development in this field over the last 10 years.

Time-domain airborne electromagnetic systems operate by abruptly shutting off a current flowing through a transmitter loop, causing a sharp variation in the magnetic flux. This variation induces currents in the ground (according to Faraday's law). The currents diffuse (due to Ohmic loss) outwards and downwards into the subsurface. Currents decay over time and diffuse with depth as function of ground conductivity, a process that occurs more slowly in highly conductive ground compared to poorly conductive ground (where the current diffuse and decay more quickly). Those currents induce a secondary time-varying magnetic field in the medium that can be measured by an induction coil in the receiver which is generally located near the transmitter. As the current penetrates deeper into the ground, the signal measurements provide information on the conductivity of the lower layers. Sedimentary environments exhibiting moderate to high resistivity in the shallow subsurface representing a particular challenge for achieving satisfactory near surface resolution using AEM measurements. As is well known, near-surface resolution is highly dependent on the specific instrument's capacity to measure the early time portion of the transient ground response. The receiver bandwidth and implemented current waveform also significantly influence the resulting near-surface resolution. An important role is also played by the transmitting current waveform and base frequency in the intensity of the induced EM ground response (Liu, 1998). Each system adopts a specific waveform at one or more base frequencies in order to fulfill precise objectives and strategies. For hydrogeological prospection, transient measuring systems should be capable of handling the great variety of signal responses likely those in environmental investigations or groundwater mapping and so they need a very wide dynamic range (Sørensen et al., 2012). A rapid shut off of the transmitter current (i.e. waveform with a short linear ramp off) induces high frequency harmonics in the primary EM field, resulting in early off-time responses

(Raiche, 1984, Fitterman and Anderson, 1987), which is appropriate for mapping shallow resistivity variation. Moreover, AEM systems are also complex to design and the acquisition of TEM data can be impaired by a variety of noise sources from both inside and outside the system, making it difficult, for example, to define an absolute time-zero, and to synchronize the transmitter and receiver (Christiansen et al., 2011). Advances in AEM system modeling have made it possible to improve near-surface resolution (Christiansen et al., 2011), and by calibrating AEM surveys using ancillary information (Foged et al., 2013; Podgorski et al., 2013).

AEM data for 3D geological model building

The Spiritwood AeroTEM survey was flown during the period from February–March 2010. The survey required approximately 5 days of flying time to cover the entire survey block, although weather restrictions resulted in approximately 4 weeks of deployment time. The survey block was aligned in the general direction of the valley as illustrated in Figure 1. The collected data consist of a series of 16 on-time gates and 17 variable width off-time gates (70 μs to 3 ms after time-off). The "full-waveform" VTEM helicopter system was tested during fall 2011, over the Spiritwood Valley area. The survey consists of three separated blocks of closely spaced lines (300 m spacing) covering approximately 220 linear km. The VTEM data strategically cover the Spiritwood area with a few lines over the northern, central, and southern parts of the AeroTEM survey block. These lines specifically followed 2 seismic profiles, one of which was also overlapped by an electrical tomography profile (figure 1). The VTEM data consists of transient data at times as early as ~20 μs after current turn-off (versus ~100 μs for standard VTEM) providing enhanced near surface resolution. For data processing and inversion we adopted the Spatial Constrained Inversions (SCI, Viezzoli et al., 2008), a full non-linear damped least squares inversion based on an exact forward solution, modeling the instrumentation's system transfer function (see chapter 1,2,3 for an in-depth discussion of the AEM data processing, inversion and algorithm description).

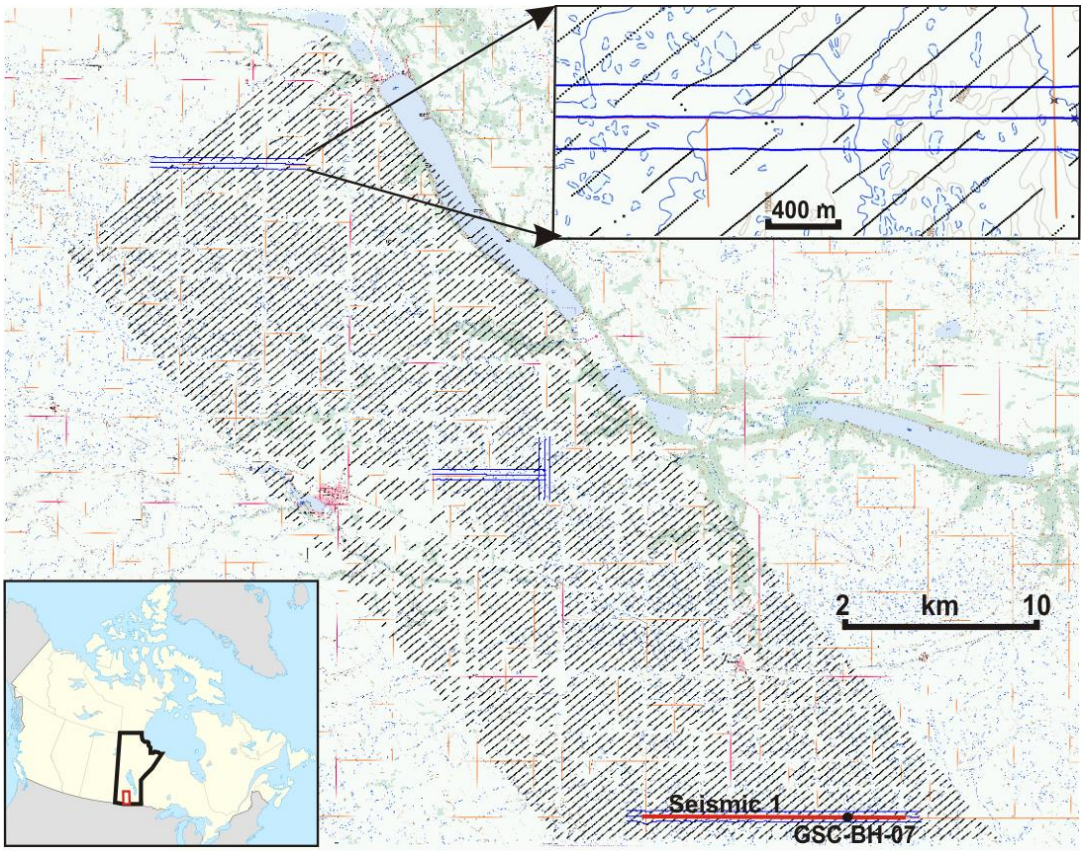

Figure 1.
Location of the Spiritwood Valley Aquifer area and the HTEM surveys in southern Manitoba, Canada (inset). The blue dots correspond to VTEM survey and the black dots to the AeroTEM survey. The solid red line is the seismic 1 profile and the black dot is the location of the borehole. The inset on top shows a close up of the overlap area in the south part of the survey block. The line spacing of the AeroTEM survey is 400 m (oblique lines) while VTEM line spacing is 300 m (horizontal lines)

This type of algorithm supports two modeling approaches: blocky models based on a limited number of layers with variable layer boundaries or "smooth models based on a large number of stacked layers in a fixed vertical discretization. We used the blocky inversion for determining layer interfaces, resistivities, evaluation of layer thicknesses and depth of penetration, taking into account that they tend to be less stable and less continuous along a flight line and that they are highly dependent on the choice of layering. On the contrary, smooth inversions offer more independence from the starting model and gradual transitions in resistivities are more obvious, which is helpful when tracing out complex geological structures, but they also produce smooth structure models with blurring of sharp formation boundaries, making them difficult to define and resulting in excessively high or low resistivity values. We used the smooth model for a better understanding of the existing geological setting while modeling the resistivity data.

3D modelling: 3D grids and Voxel

Before venturing in all sorts of interpretation and in the 3D model building, it is fundamental to have a full control of the entire set of 1D resistivity models derived from the AEM data inversion. The appropriate way to get the entire overview of the data is to work with interpolated resistivity grids instead of look at each single 1D resistivity model. It can be done by interpolating of irregular 3D grids directly from the 1D resistivity models (Pryet et al., 2011) or starting from horizontal 2D resistivity grids (at different elevation) interpolated by Kriging from the 1D models hence stacking those 2D grids into regular 3D resistivity grids (Jørgensen et al., 2005). We adopt the latter approach which, in our opinion, provides an adequate resolution of the data in terms of detail. The grids has consequently been discretized using 100 × 100 m in the X–Y direction and 5 m in the Z direction. However, it's worth to note that, due to processing and deletion of noisy data, large spacing between 1D soundings can occur. In these cases, interpolation acts to fill the occurring gaps based on the adopted search radius, and the scarcity in information present in these areas has to be carefully taken into account. To mitigate this problem, a parallel check to the 1D soundings together with the 3D resistivity grids is advisable while modeling and it guarantees that the modeler's interpretation is based on existing AEM soundings and not solely interpolated data. Once 3D resistivity grids are made, it's possible to start the 3D model building of the resistivity data. The cognitive approach and the developed tools for 3D voxel modeling are discussed in detail by Jørgensen et al., 2013. There are several tools to handle the resistivity grids in order to create voxel models. The challenge for the modeler is to convert resistivity values into geological structure and lithology. It is optimally done by combining the AEM data with the geological knowledge and, where available, other geophysical and geological data like seismic, electrical tomography, resistivity logs and borehole data. The challenge is to reproduce the highly geological heterogeneity like those found in glaciated environment which rarely is very well organized. Also, glaciated terrains often include several buried valleys of different generations with many cross-cuttings between valleys and abrupt interruptions which are very difficult and time consuming to model.

The voxel model building consisted of selection of voxel groups from based on the 3D resistivity grids (on the basis of picked resistivity values) and then assigning a lithology to that selected volume. Regarding the buried valleys in our area, the selected volume aims to represent the infill material derived by picked interval resistivity values in the resistivity grid and by using region grow tools. Region grow tools allow automatic selection of neighbouring voxels/ voxel groups with resistivity values within a selected interval as decided by the modeler (Jorgensen et al., 2013). The lower boundary of the volume can be constrained by interpreted 3D surfaces of the buried valleys. The top of the volume can be constrained by a surface which is interpreted to be the upper limit of the buried valley structure.

AeroTEM lithological voxel model

To perform geological interpretations of the Spiritwood area the output resistivity models are displayed using both averaged resistivity maps at different elevation and cross-sections (figure 2 and figure 3). Moreover, a profile view facilitates the comparison between the resistivity model and the other available ancillary information at the survey area (i.e. seismic data). The 3D resistivity grids sliced at 420 m asl (figure 4, bottom) clearly show the existence of a resistive elongated feature-like valley, approximately 10 km wide, set amongst a conductive background consisting of shale. It is known as the Spiritwood Valley Aquifer which many authors attributed as a results of preglacial fluvial incision coming from the North of USA (Cummings et al., 2012). Along the middle of the Spiritwood valley we observe two elongated features, much more narrow structures (about 1 km wide) interpreted to be inset valleys that follow the main Spiritwood valley in the north-south directions (Oldenborger 2013; Pugin et al., 2014). In addition to these valleys, a complex network of valley-like features outside the main valley are observed (figure 2, see also chapter 4). Some of the observed buried valleys are relatively narrow and reveals a complex glacial setting with many cross-cutting buried valleys. As mentioned in the previous paragraph, the resistivity model itself does not provide univocal information about lithology of the subsurface layers. However, changes in resistivity value in the model at least reveal the existing lithological

variability. Therefore, a first step before building the voxel was to make interpretation of 3D surfaces following the main resistivity contrast revealed by the resistivity model (figure 4, top). Those 3D surfaces consist of manually digitized interpretation points

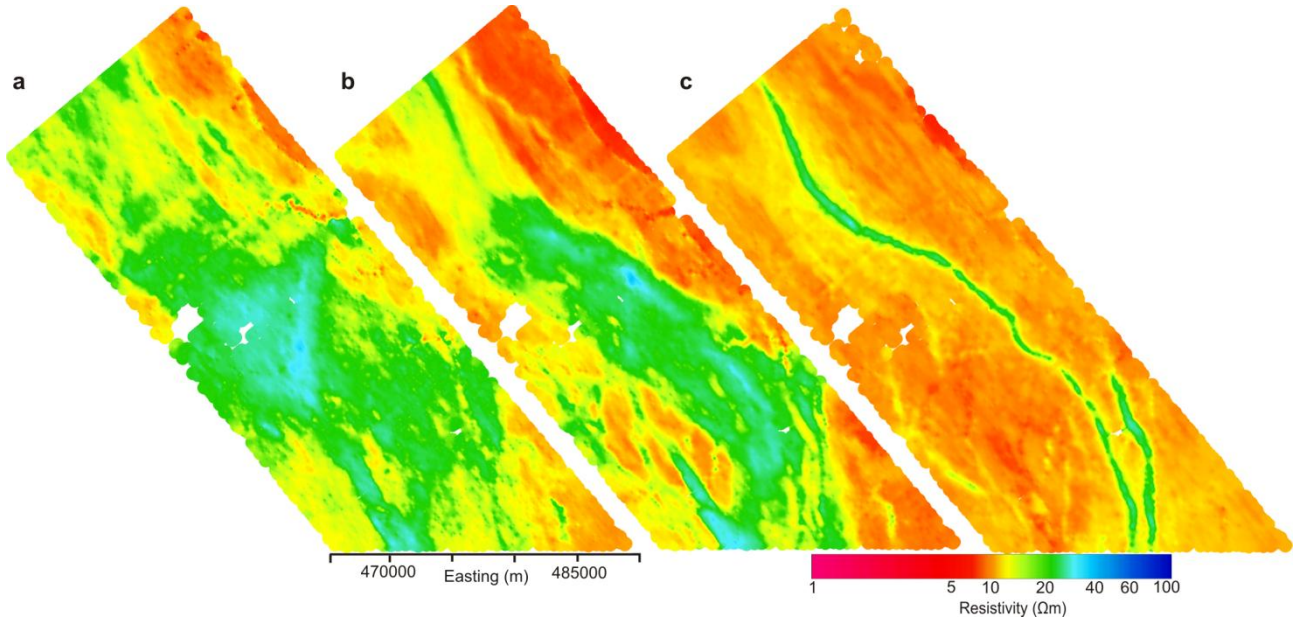

Figure 2.
Inversion results for fully-processed AeroTEM III data. The early time gates affected by residual primary field and the noisy late time gates were omitted from the inversion. The smooth (29 layers) inversion model is shown as averaged resistivity maps at different depth intervals: a) 0-10m, b) 50-60m and c) 110-120m.

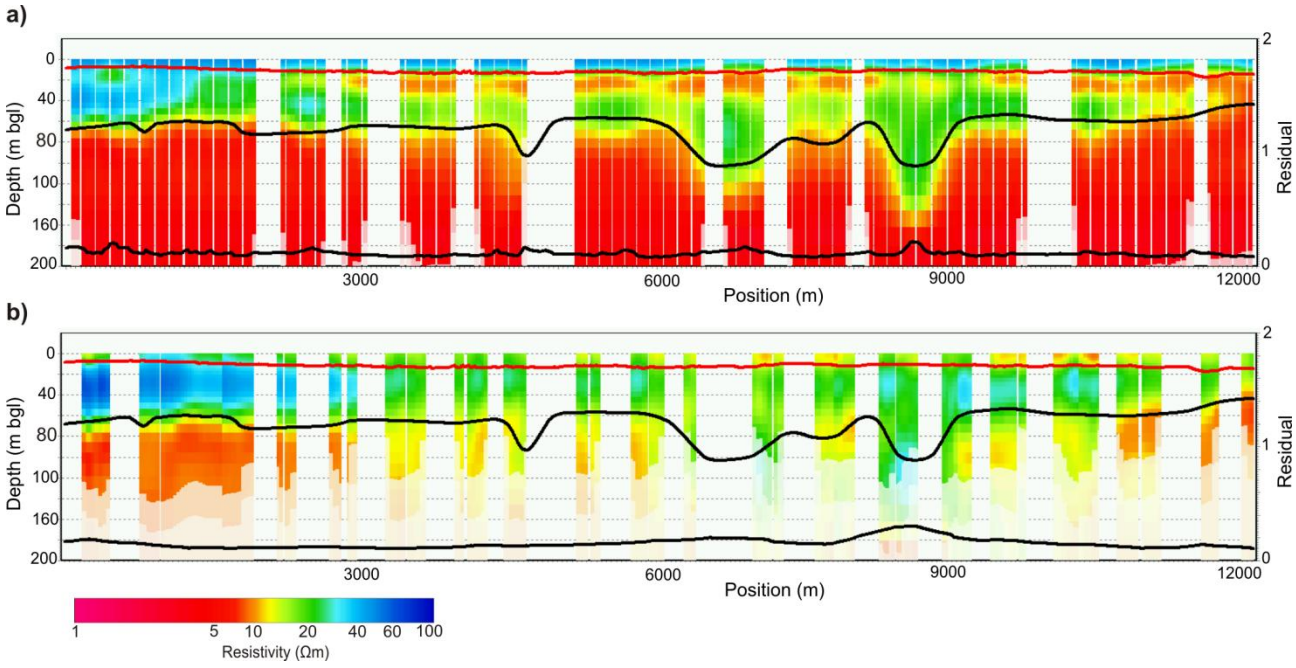

Figure 3.
a) VTEM reference model along seismic line 1 (Pugin et al., 2009a). b) AeroTEM III smooth inversion results after a -20 µs time shift applied to all Rx time gates. Solid red line is an inter-till reflection surface. Solid red line is an inter-till reflection surface. Upper solid black line is the bedrock reflection surface and lower solid black line is the data misfit.

during the cognitive interpretation of the structures imaged by AEM survey. To this end, both few layer and the smooth inversion results were jointly used in order to have the total control of the data during the interpretation. This practice is time consuming but, at the same time, allows better delineation of the structures. The resulting surfaces are shown in figure 5. The existence of a complex network of interconnected buried valleys is clearly confirmed from the observation of the 3D surfaces. These structures show different length which approximately range from few hundred meters to more than 20 kilometers long. Some buried valleys seem to be organized in interconnected networks, whereas others occur as individual elements. Apparently, those networks are easily seen at some locations from AEM response, but their interpretation have been performed alternatively using also seismic reflection profile collected over the survey area. Subsequently, all those surfaces were used to constrain the voxel. To obtain direct conversion from resistivity into lithology, a priori knowledge of the key intervals of resistivity values can significantly help to characterize the deposits in the area. Based on the general experience with material resistivities for the Spiritwood area (Crow et al., 2012, Oldenborger et al., 2013), the sediments could at best be classified in this way : 8-10 ohm m for the Cretaceous shale bedrock; 15–30 ohm m for the diamicton sequence; >35 ohm m for the melt-water sand and gravel. However, since transient electromagnetic methods are suitable for detecting conductive layer with high level of accuracy and only provide limited resolution of resistive materials, then discrimination between sand and gravel or sandy till sediments to sand can be problematic or even impossible in some cases unless there are reliable borehole information in support of AEM data interpretation. In our specific case we only have one calibrated borehole with geological stratification and measured conductivity logs (Crow et al., 2012).

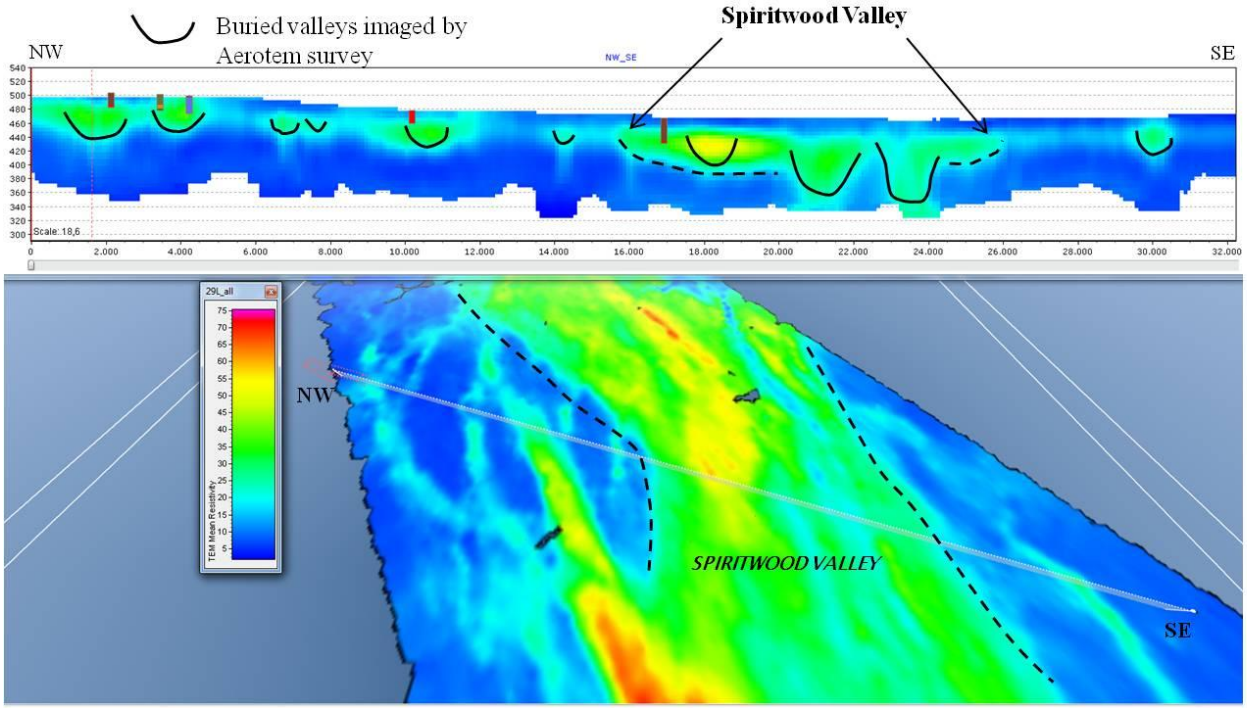

Figure 4.
Cross-section of the AeroTEM resistivity model (top). Solid black lines illustrate the buried valleys 3D surfaces interpreted from the AeroTEM resistivity model. Dashed black line represents the wider Spiritwood Valley. Averaged resistivity map of the AeroTEM survey sliced at 420 m asl (bottom). The Spiritwood valley is readily apparent as resistive feature set amongst a conductive background supposed to be the shale bedrock. Several valleys-like features are also evident as resistive structures cut into the bedrock.

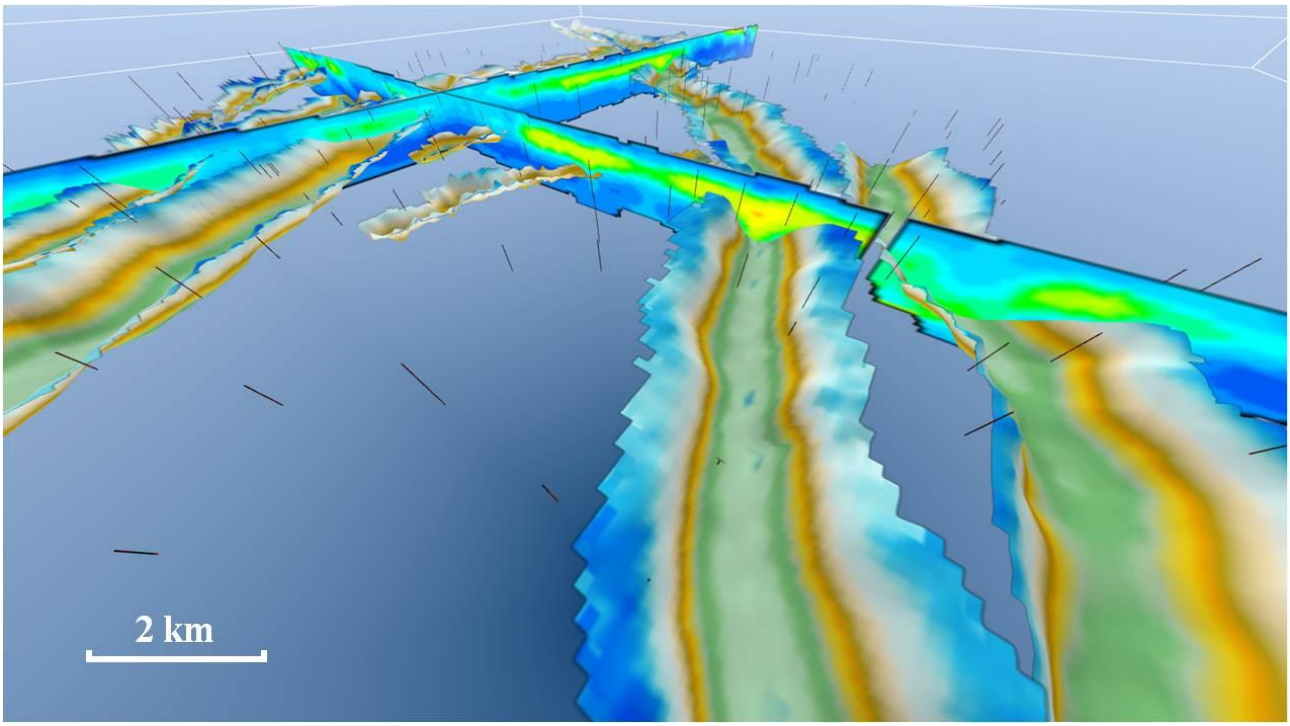

Figure 5.
3D surfaces of the buried valleys derived from the interpretation of the 3D resistivity grids. The surfaces are interpolated using a Kriging with a search radius of 100m.

All other available boreholes at the survey area are mainly water wells for drinking and agriculture use with higher uncertainties in the geological description of the samples and, even more critical, often with wrong location which in turn make those data useless in supporting any geological interpretation (see chapter 4 for details). Figure 6 show the lithological voxel-based model. In the lithological voxel model different type of buried valley were classified in terms of lithologies also according to seismic data (figure 7) (Pugin et al., 2014):

1) Regional-scale, extensive (10 km wide) known as Spiritwood Valley supposed to be formed as pre-glacial river incision (Cummings et al., 2012). This valley appear as a gently deepening of the shale bedrock. However, the 3D resistivity grids show the Spiritwood Valley as a large structure incised by several other valleys which run approximately north-south direction (figure 2 and figure 4, bottom). The Spiritwood valley is filled by different types of sediments which, according to the resistivity values, can be attributed to be the response of a thick (>70m) till package in addition to sand and gravel materials mainly filling the inset valleys (figure 6).

2) Regional-scale, much more narrow (about 1\2 km wide) valleys, set within the wider regional valley (i.e. Spiritwood). In particular, two inset valleys appear eroded into both bedrock and the regional valley sediment and filled with relatively resistive materials interpreted to be coarse-grained sand and gravel. However, as a result of the interpretation of the resistivity model, these two buried valleys seem not entirely to be filled by coarse grained materials. In fact, we observed lower resistivity values at the southern part of these two inset valleys which therefore have been interpreted to be the response of sandy\silt diamicton (till materials) (Figure 8). This interpretation was also supported by a borehole log located in the south part of the Spiritwood area (Crow et al., 2012). In fact, the borehole shows very fine to fine sand embedded in sandy silt diamicton in the first 9 m. These layers overlay a clay till varying from hard clay diamicton sediments before the drilling indicates relatively uniform till and coarse grained sediments at the bottom of the borehole (~90m). In addition, the collected geophysical logs reveal the near surface as resistive (~ 17 Ohm m) down to 9 m depth. The till package below show a lower, relatively

uniform, resistivity (~ 9 Ohm m) from 10-80 m in depth. Despite nearly uniform resistivity, the borehole samples clearly showed two till packages. The coarse-grained sediment observed at the bottom of the borehole appear to be a bit more resistive than the till sequence (~ 20 Ohm m). To this end, the two inset valleys have been assigned, southwards, a voxel with a lithological attribute representing a sandy\silty till materials (figure 8). However, the AEM resistivity model shows the same buried valleys, northwards, as higher resistivity response within the valley which, therefore, we attributed to be likely the response of coarse-grained infilling sediments (i.e. gravel and sand).

3) Local-scale, apparently discontinuous with abrupt interruption, variable widths and length (~ 1 km wide, hundreds of meters to tens kilometers length) these buried valleys are observed to cross-cut other valleys (figure 5, 6, 7, 8). This type of buried valleys is clearly identified from the resistivity model although they show very diverse resistivity range of values. Some of these valleys appear as resistive features (>40 Ohm m) interpreted to be filled by sand and gravel materials. Conversely, some of these buried valleys are imaged as less resistive features (<15 Ohm m) which we attributed to be the response of clay-rich till materials (figure 7).

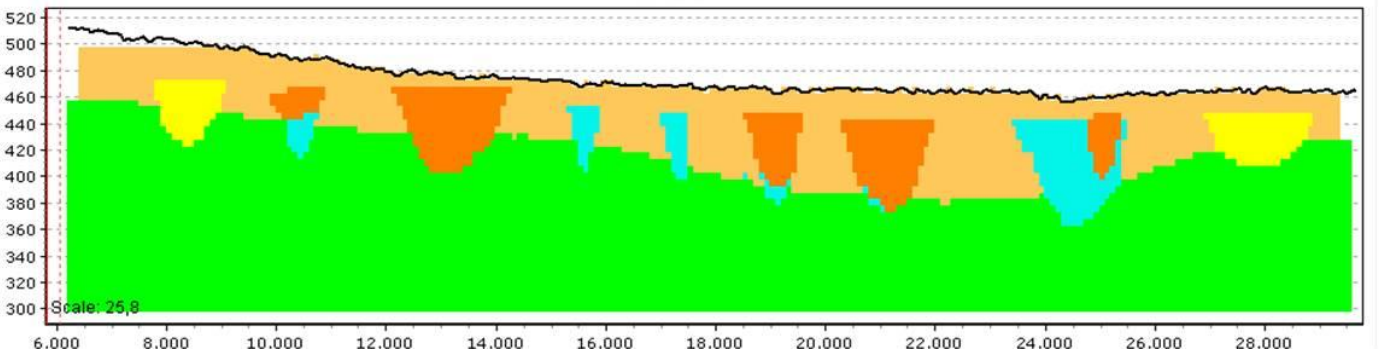

Figure 6.
Cross section East-West oriented (see figure 8 for the location of the profile) of the lithological voxel-based model obtained from the interpretation of the AeroTEM resistivity model. Solid black line is the terrain. Different lithologies are rendered with different colors based on a cognitive interpretation approach of the hydrogeological setting (e.g., gravel and sand orange, shale bedrock green, sandy\silt diamicton light blue and clay-rich till yellow).

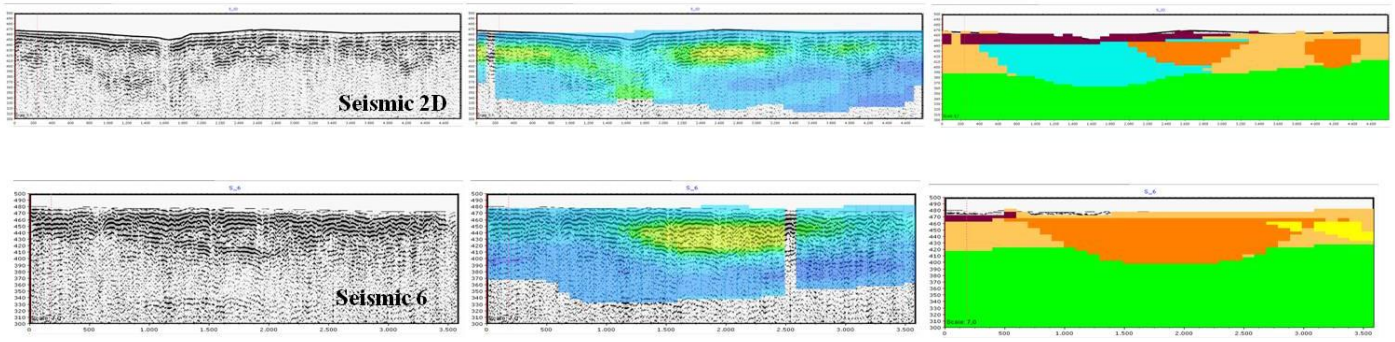

Figure 7.
From the left to the right are illustrated: seismic sections, AeroTEM inversion results along the seismic profile and the interpreted 3D lithological model. The seismic profiles 2D and 6 were adapted from Pugin et al 2009. The seismic and AEM results significantly match (within the limitation of the method) and then the 3D lithological model is derived from a combined interpretation of both geophysical data.

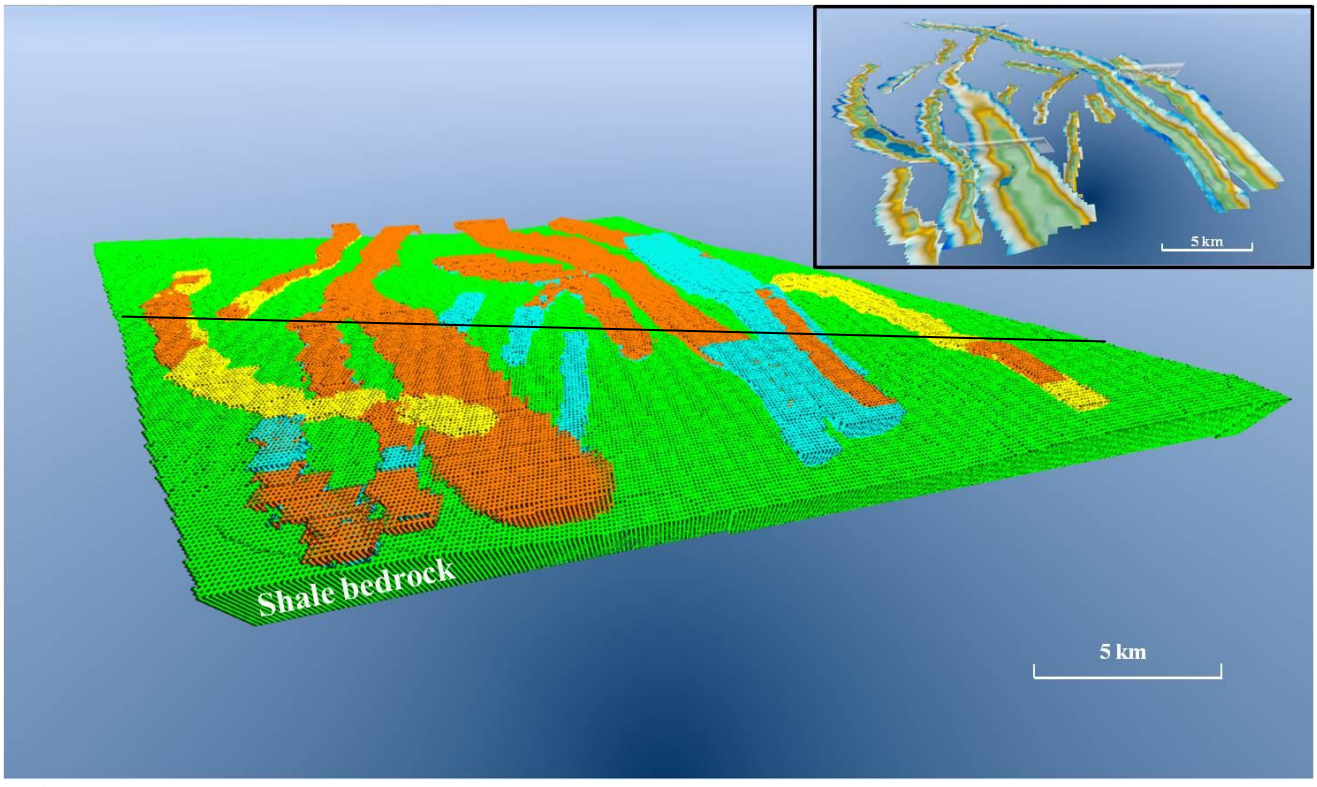

Figure 8.
3D visualization of the lithological voxel-base model of the Spiritwood survey area. Different ithologies are illustrated as in figure xxxP. The inset on top show the 3D surfaces of the buried valleys which have been used to constrain the voxel grids. The solide black line indicate the profile section of figure 6

Discussion

Buried valleys are a common feature in glacial terrains. In the Western Glaciated Plains numerous valleys were cut into Cretaceous and Tertiary bedrock units prior to the initiation of continental glaciation. Alluvial deposits, in particular Tertiary sands and gravels are generally thought to have been transported from the Rocky Mountains to the west and rest on the underlying bedrock in parts of many of these valleys (Cummings et al., 2012). Several authors have been studying Prairie buried valleys (Andriashek, 2003; Cummings et al., 2012; Gibling, 2006; Howard, 1960; Maathuis and Thorleifson, 2000; Oldenborger et al., 2013; Pugin et al., 2014; Russel et al., 2004; Schreiner, 1990; Shaver, 2010; Wiecek, 2009). Cummings et al. 2012 defined the term buried valley to describe any eroded depression that initially was incised on the surface and is now buried by overlying sediment. The term does not contribute to identify neither the origin nor stratigraphic position of these structures which implies that buried valleys may have formed by tectonic, glacial, glaciofluvial, fluvial erosion. In general, the main lithologies filling the Prairie buried valleys consist of a variety of glacial and interglacial deposits, most commonly melt-water sand and gravel, glacio-lacustrine clay and silt and clay till (Cummings et al., 2012). Such heterogeneity is extremely difficult to map using water well data alone. Geophysical methods, such as reflection seismic and, mainly, AEM survey are illustrating that such extremely complex geological setting may be mapped (Pugin et al., 2014), also combined with ERT data (Oldenborger et al., 2013), borehole logging and sampling (Crow et al., 2012). In particular, the 1D inversion approach has revealed to be perfectly viable in geological contexts of gradually varying 3D structures also when conductivity contrasts are only moderate. Conversely, in geological contexts with pronounced 3D characteristics, a 1D inversion will be strongly influenced by the 3D effects and might easily generate unreliable models. Literature includes a number of papers discussing the influence of 3D structures on 1D interpretations of TEM data, including Auken (1995), Newman et al. (1987), and Goldman et al. (1994). At Spiritwood, several buried valleys have been mapped and modelled in 3D at regional scale (several km2) and potential aquifers have been identified which in turn may be exploited as

groundwater resources. The AEM results which reflect the complexity of the geological setting has required a cognitive voxel modelling approach for the geological interpretation of the resistivity model (Jørgensen et al., 2013).

Figure 9 illustrates the results obtained from automatic conversions of resistivity into lithology. Based on the classification of the resistivity values which are supposed to be representative of the existing lithologies at Spiritwood, an automated conversion from these resistivity values into lithology has been performed as a first prior step for the 3D hydro\geological model building. The first profile (figure 9A) shows the result of the direct conversion into lithology of picked resistivity values from the conductive shale bedrock. From the bedrock we picked 10 ohm m and we select an interval of resistivity between 5 to 10 ohm m to be representative for the bedrock thereby populating all selected voxels with shale as attribute. However, in this way not only the bedrock but also most part of the near surface will be filled by voxels. This is caused by the difficulties of the AeroTEM to exactly resolve the near surface in addition to the fact that we are not really interpreting unbiased early time gates (which in turn give rise to a conductive signature of the surficial layer – see chapter 3 for details). In figure 9B the same procedure was applied in order to assign the till lithology to the voxels. An interval between 15 ohm m to 30 ohm m was applied from a picked resistivity value of 15 ohm m within the resistive layer throughout the profile down to a depth of 70 m. As a result, most of the resistive features seems to be selected except for an area between 13 km to 19 km were resistivity appears to be higher. However, the buried valleys imaged by the resistivity model are not as well as represented from this selection at all since the picked resistivity range partially overlap the intervals of both the till package and the signal supposed to be from sand and gravel materials. Instead, the resistivity model suggest the presence of clearly defined valleys structures. Between 13 and 19 km picked value suggest resistivity greater than 30 ohm m within the buried valleys which never exceed 70 ohm m. In figure 9C resistivities above 30 ohm m were assigned to be the response of sand and gravel materials. By doing this, it is more evident the existing overlap with the previous till resistivity interval, mainly within those buried

valleys located at 1 km, 5 km 7 and 8 km and the main buried valley between 20 and 21 km along the profile. In general, the buried valleys with potential sand and gravel infill show up as undetermined shaped-features and not with distinct valley shapes. Therefore, valleys are insufficiently and unclearly resolved and do not come up with resistivities that contrast with those of the surrounding sediments. This problem is also caused by the difficulties of the smooth models to resolve layer boundaries exactly. In addition, the depth of the buried valleys is not properly determined if we automatically convert resistivity into lithology. As seen from the example above, the model created by the automated conversion does not satisfactorily represent and outline the expected geology along the profile.

The model can be improved by incorporating geological background knowledge, comparing AEM data with additional geophysical data (and borehole) and by carefully considering the potential 3D effects in the inversion result during cognitive interpretation of the resistivity model. From the AEM resistivity model the Spiritwood valley appears to be about 15-20 km wide, up to 70 m deep. It is oriented approximately north-south, extending hundreds km from Manitoba, into South Dakota. There is no surficial expression of the valley as clearly evident from the digital elevation model of the Spiritwood survey area (figure 10, top). The Spiritwood valley appears to be eroded into the shale bedrock with dominantly diamictic infill materials but inter-till sands and gravels also fill numerous inset valleys lying within the wider regional valley (Cummings et al., 2012, Pugin et al., 2014). This is particularly evident for the two main inset valleys appear eroded into the Spiritwood valley from the north to the south down to the bedrock as well. Several of the local scale cross-cutting buried valleys with undulating profiles are also eroded into bedrock (figure 10, bottom). As also illustrated in figure 9, the AEM resistivity model showed that the infill materials of the Spiritwood buried valleys turn out as represented by a tight interval of resistivity values ranging from few Ohm m (>5 Ohm m) and never exceed 70 Ohm m throughout the survey area.

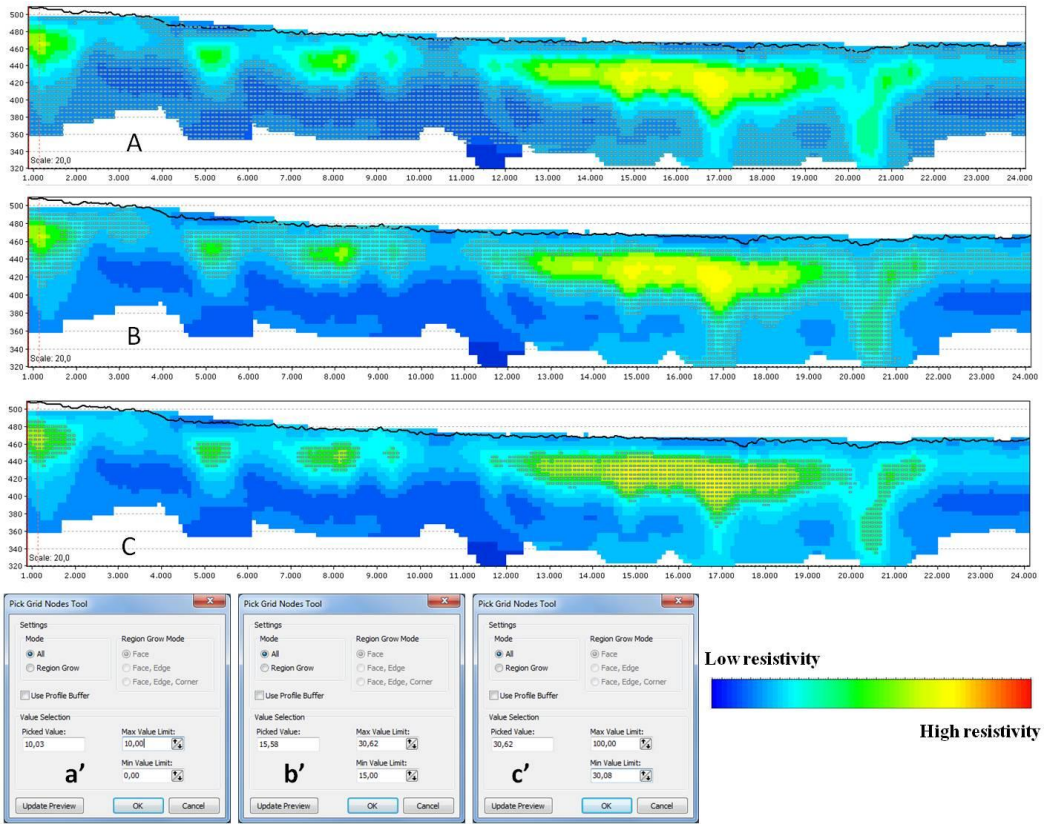

Figure 9.
Selection of voxel nodes by using the region grow tool along a section of the AeroTEM 3D resistivity grids. A), B), C), show the voxel nodes derived from the picked resistivity interval illustrated respectively in a', b' and c'.

Therefore, it's hard to evaluate if all the buried valleys imaged by the AEM surveys effectively can be potential aquifers. This is particularly true if we consider the low resistivity value at the bottom of the main inset valley where the borehole, mentioned above, cached the gravel at about 90m depth (see chapter 2 for detailed description of the borehole logs). Notoriously, buried valley aquifers are supposed to be filled by permeable sediments which in turn consist of higher resistivity compared to the more conductive aquiclude. At Spiritwood, it's worth to note that the clasts in the gravel are supposed to be mostly shale with only minor contribution from the granitic Canadian Shield. Therefore, the relatively low resistivity of the gravel material filling the buried valleys is not entirely unexpected. However, lower resistivity values might also be explained in the presence of water with higher salinity contents. As for salinity, very few data except for surface waters are available at the survey area. There are some salinity data from Wiecek (2009) which indicate the gravel salinities as high as 150 mS/m (~1 ppt). This is not in the typical range of "salty water" (normally as high as 5-6 ppt) but it is brackish. When compared to the resistivity model the

3D litholological model also shows that some buried valleys appear to be filled by very conductive materials which we interpreted to be the response of clay-rich till sediments. To this end, we might exclude these buried valley being potential aquifer since clay till consists of relatively low permeability compared to coarse grained sediments. The electrical resistivity of sediments is controlled by clay minerals, pore-water ion content and the amount of pore water itself. The translation from resistivity into lithology can only be properly done if a series of important aspects regarding the physical properties of the subsurface and the limitations of the applied methods are carefully considered and implemented. Even then, it impossible to discriminate lithology based on resistivity with certainty if two different lithologies have the same resistivity! Therefore, it is very important, while modeling, to have a basic knowledge of the existing geological setting of the area which can be derived from borehole data or other geophysical data like seismic data, electrical data.

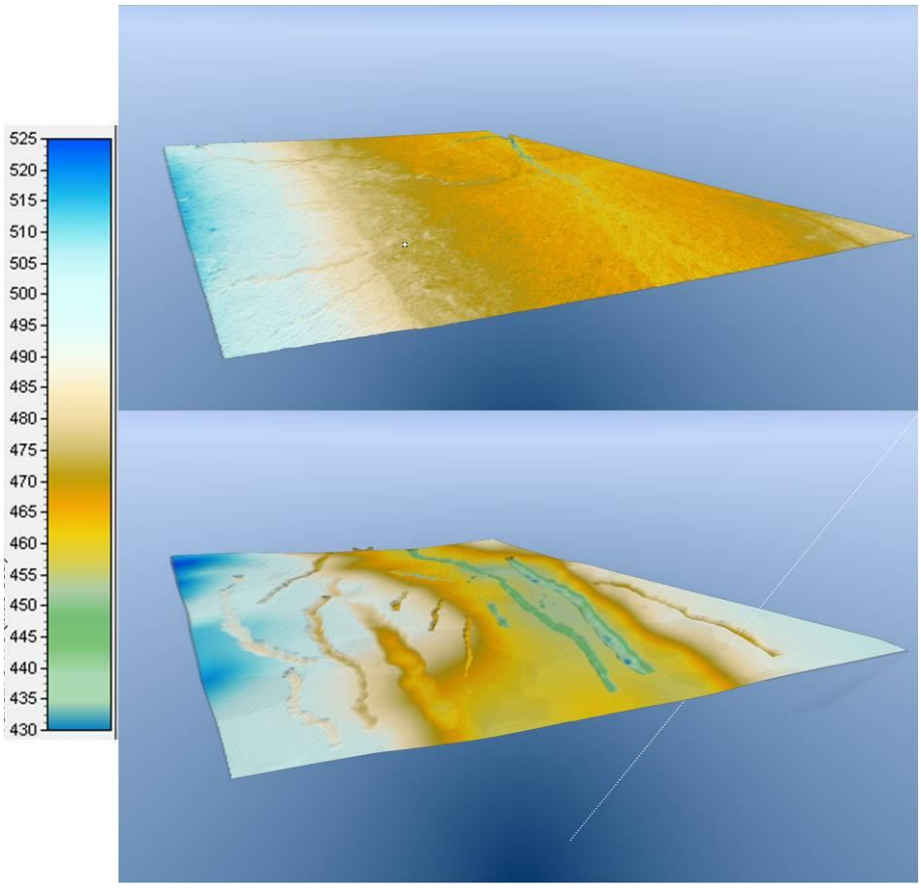

Figure 10.
Digital elevation model of the spiritwood Valley survey area (top). 3D surface of the shale bedrock derived from the interpretation of the 3D resistivity grids of the AeroTEM resistivity model (bottom). The bedrock appear to be incised by numerous valleys each of them eroded the shale at different elevation.

Final remarks

Given the importance of the Spiritwood aquifer an AEM survey together with several kilometers of seismic profiles have been performed at Spiritwood in order to deeply investigate the aquifer system. Full non linear inversions of the Spiritwood AEM datasets showed significant geological structures and clearly indicate a complex valley morphology that can be used to significantly improve geological and hydrogeological knowledge on a regional scale. To summarize, AEM inversion results revealed multiple resistive valley features inside a wider valley structure in addition to a network of many cross-cutting narrower buried valleys outside the main Spiritwood valley. The Spiritwood aquifer system consists of a complex network of glacially deposited sand and gravel bodies interbedded with till and clay-rich till, infilling a broad north-south trending Tertiary valley (the Spiritwood Valley).

The geology of glaciated areas is complex and such geology is therefore very hard to handle if the aim is to obtain a reliable 3D hydro\geological model. Moreover, detailed 3D hydro\geological models are needed in those cases where the goal of the 3D model is to e.g. predict groundwater pathways to well fields. After advanced data processing and inversion, we consider the AeroTEM output resistivity model to be the most reliable resistivity model, consistent with all available ancillary data (seismic data, ERT data and borehole logs), to be further used as input data for 3D hydrogeological model building. To this end, we applied a cognitive modeling approach which involved joint use of AEM data, seismic data, ERT data and borehole log data to obtain the final 3D lithological model of the buried valleys. A voxel approach allows a quantitative understanding of the hydrogeological setting of the area, and it can be further used to estimate the aquifers volumes (potential amount of groundwater resources) as well as hydrogeological flow model at regional scale. The resistive valleys have been interpreted to be filled by coarse grained materials (sand and gravel) to be further considered as potential ground water reservoir (aquifer) and possible pathway for groundwater flow. Other buried valleys appear as low resistive features from the resistivity model and, therefore, they have been interpreted to be filled by clay-till

sediments which likely exclude those features to be potential aquifer or groundwater pathways (figure 11). However, model reliability and resolution of the very near surface is a crucial part for groundwater mapping especially in glacial environments where multiple inter-till aquifers can occur at different depths and recharge can depend strongly of the characteristics of the entire stratigraphic sequence. Despite the AeroTEM survey has revealed to be crucial for the buried valleys mapping at regional scale (the Spiritwood Valley area), the 3D lithological voxel-based model still lack surficial detail (or can be considered inaccurate at surface) which reflect system's limitation in resolving the very near surface. The VTEM dataset (although it needed to be calibrated) showed much more details of the near surface geology and is much more reliable here. However, to be totally adequate for 3D hydro\geological model building of the buried valleys at regional scale, a wider survey with the VTEM system (with higher near surface resolution compared to AeroTEM system) is obviously advisable!

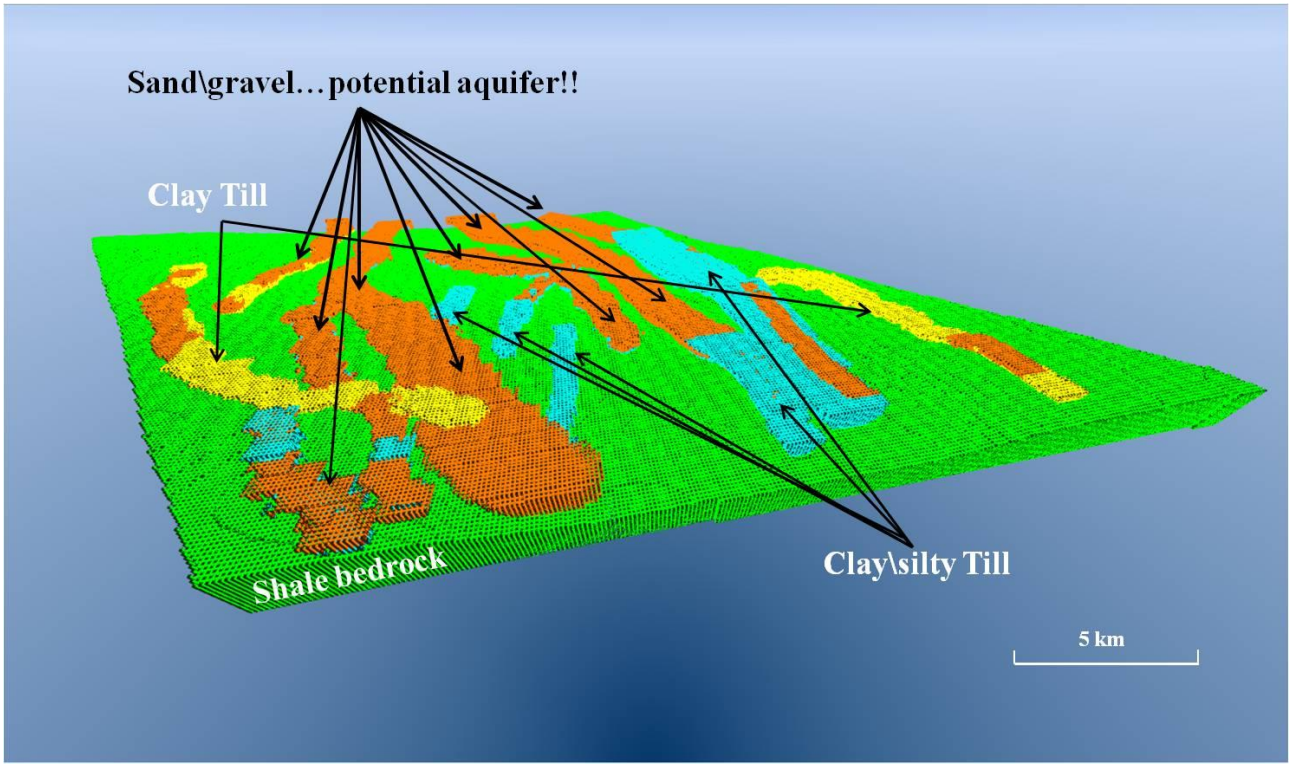

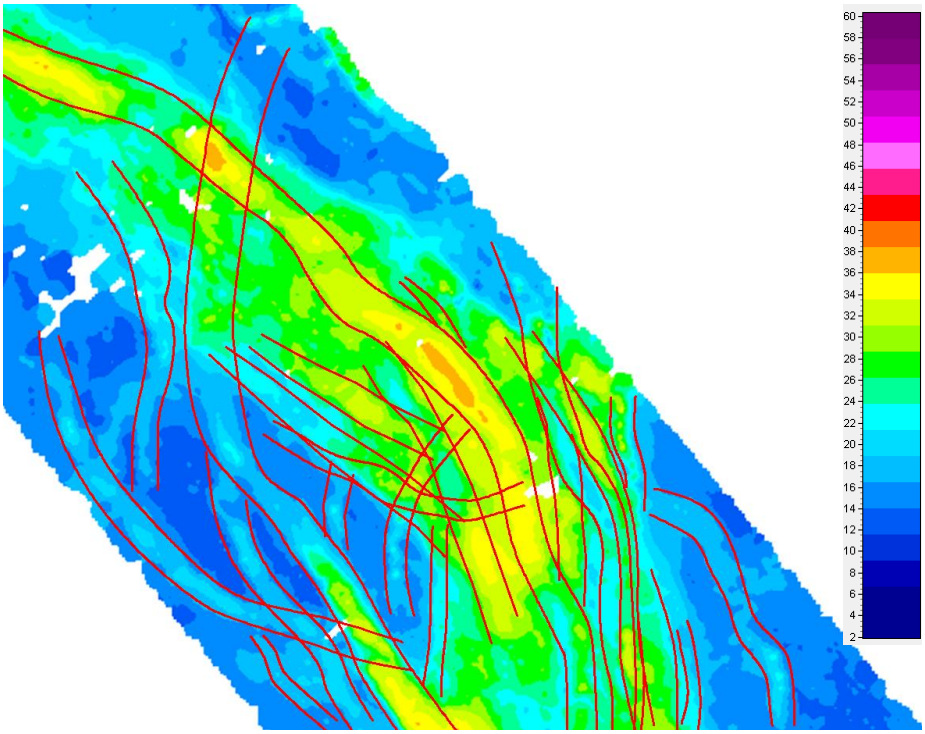

Figure 11.
3D visualization of the lithological voxel model of the Spiritwood survey area as in figure 7. Different lithologies are illustrated as in figure 6. Potential sand\gravel buried valleys aquifers are highlighted with black arrows. Few buried valleys are interpreted to be filled by clay-rich till sediments which in turn should be considered less permeable sediments, hence not potentially aquifers. Averaged resistivity map at 380 m asl with the interpreted buried valleys structures imaged by the AEM AeroTEM survey at different levels.

References

Allard M., 2007, On the origin of the HTEM species. in Proceedings: Fifth Decennial International Conference on Mineral Exploration, 355-374.

Auken, E., 1995, 1D time domain electromagnetic interpretations over 2D and 3D structures, In Proceedings of the Symposium on the Application of Geophysics to Engineering and Environmental Problems, Orlando, USA, 329–338.

Auken, E., F. Jørgensen, and K. I. Sørensen, 2003, Large-scaleTEM investigation for groundwater, Expl. Geoph., 33, 188–194.

Auken E., Christiansen A.V., Jacobsen L., and Sørensen K.I. 2008. A resolution study of buried valleys using laterally constrained inversion of TEM data, J. Appl. Geoph., 65, 10-20.

Andriashek, L.D., 2003, Quaternary geological setting of the Athabasca Oil Sands (in situ) area, northeast Alberta: Alberta Energy and Utilities Board/Alberta Geological Survey, Earth Sciences report 2002-2003.

Berg CB, Mathers SJ, Kessler H, Keefer DA (2011) Synopsis of Current Three-dimensional Geological Mapping and Modeling in Geological Survey Organizations, vol 578. Circular, Illinois State Geological Survey, Illinois.

Crow H.L., Knight R.D., Medioli B.E., Hinton M.J., Plourde A., Pugin A.J.-M., Brewer K.D., Russell H.A.J., and Sharpe D.R., 2012, Geological, hydrogeological, geophysical, and geochemistry data from a cored borehole in the Spiritwood buried valley, southwest Manitoba: Geological Survey of Canada, Open File 7079.

Christiansen, A.V., E., Auken, and A., Viezzoli, 2011, Quantification of modeling errors in airborne TEM caused by inaccurate system description, Geoph., 76, 43-52.

Cummings, D.I., Russell, H.A.J., and Sharpe, D., 2012. Buried-Valleys in the Canadian Prairies: geology, hydrogeology, and origin: Canadian Journal of Earth Sciences, 49, 987-1004.

Danielsen, J. E., Auken, E., Jørgensen, F., Søndergaard, V. H., and Sørensen, K. I., 2003, The application of the transient electromagnetic method in hydrogeophysical surveys, J. of Appl. Geoph, 53, 181–198, doi: 10.1016/j.jappgeo.2003.08.004.

Foged, N., Auken, E., Christiansen, A.V. Sørensen, K.I., 2013, Test site calibration and validation of airborne and ground based TEM-systems: Geophysics,78, 95–106.

Fitterman, D.V., Anderson, W.L., 1987, Effect of transmitter turn-off time on transient soundings. Geoexpl., 24, 131–146.

Fountain, D.K., 1998, Airborne Electromagnetic systems – 50 years of development: Expl. Geoph., 29, 1-11.

Fountain, D.K., and Smith, R.S., 2003, 55 years of AEM; 50 years of KEGS. KEGS 50th Anniversary Symposium, Toronto, Canada.

Fountain, D., Smith, R., Payne, T., and Lemieux, J., 2005, A helicopter time-domain EM system applied to mineral exploration: system and data. First Break, 23, 73-80.

Gabriel G., R., Kirsch, B., Siemon, and H., Wiederhold (2003), Geophysical investigation of buried Pleistocene subglacial valleys in Northern Germany, J. Appl. Geophys., 53, 159–180, doi:10.1016/j.jappgeo.2003.08.005.

Gibling, M.R., 2006, Width and thikness of fluvial channel bodies and valley fills in the geological record: a literature compilation and classification, Journal of sedimentary research, 76, 731-770, doi: 10.2110/jsr.2006.060.

Goldman, M., Tabarovsky, L., Rabinovich, M., 1994, On the influence of 3-D structures in the interpretation of transient electromagnetic sounding data, Geophs., 59, 889–901.

Gunnink, J. L. and Siemon, B., 2009, Combining airborne electromagnetic and drillings to construct a stochastic 3D lithological model, in: Proceedings of 15th European Meeting of Environmental and Engineering Geophysics – Near Surface 2009, Dublin, Ireland, B02.

Gunnink JL, Bosch JHA, Siemon B, Roth B, Auken E (2012) combining ground-based and airborne EM through artificial neural networks for modelling glacial till under saline ground-water conditions. Hydrol Earth Syst Sci 16:3061–3074.

Hoyer A. S., H., Lykke-Andersen, F., Jørgensen, and E., Auken (2011), Combined interpretation of SkyTEM and high-resolution seismic data. Physics and Chemistry of the Earth, 36, 1386–1397, doi:10.1016/j.pce.2011.01.001.

Howard, A.D., 1960, Cenozoic history of northeastern Montana and northwestern North Dakota, with emphasis on the Pleistocene: USGS, Professional paper 326, pp. 107.

Jørgensen, F., Sandersen, Peter B.E., Auken, E., 2003, Imaging buried Quaternary valleys using the transient electromagnetic method: Journal of Applied Geophysics, 53, 199- 213.

Jørgensen F, Sandersen PBE, Auken E, Lykke-Andersen H, Sørensen K (2005) Contributions to the geological mapping of Mors, Denmark—A study based on a large-scale TEM survey. Bull Geol Soc Den 52:53–75.

Jørgensen, F. and Sandersen P.B.E. .2009. Buried Valley mapping in Denmark: evaluating mapping method constraints and the importance of data density. Zeitschrift der Deutschen

Gesellschaft für Geowissenschaften, 160, 211–223. doi: 10.1127/1860-1804/2009/0160-0211.

Jørgensen F, Møller RR, Sandersen PBE, Nebel L (2010) 3-D geological modelling of the Egebjerg area, Denmark, based on hydrogeophysical data. Geol Surv Den Greenl Bull 20:27–30.

Jørgensen, F., Møller, Nebel, L., Jensen, N-P., Christiansen, A.V., Sandersen, P. B. E., 2013, A method for cognitive 3D geological voxel modeling of AEM data, Bulletin of Engineering Geology and the Environment, 72, pp 421-432.

Kaufmann, O., & Martin, T., 2008, 3D geological modelling from boreholes, cross-sections and geological maps, application over former natural gas storages in coal mines, Computers & Geosciences, 34, 278-290.

Legault, J. M., Prikhodko, A., Dodds, D. J., Macnae, J. C., Oldenborger, G.A., 2012, Results of recent VTEM helicopter system devel. opment testing over the Spiritwood Valley aquifer, Manitoba: in Expanded Abstracts: 25th SAGEEP Symposium on the Application of Geophysics to Engineering and Environmental Problems, 17 pp.

Liu, G., 1998, Effect of transmitter current waveform on airborne TEM response: Expl. Geophys., 29, 35–41.

Maathuis, H., and Thorleifson, L.H. 2000. Potential impact of climate change on Prairie groundwater supplies: Review of current knowledge. Saskatchewan Research Council, Publication, No. 11304-2 E00, 93 pp.

Nabighian, M. and Macnae, J., 2005, Electrical and EM methods 1980-2005, The Leading Edge, 24, 42-45.

Oldenborger G.A., Pugin A.J.-M., and Pullan S.E, 2013, Airborne time-domain electromagnetics, electrical resistivity and seismic reflection for regional three-dimensional mapping and characterization of the Spiritwood Valley Aquifer, Manitoba, Canada: Near Surface Geophysics, 11, 63-74.

Paine, J.G., and B.R.S. Minty, 2005, Airborne hydrogeophysics: Hydrogeophysics, 50, 333-357.

Podgorski, J.E., Auken, E., Schamper, C., Christiansen, A.V., Kalscheuer, T. and Green, A. G. 2013. Processing and inversion of commercial helicopter time-domain electromagnetic data for environmental assessments and geologic and hydrologic mapping. Geoph., 78, 149–159.

Pryet A, Ramm J, Chiles JP, Auken E, Deffontaines B, Violette S (2011) 3D resistivity gridding of large AEM datasets: a step-toward enhanced geological interpretation. J Appl Geophys 75:277–283. doi:10.1016/j.jappgeo.2011.07.006.

Pugin, A. J. M., Oldenborger, G. A., Cummings, D. I., Russell, H. A., & Sharpe, D. R. (2014). Architecture of buried valleys in glaciated Canadian Prairie regions based on high resolution geophysical data. Quaternary Science Reviews, 86, 13-23.

Raiber M, White PA, Daughney CJ, Tschritter C, Davidson P, Bainbridge SE (2012) Three-dimensional geological modeling and multivariate statistical analysis of water chemistry data to analyse and visualise aquifer structure and groundwater composition in the Wairau Plain, Marlborough District, New Zealand. J Hydrol 436:13–34. doi:10.1016/j.jhydrol.2012.01.045.

Raiche, A.P., Jupp, D.L.B., Rutter H. and Vozoff, K. 1985. The joint use of coincident loop transient electromagnetic and Schlumberger sounding to resolve layered structures. Geophysics, 50, 1618–1627. doi: 10.1190/1.1441851.

Royse KR (2010) Combining numerical and cognitive 3D modeling approaches in order to determine the structure of the Chalk in the London Basin. Comput Geosci 36(4):500–511. doi:10.1016/j.cageo.2009.10.001.

Russell, H A J; Hinton, M J; van der Kamp, G; Sharpe, D R., 2004, An overview of the architecture, sedimentology and hydrogeology of buried valley aquifers in Canada, in Proceedings of the 57th Canadian Geotechnical Conference and the 5th joint CGS-IAH Conference; 2004; pages 2B (26-33) (GSC Cont.# 2004085).

Sattel D., 2009, An overview of helicopter time-domain EM systems. in Extended Abstracts: ASEG, 2009.

Scharling PB, Rasmussen ES, Sonnenborg TO, Engesgaard P, Hinsby K (2009) Three-dimensional regional-scale hydrostratigraphic modeling based on sequence stratigraphic methods: a case study of the Miocene succession in Denmark. Hydrogeol J, 17(8):1913–1933. doi:10.1007/s10040-009-0475-6.

Schreiner, B.T., 1990, Lithostratigraphyc correlation of Saskatchewan tills – a mirror image of Cretaceous cedrock, Saskatchewan Research Council, Publication G 743-3-B-82.

Shaver, R.B., 2010, Buried valley aquifers – the North Dakota experience, workshop on Prairie buried valley aquifers, Saskatoon, Saskatchewan.

Siemon, B., Christiansen, A. V. and Auken, E. 2009. A review of helicopter-borne electromagnetic methods for groundwater exploration. Near Surface Geophysics, 7, 629-646. doi:10.3997/1873-0604.2009043.

Sørensen, K.I. and Nyboe, N. S., 2012, Near Surface Resolution and Turnoff Times in Airborne TEM Investigations, In Proceedings: 25th Symposium on the Application of Geophpysics to Engineering & Environmental Problems, Tucson, Arizona (USA)

Thomson S., Fountain D., and Watts T., 2007, Airborne geophysics - Evolution and revolution. In Proceedings of Exploration 07: Fifth Decennial International Conference on Mineral Exploration, 19-37.

Turner AK (2006) Challenges and trends for geological modelling and visualisation. Bull Eng Geol Environ 65(2):109–127. doi: 10.1007/s10064-005-0015-0.

Venteris ER (2007) Three-dimensional modeling of glacial sediments using public water-well data records: an integration of interpretive and geostatistical approaches. Geosphere 3(6):456–468. doi: 10.1130/ges00090.1.

Viezzoli, A., Christiansen, A.V., Auken, E., and Sørensen, K., 2008, Quasi-3D modeling of airborne TEM data by spatially constrained inversion: Geoph., 73, 105-113.

Viezzoli, A., L. Tosi, P. Teatini, and S. Silvestri (2010), Surface water–groundwater exchange in transitional coastal environments by airborne electromagnetics: The Venice Lagoon example, Geophys. Res. Lett., 37, L01402, doi:10.1029/2009GL041572.

Viezzoli A, Jørgensen F, Sørensen C (2012) Flawed processing of airborne EM data affecting hydrogeological interpretation. Ground Water. doi:10.1111/j.1745-6584.2012.00958.x.

Wiecek S., 2009, Municipality of Killarney, Turtle Mountain groundwater assessment study: W.L. Gibbons & Associates Inc.

Witherly K., 2000, The Quest for the Holy Grail in Mining Geophysics. The Leading Edge, 19, 270-274.

APPENDIX

The VTEM 3D lithological model

Previous investigations of the Spiritwood VTEM data resulted in a VTEM model that is consistent with existing seismic, ERT and borehole data (see chapter 3). The VTEM model was calibrated to the supporting data via a small time-shift in the VTEM data gates relative to ramp-off . The source of the time shift was attributed to timing or turn-off errors, but the calibration procedure is independent of the source of noise. The calibrated VTEM model exhibits detailed delineation of the very near surface and other resistive anomalies associated to the valley fill (figure 3).

We also performed the inversion of the “original" VTEM datasets without any removal of data gates and without any processing for early-time bias, cultural noise, late-time noise, or calibration. Figure A shows the inversion results along a flight line. The overburden structure reverts to be a conductor over a resistor as opposed to a resistor over a conductor (figure 2, top). The conductive layer near 15 m depth disappears completely. Also, the data residual is mostly above 1 (not shown here) which means that we’re not fitting observed data within noise level.

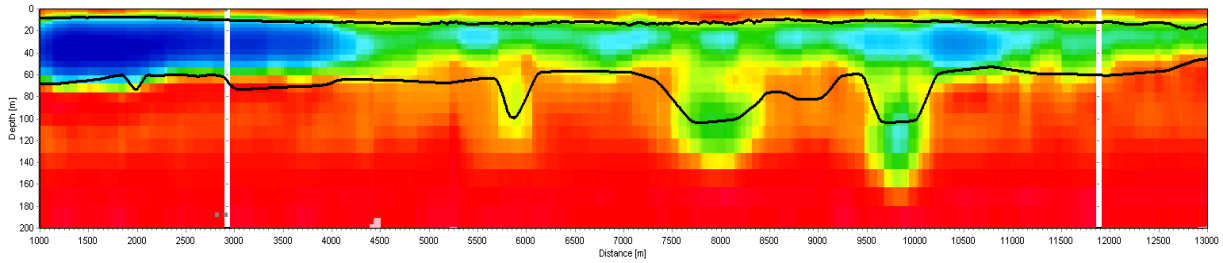

Figure A
Unprocessed VTEM smooth inversion results with all Rx time gates along seismic line 1. Upper solid black line is the shallower till reflection surface and lower solid black line is the bedrock shale reflection.

A lithological voxel-based model has been interpreted for both the un-calibrated (and un-processed) and the calibrated (fully processed) VTEM results. The voxel discretization is 100 × 100 m in the X–Y direction and 5 m in the Z direction. The 3-D modelling was carried out in two steps: first, 3D surfaces were previously interpreted and interpolated based on VTEM resistivity grids and, subsequently, those surfaces were used to constrain the 3D lithological model (figure B). Since different resistivity values are due to variations in filling materials (higher resistivity for coarse-

grained materials and lower resistivity for finer-clayey ones), each lithology were interpreted based on picked resistivity values directly from the VTEM resistivity grids. Figure C reports the geological models derived from the "original" and the revisited VTEM waveform, over the same volume of the subsurface. The differences in the geological models are evident. The top model matches all available ancillary information (ERT, seismic, boreholes, priori geological knowledge- and the AEM data). The bottom model is inaccurate for many reasons, including a) artificial ubiquitous shallow clay cap cover that would prevent surficial recharge, shows, b) erroneous depth estimate of buried valleys, c) overestimation of aquifers porosity. Extraction or management of the GW resources based on this model would most likely bring unwelcomed consequences.

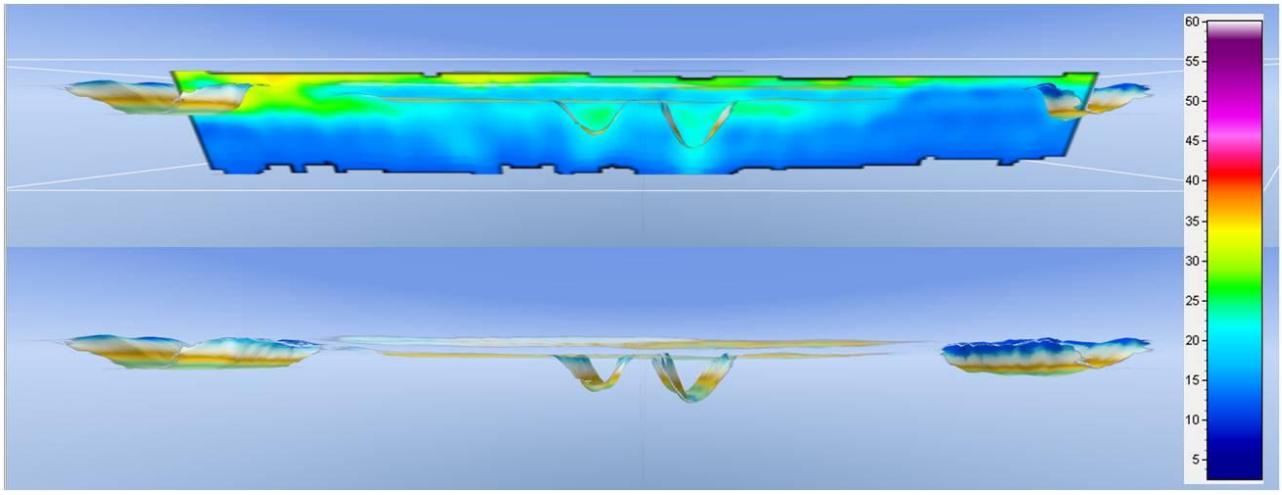

Figure B.
Cross section of the calibrated VTEM resistivity model and the interpreted 3D surfaces of the existing buried valleys (top). 3D surfaces of the buried valleys used to constrain the voxel (bottom).

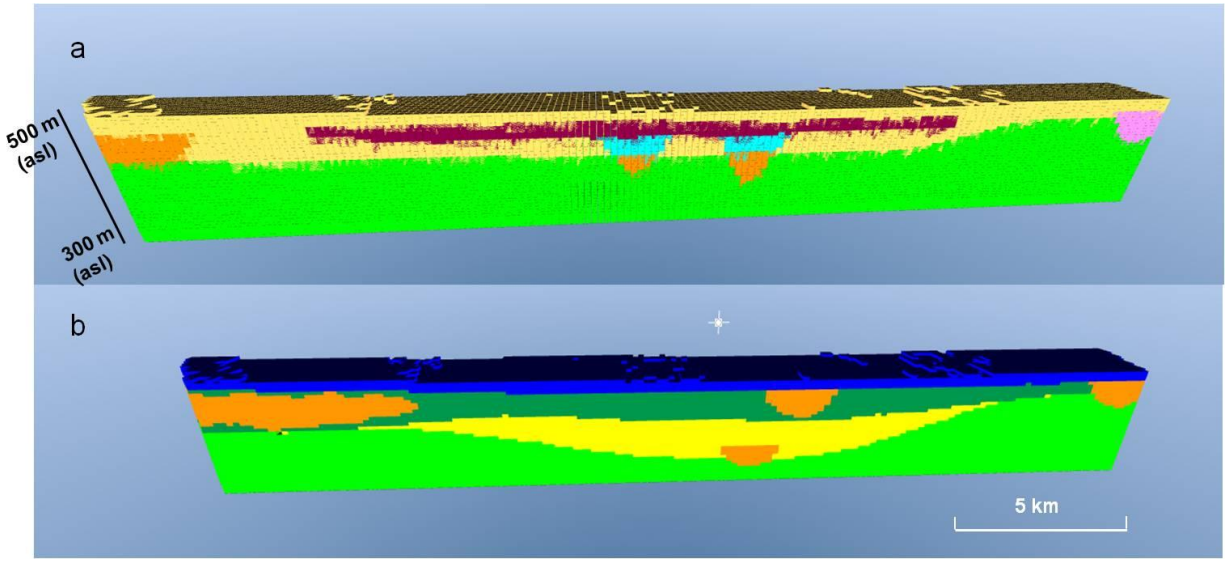

Figure C.
Voxel based lithological model derived from the calibrated VTEM resistivity model (top) and the uncalibrated VTEM resistivity model (bottom). Different lithologies are rendered with different colors (e.g., gravel orange, shale bedrock green, clay-rich till blue and purple, till matrix light brown).